

Sheffield Hallam University

Cathodic Protection of Corroded Pre-stressed Tendons

ELOMARI, Ibrahim Ramadan

Available from the Sheffield Hallam University Research Archive (SHURA) at:

<http://shura.shu.ac.uk/25590/>

A Sheffield Hallam University thesis

This thesis is protected by copyright which belongs to the author.

The content must not be changed in any way or sold commercially in any format or medium without the formal permission of the author.

When referring to this work, full bibliographic details including the author, title, awarding institution and date of the thesis must be given.

Please visit <http://shura.shu.ac.uk/25590/> and <http://shura.shu.ac.uk/information.html> for further details about copyright and re-use permissions.

Cathodic Protection of Corroded Pre-stressed Tendons

Ibrahim Ramadan Elomari

A thesis submitted in partial fulfilment of the requirements of
Sheffield Hallam University
for the degree of Doctor of Philosophy

April 2019

Dedication

I would like to dedicate my thesis to my beloved late parents who always believed in my ability to be successful in the academic arena. You are gone but your belief in me has made the dream of doing this project into reality. I know they would be proud and I will forever be grateful for the knowledge and values they instilled in me.

Abstract

The corrosion of reinforcement in concrete, whether conventional or pre-stressed, remains a significant cause for the loss of durability of reinforced concrete structures. Corrosion costs the UK economy between 3% to 4% of Gross National Product. This is, in turn, has resulted in the development of greatly enhanced methods of remediation and life extension. One possible approach is to use Cathodic Protection (CP) to control further deterioration. CP of reinforcing steel in concrete structures has proved to be effective for preventing or controlling corrosion and been used successfully for over 25 years. CP is able to stop corrosion in a reliable and economical way where the environment has caused reinforcement corrosion and subsequent concrete damage. However, concerns exist about the ability of CP to avert deterioration in pre-stressed structures due to hydrogen generation and subsequent embrittlement of the tendons. This research investigates the performance of pre-stressed steel tendon exposed to an impressed current cathodic protection (ICCP) at varying potentials on a long-term basis to establish its effect on strength and establish optimised criteria for CP that can be safely applied to deteriorated pre-stressed structures.

Twelve timber moulds were manufactured for applying the pre-stressing technique to test specimens. Tendons measuring 5.4mm diameter were selected in both the galvanised and ungalvanised state. Two levels of pre-stressing have been investigated, namely low level (300-400 MPa) and high level (800-1200 MPa). Three different degrees of corrosion Stage I, II and III with target losses of cross-sectional of 0-1 %, 2-4 % and 4-7 % respectively, were employed to replicate in-situ conditions. The actual degree of corrosion was verified gravimetrically by weighing the tendons both before and after testing. The tendons were pre-stressed in two types of electrolyte, namely a saline solution and a sand/cement mortar representing mortar. Upon completion of the corrosion phase using an anodic impressed current method, Impressed Current Cathodic Protection (ICCP) was applied to the tendons at two levels of polarization, normal protection (ICCP-N) in the range of -650 to -750 mV vs Ag/AgCl/ 0.5M KCl and over protection (ICCP-O) ranging between -850 to -1300 mV vs Ag/AgCl/ 0.5M KCl for an extended period to both ungalvanised

and galvanised pre-stressed steel tendons, to investigate its effect. The potentials of the pre-stressed steel tendon and potential decay resulting from the application of ICCP were monitored and analysed. The strain in the tendons was also monitored throughout the corrosion and ICCP phases to establish pre-stress losses. Finally, the mechanical properties were investigated and the tendon surfaces and fracture modes inspected using an Infinite Focus Microscope (IFM) and Scanning Electronic Microscope (SEM).

The results confirmed that accelerated corrosion is a reliable technique for generating the corrosion of steel. ICCP can be used in the corroded pre-stressed tendons as the long-term application shows there is no significant effect on the surface or damage of the both types of tendons with low or high levels of pre-stress. There has been a long term loss in service stress which due to corrosion, due to ICCP or a combination of both. From the results, the loss is more likely to be corrosion induced rather than ICCP. A higher degree of corrosion leads to a higher loss in pre-stress in highly pre-stressed tendons, which is an additional loss that should be accounted for at the design stage.

Declaration

I hereby declare that no portion of the work referred to in this thesis has been submitted in support of an application for another degree or qualification of this or any other University or other institution of learning. All sources of information have been made duly acknowledged.

Ibrahim Ramadan Elomari

April 2019

Acknowledgements

I would like to express my sincere gratitude to Professor Fin O'Flaherty of the Centre for Infrastructure Management, Sheffield Hallam University, for his guidance, support and patience throughout this research project.

I also gratefully acknowledges the contributions, sincere assistance, guidance and supervision of Professor Paul Lambert (Mott MacDonald) and the Centre for Infrastructure Management, Sheffield Hallam University.

I also greatly appreciate and wishes to thank the valuable assistance given by the staff of the Material Engineering Research Institute (MERI) and the technicians of Construction Materials Laboratory.

I acknowledges the Ministry of Higher Education & Scientific Research in Libya for the provision of funding which was helpful in completing this research project.

Many thanks for my family members for their support, encouragement, and sacrifice that gave me the courage and determination to complete my study.

Most importantly, I wish to express my deepest gratitude to my wife, Fairouz, for her patience and tolerance over the study period. I could not be able to finish this work without her support. Thank you for being with me and for your appreciated sacrifices. Thank you for my wonderful children, Ahmed, Mhmud, Mohamed, Ameer and new born Yaseen, who have been source of unending inspiration.

Table of Contents

Dedication.....	ii
Abstract	iii
Table of Contents.....	vii
Notation	v
List of Figures	vii
List of Tables.....	vii
Chapter 1 - Introduction and Thesis Outlined	1
1.1 Introduction	1
1.2 Aims of the research	5
1.3 Scope of study	5
1.4 Thesis outline.....	6
Chapter 2 - Literature Review	8
2.1 Introduction	8
2.2 Pre-stressed concrete principles.....	8
2.3 Deterioration of reinforced concrete structure	11
2.3.1 Deterioration stages.....	11
2.3.2 Factors influencing rates of deterioration	13
2.4 Corrosion mechanisms	15
2.4.1 Definition of corrosion	15
2.4.2 Principle of corrosion	15
2.5 Forms of corrosion	16
2.5.1 General Corrosion.....	17
2.5.2 Localised corrosion	17
2.6 Corrosion of steel in concrete	18
2.6.1 Introduction	18
2.6.2 Corrosion process.....	19

2.6.3 Corrosion of pre-stressing steel in concrete.....	22
2.7 Cathodic Protection.....	29
2.7.1 Historical foundation of cathodic protection	29
2.7.2 Theoretical basis for cathodic protection.....	29
2.7.3 Methods of Applying Cathodic Protection	30
2.7.4 Anode selection	33
2.7.5 Electrolysis.....	33
2.7.6 Design criteria for CP.....	35
2.7.7 Reference electrode (Half-Cell).....	37
2.7.8 Hydrogen embrittlement.....	38
2.8 Conclusion of review.....	38
Chapter 3 - Preliminary Experimental Works	40
3.1 Introduction	40
3.2 Aims and Objectives	40
3.3 Preliminary Experimental Programme	40
3.4 Selection of strain gauges and determination of slippage.....	42
3.5 Accelerating corrosion of the tendon.....	44
3.5.1 Faraday's Law.....	44
3.6 Optimisation of ICCP	53
3.7 Concluding remarks.....	56
3.7.1 Loss in stress-due to slippage.....	56
3.7.2 Effect of corrosion on the tendon	56
3.7.3 Effect of Impressed Current Cathodic Protection (ICCP) on the tendon.....	56
Chapter 4 - Experimental Methodology	57
4.1 Introduction	57
4.2 Objectives of investigation	58

4.3 Details of the experimental programme	58
4.4 Preparation of moulds	62
4.5 Preparation and pre-stressing system	62
4.6 Electrochemical Techniques	66
4.6.1 Potential inspection technique	66
4.6.2 Half-cell potential	66
4.6.3 Experimental Procedure	68
4.7 Impressed Current Cathodic Protection (ICCP)	71
4.7.1 Design of ICCP for corrosion control.....	72
4.8 Hydrogen test.....	73
4.9 Materials	74
4.9.1 Tendon.....	74
4.9.2 MMO Titanium Mesh.....	75
4.9.3 Cement	75
4.9.4 Aggregates.....	75
4.9.5 Sodium Chloride	76
4.9.6 Calcium Hydroxide.....	77
4.9.7 Di-ammonium Hydrogen Citrate.....	77
4.10 Apparatus.....	77
4.10.1 DC Power Supply.....	77
4.10.2 Reference Electrode (half-cell).....	77
4.10.3 Digital Voltage Meter.....	79
4.10.4 Data Logger	79
4.10.5 Strain Gauges	80
4.10.6 Hydraulic Jack.....	81
4.10.7 Load Cell.....	81
4.11 Analytical Methodology	81

4.11.1 Scanning Electronic Microscopy (SEM)	81
4.11.2 X-Ray Diffraction (XRD)	85
4.11.3 Infinite Focus Microscope (IFM)	85
4.11.4 Tensile Test	86
4.11.5 Compressive strength	88
4.11.6 Visual examination	89

Chapter 5 - Effect of accelerated corrosion on the applied service

stress in the tendon.....	90
5.1 Introduction	90
5.2 The objectives of the tests	90
5.3 Anodic impressed current technique	91
5.4 Experimental Works	92
5.4.1 Test programme.....	92
5.4.2 Tests in saline electrolyte.....	93
5.4.3 Test in mortar electrolyte	94
5.4.4 Pre-tensioning and installing strain gauges.....	96
5.5 Accelerated corrosion process.....	99
5.5.1 Corrosion of tendons in saline solution	100
5.5.2 Corrosion of tendons in mortar.....	102
5.6 Results and discussion	104
5.6.1 Visual observation.....	104
5.6.2 Surface condition of the corroded tendons	106
5.6.3 X-ray Diffraction (XRD)	113
5.6.4 Diameter and weight loss.....	114
5.6.5 Loss in service stress.....	122
5.7 Conclusions	141

Chapter 6 - Effect of Cathodic protection on tendon - Normal Protection	143
6.1 Introduction	143
6.2 The objectives of the tests	144
6.3 Impressed Current Cathodic Protection (ICCP)	145
6.3.1 Anode	147
6.3.2 Current density requirement.....	147
6.3.3 ICCP with hydrogen embrittlement	147
6.4 Experimental Work.....	148
6.4.1 Specimen design, mortar mix, pre-tensioning and accelerated corrosion	150
6.4.2 Application of impressed current cathodic protection (ICCP).....	151
6.4.3 Design criteria	153
6.4.4 Polarisation and Depolarisation Criteria	154
6.5 Results and discussion	155
6.5.1 Visual observation.....	155
6.5.2 Infinite Focus Microscope (IFM)	159
6.5.3 Potential.....	162
6.5.4 Monitoring of Condition and Performance.....	165
6.5.5 Effect of ICCP-N on the applied service stress	169
6.5.6 Effect of ICCP-N on the mechanical properties of the tendon.....	174
6.5.7 Conclusion	201
Chapter 7 - Effect of Cathodic protection on steel tendons Overprotection	203
7.1 Introduction	203
7.2 The objectives of the tests	203

7.3 Impressed Current Cathodic Protection (ICCP)	204
7.4 Experimental works.....	204
7.4.1 Specimens design, mortar mix, pre-tensioning and accelerated corrosion	206
7.4.2 Application of impressed current cathodic protection (ICCP).....	206
7.4.3 Design criteria	209
7.4.4 Polarization and Depolarization Criteria	209
7.5 Results and discussion	210
7.5.1 Visual observation.....	210
7.5.2 Infinite Focus Microscope (IFM).....	214
7.5.3 Potential.....	217
7.5.4 Monitoring of Condition and Performance.....	221
7.5.5 Effect of ICCP-O on the applied service stress	226
7.5.6 Effect of ICCP-O on the mechanical properties of the tendon.....	231
7.5.7 Summary of comparison between the effects of applying cathodic protection at normal and overprotection levels ...	256
7.5.8 Conclusions	272
Chapter 8 - Conclusions and recommendations for future works	275
8.1 General conclusions	275
8.2 Effect of corrosion on the tendon	276
8.3 Effect of Normal Impressed Current Cathodic Protection (ICCP- N) on the tendons	276
8.4 Effect of Overprotection by Impressed Current Cathodic Protection (ICCP-O) on the tendons	277
8.5 Recommendations for further research.....	279

Appendix 1.....	280
Appendix 2.....	282
References.....	283

Notation

The great majority of the symbols listed below are essentially those used in the current British Practice. Less frequently used symbols and symbols which have different meanings in different contexts are defined where they are used.

A	atomic weight of iron (56 gram/mol)
γ	density of metal (7.86 g/cm ³)
F	Faraday's constant (96,500 Coulombs)
Z	valence of iron which is (2)
a	tendon surface area before corrosion (cm ²)
Φ	nominal perimeter of the tendon (mm)
I	electric current (A)
t	time (sec)
i	corrosion current density (A/cm ²)
R	metal section loss per year
T	the period of corrosion after initiation (year)
Δw	weight loss due to corrosion in (g)
δ	material loss
2RT/D (%)	degree of corrosion (%)
V	applied voltage (mV)
DVM	digital voltage meter
E	potential drop of tendon
$\Delta\mu\varepsilon$	the strain in microstrain
F_1	datum frequency of the VWSG (Hz).
F_2	subsequent frequency of the VWSG (Hz).
CP	Cathodic Protection
ICCP	Impressed Current Cathodic Protection
ICCP-N	Impressed Current Cathodic Protection-Normal Protection
ICCP-O	Impressed Current Cathodic Protection-Over Protection
D1	mean diameter of tendon before corrosion
D2	mean diameter of tendon before corrosion
$\Delta d1$	actual diameter loss of tendon
$\Delta d2$	theoretical weight loss of tendon
$\%\Delta d$	percent error in diameter reduction

W_1	weight of tendon before corrosion
W_2	weight of tendon after corrosion
Δw_1	weight loss of tendon
Δw_2	theoretical weight loss of tendon
$\% \Delta w$	percent error in weight loss

List of Figures

Figure 1.1 Some of the applications of pre-stress concrete structures	2
Figure 1.2 LNG bund wall	3
Figure 1.3 Preload system of bund wall	4
Figure 1.4 Corrosion on preloaded tendon in a bund Wall.....	5
Figure 2.1 Examples of stress-strain curves for reinforcing and pre-stressing steels [10]	9
Figure 2.2 The stages of corrosion of steel in concrete [16]	12
Figure 2.3 Causes of deterioration of reinforced concrete structures [10].....	14
Figure 2.4 Breakdown of the protective passive film on a steel bar in concrete [27]	18
Figure 2.5 Schematic illustration of the corrosion of reinforcement steel in concrete [16], [29]	20
Figure 2.6 Potential-pH equilibrium diagram of iron in aqueous solutions [32].....	21
Figure 2.7 (a) Corrosion of Pre-stressing Wires [35] (b) Corroded wires of a strand from a simulated tendon [36].....	23
Figure 2.8 Severe corrosion and minimal rust staining on pre-stressing wires [37]	23
Figure 2.9 Pitted PT wires with (a) grout [Cl-] 0.80 wt% cement, pit depth 0.12 mm, and no physical grout deficiency and (b) grout [Cl-] 2.00 wt% cement, pit depth 0.46 mm and a grout void [36]	25
Figure 2.10 Stress corrosion cracking in a corrosion pit on steel [39]	25
Figure 2.11 Pitting induced stress corrosion cracking [42].....	26
Figure 2.12 Sequence of phenomena that lead to the initiation and propagation of hydrogen induced cracks and subsequent failure in two materials (A and B) with different fracture toughness (d_{cr} = critical flaw size; t_i = incubation time, t_r = time of failure) [10]	26
Figure 2.13 Brittle fracture of pre-stressing wire [37]	27

Figure 2.14 Fracture surface of a pre-stressing bar that failed due to hydrogen embrittlement [10]	28
Figure 2.15 Schematic diagram of cathodic protection using sacrificial anodes [55]	31
Figure 2.16 Schematic diagram of cathodic protection using the impressed-current technique [55].....	32
Figure 2.17 Potential decay curve [78].....	36
Figure 3.1 Placing and taking readings of both DEMEC and VW strain gauges	42
Figure 3.2 Slippage compensation with increasing applied pre-tensioning force.....	44
Figure 3.3 Appearance of tendon throughout the corrosion period	47
Figure 3.4 Gross loss in tendon with low pre-stress over the test period	52
Figure 3.5 Gross loss in tendon with high pre-stress over the test period.....	52
Figure 3.6 Hydrogen just being generated on tendon S-G-H-II-1.....	53
Figure 3.7 Applied current and voltage versus test period	54
Figure 4.1 Timber mould on a wisa-form base.....	62
Figure 4.2 Pre-stressing set-up.....	64
Figure 4.3 Pre-stressing system in operation.....	65
Figure 4.4 Wedges and U shape washers to minimise the slippage losses.....	65
Figure 4.5 Trial test using load cell to determine the losses	66
Figure 4.6 Schematic diagram of half-cell circuit.....	67
Figure 4.7 The schematic diagram of acceleration corrosion test.....	69
Figure 4.8 Schematic diagram of ICCP set-up.....	71
Figure 4.9 ICCP Components	72
Figure 4.10 ICCP test in progress.....	73
Figure 4.11 Hydrogen test machine	74
Figure 4.12 DC Multi-Channel Power Supply	77

Figure 4.13 Reference electrode.....	78
Figure 4.14 Digital voltmeter	79
Figure 4.15 Data logger Type 85D.....	79
Figure 4.16 (a) Demec digital strain gauge, (b) Digital vibrating wire strain gauge.....	80
Figure 4.17 Hydraulic hollow cylinder Jack	81
Figure 4.18 Scanning Electronic Microscopy (SEM)	82
Figure 4.19 SEM principle schematic diagram [88].....	83
Figure 4.20 Cutting SEM samples	84
Figure 4.21 Aluminium holder with a double sticky carbon film.....	84
Figure 4.22 X-Ray Diffraction (XRD).....	85
Figure 4.23 Infinite Focus Measurement (IFM) (a), taking image (b)	86
Figure 4.24 Tensile test machine ESH600 and extensometer	88
Figure 4.25 Compressive test machine.....	88
Figure 5.1 Test set-up for saline electrolyte	93
Figure 5.2 Specimens dimension (mm)	94
Figure 5.3 Casting the mortar and testing the cubes	95
Figure 5.4 Pre-stressing System (a) mould; (b) strain gauge; (c) laptop; (d) data logger; (e) hydraulic jack connected to hand pump.....	97
Figure 5.5 Batch 1 with pre-stressed tendons ready for accelerated corrosion.....	101
Figure 5.6 Batch 1 specimens under accelerated corrosion	101
Figure 5.7 Batch 1 specimens under accelerated corrosion	102
Figure 5.8 Specimens and cubes ready for casting	102
Figure 5.9 Schematic diagram shows the test set-up for one batch.....	103
Figure 5.10 Set of specimens under accelerated corrosion - Batch 2.....	104
Figure 5.11 Specimens under accelerated corrosion.....	105

Figure 5.12 Corrosion of the tendons in the saline solution and colour changes	105
Figure 5.13 Cracks at each stage of corrosion during accelerated corrosion process.....	106
Figure 5.14 Removal of corrosion products with di-ammonium hydrogen citrate solution.....	107
Figure 5.15 Surface of tendon after corrosion - Batch 1	108
Figure 5.16 Surface of tendon after corrosion - Batch 2	108
Figure 5.17 Surface of tendon after corrosion - Batch 3	109
Figure 5.18 Surface of tendon after corrosion - Batch 4	109
Figure 5.19 Specimen under surface investigation by IFM	111
Figure 5.20 Gross loss in tendon pre-stress over corrosion period (30% UTS)	124
Figure 5.21 Net loss in tendon pre-stress over corrosion time (30% UTS)	125
Figure 5.22 Gross loss in tendon pre-stress over corrosion time (80% UTS)	125
Figure 5.23 Net loss in tendon pre-stress over corrosion period (80% UTS) ..	126
Figure 5.24 Loss in pre-stress due to corrosion Stage II.....	127
Figure 5.25 Loss in pre-stress due to corrosion Stage III.....	127
Figure 5.26 Relationship between degree of corrosion and different levels of pre-stress.....	128
Figure 5.27 Gross loss in tendon pre-stress during corrosion period (30% UTS) - Batch 2	129
Figure 5.28 Gross loss in tendon pre-stress during corrosion period (30% UTS) - Batch 3	130
Figure 5.29 Gross loss in tendon pre-stress during corrosion period (80% UTS) - Batch 2	130
Figure 5.30 Gross loss in tendon pre-stress during corrosion period (80% UTS) - Batch 3	131

Figure 5.31 Average loss in tendon pre-stress during corrosion period (80% UTS) - Batch 2 & 3	131
Figure 5.32 Average loss in pre-stress due to corrosion Stage II - Batch 2 & 3	132
Figure 5.33 Average loss in pre-stress due to corrosion Stage III - Batches 2 & 3	133
Figure 5.34 Relationship between degree of corrosion and different levels of pre-stress - Batches 2 & 3	134
Figure 5.35 Gross loss in tendon pre-stress during corrosion period (80% UTS) - Batch 4, Group 1	136
Figure 5.36 Gross loss in tendon pre-stress during corrosion period (80% UTS) - Batch 4, Group 2	136
Figure 5.37 Net loss in tendon pre-stress during corrosion period (80% UTS) - Batch 4, Group 1	137
Figure 5.38 Net loss in tendon pre-stress during corrosion period (80% UTS) - Batch 4, Group 2	137
Figure 5.39 Relationship between degree of corrosion and the loss in pre-stress (80% UTS).....	138
Figure 5.40 Net loss in galvanised and ungalvanised tendon pre-stress during corrosion period (Stage II).....	139
Figure 5.41 Net loss in galvanised and ungalvanised tendone pre-stress during corrosion period (Stage III).....	140
Figure 5.42 Relationship between degree of corrosion and the average loss in pre-stress in galvanised and ungalvanised tendon (80% UTS) ...	141
Figure 6.1 Schematic diagram of the principle of ICCP	146
Figure 6.2 Wooden supports to facilitate storage of specimens.....	151
Figure 6.3 Setup of specimens under application of ICCP-Normal protection	152
Figure 6.4 Polarization-Depolarisation [119].....	155

Figure 6.5 Yellow spots on the mortar surface for ungalvanised tendons with Low Level of pre-stress	157
Figure 6.6 Yellow spots on the mortar surface for ungalvanised tendons with High Level of pre-stress.....	158
Figure 6.7 No yellow spots on the mortar surface for galvanised tendons with High Level of pre-stress.....	159
Figure 6.8 Microstructure of ungalvanized tendons surface.....	160
Figure 6.9 Microstructure of ungalvanized tendons surface with High Level of pre-stress.....	161
Figure 6.10 Microstructure of galvanised tendons surface with High Level of pre-stress.....	162
Figure 6.11 "ON" potential of ungalvanised tendons during applying ICCP-Normal Protection, 30% UTS.....	164
Figure 6.12 "ON" potential of ungalvanised tendons during applying ICCP-Normal Protection, 80% UTS.....	164
Figure 6.13 "ON" potential of galvanised tendons during applying ICCP-Normal Protection, 80% UTS.....	165
Figure 6.14 Instant-Off potential of ungalvanised tendons, 30% UTS.....	166
Figure 6.15 Instant-Off potential of ungalvanised tendons, 80% UTS.....	166
Figure 6.16 Instant-Off potential of galvanised tendon, 80% UTS	167
Figure 6.17 Potential decay of ungalvanised tendons.....	168
Figure 6.18 Potential decay of galvanised tendons.....	168
Figure 6.19 DEMEC pips placing for contraction measurements.....	169
Figure 6.20 Service stress in the ungalvanised tendons over the ICCP-N period, Batch 2 (30% UTS)	171
Figure 6.21 Service stress in the ungalvanised tendons over the ICCP-N period, Batch 2 (80% UTS)	172
Figure 6.22 Service stress in the ungalvanised tendons over the ICCP-N period, Batch 2 (30% & 80% UTS).....	172

Figure 6.23 Service stress in pre-stressed galvanised tendon over the ICCP-N period, Batch 4 (80% UTS).....	173
Figure 6.24 Relationship between Stages of corrosion and the loss in service stress in ungalvanised and galvanised tendons (80% UTS) during the ICCP-N period.....	174
Figure 6.25 Stress-Strain curve for as-received ungalvanised tendons	176
Figure 6.26 Stress-Strain curve for as-received galvanised tendons	176
Figure 6.27 Fracture modes for ungalvanised and galvanised as-received tendons	177
Figure 6.28 Location of failure mode.....	178
Figure 6.29 Stress-strain curves for the ungalvanised tendons, ICCP-N, 30% UTS	185
Figure 6.30 Stress-strain curves for the ungalvanised tendons, ICCP-N, 80% UTS	185
Figure 6.31 Comparison of stress-strain curves for all ungalvanised tendons, ICCP-N, 30% & 80% UTS.....	186
Figure 6.32 Comparison stress-strain curves for galvanised tendons, ICCP-N, 80% UTS	186
Figure 6.33 Comparison between ungalvanised and galvanised stress-strain curves, ICCP-N, 80% UTS, Stage I corrosion	187
Figure 6.34 Comparison between ungalvanised and galvanised stress-strain curves, CP-N, 80% UTS, Stage II corrosion.....	187
Figure 6.35 Comparison between ungalvanised and galvanised stress-strain curves, ICCP-N, 80% UTS, Stage III corrosion	188
Figure 6.36 Ductility measurement	189
Figure 6.37 Relationship between normal CP potential and hydrogen embrittlement ratio, Low Level pre-stress and, ungalvanised tendons....	190
Figure 6.38 Relationship between normal CP potential and hydrogen embrittlement ratio, High Level pre-stress and, ungalvanised tendons...	190

Figure 6.39 Relationship between normal CP potential and hydrogen embrittlement ratio, High Level pre-stress and, galvanised tendons.....	191
Figure 6.40 SEM micrographs and images showing the fracture mode of the as-received ungalvanised tendon	193
Figure 6.41 SEM micrographs and images showing the fracture mode of the as-received galvanised tendon	194
Figure 6.42 SEM images for ungalvanised tendon (M-U-L-I-N-1), 30% UTS.....	195
Figure 6.43 SEM images for ungalvanised tendon (M-U-L-I-N-2), 30% UTS.....	196
Figure 6.44 SEM images for ungalvanised tendon (M-U-L-III-N-3), 30% UTS.....	196
Figure 6.45 SEM images for ungalvanised tendon (M-U-H-I-N-1), 80% UTS.....	197
Figure 6.46 SEM images for ungalvanised tendon (M-U-H-II-N-2), 80% UTS.....	198
Figure 6.47 SEM images for ungalvanised tendon (M-U-H-III-N-3), 80% UTS.....	198
Figure 6.48 IFM image (50X magnification, 1mm length, 6x2 image) for specimen M-G-H-III-3	199
Figure 6.49 SEM images for galvanised tendon (M-G-H-I-N-1), 80% UTS.....	200
Figure 6.50 SEM images for galvanised tendon (M-G-H-II-N-2), 80% UTS....	200
Figure 6.51 SEM images for galvanised tendon (M-G-H-III-N-3), 80% UTS...	201
Figure 7.1 ICCP-O specimens pre-stressed and cast.....	206
Figure 7.2 Power supplies to generate the target potential.....	207
Figure 7.3 Set-up of specimens under the application of ICCP overprotection	208
Figure 7.4 Set-up of unstressed Ugalvanised & Galvanised tendons under application of ICCP-O	209

Figure 7.5 Yellow spots on the mortar surface for ungalvanised tendons with Low Level of pre-stress	211
Figure 7.6 Yellow spots on the mortar surface for ungalvanised tendons with High Level of pre-stress.....	212
Figure 7.7 Yellow spots on the mortar surface for galvanised tendons with High Level of pre-stress	213
Figure 7.8 Microstructure of ungalvanized tendon surface	214
Figure 7.9 Microstructure of ungalvanized tendon surface with High Level of pre-stress.....	215
Figure 7.10 Microstructure of galvanized tendon surface with High Level of pre-stress.....	216
Figure 7.11 Microstructure of ungalvanised & galvanized tendon surface	216
Figure 7.12 "ON" potential of ungalvanised tendon during application of ICCP-Overprotection, 30% UTS	219
Figure 7.13 "ON" potential of ungalvanised tendon during application of ICCP-Overprotection, 80% UTS	219
Figure 7.14 "ON" potential of galvanised tendon during application of ICCP-Overprotection, 80% UTS	220
Figure 7.15 "ON" potential of un-stressed galvanised & ungalvanised tendons during application of ICCP-Overprotection.....	220
Figure 7.16 Instant-Off potential of ungalvanised tendons, 30% UTS.....	222
Figure 7.17 Instant-Off potential of ungalvanised tendons, 80% UTS.....	222
Figure 7.18 Instant-Off potential of galvanised tendons, 80% UTS.....	223
Figure 7.19 Instant-Off potential of Un-stressed galvanised tendons, 80% UTS.....	223
Figure 7.20 Potential decay of ungalvanised tendons.....	224
Figure 7.21 Potential decay of galvanised tendons.....	225
Figure 7.22 Potential decay of unstressed galvanised & ungalvanised tendons.....	225
Figure 7.23 Monitoring contraction of timber moulds	226

Figure 7.24 Service stress in pre-stressed ungalvanised tendon over the ICCP-O period, Batch 3 (30% UTS).....	228
Figure 7.25 Service stress in pre-stressed ungalvanised tendon over the ICCP-O period, Batch 3 (80% UTS).....	229
Figure 7.26 Service stress in pre-stressed ungalvanised tendons over the ICCP-O period, Batch 3 (30% & 80% UTS)	229
Figure 7.27 Service stress in pre-stressed galvanised tendons over the ICCP-O period, Batch 4 (80% UTS).....	230
Figure 7.28 Relationship between stages of corrosion and the loss in service stress in the ungalvanised and galvanised tendons (80% UTS) over the ICCP-O period	231
Figure 7.29 Location of failure.....	232
Figure 7.30 Stress-Strain curve for ungalvanised tendons, 30% UTS	239
Figure 7.31 Stress-Strain curve for ungalvanised tendons, 80% UTS	239
Figure 7.32 Stress-Strain curve for galvanised tendons, 80% UTS	240
Figure 7.33 Stress-Strain curve for ungalvanised tendons (unstressed).....	240
Figure 7.34 Stress-Strain curve for galvanised tendons (unstressed).....	241
Figure 7.35 Relationship between overpotential and the hydrogen embrittlement ratio, Low Level pre-stress, ungalvanised tendon	243
Figure 7.36 Relationship between over potential and the hydrogen embrittlement ratio, High Level pre-stress, ungalvanised tendon, 80% UTS.....	244
Figure 7.37 Relationship between over potential and the hydrogen embrittlement ratio, High Lvel pre-stress, galvanised tendon, 80% UTS.....	244
Figure 7.38 Relationship between overpotential and the hydrogen embrittlement ratio, ungalvanised tendon (Batch 5).....	245
Figure 7.39 Relationship between overpotential and the hydrogen embrittlement ratio, galvanised tendon (Batch 5).....	245

Figure 7.40 SEM images for ungalvanised tendon (M-U-L-I-O-1), 30% UTS.....	247
Figure 7.41 SEM images for ungalvanised tendon (M-U-L-II-O-2), 30% UTS.....	247
Figure 7.42 SEM images for ungalvanised tendon (M-U-L-III-O-3), 30% UTS.....	248
Figure 7.43 SEM images for ungalvanised tendon (M-U-H-I-O-1), 80% UTS.....	249
Figure 7.44 SEM images for ungalvanised tendon (M-U-H-II-O-2), 80% UTS.....	249
Figure 7.45 SEM images for ungalvanised tendon (M-U-H-III-O-3), 80% UTS.....	250
Figure 7.46 SEM images for galvanised tendon (M-G-H-I-O-1), 80% UTS.....	251
Figure 7.47 SEM images for galvanised tendon (M-G-H-II-O-2), 80% UTS....	251
Figure 7.48 SEM images for galvanised tendon (M-G-H-III-O-3), 80% UTS...	252
Figure 7.49 SEM images for ungalvanised tendon (5-U-O-1), Batch 5	253
Figure 7.50 SEM images for ungalvanised tendon (5-U-O-2), Batch 5	253
Figure 7.51 SEM images for ungalvanised tendon (5-U-O-3), Batch 5	254
Figure 7.52 SEM images for galvanised tendon (5-G-O-1), Batch 5.....	255
Figure 7.53 SEM images for galvanised tendon (5-G-O-2), Batch 5.....	255
Figure 7.54 SEM images for galvanised tendon (5-G-O-3), Batch 5.....	256
Figure 7.55 Comparison of loss in service stress for ungalvanised tendons (30% & 80% UTS).....	257
Figure 7.56 Comparison of loss in service stress for galvanised tendons (80%UTS)	258
Figure 7.57 Comparison of mechanical properties for ungalvanised tendons with low level of pre-stress exposed to ICCP-N & ICCP-O (1) ..	259
Figure 7.58 Comparison of mechanical properties for ungalvanised tendons with a low level of pre-stress exposed to ICCP-N & ICCP-O (2)	259

Figure 7.59 Comparison of mechanical properties for ungalvanised tendons with High Level of pre-stress exposed to ICCP-N & ICCP-O (1)	260
Figure 7.60 Comparison of mechanical properties for ungalvanised tendons with High Level of pre-stress exposed to ICCP-N & ICCP-O (2)	261
Figure 7.61 Comparison of mechanical properties for galvanised tendons with High Level of pre-stress exposed to ICCP-N & ICCP-O (1).....	262
Figure 7.62 Comparison of mechanical properties for galvanised tendons with High Level of pre-stress exposed to ICCP-N & ICCP-O (2).....	262
Figure 7.63 Relationship between polarisation potential and hydrogen embrittlement ratio for ungalvanised tendons, Low Level, Stage II	263
Figure 7.64 Relationship between polarisation potential and hydrogen embrittlement ratio for ungalvanised tendons, Low Level, Stage III	264
Figure 7.65 Relationship between polarisation potential and hydrogen embrittlement ratio for ungalvanised tendons, High Level, Stage II	264
Figure 7.66 Relationship between polarisation potential and hydrogen embrittlement ratio for ungalvanised tendons, High Level, Stage III	265
Figure 7.67 Relationship between polarisation potential and hydrogen embrittlement ratio for galvanised tendons, High Level, Stage II	266
Figure 7.68 Relationship between polarisation potential and hydrogen embrittlement ratio for galvanised tendons, High Level, Stage III	266
Figure 7.69 Comparison of fracture mode for ungalvanised tendons (30% UTS)	267
Figure 7.70 Comparison of fracture mode for ungalvanised tendons, (80% UTS)	269
Figure 7.71 Comparison of fracture mode for galvanised tendons (80% UTS)	270
Figure 7.72 Comparison of fracture mode for ungalvanised and galvanised tendons (unstressed samples)	271

List of Tables

Table 2.1 Different types of pre-stressing steel [10].....	10
Table 2.2 Examples of corrosion of steel in concrete [22].....	16
Table 3.1 Preliminary Experimental Test Program.....	41
Table 3.2 Calculating tendon slippage using load cell	43
Table 3.3 Tendon test parameters	48
Table 3.4 Corrosion design criteria	49
Table 3.5 Actual strain and stress in the tendons	50
Table 3.6 Stress and strain in the tendons.....	51
Table 3.7 Pilot CP test in a saline solution.....	53
Table 3.8 Test results of the ICCP application	55
Table 4.1 Detailed Experimental Programme	60
Table 4.2 Composition of galvanised and ungalvanised tendons	75
Table 4.3 Specification of MMO titanium mesh.....	76
Table 4.4 Reference electrodes for measurement and calibration.....	78
Table 4.5 Geosense VW Strain Gauges Specifications	80
Table 4.6 Settings for SEM images.....	84
Table 5.1 Tests programme.....	92
Table 5.2 Compressive strength of mortar at 28 days	96
Table 5.3 Convert obtained strain to applied service stress for tendons.....	98
Table 5.4 Corrosion of tendon - test programme	100
Table 5.5 Maximum crack width at each stage of corrosion during accelerated corrosion process	106
Table 5.6 Characteristics of tendon corrosion.....	110
Table 5.7 IFM results	112
Table 5.8 Mass and diameter loss of Batch 1	118
Table 5.9 Mass and diameter loss of Batch 2	119

Table 5.10 Mass and diameter loss of Batch 3	120
Table 5.11 Mass and diameter loss of Batch 4	121
Table 5.12 Corrosion design criteria	122
Table 5.13 Variation in stress in the tendons during accelerated corrosion	123
Table 5.14 Residual service stress due to corrosion.....	128
Table 5.15 Residual service stress due to corrosion (Batch 2 & 3)	133
Table 5.16 Batch 4 galvanised tendons	135
Table 5.17 Residual service stress due to corrosion Batch 4	138
Table 6.1 Test programme.....	149
Table 6.2 ICCP Normal-protection	150
Table 6.3 Potential before applying ICCP-N (Rest Potential).....	163
Table 6.4 Timber mould contraction (microstrain).....	169
Table 6.5 Effect of ICCP-N on the applied service stress	170
Table 6.6 Residual service stress in the pre-corroded tendons under the effect of ICCP	174
Table 6.7 Tensile properties of the as-received tendons	175
Table 6.8 Mechanical properties of the tendons after applying CP-Normal Protection.....	179
Table 6.9 Summary of mechanical properties (Young's modulus, 0.2% Proof strength and Ultimate tensile strength).....	183
Table 6.10 Summary of mechanical properties (Elongation, Toughness and Ductility)	184
Table 7.1 Test Programme	204
Table 7.2 ICCP Overprotection	205
Table 7.3 Potential before applying ICCP-O (Rest Potential)	217
Table 7.4 The average timber mould contraction (strain).....	226
Table 7.5 Effect of ICCP-O on the applied service stress	227

Table 7.6 Residual service stress in the pre-corroded tendons under the effect of ICCP-O.....	231
Table 7.7 Mechanical properties of the tendons after applying ICCP-O	233
Table 7.8 Summary of mechanical properties (Young's modulus, 0.2% Proof strength and Ultimate tensile strength)	235
Table 7.9 Summary of mechanical properties (Elongation, Toughness and Ductility)	236
Table 7.10 Hydrogen investigation.....	242

1 Introduction and Thesis Outline

1.1 Introduction

In most environments concrete provides steel with a relatively high degree of protection against corrosion and, in turn, the steel is an excellent source of reinforcement for the concrete. The concrete produces a protective passivating film on the surface of the steel. This passive film is created by the high alkalinity of the concrete. Typically, the pH of the concrete is approximately 13 [1]. Concrete reinforced with steel is a durable construction product and should provide many years of maintenance-free use if properly designed and constructed. However, there are a significant number of cases where problems have occurred due to the corrosion of the steel reinforcement in the structures due to poor design and workmanship and as a result of exposure to aggressive environments, for example, motorway bridges, car parks and marine structures. Pre-stressed steel can also corrode in a similar way to conventional reinforced concrete.

Cathodic Protection (CP) has been successfully used to mitigate corrosion by providing protection to buried and submerged metallic structures for almost two hundred years [2]. More recently, the method has been successfully applied to reinforced concrete. However, there is some concern about applying CP on pre-stressed tendons due to the risk of hydrogen embrittlement which may lead to premature rupture.

Due to the compression of concrete in pre-stressed concrete structures, cracking is better controlled as well as allowing a reduction of the cross-sectional area of a member, thus offering an extended range of options for many types of structures including bridges and buildings. Pre-stressed concrete tanks are used in water treatment and distribution systems, waste water collection and treatment systems and storm water management. Other applications include liquefied natural gas (LNG) containment structures and bunds, large industrial process tanks and bulk storage tanks (Figure 1.1)



Figure 1.1 Some of the applications of pre-stress concrete structures

A particular type of structure which will benefit from the research are bund walls. These provide secondary containment in the event of a rupture of holding tanks (Figure 1.2). These are constructed using the 'Preload' system, where high tensile tendons are wound under tension around the walls to provide support to the structure. The tendons are then sprayed with gunite to provide a durable, smooth finish.



Figure 1.2 LNG bund wall

The bund walls can be up to 20m high and 60m-70m in diameter. Circumferential bands are equispaced throughout its height and recessed some 80 mm into the outer face of a 500 mm thick wall. Each band can be 500 mm deep in elevation and, depending on its position, can contain between 240 and 380 small diameter galvanized steel wires each stressed to 1.5 metric tonnes [3].

The basis of the Preload system of design and construction of pre-stressed concrete circular structures is the Preload stressing machine or wire winder, developed around 1943 for the purpose of applying large quantities of stressed high tensile steel wire to circular structures in a rapid and efficient manner (Figure 1.3).

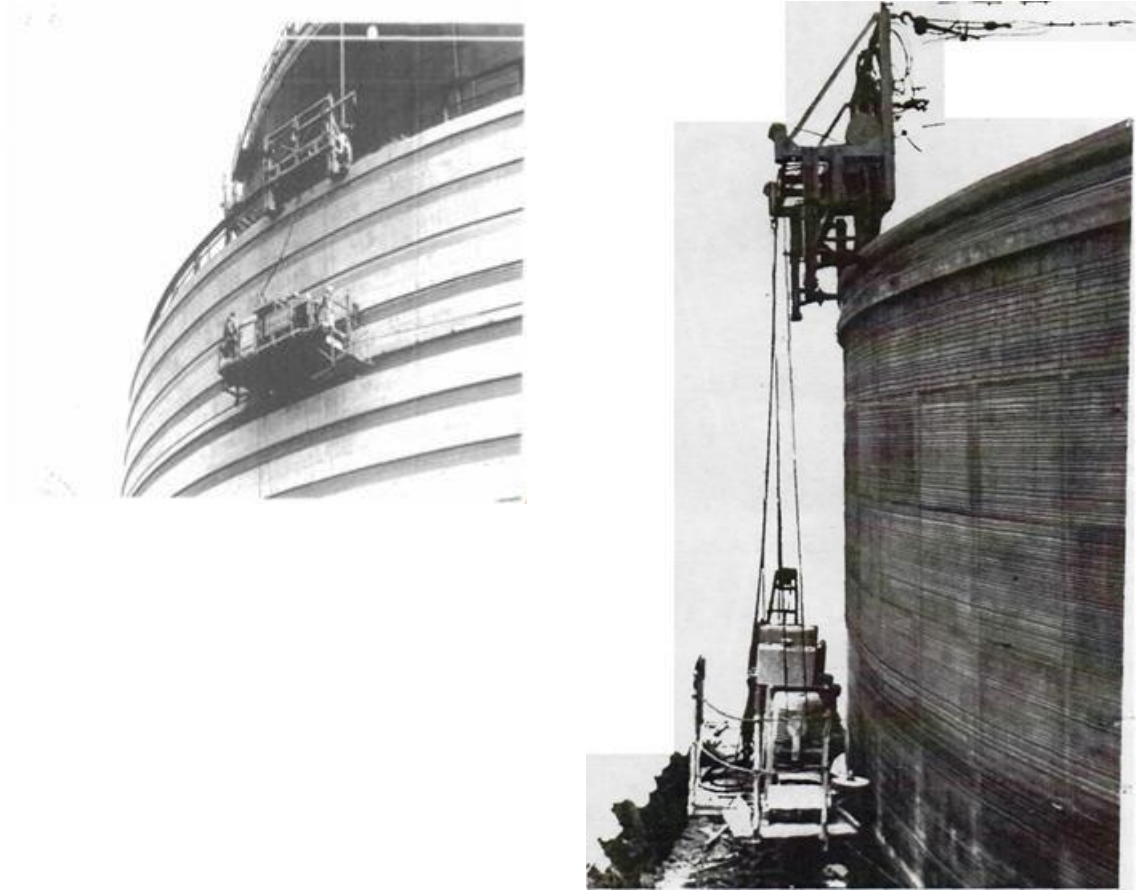


Figure 1.3 Preload system of bund wall

The United Kingdom, along with many other nations, is now facing growing concerns with regard to the safety of these structures. Corrosion of the wire tendons has become an issue (Figure 1.4) and an assessment of their residual strength, in addition to proposing new methods for strengthening and increasing their service life, is required.

Cathodic protection of steel in concrete is a well-established and proven technique. It mitigates the steel corrosion process, eliminating the danger of further cracking and spalling and enabling the structure to reach its full design life. CP has been successfully employed on both new and existing reinforced concrete currently suffering, or at future risk, of steel corrosion. In many cases, CP provides the most practical and cost effective medium to long term solution to deal with the corrosion problem [4]. In this research, the key to a successful outcome is to ensure that the Impressed Current Cathodic Protection (ICCP) operates in a manner which reduces the risk of hydrogen embrittlement for certain sensitive grades (where the ultimate tensile strength is high with grade

270 and tensile strength about 1800MPa [5]) of pre-stressed steel under tension.



Figure 1.4 Corrosion on preloaded tendon in a bund Wall

1.2 Aims of the research

This research study will develop a better understanding of applying ICCP to pre-stressed concrete structures by monitoring an extended application of ICCP with the aim of optimising the design criteria to avoid further damage to the tendons. Previous researchers have stated their concerns about applying ICCP on pre-stressed concrete structures due to the potential risks of hydrogen embrittlement. However, there is no clear evidence that ICCP causes failure of pre-stressed concrete structures. In addition, the contribution of this research is to determine where ICCP can be safely applied to pre-stressed concrete structures which will significantly aid their management to ensure they can remain in-service and increasing their service life.

1.3 Scope of study

In order to fulfil the aims of the research, a carefully designed scope of work has been adopted and is as follows:

- Develop a pre-stressing mould to enable different tensioning stresses to be applied to the tendons in the laboratory
- Select suitable strain measuring techniques for monitoring strains in the pre-stressing system throughout the test process

- Develop an experimental plan to include test variables such as the degree of corrosion, levels of pre-stress in the tendon, type of steel (galvanised/ungalvanised) and different CP potentials
- Apply an accelerated corrosion technique to induce corrosion in the tendon and monitor strain throughout
- Apply CP to the tendons as required by the experimental plan and monitor strains
- Investigate the effect of applied impressed current cathodic protection (ICCP) with different potentials on ungalvanised and galvanised tendons

1.4 Thesis outline

This thesis is divided into eight chapters, including this introductory Chapter 1.

Chapter 2 presents a detailed literature review of the corrosion of reinforcement and pre-stressing steel in concrete and associated repair techniques. It includes the principles, process, causes and influence of corrosion on the steel in concrete structures. It also discusses the repair techniques available to treat the corroded reinforcement and, in particular, the application of cathodic protection.

Chapter 3 introduces the preliminary experimental works, including materials, test equipment and laboratory work to confirm that the pre-stressing technique and strain monitoring in the tendons has worked successfully. It is also necessary to validate the accelerated corrosion method and employ ICCP in such a manner that a range of potentials can be applied to the tendons.

Chapter 4 provides a detailed experimental programme, appropriate to study the behaviour of pre-stressed tendons under the effects of applied ICCP, both normal and overprotection, with different levels of service pre-stress. It includes details of the materials used and the experimental procedures and techniques.

Chapter 5 investigates the effect of accelerated corrosion on the pre-stressed tendons. A total 12 timber moulds were manufactured to act as a pre-stressing rig with dimensions 200mm x 95mm x 675mm. The cast mortar samples, representing gunite, measured 100mm x 90mm x 320mm. Samples of Batch 1 to 4 were subjected to corrosion with three different degrees, Stage I (0-1 %), Stage II (2-4 %) and Stage III (4-7 %). During generation of the corrosion, the

loss of stresses were monitored. After applying the different pre-degrees of corrosion, the weight loss and diameter loss of exposed tendons were determined.

Chapter 6 describes the application of ICCP with normal protection (-650mV to -750mV, ICCP-N). The losses of applied service stress during the application of ICCP-N were calculated. The potentials and potential decays of tendons were also recorded. The results were assessed with respect to loss of applied stress, mechanical properties, embrittlement ratios and fracture modes using different assessment techniques. The potential decays of the steel met recognised ICCP standards.

Chapter 7 describes the application of ICCP with over protection (-800mV to -1300mV, ICCP-O). The losses of applied service stress during the application of ICCP-O were calculated. The potentials and potential decays of tendons were also recorded. The results were assessed with respect to loss of applied stress, mechanical properties, embrittlement ratios and fracture modes using different assessment techniques. Comparisons have been made between the application of ICCP-N and ICCP-O.

Chapter 8 provides a summary of the key conclusions for the thesis and recommendations for further research, followed by references and appendixes.

2 Literature Review

2.1 Introduction

The first documented wrapped high-strength wire in a continuous spiral on the exterior of cylindrical concrete tanks was in 1942. A similar design has been used in the construction of large liquefied natural gas (LNG) bund walls, and in years past, some were used for the storage of low-level radioactive materials [6]. Durability, however, has become an issue due to corrosion of the tendons. Similar issues have been reported for tanks belonging to water companies.

In general, corrosion is caused by the damaging attack of chloride ions penetrating by diffusion (and/or alternative penetration mechanisms) from the environment, by incorporation into the concrete mixture, by carbonation of the concrete cover, or their combination [7]. It is suggested that losses in the structural performance of concrete members with corroded reinforcement are caused by three factors, namely, reduction within the effective cross-sectional area of concrete due to cracking in the cover zone, losses in the mechanical performance of reinforcement due to the reduction in their cross-sectional area and losses in the bond of concrete with reinforcements [8].

2.2 Pre-stressed concrete principles

Pre-stressed concrete is a particular form of reinforced concrete. Pre-stressing involves the application of an initial compressive load on a structure to reduce or eliminate the internal tensile forces and, thereby, control or eliminate cracking. The initial compressive load is imposed and sustained by highly tensioned steel reinforcement reacting on the concrete. With cracking reduced or eliminated, a pre-stressed section is considerably stiffer than the equivalent (usually cracked) reinforced section. Pre-stressing may also impose internal forces which are of opposite sign to the external loads and may therefore significantly reduce or even eliminate deflection. The use of high-strength steel is, therefore, not only an advantage to pre-stressed concrete, it is a necessity. Pre-stressing results in lighter members, longer spans, and an increase in the economical range of application of reinforced concrete. [9].

Pre-stressing steel, used for pre-tensioned (tensioning the steel before casting the concrete) or post-tensioned (tensioning the steel after casting and hardening the concrete) structures, can be in the form of wires, strands, or bars. The main requirement for these products is a high value of the yield strength (Figure 2.1) [10]. The strength of pre-stressing steel may vary according to the production technology, the metallurgical composition, and the geometry.

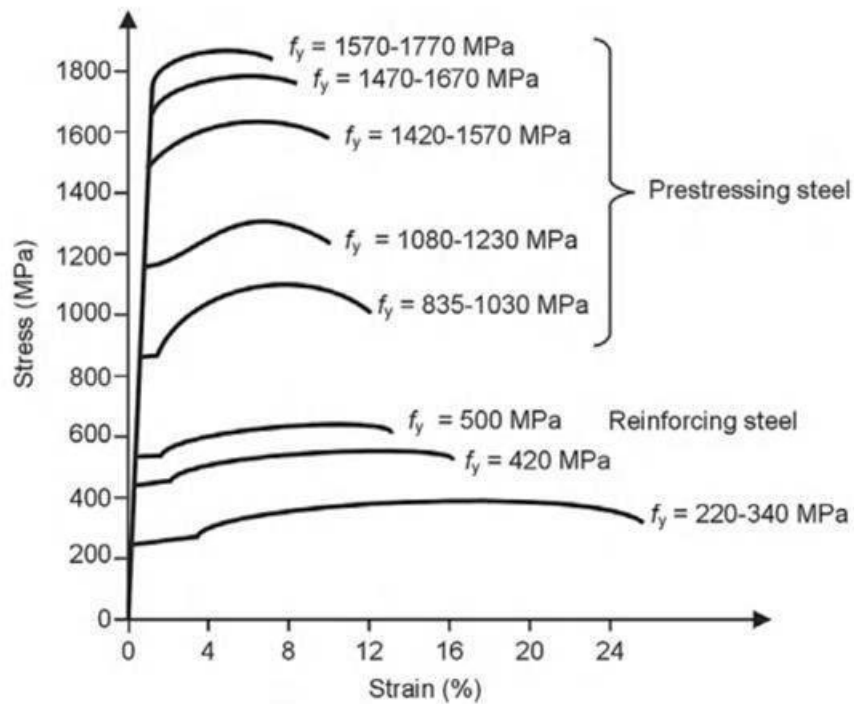


Figure 2.1 Examples of stress-strain curves for reinforcing and pre-stressing steels [10]

Compared to reinforcing steel, much higher strength levels must be obtained, and thus higher levels of carbon are used. In order to obtain high yield strength values, tendons can be cold worked, hot rolled, or quenched and tempered (Table 2.1) [10].

The following sections investigate the various deterioration mechanisms which influence the performance of steel in concrete, irrespective of whether it is conventional reinforcing steel or pre-stressed steel.

Table 2.1 Different types of pre-stressing steel [10]

<i>Type</i>	<i>Shape, surface</i>	<i>Diameter (mm)</i>	<i>Anchorage System</i>	<i>Strength Class (MPa)</i>	<i>Production (tonne/year)</i>
Cold deformed	Round-smooth	4-12.2	Wedge or button heads	1570-1860*	1,000,000
Wire	Round-profiled	5-5.5			
Strand	Round-smooth (7wires)	9.3-15.5		1700-2060*	
Hot rolled	Round-smooth	26-36		1030-1230	50,000 (Germany, UK)
Bar	Round-ribbed	26.5-36			
Quenched and tempered wire	Round-smooth	6-14		1570	5,000 (Germany, UK)
	Round-ribbed	5-14			
	Oval-ribbed	40-120			

* In Germany max. 1770MPa.

2.3 Deterioration of reinforced concrete structure

The concrete rarely deteriorates due to one isolated cause, and concrete can suffer from various mechanisms of deterioration [11]. Environmental species such as chloride salts, oxygen, moisture or carbon dioxide can penetrate the concrete cover and can eventually lead to corrosion of embedded steel reinforcement. As the steel corrodes, apart from the resulting loss in its cross-sectional area, the corrosion products expand in volume causing cracking, rust staining and spalling of the concrete cover zone [12]. Reinforced concrete is usually durable and cost effective, which has resulted in its widespread use for the construction. However, it has become increasingly apparent that attack by aggressive agents such as chloride ions, leading to corrosion of embedded steel, may cause a structure to deteriorate prematurely. The corrosion of reinforcing steel due to chloride transport in concrete structures in marine environments has received increasing attention in recent years because of its widespread occurrence and the high cost of repair [13].

The detrimental role that corrosion of embedded steel rebars plays in the service life of reinforced concrete is well documented, costing the United Kingdom an estimated £550m per annum. The problem is also widespread overseas, i.e. it has been reported that corrosion costs in the United States alone are estimated to be close to \$300 billion a year, or approximately 3.2% of the United States gross domestic product [14]. The US Federal Highway Administration published a report in 2001 that stated the estimated cost of corrosion of highway bridges was between \$6.43 and \$10.15 billion. This problem drains resources in both the public and private sectors. Implementation of solutions is needed, both in the design of structures resistant to corrosion and the rehabilitation of structures suffering the effects of corrosion.

2.3.1 Deterioration stages

The majority of reinforced concrete performs satisfactory if designed, constructed and maintained correctly. They may only suffer from minor issues throughout their lifespan. A minority of structures do, however, suffer more serious durability issues as a result of a combination of environmental, design and construction [15].

The state of corrosion of steel in concrete may be expected to change as a function of time. Corrosion process has three distinct stages, namely depassivation, propagation and final state as shown in Figure 2.2 [16]. Depassivation is the loss of oxide (passive) layer over the rebar, which is initially formed due to the high alkalinity of concrete. The process of depassivation takes an initiation period, t_p , which is the time from construction to the time of initiation of corrosion (depassivation).

The propagation phase starts from the time of depassivation, t_p , to the final state, is reached at a critical time, t_{cr} , at which corrosion would produce spalling of concrete cover or cracking through the whole of concrete cover. During the propagation period, i.e. corrosion period, t_{cor} , which begins at the moment of depassivation, the rebar corrosion is usually assumed to be in a steady state, as indicated by a straight line in Figure 2.2. The critical time, t_{cr} , as defined above can be expressed as [16]:

$$t_{cr} = t_p + t_{cor} \quad (2.1)$$

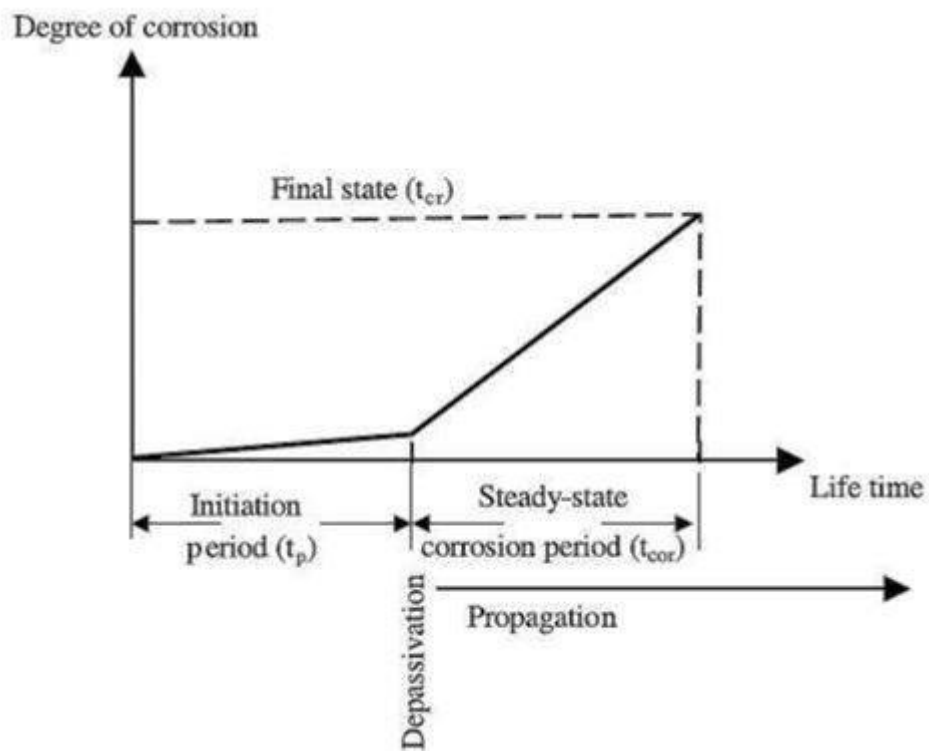


Figure 2.2 The stages of corrosion of steel in concrete [16]

2.3.2 Factors influencing rates of deterioration

Concrete provides a highly alkaline environment (generally $\text{pH} > 13$) [17], created by the hydroxides of sodium, potassium and calcium released during the various hydration reactions. In addition, the concrete acts as a physical obstacle to most of the substances which will cause degradation of the reinforcement. The steel remains passive and any small breaks in the stable protective oxide film are soon repaired. However, if the alkalinity of the concrete surrounding the reinforcement is reduced, for example by reaction with atmospheric carbon dioxide (carbonation), or if de-passivating chloride ions are made available at the surface of the steel then corrosion may occur. As a result of corrosion initiation, the loss of steel section and spalling of cover occurs. The rate of deterioration can be affected by the depth of the concrete cover, if the depth is inadequate the concrete can be exposed to high corrosion risk. Cracked cover due to large shrinkage and movement cracks can be direct consequences of corrosion. Presence of chloride ions can be another vital factor causing corrosion of reinforcement. Chloride can be induced to the concrete either during the mixing of concrete or after casting the concrete from an external source like sea water. When chloride ions have reached the reinforcement in adequate amounts, they break down the oxide layer that is normally maintained by the alkaline environment and protects the steel. Carbon dioxide present in the atmosphere combines with moisture in the concrete to form carbonic acid. This reacts with the calcium hydroxide and other alkaline hydroxides in the pore water resulting in a reduction in the alkalinity of the concrete [15].

Corrosion of embedded reinforcement is the most common cause of deterioration of reinforced concrete (RC) structures and a major economic cost for maintenance of national infrastructures. This will affect the residual capacity of the RC structures and, therefore, is of concern to those who are in charge of ensuring safe operation of concrete structures [18].

There is a large amount of literature on the corrosion of reinforcement which is mainly focused on corrosion induced cover cracking, corrosion prevention and repair of corrosion damaged structures. In the recent years, researchers have studied the effect of corrosion on residual capacity and mechanical properties of reinforcing bars. In most previous studies researchers have used accelerated

corrosion techniques on embedded steel in concrete to generate the corrosion procedure in the laboratory environment as well as taking reinforcing bar samples from corroded bridges. A key aspect that almost all these researchers agree on is that the corrosion does not change the fundamental mechanical properties of reinforcing steel such as modulus of elasticity; however, non-symmetrical pitting corrosion along the bar can change the load-extension response of reinforcement in a tension test [18].

The basic problem associated with the deterioration of reinforced concrete due to corrosion is not that the reinforcing itself is reduced in mechanical strength, rather that the products of corrosion exert stresses inside the concrete that cannot be supported by the limited plastic deformation of the concrete, and therefore the concrete cracks. This leads to a weakening of the bond and anchorage between concrete and reinforcement which directly affects the serviceability and ultimate strength of concrete elements within a structure [19]. Degradation processes and causes of deterioration of reinforced concrete can be classified and summarized in Figure 2.3 [10].

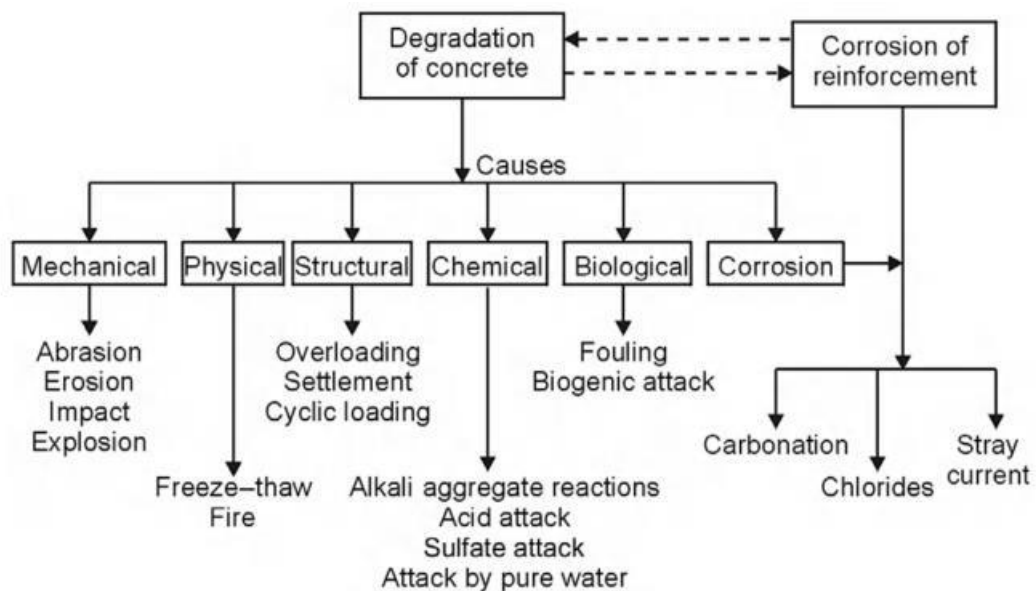


Figure 2.3 Causes of deterioration of reinforced concrete structures [10]

2.4 Corrosion mechanisms

2.4.1 Definition of corrosion

ASTM terminology (G 15) defines corrosion as “the chemical or electrochemical reaction between a material, usually a metal, and its environment that produces a deterioration of the material and its properties.” For steel embedded in concrete, corrosion results in the formation of rust which has at least two to four times the volume of the original steel and none of its beneficial mechanical properties. Corrosion can also produce pits or holes on the surface of reinforcing steel, reducing strength capacity as a result of the reduced cross-sectional area [20].

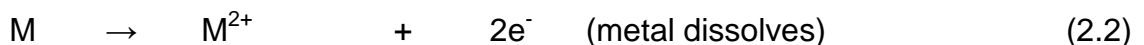
Corrosion, typically defined as the deterioration of metals through the combined actions of oxygen, other metals, and salts, has a major impact on industrial economies. But despite the damage it does, and the seriousness of the issue in economic terms, awareness of ways corrosion can be controlled is often less well understood [21].

2.4.2 Principle of corrosion

In its simplest form, the corrosion process can be described by two metals in an electrolyte, joined by a conductive metal path to permit electrons to pass from anode to cathode.

In reality, when a metal corrodes, anodic and cathodic areas can be formed on a single surface in contact with the aggressive aqueous environment. As a result, corrosion can occur at a large number of sites over the surface of the metal. The reactions occurring at the anodic and cathodic sites can be represented as follows:

Anode:

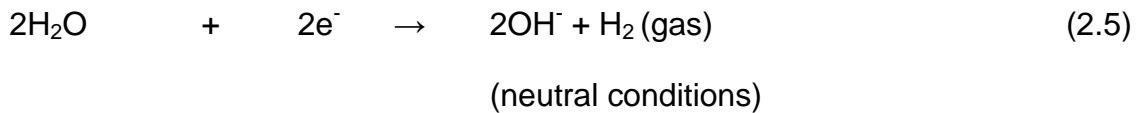
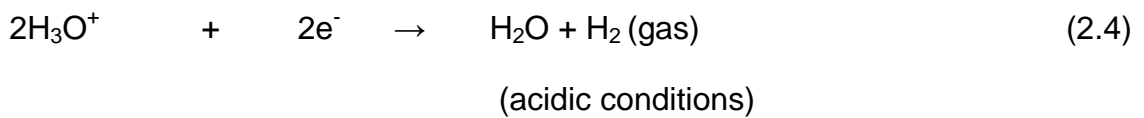


Cathode:

In well aerated neutral and alkaline environments, (2.3)



In some cases especially in acidic conditions, or in the absence of oxygen, the following reactions can occur:



Dissolved metal ions react with hydroxyl ions to form corrosion products. Production of hydrogen at the cathode can lead to failure in some materials, e.g. high strength low alloy steels, due to hydrogen embrittlement in areas that are stressed [22].

2.5 Forms of corrosion

Corrosion can be categorized in several ways. These can be due to the nature of the appearance of the damage, mechanism of attack, nature of the application and preventive methods [23]. One of the earliest classification of corrosion was by Fontana [24]. He categorized corrosion into eight forms. More recently, others [23], [25] have categorized corrosion into thirteen forms. However, for the purpose of this study it is sufficient to categorise corrosion as either general or localised, as discussed below. Table 2.2 describes examples of corrosion of steel in concrete [22].

Table 2.2 Examples of corrosion of steel in concrete [22]

<i>Forms of corrosion</i>	<i>Description</i>
General	Carbonation induced corrosion and spalling
Pitting	Chloride ion induced localised corrosion due to de-icing salts
Crevice	Under-film corrosion of organically coated reinforcement
Bimetallic	Interaction between dissimilar metals (e.g. conventional and stainless steel)

2.5.1 General Corrosion

This form of corrosion results in a uniform attack of the steel surface, often resulting in an 'orange peel' effect. The rate of penetration due to general corrosion is less than that of more localised forms of corrosion, such as pitting or crevice, though it often results in a greater degree of rust generation and staining. For most commonly available materials, 'typical' corrosion rates are readily obtainable and can be used to determine the expected life of the unprotected material in a specific environment where contamination of product or aesthetics are not an important consideration. Other than changing the specified materials, it is difficult to design against general corrosion. As a result, coating or cathodic protection (CP) techniques may have to be employed in order to prevent this form of corrosion [22].

General corrosion is also commonly referred to as uniform corrosion. It is defined as a chemical or electrochemical reaction that takes place along the entire or a large part of the surface of a metal that is exposed to a corrosive environment, resulting in the loss of metal and, potentially, eventual failure [24].

2.5.2 Localised corrosion

2.5.2.1 Pitting corrosion

Pitting corrosion is a form of localised corrosion and is defined as 'cavities or holes with the surface diameter about the same or smaller than the depth' [24]. These holes may be small or large in diameter, but they are usually small in most cases. Pitting is considered to be potentially more dangerous than uniform corrosion because it is more difficult to detect, predict, and design against. Pitting corrosion occurs when discrete areas of a material undergo rapid attack while most of the adjacent surface remains virtually unaffected [25].

2.5.2.2 Galvanic Corrosion or Bimetallic Corrosion

Galvanic corrosion takes place when dissimilar metallic materials are brought into contact with one another in the presence of an electrolyte. The potential difference between the two metals produces electron flow between them [24], [25].

2.6 Corrosion of steel in concrete

2.6.1 Introduction

Corrosion of steel in concrete was first reported in marine structures and chemical manufacturing plants [17]. Corrosion of steel reinforcement is a major problem influencing the long-term performance of reinforced concrete structures. Within the presence of chloride, the steel protective passive layer is locally destroyed and unprotected steel areas dissolve. The formation of corrosion products (rust) involves a considerable volume increase, i.e. the volume of corrosion products is greater than that of original steel bar. Therefore, expansive stresses are induced around corroded steel bars causing possible cracking, spalling of concrete cover and loss of bond between steel/concrete, and therefore reducing the serviceability of concrete structures [26].

Concrete, in general, provides protection to steel reinforcement because of two reasons, (a) concrete provides a highly alkaline environment to steel reinforcement which passivates the steel surface and, hence, prevents it from corrosion, and (b) concrete helps prevent the ingress of corrosion species, like oxygen, chloride ions, carbon dioxide and water, in low water-cement ratio concrete [27].

Once the alkaline environment is destroyed, the protective oxide layer on the steel surface is destroyed and corrosion initiates. The formation of protective oxide layers and their breakdown is shown in Figure 2.4. The protective oxide layers that developed are either Fe_2O_3 or Fe_3O_4 , both are stable in concrete. The most stable layer in concrete is Fe_2O_3 written as $\gamma\text{-FeOOH}$ that it is the hydrated form of Fe_2O_3 . [27].

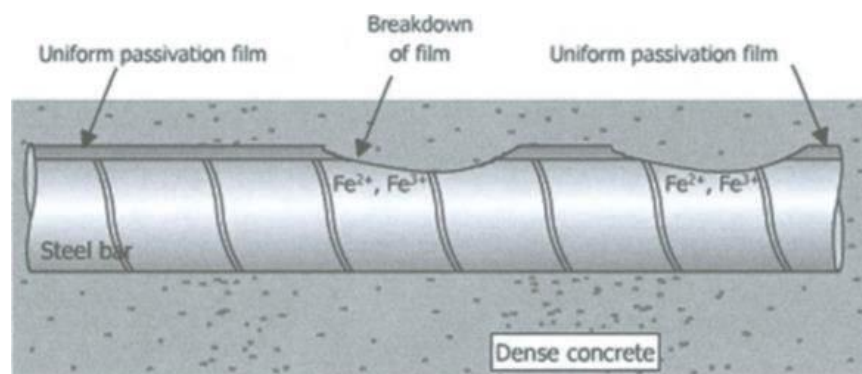


Figure 2.4 Breakdown of the protective passive film on a steel bar in concrete

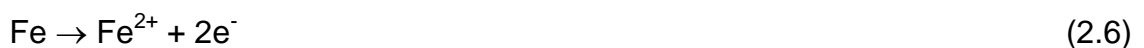
[27]

In the case of carbonation, the reinforcement is subject to general corrosion while chloride ions can initiate the pitting form of attack.

2.6.2 Corrosion process

The corrosion process of steel in concrete is a function of many variables such as the steel surface, concrete properties, and the environment in which the concrete is used [28]. It is a chemical reaction involving the transfer of charge (electrons) from one specie to another. For an electrochemical reaction to occur (in the absence of an external electrical source) there must be two half-cell reactions: one capable of producing electrons (the anodic reaction) and one capable of consuming electrons (the cathodic reaction) [29]. The surface of the corroding steel functions as a mixed electrode that is a composite of anodes and cathodes electrically connected through the body of steel itself, upon which coupled anodic and cathodic reactions take place. Concrete pore water functions as an aqueous medium, i.e., a complex electrolyte [16].

Under this condition and in the presence of oxygen and water, positively charged ferrous ions dissolve into the pore solution according to the anodic reaction [30]:



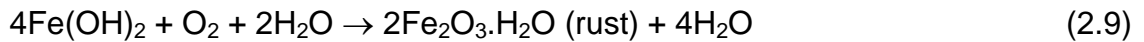
The electrons produced by this reaction are conducted through the steel to neighbouring regions where oxygen is reduced according to the cathodic reaction:



To complete the circuit of charge movement, hydroxide ions migrate from the cathode to the anode to produce ferrous hydroxide, $\text{Fe}(\text{OH})_2$ (2.8).



In the presence of further oxygen and moisture, Fe(OH)_2 is then converted to rust according to equations (2.9) .



These process are summarised in Figure 2.5. The anodic reaction represents the dissolution of the metal. The flux of ions and electrons respectively can be taken as a measure of the corrosion rate. This can be given as mass lost per unit of time and area, as a reduction of the thickness per unit of time or as current density (current per unit of area) [31].

Four conditions must exist for corrosion to occur:

- An anode (corroding) and a cathode (protected) component
- An electrical potential between the anode and the cathode
- The anode and cathode must be immersed in an electrolyte, which is an electrically conductive fluid
- The anode and cathode must be connected by a metal path of low resistance

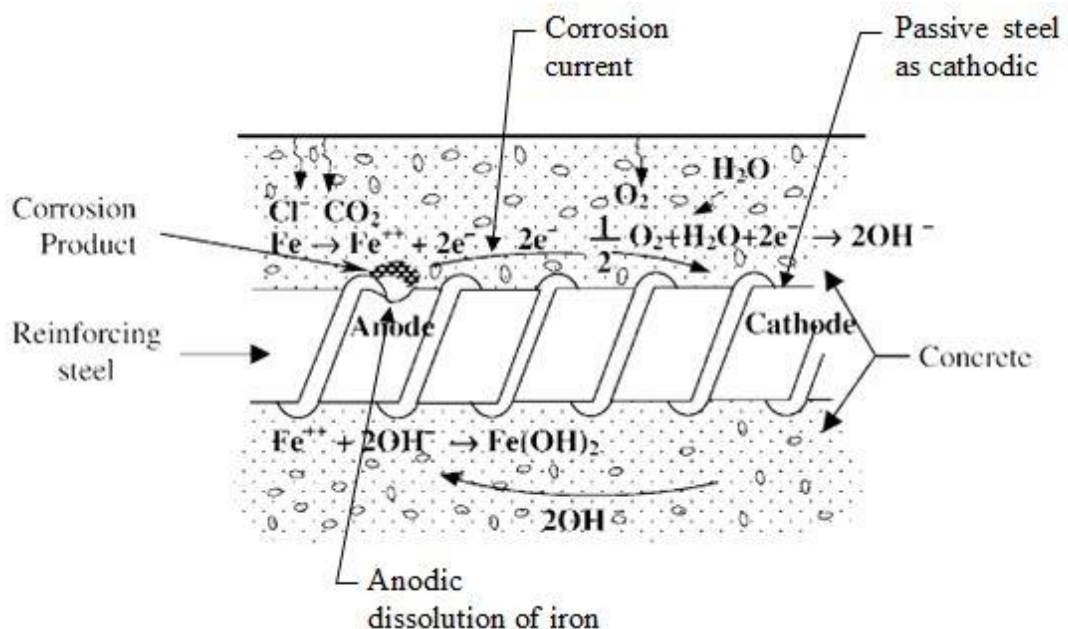


Figure 2.5 Schematic illustration of the corrosion of reinforcement steel in concrete [16], [29]

Based on Faraday's Law, the magnitude of the corrosion current is a direct measure of the rate of corrosion of the steel. Thus, corrosion current (determined per unit area of reinforcement) of 1 A/m^2 is equivalent to an average oxidation or dissolution of 1.16 mm per year from the surface of the steel. Faraday's Law and its application are described in Section 3.5.1. As in any other electrical circuit, the corrosion current is limited by the resistance of the circuit. In this case, the important factor is the electrical resistance of the concrete.

While the electrical resistance of the concrete is one of the factors controlling how fast corrosion can occur (i.e. the reaction kinetics), the parameters determining whether or not corrosion is actually possible (the reaction thermodynamics) are the pH of the concrete pore solution and the electrochemical potential existing at the steel surface. One can determine theoretically whether or not the reactions are thermodynamically possible and values of E as a function of pH for which the above reactions are in equilibrium can easily be calculated and are available in graphical form as illustrated in Figure 2.6 [32].

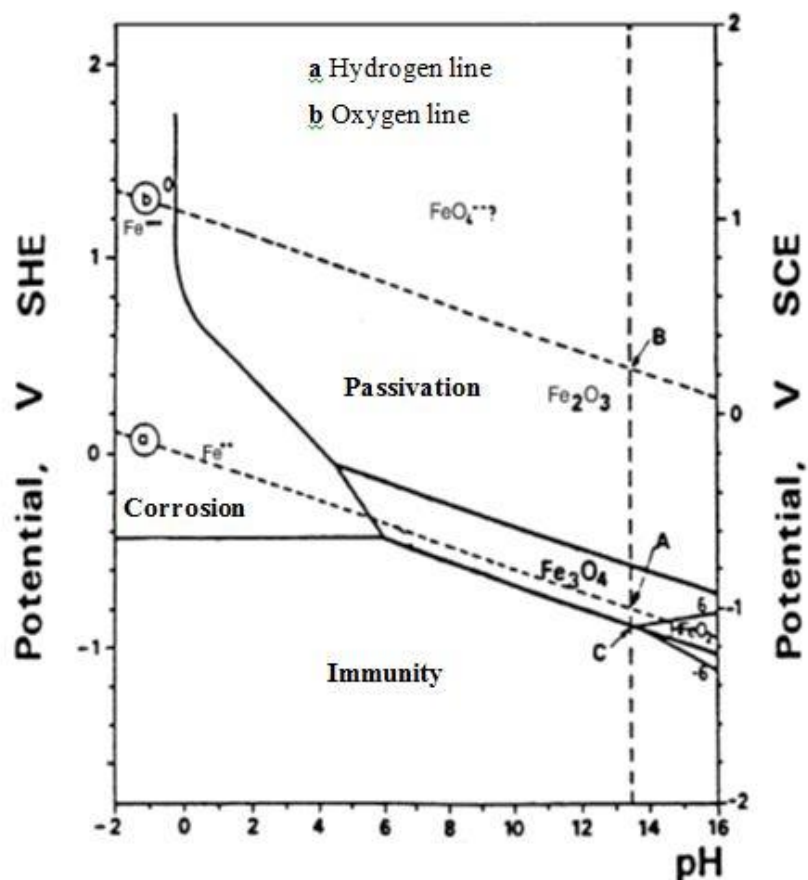


Figure 2.6 Potential-pH equilibrium diagram of iron in aqueous solutions [32]

From the diagram of the equilibrium phases of iron in aqueous solutions as a function of pH and electrochemical potential, at pH 13.5, iron is in equilibrium with Fe_3O_4 at $E = -1125 \text{ mV SCE}$ (saturated calomel electrode), equivalent to -881 mV SHE (standard hydrogen electrode), point "C" in Figure 2.6. At potentials lower than this, iron is the stable phase and, therefore, corrosion cannot occur. At higher values of the potential, Fe_3O_4 or Fe_2O_3 is the stable phase and corrosion (or oxidation) can occur. In theory, the more positive the potential, the higher will be the corrosion rate. However, at high pH (>9) in the presence of O_2 , the oxide forms a passive film on the surface of the iron. This film acts as a protective coating but is not completely protective. Thus, corrosion is not stopped but the rate of corrosion is reduced to an insignificant level. The second effect of this passive film is that there is no unique value of the corrosion potential. Its highest possible value is determined by the equilibrium potential of O_2 , the dashed line in Figure 2.6. In aerated concrete of pH 13.5, the highest potential of the steel would thus be $+175 \text{ mV SCE}$ (point "B" in Figure 2.6). The lowest potential at which the passive film has been experimentally found to be stable at this pH is -594 mV SCE . In practice, the steel can adopt any potential within this range and still be passivated depending on the O_2 concentration [29], [32].

2.6.3 Corrosion of pre-stressing steel in concrete

As far as corrosion behaviour is concerned, pre-stressing steel needs to be distinguished from reinforcing steel with regard to hydrogen embrittlement, since it only affects the former; this has been illustrated in the above sections. In noncarbonated and chloride-free concrete, the passivity of low-alloyed steels is not influenced appreciably by their composition, structure or surface conditions. Therefore, the usual thermal or mechanical treatments or the roughness of the surface of the rebars have negligible influence on their corrosion behaviour. Even the presence of magnetite scale that often covers the surface of the bars, which can cause dangerous localized attack on steel in contact with neutral solutions (such as fresh water or seawater), is not dangerous in concrete. In fact, noncarbonated and chloride-free concrete passivates all the surface of the steel. If adherent oxide films are present, they do not create problems. If the oxide layer contains chlorides, because for example, it is formed in a marine environment, it must be removed completely because it can hinder passivation.

Once the steel becomes active due to carbonation of concrete or chloride penetration, the influence of chemical composition, microstructure and surface finishing is still of secondary importance, because kinetic control of the corrosive process is of the ohmic type, or dependent on oxygen diffusion and thus on characteristics of the concrete (and in particular its moisture content) rather than on those of the metal. Nevertheless, it was shown that the susceptibility of steel to pitting corrosion in chloride-contaminated concrete may be slightly affected by the surface condition of the steel [10].

For many pre-stressed structures exposed to marine environment and de-icing salts, attack by chloride ion is the chief factor that causes corrosion of steel bars. Durability failures of pre-stressed structures caused by chloride contamination are happening continuously all over the world [33]. Offshore structures, piers, dams, docks or harbours are also attacked by chlorides from seawater especially in the tidal, splash and spray water zones [34]. Figure 2.7 and Figure 2.8 show the corrosion of pre-stressed steel wires.



Figure 2.7 (a) Corrosion of Pre-stressing Wires [35] (b) Corroded wires of a strand from a simulated tendon [36]



Figure 2.8 Severe corrosion and minimal rust staining on pre-stressing wires [37]

Forms of corrosion are discussed in Section 2.5, The most common types of corrosion that affect pre-stressing steels are uniform corrosion, localized or pitting corrosion and stress corrosion. Hydrogen embrittlement had for some time been considered as a separate type. However, now it is being considered as a variation of stress corrosion. Brittle fracture of pre-stressing steel by either stress corrosion or hydrogen embrittlement is especially dangerous and of grave concern to engineers and designers. Fretting corrosion is another type that is becoming of increasing concern. Other types of corrosion are crevice corrosion and stray current corrosion [33].

2.6.3.1 Stress corrosion cracking

Stress corrosion cracking (SCC) is a type of highly localized corrosion that produces cracking as a result of the simultaneous presence of corrosion and tensile stress. This phenomenon is of importance because it can occur at stresses within the range of design stresses. Although many mechanisms have been postulated, none completely explains the phenomenon of stress corrosion cracking. The process of corrosion produces a discontinuity on the surface of the metal (a pit), thus providing a stress raiser. Stress corrosion cracks have often been observed to originate at the base of a pit (Figure 2.9). Once a crack has started, there is a large stress concentration at the tip of the crack, with subsequent crack propagation. Cracks propagate either along grain boundaries (intergranular) or on slip planes within the crystal lattice (transgranular) (Figure 2.10). Eventually, these cracks can cause sufficient reduction in cross section to precipitate a brittle failure [33]. The chemical reactions of corrosion should be considered as described in Section 2.6.

Pitting corrosion of steel usually is readily recognised. Individual shallow pits, and in later stages, deep and sometimes connected pits can be seen with the eye. Pitting corrosion starts when the passive oxide film breaks down in a chloride-rich environment. Once the passive film is breached, an electrochemical cell becomes active. Iron goes into solution in the more anodic bottom of the pit, diffuses toward the top, and oxidizes to iron oxide. The concentration of the iron chloride solution in a pit can increase as the pit deepens. Pitting can penetrate deep into the steel, creating a situation where the steel could fail [38].



Figure 2.9 Pitted PT wires with (a) grout [Cl⁻] 0.80 wt% cement, pit depth 0.12 mm, and no physical grout deficiency and (b) grout [Cl⁻] 2.00 wt% cement, pit depth 0.46 mm and a grout void [36]

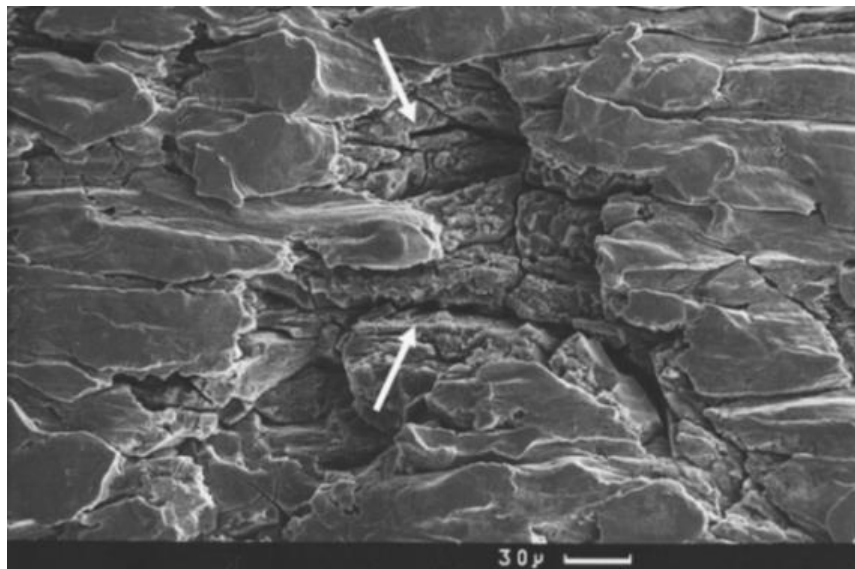


Figure 2.10 Stress corrosion cracking in a corrosion pit on steel [39]

In concrete structures, the medium is mostly alkaline and acid solutions are limited to exceptions. Nevertheless, in natural environments the pitting induced SCC can take place (Figure 2.11). In pre-stressed construction carbonation of concrete and mortar as well as chloride contamination are responsible for local corrosion attack.

Crevice corrosion and pitting corrosion are problems in practice and they are well documented in the literature [40]. Several methods have been used to measure the pitting potential, such as potentiostatic methods, potentiokinetic methods, galvanostatic methods, etc.[40], [41].

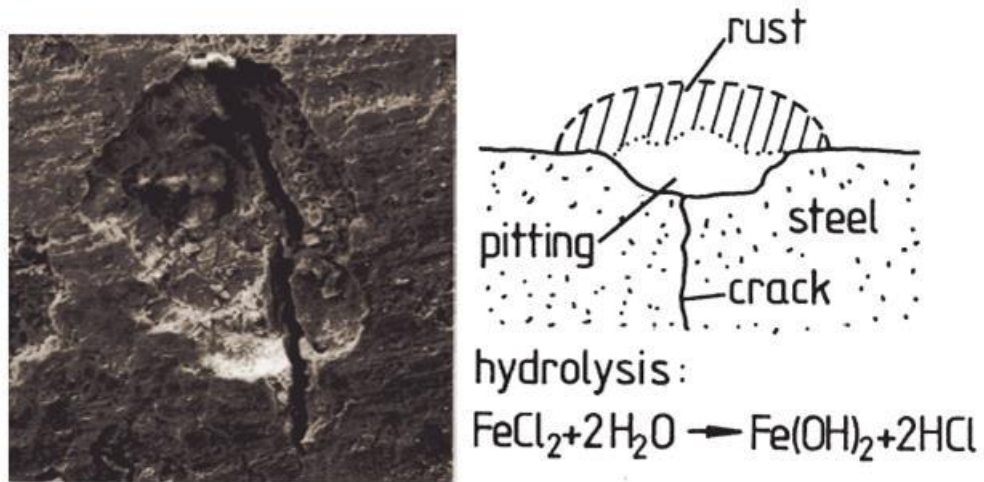


Figure 2.11 Pitting induced stress corrosion cracking [42]

Fracture of high-strength steel due to SCC normally takes place in three stages (Figure 2.12): (i) a first stage of incubation or crack initiation; (ii) a second stage of slow (subcritical) propagation of cracks; (iii) a third stage of fast propagation, which occurs when some critical conditions are reached and suddenly leads to failure [10]

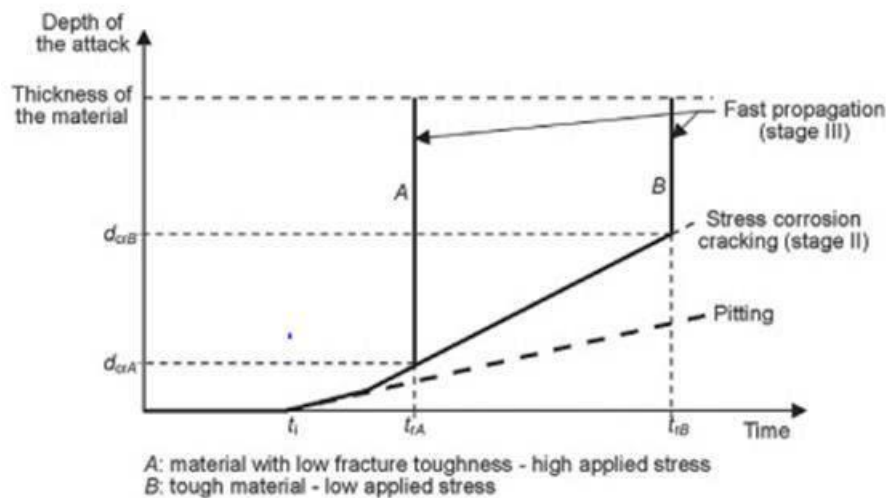


Figure 2.12 Sequence of phenomena that lead to the initiation and propagation of hydrogen induced cracks and subsequent failure in two materials (A and B) with different fracture toughness (d_{cr} = critical flaw size; t_i = incubation time, t_r = time of failure) [10]

The hydrogen affects the microstructure and the stability of passive films. It has been found that hydrogen increases the disorder of passive films, and consequently the pitting susceptibility. In addition, hydrogen-induced drop of

breakdown potential facilitates the initiation of pitting, and increases the pitting density and growth rate [43].

2.6.3.2 Hydrogen Embrittlement

Hydrogen embrittlement (HE) cracking of steel under stress occurs when atomic hydrogen penetrates into the metal structure, where it recombines to hydrogen molecules, producing an internal pressure in the metal. Absorption of atomic hydrogen by the pre-stressing steel usually occurs by cathodic charging, which happens in a corrosive environment when the steel is electrically coupled to a more anodic metal, for example, zinc coating. The atomic hydrogen may be formed by the corrosion process itself or as a result of some manufacturing operation, such as pickling. Cracking of the metal may be initiated as a result of the internal pressure developed by the hydrogen molecules causing tensile stress, or in combination with a critical external tensile stress. Atomic hydrogen may enter the metal over an extended period of time. Rupture due to hydrogen embrittlement has occurred several years after installation [33].



Figure 2.13 Brittle fracture of pre-stressing wire [37]

In sensitive steels the hydrogen under the effect of mechanical stresses can create pre-cracks in critical structural areas such as grain boundaries. These cracks may grow and result in material fracture. Special conditions have to exist to activate the formation of adsorbable hydrogen atoms [42]. SCC and the

subsequent failure of steel (Figure 2.13) and construction may occur if the protection is not guaranteed from the beginning as a result of poor workmanship, or it is lost because of deterioration of the construction in the course of the time, or the pre-stressing reinforcement is pre-damaged during handling. Also, an application of unsuitable materials for pre-stressing steel, injection mortar or concrete can alone or in combination with other factors favour SCC.

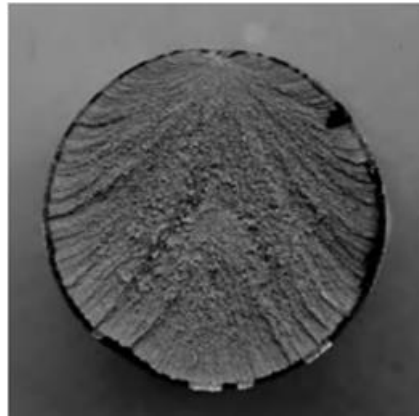


Figure 2.14 Fracture surface of a pre-stressing bar that failed due to hydrogen embrittlement [10]

The use of galvanized steel tendons in pre-stressing structures is normally restricted to the external application of non-adherent type. The reason for this limitation is the possibility of failure due to the risk of hydrogen embrittlement of the bare steel that can arise when loaded galvanized tendons or wires are in direct contact with high alkaline cement based materials. However, there is insufficient evidence to this restriction that claims for a deeper investigation [44]. For example, the pre-stressing steel in the bund walls highlighted in Chapter 1 was galvanised and this research project will investigate their performance with respect to hydrogen embrittlement. Figure 2.14 shows the fracture surface of a pre-stressing steel that failed due to hydrogen embrittlement.

Despite the major technical importance of hydrogen embrittlement, and the significant of research work on the subject, the mechanism of hydrogen embrittlement remains uncertain. In considering hydrogen embrittlement mechanisms, it is important to recognise the concentration of hydrogen in the steel, as matrix concentrations are very low, typically of the order of one atom of hydrogen for every 10^6 iron atoms. It can be difficult to understand how such

small amounts of hydrogen can modify fracture properties. Details of HE are given in ref. [45].

2.7 Cathodic Protection

2.7.1 Historical foundation of cathodic protection

Cathodic protection was first applied by Sir Humphry Davy in 1824 to reduce the corrosion of the copper sheathed hulls of warships by attaching anodes of a less noble metal than the copper itself [73]. After Davy's discovery, Faraday examined the corrosion of cast iron in sea water and found that it corrodes faster near the water surface than deeper down. In 1834 he discovered the quantitative connection between corrosion weight loss and electric current. With this discovery he laid the scientific foundation of electrolysis and cathodic protection. In the 1890s, one of the first practical applications of impressed current cathodic protection was made by Thomas Edison, when he developed a system to protect ship hulls. Impressed current CP was developed as a practical way of reducing corrosion with the invention of DC generators and efficient storage batteries allowing initial applications were to underground structures from around 1910 [46]. During the 1920s, steel pipelines in North America were treated with CP and its success led to its popularity and diversification of its application. In 1959, the use of ICCP in reinforced concrete was trialled by Richard Stratfull who applied ICCP to a bridge deck suffering from chloride-induced corrosion. Thereafter, its application in reinforced concrete became more widespread [47], [48]. This extended to buildings, tunnels, marine structures and substructures throughout the USA and Europe in the 1980s [49]. Existing damage to the concrete must be repaired before a CP system can be installed, though the extensiveness of repair is much less than what is required for repair-only cases [49].

2.7.2 Theoretical basis for cathodic protection

CP provides external electrons to the steel to be protected by introducing a new anode into the system. The steel becomes the cathode and further aggressive corrosion is prevented or reduced [50]. Cathodic protection is a unique technique of corrosion protection amongst all other methods as it mitigates corrosion and it is possible to stop corrosion completely. CP works on the basic principle where electrons are supplied from an external anode to the metal

intended for protection, transforming it into the cathode (negatively polarised). In other words, electrons from an external anode substitute for the electrons that would have otherwise been lost from the oxidation of the metal through the anodic reaction, thus preventing corrosion.

The mechanism of ICCP works on the application of an external direct current which polarizes the surface of the metal to be protected to the thermodynamic potential of the anode, i.e. the surface reaches equipotential with the anode. As a result, corrosion current is prevented from flowing, thus stopping the metal from corroding [51]. More detailed theoretical explanation of cathodic protection is given in [52].

2.7.3 Methods of Applying Cathodic Protection

There are essentially two methods of applying cathodic protection, namely the galvanic sacrificial anode cathodic protection (SACP) and the impressed current cathodic protection (ICCP) technique. Both systems have an anode, a continuous electrolyte between the anode to the element being protected and an external wire connection system. ICCP systems typically require a constant low direct current (DC) power supply to each independently controlled anodic zone [53]. This DC power source is normally from an electrical grid or generators for more remote locations, both of which are usually unsustainable sources of energy [54].

2.7.3.1 Galvanic or sacrificial anode cathodic protection

The sacrificial anode technique uses the natural potential difference that exists between the structure and a second metal in the same environment to provide the driving voltage. No power source is employed. Moreover, the dissolution of the second metal, that is, the sacrificial anode, provides the source of electrons for cathodic polarization of the structure. Thus, while the impressed-current anode may be more noble or more base than the protected structure because the power source forces it to act as an anode, the sacrificial anode must be spontaneously anodic to the structure, that is, be more negative in the galvanic series for the given environment. Thus, in principle, zinc, aluminum, or magnesium could be used to protect steel, and iron to protect copper. Figure 8 illustrates the use of a sacrificial anode for cathodic protection [52]. Compared to ICCP, galvanic systems have the advantage of being independent to external

electric power and are less liable to cause interaction on adjacent structures [65]. However, the SACP anode lifespan tends to be shorter than ICCP, as the material is eaten-away. While a low driving voltage may be undesirable for most reinforced concrete structures, it is a safer choice for pre-stressed structures. As low resistivity is a requirement for effective galvanic protection [67], the main limitation of this type of cathodic protection for use with reinforcement is the relatively high resistance of the cover concrete. SACP systems provide a low current, limiting its effectiveness in high resistance environments. These systems are often used on oil platforms for both concrete and steel structures below water [67].

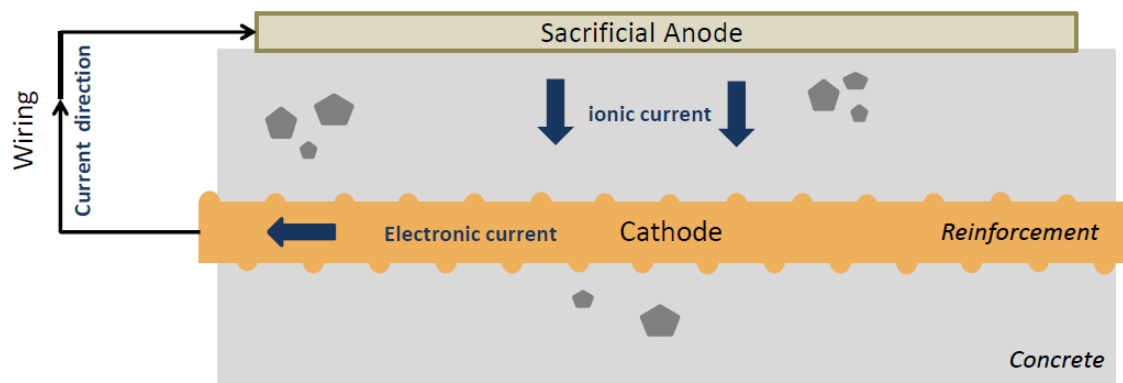


Figure 2.15 Schematic diagram of cathodic protection using sacrificial anodes [55]

2.7.3.2 Impressed current cathodic protection

Impressed current systems are the most commonly used for reinforced concrete [53], [56]–[62]. ICCP is used where electrolyte resistivity is high and galvanic anodes cannot economically deliver enough current to provide protection. Figure 2.16 illustrates the use of an external power supply to provide the cathodic polarization of the structure. The circuit comprises the power source, an auxiliary or impressed current electrode, the corrosive solution, and the structure to be protected. The power source drives a positive current from the impressed current electrode through the corrosive solution and onto the structure. The structure is thereby cathodically polarized (its potential is lowered), and the positive current returns through the circuit to the power supply. Thus, to achieve cathodic protection, the impressed current electrode

and the structure must be in both electrolytic and electronic contact. The power supply is usually a transformer/rectifier that converts AC power to DC [52].

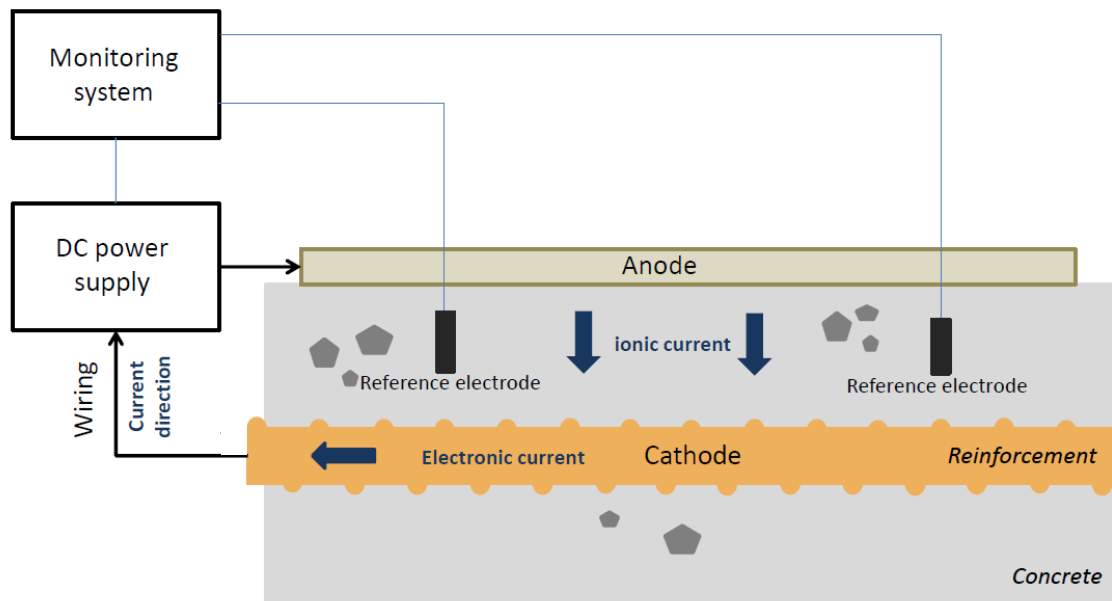


Figure 2.16 Schematic diagram of cathodic protection using the impressed-current technique [55]

Impressed current installations are able to supply a relatively large current, providing high DC driving voltages which, unlike SACP, allow them to be used in most types of electrolytes. Also unlike SACP, Impressed current systems can provide a flexible current output that can accommodate changes in the structure being protected [63]. ICCP is employed widely in the repair of reinforced concrete structures suffering from corrosion but it has only rarely been considered for pre-stressed concrete structures. This is for two reasons. The first is that in general pre-stressed construction is not as conventional reinforced concrete and is consequently in a better condition. This, however, will not be the case permanently. There are pre-stressed concrete elements that are beginning to show evidence of corrosion, spalling and delamination [35]. The second concern is with regards to the risk of hydrogen embrittlement which can result in brittle failure of a tendon [64], [65]. The steel becomes brittle due to the absorption of hydrogen so inducing stress corrosion cracking and leading to premature failure of the steel. This effect occurs on high strength stressed steel tendons such as pre-stressed or post-tensioned tendons.

2.7.4 Anode selection

Anodes for SACP systems are made from less noble material than the steel being protected and are consumed preferentially to create the cathodic protection current [66]. Typical materials used are zinc, aluminium or magnesium. These metals are often alloyed to improve the long-term performance and dissolution characteristics, for example Aluminium-Zinc-Indium. Zinc and its alloys are the most commonly used for reinforcement in concrete structures [67]. The main drawback is “passivation” of zinc in this environment which creates an oxide layer on the surface that changes its potential. Therefore, zinc alloys may be used instead to reduce the formation of this layer. For reinforced structures sacrificial anodes can be a zinc mesh and overlay, or a zinc sheet attached to the concrete using a conductive gel or flame sprayed zinc [49]. Aluminium and magnesium and their alloys are used less regularly as their oxides and corrosion products can attack the concrete [67]. However, examples exist where they have been used successfully [68]. Examples of anodes used for ICCP include magnetite, carbonaceous materials (graphite), high silicon iron, lead/lead oxide, lead alloys and platinised materials such as titanium [69] which can provide relatively large protection currents without compromising durability [49].

The most common and reliable ICCP anode is the activated titanium expanded mesh with a surface coating of mixed metal oxides and covered with a cementitious overlay [49]. The mixed metal oxide coating acts as the anode while the titanium provides a stable base material [70]. Titanium conductors are spot welded at regular intervals to facilitate the connection to the current source [80]. Although titanium mesh/overlay systems are costly and heavy, they are robust with a life expectancy of over 25 years [49]. This type has a high tolerance for external moisture so surface preparation is very important to ensure good cover provided.

2.7.5 Electrolysis

As a result of the electrical potential difference between the anode and the cathode, water is reduced to hydroxide ions at the reinforcement. After the available oxygen has been consumed according to reaction (2.7), the cathodic reaction produces hydroxide and hydrogen gas. At the external anode, water or hydroxide is oxidised to oxygen and hydrogen ions respectively. These

reactions are referred to as electrolysis, which results in a pH increase at the reinforcement, and this is the most important process for realkalisation [71].

The rate of oxygen reduction is determined by the rate of diffusion of oxygen in concrete whereas the water reduction reaction is controlled by the kinetics of the charge transfer process [72]. The reactions lead to an increase in alkalinity at the cathode, restoring and maintaining steel passivation.

The primary anodic reaction for sacrificial anodes is spontaneous and involves ionisation of the metal. In neutral or alkaline solutions the metal cation will be unstable and become hydrolysed. Anodic reactions for impressed current systems are widely held to be the generation of oxygen, water and chlorine gas with the overall effect of lowering the local pH. In neutral solutions oxygen is evolved and in alkaline solutions, water also evolved as follows:



Chlorine evolution is possible at inert electrodes at relatively small concentrations of chloride ions [73]:



The anode material directly influences the reactions occurring and these are likely to change with time as the environment adjacent to the anode varies. This may be due to reaction products inculcating secondary reactions or due to external factors such as variation in temperature and moisture. Concrete in contact with the anode may become dehydrated as water is consumed and calcium silicates and aluminates may become unstable in the less alkaline conditions, resulting in a deterioration of the anode/concrete interface. In addition, corrosion of the anode material may occur due to the development of an aggressive operating environment. These factors have often been ignored by other workers when considering the long term durability of CP systems. Accelerated and long-term testing of CP systems has confirmed that production of some anodic products leads to acidification at anode/concrete interfaces with subsequent local modifications to cement paste [74], [75].

2.7.6 Design criteria for CP

The main effect of applying cathodic protection is to polarise the steel, i.e. drive the potential of the steel to more negative values. Consequently, measurement of this change is the most common method used to determine the effectiveness of cathodic protection. The secondary effects of cathodic protection include repelling chloride ions from the steel surface and increasing the pH local to the steel. These factors result in a reduction in the corrosive conditions and hence a reduction in the corrosion rate and can be used in assessing the effectiveness of cathodic protection. As indicated in Section 2.6.3.2, one aspect of cathodic protection applied to pre-stressed concrete structures is the risk of hydrogen embrittlement. High-strength steel (used in pre-stressing) can be susceptible to hydrogen embrittlement; however, the overall risk is also dependent on the levels of tensile stress in the component, the environment (in particular pH) and the degree of polarisation of the steel (i.e. potential). It is worth noting that the absolute protection potential for steel in concrete is rarely achieved and so it could be considered that the risk of reaching the hydrogen evolution potential is low. NACE State-of-the-art gives report (01102 Criteria for Cathodic Protection of Pre-stressed Concrete Structures [76]) guidance on how to assess the susceptibility of the pre-stressing systems of a particular structure to the risk of hydrogen embrittlement [48].

It is recommended that commissioning of CP systems should start at a low level of current density for the initial part of the commissioning period to avoid any adverse effects on the anode durability. Intermediate tests can be then carried out, typically 14 days after energising, to determine what adjustments are needed to satisfy the operating criteria. The international standard for cathodic protection of steel in concrete, item 8.6 (BS EN ISO 12696:2016) [77] states: for any structure, any representative steel in concrete location shall meet any one of the following criteria :

- An “Instantaneous (or Instant) OFF” potential more negative than -720 mV with respect to Ag/AgCl/0,5 M KCl; or
- A potential decay over a maximum of 24h of at least 100mV from "Instantaneous OFF"; or
- A potential decay over an extended period (typically 24 h or longer) of at least 150 mV from the instant off subject to a continuing decay and the

use of reference electrodes (not potential decay probes) for the measurement extended beyond 24 h.

The decay is independent of the nature of the reference electrode used or any variation in its absolute potential in the long term. Historically it has been common to use a decay period of 4 hours although it should be noted that other intervals (such as 24 hours) might be suitable depending on the nature of the structure and surrounding environment. When current is applied to the anode system there will be an associated error in potential measured between the reference electrode and the steel termed the IR drop. The current must therefore first be switched off to obtain the true fully polarised potential of the steel, termed the instant-off potential. However, the steel will depolarise shortly after with a characteristic exponential decay curve as illustrated in Figure 2.17.

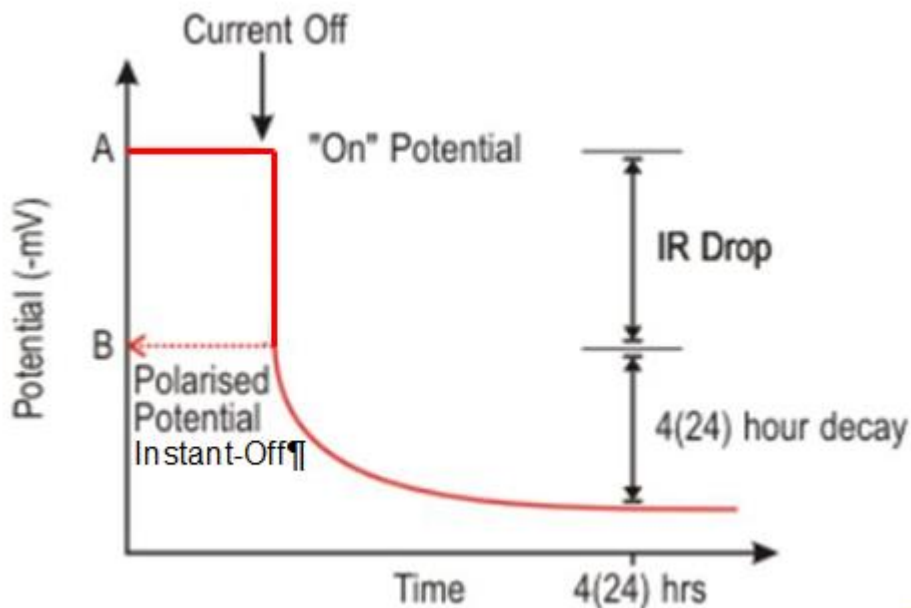


Figure 2.17 Potential decay curve [78]

In order to obtain an accurate measurement of decay, the instant-off potential must be measured within a very short time window, typically 0.1 to 0.4 seconds after the current is switched off. The reinforcement will continue to depolarise and the potential decay is measured after a period of 4 hours (or other suitable intervals) from switch off. The accurate measurement of the instant-off potential is essential to determine the value of potential decay.

A further requirement of the operating criteria is that no instant-off potential more negative than -1100mV with respect to Ag/AgCl/0.5MKCl is permitted, to avoid the possibility of hydrogen evolution which may cause embrittlement of sensitive steels.

However, it is most unlikely that these levels of potential will be reached in a properly operated system. The performance monitoring should thus be designed to ensure that the steel is polarised to the correct level of potential to achieve protection, but not excessively so [78]. However, this project will investigate this claim further and a range of instant-off potentials will be used for protecting the pre-stressing steel. Therefore, three factors must be taken into account when controlling CP system [47] :

1. There must be sufficient current to overwhelm the anodic reactions and stop or severely reduce the corrosion rate.
2. The current must stay as low as possible to minimise the acidification around the anode and the attack of the anode for those that are consumed by the anodic reactions.
3. The steel should not exceed the hydrogen evolution potential, especially for pre-stressed steel to avoid hydrogen embrittlement.

2.7.7 Reference electrode (Half-Cell)

Reference electrode is the potential difference between any metal and its surrounding electrolyte. This variation is referred to as polarization. The potential difference is also dependent on the types of chemical reaction occurring at the metal surface. The metal/electrolyte potential difference may be measured using a reference electrode. Since the measured potential difference will also depend on the type of reference electrode which is used the type of reference electrode should always be stated [79]. Reference electrodes are used to measure the potential of the reinforcing steel and can be either embedded in the concrete permanently or can be portable/surface mounted for application to the external concrete face, as follows [48]:

- Surface-mounted reference electrodes are normally double-junction silver/silver chloride/potassium chloride (Ag/AgCl/0.5M KCl) reference electrodes.

- Embedded reference electrodes are normally double-junction silver/silver chloride/ potassium chloride (Ag/AgCl/0.5M KCl) or manganese dioxide/sodium hydroxide (MnO₂/NaOH).
- Other embedded probes, not strictly reference electrodes but considered suitable for at least potential decay measurements, are sometimes used, typically graphite and activated titanium. These have the advantage of projected longer life than the true reference electrodes [48].

However, the preferred reference electrode for site use is the silver/silver chloride/potassium chloride (SSC) electrode. This requires less maintenance, is more reliable and less prone to leaking than the copper/copper sulfate electrode, which is still quite widely used. SSC electrodes must not be allowed to dry out or they risk being irreversibly damaged [80].

2.7.8 Hydrogen embrittlement

Hydrogen embrittlement in the tendon was discussed in Section 2.6.3.2. However, this Section discusses the influence of ICCP on the tendon. Failures of pre-stressing wires due to HE as a consequence of cathodic polarization has not been reported. Cathodic polarization of pre-stressing wires in concrete structures may occur as a result of stray currents and/or of cathodic protection. It has been indicated that hydrogen evolution occurs on steel in a simulated concrete environment at a potential of about -1.17 V (SCE) [81]. It is now reasonably well established that cathodic protection of normal reinforcing steels, designed and operated to the International Standards now published, presents little risk of hydrogen embrittlement. Cathodic protection of pre-stressed elements requires particular care and rigour in design and operation [48]. High strength steels and steels subjected to high stress levels may be adversely affected by hydrogen and may either embrittle or crack. Care is, therefore, needed in both material selection and design in order to minimize such possible harmful effects [79].

2.8 Conclusion of review

From the review of the literature concerning the corroded reinforced concrete, corrosion is one of the main causes of deterioration. The corrosion has a detrimental effect on the durability of reinforced concrete structures and is reduces the structures service life. However, the steel can resist corrosion if the

conditions such as alkalinity of the surrounding concrete, adequate cover to reinforcement, good quality of concrete, the bond between the steel and concrete and attention to the environment during the construction are provided. The steel in pre-stressed concrete can corrode just like that in conventionally reinforced concrete. Once corrosion occurs on the steel, there is a need to control. Cathodic protection (CP) has proved particularly effective for preventing corrosion in conventionally reinforced concrete structures at risk of corrosion as the result of carbonation or chlorides but has been actively avoided for pre-stressed structures. The main concern regarding the use of CP with pre-stressed steel has been the possible generation of hydrogen as a result of over-protection and the associated risks of hydrogen embrittlement (HE) of the steel tendons.

As structures containing pre-stressed elements age, the risk of corrosion related damage increases along with the need for effective methods of remediation. While the majority of pre-stressed post-tensioned structures are unsuitable for CP because of the presence of a metal or polymer duct, the majority of pre-cast pre-stressed components such as bridge beams and deck slabs are at least capable of being protected provided concerns about HE can be dealt with effectively. Similarly, pre-load structures, generally tanks or bunds that are constructed from pre-cast elements then strengthened with a tensioned strand laid into a groove and encased in gunite, would benefit from the application of CP provided the HE concerns can be addressed.

By understanding the effect of ICCP on pre-stressed high strength ungalvanised and galvanised tendons as used in such components, and optimising the criteria for protecting them with CP, it will be possible to develop safe and effective methods of remediation with a greatly reduced need for break-out and possible release of pre-stress. This research is therefore directed at generating the necessary information to permit such a repair strategy to be assessed and developed.

3 Preliminary Experimental Works

3.1 Introduction

Twelve pre-stressing timber moulds were developed for use in the project. These had a dual purpose (i) to act as shuttering to restrain the mortar (gunite); (ii) to enable the tendons to be pre-stressed. A preliminary test was conducted on one tendon pre-stressed in one mould using different types of strain gauges the aim is to select a suitable strain gauge technique with enough strain capacity. The main aim of the strain measuring was to enable the strain, and hence the stress, to be monitored throughout the test i.e. during the pre-stressing, the accelerated corrosion of the tendon and the application of the ICCP. After several trials with modifications and adjustments as necessary, preliminary tests including corrosion and ICCP on a tendon were performed.

3.2 Aims and Objectives

The aim of these laboratory-based preliminary tests was to confirm that the pre-stressing technique and strain monitoring in the tendons worked successfully; validate the accelerated corrosion method and to perform ICCP so that a range of potentials could be applied to the tendon. This included over and under protecting the tendon by varying the potential applied to the tendons.

3.3 Preliminary Experimental Programme

The experimental works were carried out in The Construction Materials Laboratory at Sheffield Hallam University. Different variables were considered in the test schedule and these included the degree of corrosion in the tendons, their levels of pre-stress and type of tendon (galvanised or ungalvanised) (Table 3.1). Referring to Table 3.1, three series are given, labelled 1, 2 and 3 representing the galvanised and ungalvanised tendons (Col. 1). The electrolyte is either a saline solution (3% by weight sodium chloride) or a sand/cement mortar representing gunite (Col. 2). Each tendon is given a unique code e.g. S-U-L-I-1 based on Electrolyte (solution or mortar) -Type of tendon (Galvanised or Ungalvanised) - Pre-stress level (Low or High) -Degree of Corrosion (Stage I or Stage II or Stage III) - Sample Number (1) (Col. 3). The type of tendons studied (galvanised or ungalvanised) is given in Col.4. The level of pre-load (pre-stress)

in the tendons normally used on site is about 1000 N/mm². It was considered that not all tendons in-situ may be exposed to the same levels of pre-stress after long service conditions resulting in losses and corrosion. Therefore, these tests included a high level of pre-stress (800-1200N/mm²), and a low level (300-400 N/mm²) target pre-stress (Col.5).

Table 3.1 Preliminary Experimental Test Program

Series	Type of Electrolyte	Test Code	Tendon Type	Target Stress	Corrosion Degree	ICCP
				(MPa)	Stage	mV
(1)	(2)	(3)	(4)	(5)	(6)	(7)
1	Solution	S-U-L-I-1	Un-Galvanized	Low	I	
		S-U-L-II-2		Low	II	Over-protection
		S-U-L-III-3		Low	III	Over-protection
		S-U-H-I-1		High	I	
		S-U-H-II-2		High	II	Over-protection
		S-U-H-III-3		High	III	Over-protection
2	Solution	S-G-H-III-1	Galvanized	High	II	
3	Mortar	M-U-L-I-1	Un-Galvanized	Low	I	
		M-U-H-II-2		Low	II	
		M-U-L-III-3		Low	III	
		M-U-H-I-1		High	I	
		M-U-H-II-2		High	II	
		M-U-H-III-3		High	III	

Key: U-Ungalvanised, G-Galvanised, S-Solution electrolyte, M-Mortar electrolyte, H-High level of pre-stress (800-1200 MPa), L-Low level of pre-stress (300-400 MPa), I- Stage I degree of corrosion Stage I (0-1 %), II-Stage II degree of corrosion (2-4 %), III-Stage III degree of corrosion (4-7 %), 1, 2, 3-Sample numbers.

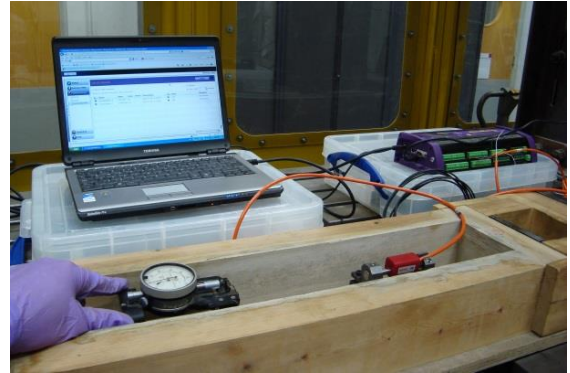
The corrosion current density was kept constant at 1 mA/cm² to enable corrosion to be conducted in a reasonable time. Three different degrees of accelerated corrosion were considered, namely Stage I (0-1%), Stage II (2-4%) and Stage III (4-7%), loss of cross-sectional area (Col. 6). These stages correspond to those which are typically used when conducting on-site inspections where corrosion is present in pre-load structures. One galvanised specimen was subjected to both accelerations of corrosion and ICCP (S-G-H-III-1). In addition, four specimens were exposed to corrosion followed by ICCP, overprotection (-950 to -1200mV) (col. 7), conducted in solution electrolyte.

3.4 Selection of strain gauges and determination of slippage

A number of tests were carried out in order to identify suitable strain gauges that can work within the range of the target stress of the tendon. Two different DEMEC mechanical strain gauges of 100mm and 200mm length were used along with two vibrating wire (VW) strain gauges 89mm and 150mm length as shown in Figure 3.1 (a) and (b).



(a) Placing DEMEC pins (100mm) and VW strain gauge (89mm) on the tendon



(b) Taking reading of both DEMEC mechanical strain and VW strain gauges

Figure 3.1 Placing and taking readings of both DEMEC and VW strain gauges

Several pilot tests on pre-stressed tendons were conducted with the aim being to optimise the pre-tensioning technique and to determine the slippage of the applied stress in the tendon (Table 3.2). Slippage is a loss in pre-stress when the loading apparatus is removed to transfer the load to wedges, this is explained more in next the chapter. The results of the slippage investigation are given in Table 3.2. Different pre-tensioning stresses were applied to determine losses upon transfer of load to the wedges. The specimen identification is given in Col. 1, the corresponding load is given in Col. 2 and resulting stress, σ , is given in Col. 3, obtained from $\sigma = (E) (\epsilon)$ where E is the elastic modulus and ϵ is the strain as measured during loading. The actual load after releasing the tensioning force is given in Col. 4 and this was repeated four times for each specimen. This load is averaged in Col. 5. The average stress after release of the pump is given in Col. 6 and averaged in Col. 7. The loss in load due to slippage is given in Col. 8 and this is averaged in Col. 9 for each of the four specimens. The average loss in stress due to slippage is then calculated in Col. 10.

Table 3.2 Calculating tendon slippage using load cell

Test No.	Force before releasing the pump pressure		Force after releasing the pump pressure				Slippage (kN)	Average Slippage (kN)	Average Slippage Stress (MPa)
	Reading (kN)	Stress (MPa)	Reading (kN)	Ave. Reading (kN)	Stress (MPa)	Ave. Stress (MPa)			
(1)	(2)	(3)	(4)	(5)	(6)	(7)	(8)	(9)	(10)
A	14.7	641.86	10.34	10.30	451.48	450.06	4.36	4.39	191.79
			10.33		451.04		4.37		
			10.30		449.73		4.40		
			10.26		447.99		4.44		
B	19.5	851.44	14.55	14.45	635.31	630.94	4.95	5.05	220.50
			14.50		633.12		5.00		
			14.38		627.88		5.12		
			14.37		627.45		5.13		
C	22.9	999.90	17.89	17.77	781.14	775.90	5.01	5.13	223.99
			17.75		775.03		5.15		
			17.73		774.16		5.17		
			17.71		773.28		5.19		
D	27.9	1218.22	20.23	20.04	883.32	875.13	7.67	7.857	343.08
			20.20		882.01		7.70		
			20.15		879.82		7.75		
			19.59		855.37		8.31		

Figure 3.2 shows the required applied force to reach the target stress and its slippage. This slippage is increment with the increase of applied pre-tensioning forces. The force, F, allowing for slippage can be obtained from the equation $F=0.0288 \sigma$ shown on Figure 3.2. The target stress 600, 800, 1000 and 1200 MPa corresponds to allowable forces for slippage of 17.28, 23.04, 28.80 and 34.56 kN.

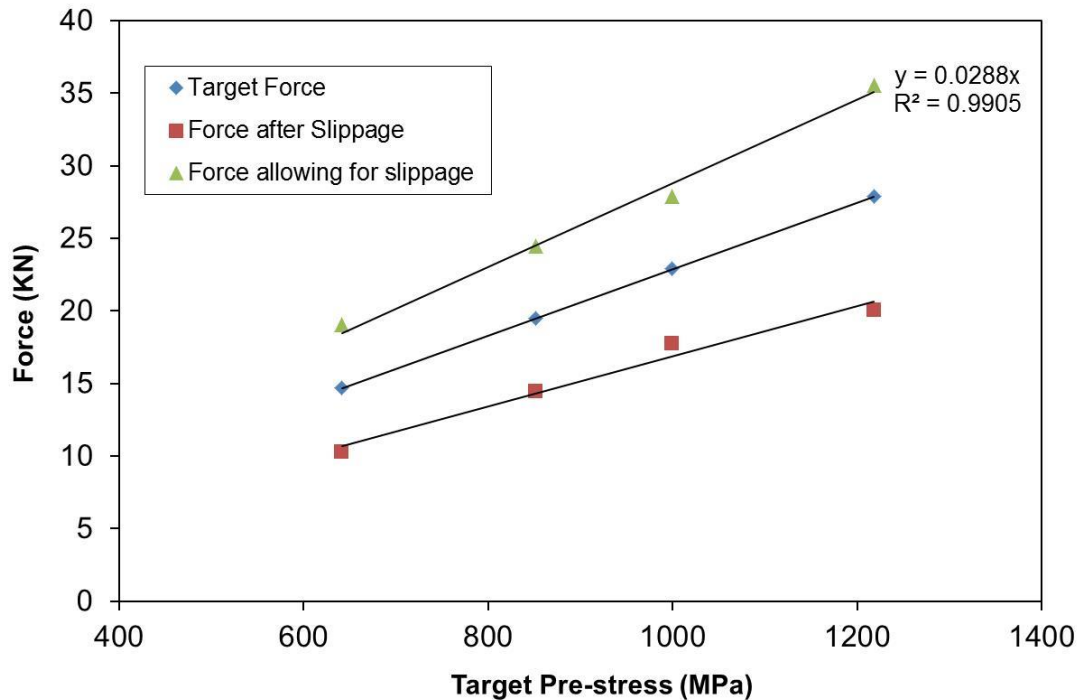


Figure 3.2 Slippage compensation with increasing applied pre-tensioning force

3.5 Accelerating corrosion of the tendon

Preliminary tests were conducted before commencing the research programme to validate the accelerated corrosion technique.

3.5.1 Faraday's Law

The relationship between corrosion current density and the weight of metal lost due to corrosion was determined by applying Faraday's Law (Equation 3.1):

$$\Delta\omega = \frac{A \times I \times t}{Z \times F} \quad \text{Equation 3.1}$$

where:

$\Delta\omega$ = weight loss due to corrosion in (g),

A = atomic weight of iron (56 g),

I = electrical current in (A),
 t = time in (sec.),
 Z = valence of iron which is 2,
 F = Faraday's constant (96 500 coulombs).

The metal weight loss due to corrosion can also be expressed as:

$$\Delta\omega = a \times \delta \times \gamma \quad \text{Equation 3.2}$$

where:

a = tendon surface area before corrosion (cm^2),
 δ = material cross sectional loss (cm),
 γ = density of material (7.86 g/cm^3).

The corrosion current can be expressed as:

$$I = i \times a \quad \text{Equation 3.3}$$

where:

i = corrosion current density (Amp/cm^2).
 a = tendon surface area before corrosion (cm^2)

Therefore, combining Equations 3.1, 3.2 and 3.3 gives:

$$a \times \delta \times \gamma = \frac{A \times I \times t}{Z \times F} = \frac{A \times i \times a \times t}{Z \times F} \quad \text{Equation 3.4}$$

Therefore,

$$\delta = \frac{A \times i \times t}{\gamma \times Z \times F} \quad \text{Equation 3.5}$$

R is defined as the metal section loss per year (cm/year)

Substituting known values, in which $t=365$ days, into Equation 3.5 and simplifying gives:

$$R = \frac{A \times i \times t}{\gamma \times Z \times F} = \frac{56 \times i \times 365 \times 24 \times 60 \times 60}{7.86 \times 2 \times 96500} = 1165 \times i \text{ (cm/year)} \quad \text{Equation 3.6}$$

For a corrosion rate (*i*) of 1 (mA/cm²), *R* equals 1.165 (cm/year) (from Equation 3.6). If, as in a reinforced concrete structure, the period of corrosion after initiation is *t'* years, then

$$\text{Metal loss after } t' \text{ years} = R \times t \text{ (cm)} \quad \text{Equation 3.7}$$

Therefore, percent reduction in rebar diameter after (*t'*) years is

$$t' = \frac{2 \times R \times t}{D} \times 100 \quad \text{Equation 3.8}$$

The expression $[2 \times R \times (t/D)]\%$, which represents a reduction in rebar diameter due to corrosion over *t'* years, is also defined as the degree of reinforcement corrosion [82]. For the purpose of this study the degree of corrosion $m = [2 \times R \times (t/D)]\%$.

Table 3.3 shows the parameters of the tendons under test and Table 3.4 shows the corrosion design criteria for the same specimens. Table 3.5 shows the strains in the tendons which are converted to stresses by applying $\sigma = E \varepsilon$ where *E* is taken as 220 GPa. The preliminary results indicate that there is a loss in pre-stress due to corrosion and also the loss of pre-stress increased as the degree of corrosion increased.

Figure 3.3 (a) and (b) shows the appearance over time of the galvanized tendon after completion of corrosion and before inducing the ICCP. The galvanized steel tendon after one day exposed to corrosion was covered with a white zinc corrosion product [Figure 3.3 (b)] and ferrous rust was spread widely in the specimens after completion of corrosion on day 3 [Figure 3.3 (c)]. Figure 3.4 and Figure 3.5 show a reduction in service stress of the ungalvanised tendon over the entire test period for target pre-stresses Low and High levels respectively. At Stage I degree of corrosion, stage I losses are very similar, while there is a greater difference in loss of pre-stress due to stage II corrosion. This indicates that the loss in service stress is more dependent on the degree of

corrosion and less dependent on the initial pre-stress in the tendon. The 0% tendons, although not subjected to corrosion, also suffer a reduction in pre-stress, perhaps as a result of compression in the timber moulds or relaxation. Extra care was taken to ensure all tendons were stable before the commencement of the accelerated corrosion process.



(a) Before start of corrosion



(b) After one day of corrosion, tendon covered by white zinc corrosion products



(c) After completion of corrosion (degree of corrosion: Stage II) and before removing corrosion substance of ferrous rust



(d) After completion of corrosion and removing corrosion substance

Figure 3.3 Appearance of tendon throughout the corrosion period

Table 3.3 Tendon test parameters

Test ID	Tendon Type	Tendon Diameter	Tendon Length	Tendon Corroded Length	Target Stress	Solution		Corrosion Degree	Current Density	Comments
	G/U**	(cm)	(cm)	(cm)	(MPa)	Water (litre)	Sodium Chloride (g)	Stage	(mA/cm ²)	
S-G-H-II	G	0.54	140	32	H	1000	30	II	1	
S-U-L-I	U	0.54	140	30.7	L	1000	30	I	1	Control
1-U-L-II	U	0.54	140	30.7	L	1000	30	II	1	
1-U-L-III	U	0.54	140	30.7	L	1000	30	II	1	
1-U-H-I	U	0.54	140	30.7	H	1000	30	I	1	Control
1-U-H-II	U	0.54	140	30.7	H	1000	30	II	1	
1-U-H-III	U	0.54	140	30.7	H	1000	30	II	1	

Key: U-Ungalvanised, G-Galvanised, S-Solution electrolyte, M-Mortar electrolyte, H-High level of pre-stress (800-1200 MPa), L-Low level of pre-stress (300-400 MPa), I- Stage I degree of corrosion Stage I (0-1 %), II-Stage II degree of corrosion (2-4 %), III-Stage III degree of corrosion (4-7 %), 1, 2, 3-Sample numbers.

Table 3.4 Corrosion design criteria

Test ID*	Tendon Type	Applied Stress (MPa)	Target Corrosion Degree Stage	Current (mA/tendon)	Duration of Accelerated Corrosion (days)	Tendon weight		Weight Lost		Comments
						Before Corrosion (g)	After Corrosion (g)	(g)	(%)	
S-G-H-II	G	658.27	I	54.29	2.54	260.79	248.07	12.72	4.88	
S-U-L-I	U	384.84	I	0	0	261.67	261.20	0.47	0.00	Control
1-U-L-II	U	453.26	II	52.08	2.54	267.63	256.24	11.39	4.26	
1-U-L-III	U	442.71	III	52.08	5.08	251.00	235.62	15.38	6.13	
1-U-H-I	U	1295.82	I	0	0	266.62	266.50	0.12	0.00	Control
1-U-H-II	U	1150.71	II	52.08	2.54	259.29	248.62	10.67	4.12	
1-U-H-III	U	1139.89	III	52.08	5.08	260.06	244.73	15.33	5.89	

Key: U-Ungalvanised, G-Galvanised, S-Solution electrolyte, M-Mortar electrolyte, H-High level of pre-stress (800-1200 MPa), L-Low level of pre-stress (300-400 MPa), I- Stage I degree of corrosion Stage I (0-1 %), II-Stage II degree of corrosion (2-4 %), III-Stage III degree of corrosion (4-7 %), 1, 2, 3-Sample numbers.

Table 3.5 Actual strain and stress in the tendons

Days	<i>Tendon</i> S-G-H-III-1		<i>Tendon</i> S-U-L-I-1		<i>Tendon</i> 1-U-L-II-2		<i>Tendon</i> 1-U-L-III-3		Comments
	<i>Strain</i>	<i>Stress</i>	<i>Strain</i>	<i>Stress</i>	<i>Strain</i>	<i>Stress</i>	<i>Strain</i>	<i>Stress</i>	
	($\mu\varepsilon$)	(MPa)	($\mu\varepsilon$)	(MPa)	($\mu\varepsilon$)	(MPa)	($\mu\varepsilon$)	(MPa)	
	1	2992.14	658.27	1749.28	384.84	2060.29	453.26	2012.30	
2	2994.81	658.86	1733.30	381.33	2021.17	444.66	1966.30	432.59	
3	2965.64	652.44	1712.84	376.82	1979.58	435.51	1917.39	421.83	
4	2925.10	643.52	1681.56	369.94	1926.04	423.73	1843.01	405.46	
5	-	-	1665.62	366.44	1908.28	419.82	1802.57	396.57	
6	-	-	1647.61	362.47	1886.34	414.99	1753.54	385.78	

Key: U-Ungalvanised, G-Galvanised, S-Solution electrolyte, M-Mortar electrolyte, H-High level of pre-stress (800-1200 MPa), L-Low level of pre-stress (300-400 MPa), I- Stage I degree of corrosion Stage I (0-1 %), II-Stage II degree of corrosion (2-4 %), III-Stage III degree of corrosion (4-7 %), 1, 2, 3-Sample numbers.

Table 3.6 Stress and strain in the tendons

Days	<i>Tendon</i>		<i>Tendon</i>		<i>Tendon</i>		<i>Comments</i>
	<i>U-H-I-1</i>		<i>U-H-II-2</i>		<i>U-H-III-3</i>		
	<i>Strain</i>	<i>Stress</i>	<i>Strain</i>	<i>Stress</i>	<i>Strain</i>	<i>Stress</i>	
	<i>($\mu\epsilon$)</i>	<i>(MPa)</i>	<i>($\mu\epsilon$)</i>	<i>(MPa)</i>	<i>($\mu\epsilon$)</i>	<i>(MPa)</i>	
1	5890.09	1295.82	5230.52	1150.71	5181.34	1139.89	
2	6034.66	1327.63	5159.01	1134.98	5086.19	1118.96	
3	6437.22	1416.19	5093.92	1120.66	5004.73	1101.04	
4	6036.63	1328.06	4989.59	1097.71	4848.47	1066.66	
5	6453.09	1419.68	4873.62	1072.20	4803.36	1056.74	

Key: U-Ungalvanised, G-Galvanised, S-Solution electrolyte, M-Mortar electrolyte, H-High level of pre-stress (800-1200 MPa), L-Low level of pre-stress (300-400 MPa), I- Stage I degree of corrosion Stage I (0-1 %), II-Stage II degree of corrosion (2-4 %), III-Stage III degree of corrosion (4-7 %), 1, 2, 3-Sample numbers.

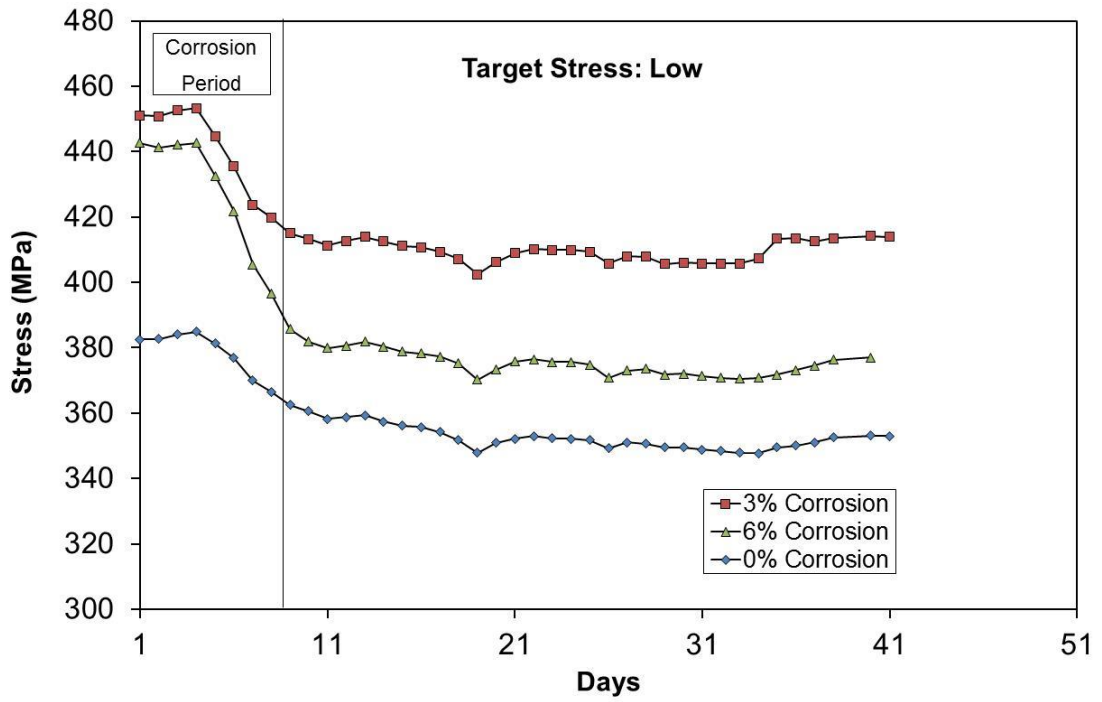


Figure 3.4 Gross loss in tendon with low pre-stress over the test period

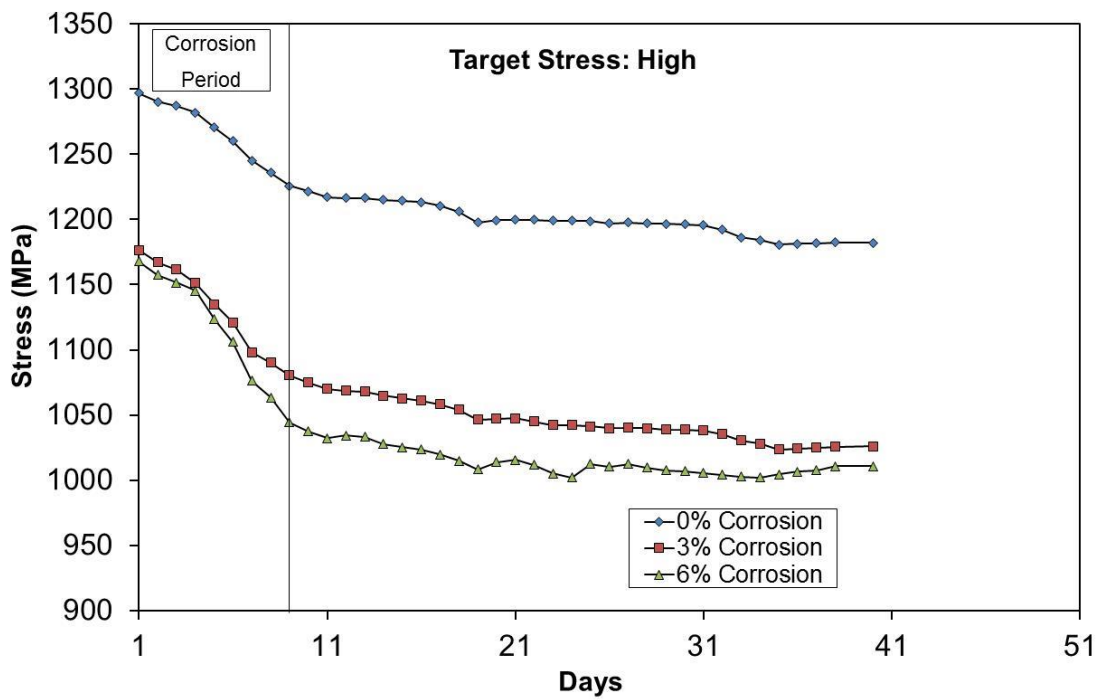


Figure 3.5 Gross loss in tendon with high pre-stress over the test period

3.6 Optimisation of ICCP

A test was initially conducted on one pre-stressed galvanised tendon (S-G-H-II) to evaluate its operation (Figure 3.6) and Table 3.7 shows the tendon parameters. Table 3.4 and Table 3.7 provide details of the test.



Figure 3.6 Hydrogen just being generated on tendon S-G-H-II-1

Table 3.7 Pilot CP test in a saline solution

<i>Specimen ID</i>	<i>Electrolyte</i>	<i>Surface Area (cm²)</i>	<i>Applied Voltage (V)</i>
S-G-H-II-1	NaCl (3%) and Ca(OH) ² (4%)	54.29	2.53

Key: U-Ungalvanised, G-Galvanised, S-Solution electrolyte, M-Mortar electrolyte, H-High level of pre-stress (800-1200 MPa), L-Low level of pre-stress (300-400 MPa), I- Stage I degree of corrosion Stage I (0-1 %), II-Stage II degree of corrosion (2-4 %), III-Stage III degree of corrosion (4-7 %), 1, 2, 3-Sample numbers.

After completing ICCP and removing the tendon from the mould, it was observed that a passivating layer had formed around the surface along the length of the tendon exposed to the electrolyte. This confirms the effectiveness of ICCP in protecting the tendon from corrosion and its contribution to preserving the alkalinity of the electrolyte around the tendon. The pH was kept constant at around 12 during the test period. Table 3.8 shows that the applied stress stays fairly constant over the period of the test at around 611 MPa while

potentials ON and Off fluctuated slightly perhaps due to the difficulties in measuring to millivolts using a hand-held DVM. Using the reference electrode types Silver/Silver Chloride (Ag/AgCl/KCl 0.5M SSC) and digital voltage meter (DVM), the instant-off was adjusted just to generate hydrogen from the beginning of the test. Figure 3.7 shows that the current passing through the tendon increased at the beginning of the test period reach to 244mA and then started to reduce as the test period increased, while the voltage stayed constant through the same period of the test (2.53V). This variation in current is attributed to the passivating layer on the surface of the tendon that prevented the oxygen ingress into the tendon over the time. After completing the ICCP, the tendon was cleaned with a solution of 5% di-ammonium hydrogen citrate and reweighed to calculate the weight loss from the corrosion period. Table 3.4 shows that the weight loss of galvanised tendon was 4.87%, higher than the Stage II target so closer monitoring is required in the main tests to ensure the actual is closer to the target loss in corrosion.

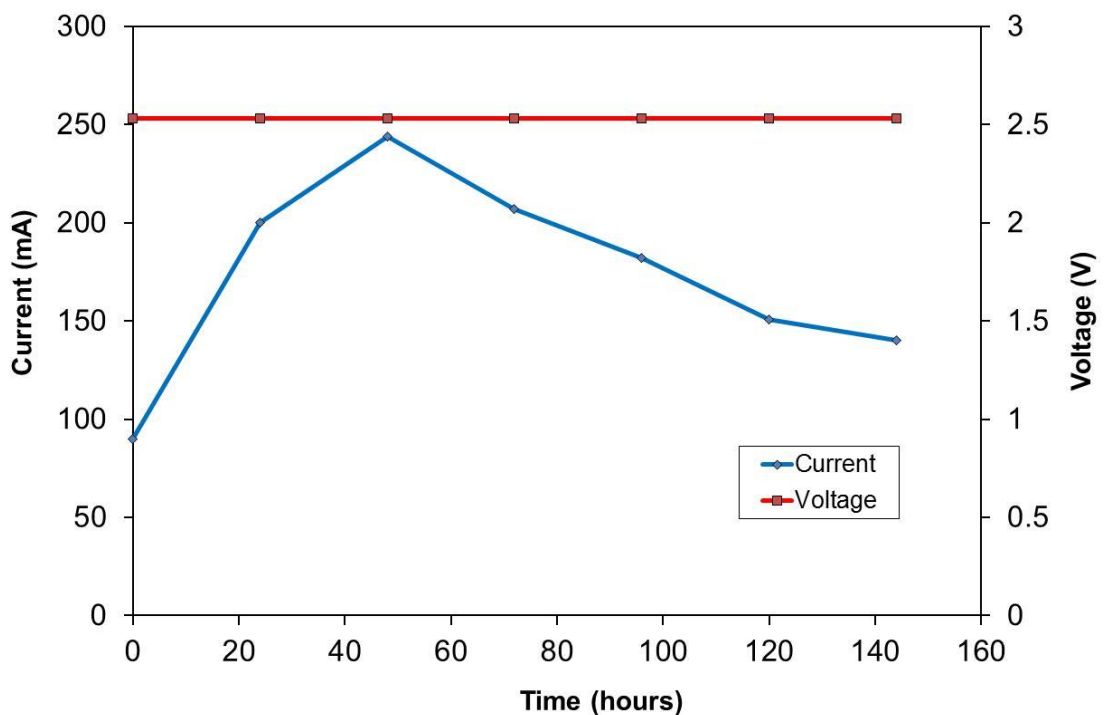


Figure 3.7 Applied current and voltage versus test period

Table 3.8 Test results of the ICCP application

Day	Strain ($\mu\epsilon$)	Stress (MPa)	Initial	Potential	Instant	Voltage (V)	Current (mA)	Applied	Mould Strain		pH	Temperature ($^{\circ}$ C)
			Potential	ON	OFF			Current	1	2		
			(mV)	(mV)	(mV)			Density (mA/cm 2)	($\mu\epsilon$)	($\mu\epsilon$)		
1	2285	599.24	-812	-1284	-1130	2.58	90	1.66	56.91	37.94	12.45	15.1
2	2295	611.63		-1328	-1180	2.53	200	3.68	37.94	-5.42	12.64	21.3
3	2293	609.15		-1396	-1195	2.53	244	4.49	-5.42	-21.68	12.72	20
4	2295	611.63		-1424	-1200	2.53	207	3.81	18.97	18.97	12.57	20.9
5	2295	611.63		-1328	-1175	2.53	182	3.35	8.13	5.42	12.45	20.5
6	2295	611.63		-1260	-1160	2.53	151	2.78	21.68	5.42	12.34	20.3
7	2292	607.91		-1242	-1165	2.53	140	2.58	27.1	5.42	12.27	20.3

3.7 Concluding remarks

Based on the preliminary tests, the methodology was shown to work successfully. This includes procuring all the materials and equipment required for the whole project. A total of 12 pre-stressing moulds were manufactured, several tests on pre-stressed tendons were conducted to quantify the slippage, validate the accelerated corrosion technique and determine that ICCP can be successfully applied.

3.7.1 Loss in stress-due to slippage

A simple equation was developed which will determine the increase in pre-stress to be applied beyond the low (300-400MPa) and high (800-1200MPa) targets to ensure the final stress is as required. It is too much to expect that all final pre-stresses will be exactly as planned but a pre-stress in the range $\pm 5\%$ will suffice.

3.7.2 Effect of corrosion on the tendon

A unique outcome of the work will be the ability to relate the degree of corrosion to a loss in pre-stress. The preliminary research has shown that a higher degree of corrosion leads to a higher loss in pre-stress. The work to date considered only three levels of corrosion Stage I (0-1%), Stage II (2-4%) and Stage III (4-7%) and two levels pre-stress low (300-400MPa) and high (800-1200MPa)

3.7.3 Effect of Impressed Current Cathodic Protection (ICCP) on the tendon

The application of ICCP shows that there is no change in the applied stress through the test period of ICCP. Although a potential of -1400mV was applied, more than the stated limits in international standards, there was no visual damage to the tendon. However, the tendon is yet to be tested to determine if there has been a decrease in ultimate tensile strength (UTS). This is likely due to the loss in cross-sectional area as a result of corrosion but it is only when it is compared to an uncorroded, ICCP applied tendon can a true influence be established.

The next chapter will describe the materials need and explain the methodology that was employed with more details for the purpose of this research work.

4 Experimental Methodology

4.1 Introduction

Deterioration of reinforced concrete can take many forms; the most obvious is the change in appearance caused by corrosion of the reinforcement. Many studies have shown that corrosion of reinforcement is the single most common source of damage and it is usually clear that low quality concrete, inadequate cover to the reinforcement or the presence of impurities (and sometimes all three) is the prime cause. Much of the deterioration of concrete can only occur in the presence of water since aggressive agents will penetrate concrete and react harmfully with the cement paste only when dissolved in water [83]. This problem has been investigated in many organisations such as the Corrosion Prevention Association (CPA), the National Association of Corrosion Engineers (NACE), Institute of Corrosion, The Concrete Society, and American Concrete Institute (ACI) through their publications and several international conferences.

The economic factor is a very important motivation for much of the current research in corrosion. Losses sustained by industry and by governments amount to many billions of dollars annually, approximately \$ 276 billion in the United States, or 3.1% of the Gross Domestic Product (GDP), according to a recent study [51]. It has been estimated that about 25 – 30% of this total could be avoided if currently available corrosion technology were effectively applied. Studies of the cost of corrosion to Australia, Great Britain, Japan, and other countries have also been carried out. In each country studied, the cost of corrosion is approximately 3 – 4 % of the Gross National Product [51]. As a result, as civil infrastructure is age, owners have to spend an increasing percentage of their budgets on rehabilitation (or replacement) of existing concrete structures. Thus, there is obviously a strong financial incentive to extend the service life of existing structures [84]. Impressed Current Cathodic Protection (ICCP) technique is a system that can prevent further corrosion and extend the service life of the structure. However, using this technique in pre-stressed concrete is still limited due to concerns about hydrogen embrittlement in the tendon.

The aim of this research, therefore, is to determine the effect of applying cathodic protection to pre-stressed steel tendons. It will be applied as both normal and over protection when the tendon is subjected to varying degrees of corrosion. This chapter describes the materials, methods, and analytical techniques used for the purpose of this research work taking into consideration the output of the preliminary experimental works.

4.2 Objectives of investigation

The principle objectives of the experimental work are to:

- validate and develop the pre-stressing technique using vibrating wire strain gauge (VWSG), to apply the target force and monitor the strain
- develop an effective technique for accelerating corrosion of pre-stressed tendons in concrete
- study the behaviour of pre-stressed tendons under the effect of applied impressed current cathodic protection (ICCP), both normal and overprotection, with different levels of service pre-stress and with unstressed tendons
- develop a better understanding of the effect of ICCP on pre-stressed tendons in terms of mechanical properties
- investigate the effect of different degrees of corrosion on different levels of applied service pre-stress for ungalvanised and galvanised tendons

4.3 Details of the experimental programme

The Construction Materials laboratory at Sheffield Hallam University was used to carry out the investigations. Different batches of specimens were tested to fulfill the objectives of the research. Referring to Table 4.1, Batch R refers to the as-received tendons and used as control samples for comparison with the other batches. Batch 1 investigated the influence of applied ICCP overprotection on the ungalvanised tendons pre-tensioned to various levels of service stress, conducted in a saline electrolyte and exposed to different stages of corrosion. Batch 2 investigated the influence of applied ICCP normal protection on the ungalvanised tendons tensioned to low and high levels of service pre-stress embedded in mortar/gunite electrolyte and exposed to different stages of corrosion. Batch 3 investigated the influence of applied ICCP overprotection on the ungalvanised tendons tensioned to low and high levels of service pre-stress

in a mortar/gunite electrolyte and exposed to different stages of corrosion. Batch 4 investigated the influence of applied ICCP normal and overprotection on the galvanised tendons tensioned to high levels of service pre-stress and placed in a mortar/gunite electrolyte and exposed to different stages of corrosion. Batch 5 investigated the influence of applied ICCP overprotection on unstressed ungalvanised and galvanised tendons in a saline electrolyte. A total of 31 specimens (Table 4.1) were tested.

Mortar prisms made of sand, cement and water with length of 575 mm and with a cross-section of 90 mm deep and 100 mm wide were used in the investigation. Prisms were cast using timber moulds. Each mortar prisms was reinforced with one high tensile tendon of 5.4 mm diameter.

Table 4.1 Detailed Experimental Programme

No.	Batches	Type of Electrolyte	Tendon Type	Target Stress	Corrosion Degree	Test Code	Applied Processes		
				(MPa)	Stage				
1	R		U			U-R-1			
2						U-R-2			
3						U-R-3			
4						G		G-R-1	
5			G-R-2						
6			G-R-3						
7			G-R-4						
8						G-R-5			
1	1	Solution	U	Low	I	S-U-L-I-1	Pre-stressing		
2						II	S-U-L-II-O-2	Pre-stressing + Corrosion + ICCP (Over)	
3						III	S-U-L-III-O-3	Pre-stressing + Corrosion + ICCP (Over)	
4						High	I	S-U-H-I-1	Pre-stressing
5							II	S-U-H-II-O-2	Pre-stressing + Corrosion + ICCP (Over)
6							III	S-U-H-III-O-3	Pre-stressing + Corrosion + ICCP (Over)
7							Solution	G	High
8	2	Mortar	U	Low	II	M-U-L-X-1	Pre-stressing		
9						III	M-U-L-II-N-2	Pre-stressing + Corrosion + ICCP(Normal)	
10						III	M-U-L-III-N-3	Pre-stressing + Corrosion + ICCP(Normal)	
11						High	I	M-U-H-X-1	Pre-stressing

Key: U-Ungalvanised, G-Galvanised, S-Solution electrolyte, M-Mortar electrolyte, H-High level of pre-stress (800-1200 MPa), L-Low level of pre-stress (300-400 MPa), I- Stage I degree of corrosion Stage I (0-1 %), II-Stage II degree of corrosion (2-4 %), III-Stage III degree of corrosion (4-7 %), N-Normal protection, O-Overprotection, X&X1-No corrosion and No CP, 1, 2, 3-Sample numbers.

Table 4.1 Experimental Programme - Cont.

No.	Batches	Type of Electrolyte	Tendon Type	Target Stress (MPa)	Corrosion Degree Stages	Test Code	Applied Processes
12					II	M-U-H-II-N-2	Pre-stressing + Corrosion + ICCP(Normal)
13					III	M-U-H-III-N-3	Pre-stressing + Corrosion + ICCP(Normal)
14	3	Mortar	U	Low	I	M-U-L-X1-1	Pre-stressing + Casting
15					II	M-U-L-II-O-2	Pre-stressing + Corrosion + ICCP (Over)
16					III	M-U-L-III-O-3	Pre-stressing + Corrosion + ICCP (Over)
17				High	I	M-U-H-X1-1	Pre-stressing + Casting
18					II	M-U-H-II-O-2	Pre-stressing + Corrosion + ICCP (Over)
19					III	M-U-H-III-O-3	Pre-stressing + Corrosion + ICCP (Over)
20	4	Mortar	G	High	I	M-G-H-X-1	Pre-stressing + Casting
21					II	M-G-H-II-N-1	Pre-stressing + Corrosion + ICCP(Normal)
22					III	M-G-H-III-N-3	Pre-stressing + Corrosion + ICCP(Normal)
23				High	I	M-G-H-X1-1	Pre-stressing + Casting
24					II	M-G-H-II-O-2	Pre-stressing + Corrosion + ICCP (Over)
25					III	M-G-H-III-O-3	Pre-stressing + Corrosion + ICCP (Over)
26	5	Solution	G	Unstressed		S-G-O-1	ICCP (Over)
27						S-G-O-1	ICCP (Over)
28						S-G-O-3	ICCP (Over)
29			U			S-U-O-1	ICCP (Over)
30						S-U-O-2	ICCP (Over)
31						S-U-O-3	ICCP (Over)

Key: U-Ungalvanised, G-Galvanised, S-Solution electrolyte, M-Mortar electrolyte, H-High level of pre-stress (800-1200 MPa), L-Low level of pre-stress (300-400 MPa), I- Stage I degree of corrosion Stage I (0-1 %), II-Stage II degree of corrosion (2-4 %), III-Stage III degree of corrosion (4-7 %), N-Normal protection, O-Overprotection, X&X1-No corrosion and No CP, 1, 2, 3-Sample numbers.

4.4 Preparation of moulds

A total of 12 timber moulds/pre-stress beds were designed, manufactured and developed as shown in Figure 4.1. The timber mould was fastened to a plywood or wisa-form base and was used:

- pre-load the tendon
- provide formwork for the cast gunite/mortar or space for the solution in a plastic tray
- conduct accelerated corrosion
- conduct cathodic protection

A sketch of the complete pre-stressing apparatus is shown in Figure 4.2.



Figure 4.1 Timber mould on a wisa-form base

4.5 Preparation and pre-stressing system

The main components of the test system are as follows (Figure 4.2 and Figure 4.3):

- a hollow cylinder to apply the load (Enerpac RCH 121) and a hand pump as described in Section 4.10.6
- a vibrating wire strain gauge on the tendon and connected to a laptop to monitor the stress in the tendons as described in Section 4.10.5
- wedges to grip the tendons during pre-loading and bond testing (PAUL Grips F24B-16 Bayonet)
- mild steel end plates to spread the load and prevent piercing of the timber mould during loading

- drilled M16 mild steel bolts at either end, through which the tendons passed, and threaded into the end plates to facilitate releasing of the pre-load
- a thrust bearing inserted at the bolt head at the loading end to prevent damage to the tendon/mortar bond during the release of load
- a data logger to record and log the strain readings from the strain gauges

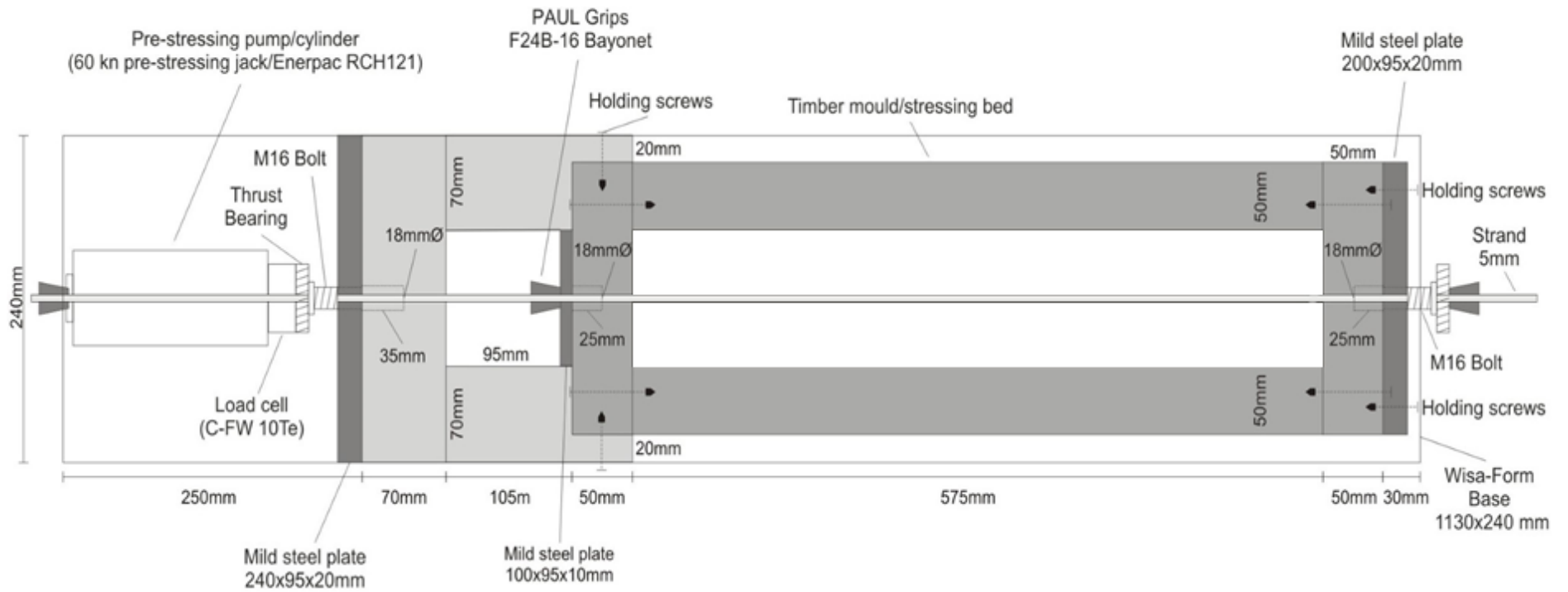


Figure 4.2 Pre-stressing set-up

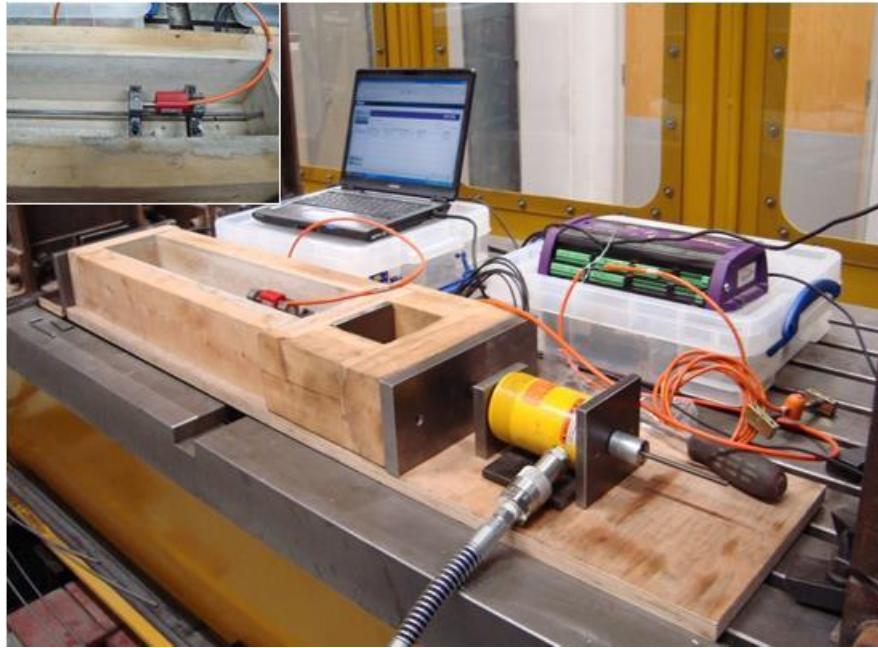


Figure 4.3 Pre-stressing system in operation

In order to remove the loading apparatus for use on the subsequent mould, wedges were used at either end to maintain the pre-load in the tendon. Losses due to slippage were minimised by inserting U shaped washers between the end plate and wedge at the loading end. Washers ranged from 0.5mm to 4mm in thickness and were combined to give a thickness appropriate to the gap to be filled (Figure 4.4).

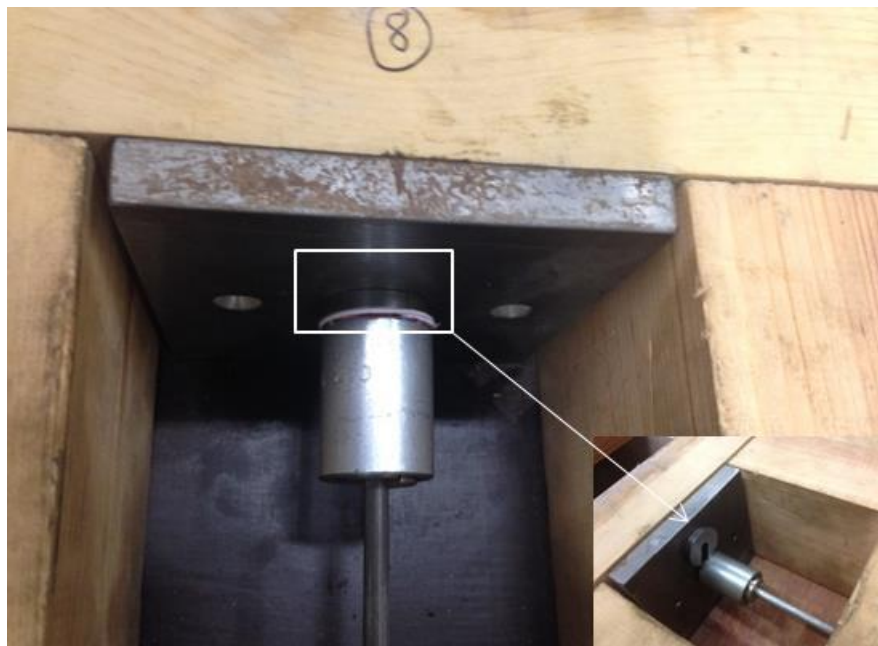
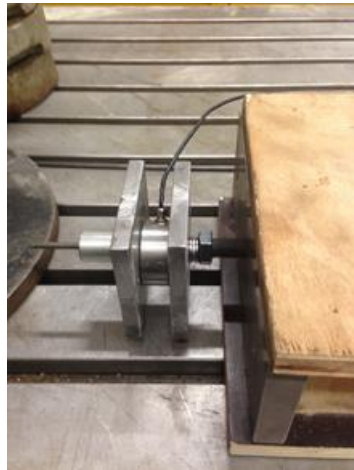


Figure 4.4 Wedges and U shape washers to minimise the slippage losses

The target stress was exceeded by approximately 5 MPa to allow for the losses, based on trials conducted with the load cell in place and monitoring the drop-off in load (Figure 4.5 (a) and (b)). The preliminary work enabled the target pre-stress to be more accurately determined due to a better understanding of slippage losses within this pre-stressing system (Section 3.7.1)



(a) Load cell



(b) Pre-stressing in progress

Figure 4.5 Trial test using load cell to determine the losses

4.6 Electrochemical Techniques

4.6.1 Potential inspection technique

In order for the corrosion process to take place, there must be differences in potential; anodic and cathodic surface zones of the steel must be connected electrically. A flow of electrons and ions between them must be possible. The electrolytic connection is represented by the saline solution or damp mortar. A digital voltmeter (DVM) is used to measure the potential between the anodes (the tendons) and the cathode (mixed metal oxide) in both solution and mortar electrolyte.

4.6.2 Half-cell potential

The main purpose of the half-cell method is to measure the actual potential of the tendon. The components of the system are a reference electrode, DVM and connecting cables. The negative lead of DVM is connected to the reference electrode whereas the positive lead is connected to the tendon. With a suitable scale of DVM the reading of potential can be taken (Figure 4.6). Since the test

involves both a solution and a mortar as the electrolyte, extra preparation is required when dealing with the mortar due to the higher resistance.

The mortar surface, an overlaying material, or both must be pre-wetted to decrease the electrical resistance of the circuit. A test to determine the need for pre-wetting may be conducted as follows:

The half-cell to be placed on the surface of the mortar and the DVM to be observed for one of the following conditions:

1. The measured value of the half-cell potential does not change or fluctuate with time.
2. The measured value of the half-cell potential changes or fluctuates with time.

If Condition 1 is observed, pre-wetting the concrete surface is not necessary. However, if Condition 2 is observed, pre-wetting is required for an amount of time such that the voltage reading is stable (± 0.02 V) when observed for at least 5 mins. If pre-wetting cannot obtain Condition 1, either the electrical resistance of the circuit is too great to obtain valid half-cell potential measurements of the steel. However, the previous testing by the research team has shown that Condition 1 can be met. If the mortar is saturated, the availability of oxygen to the steel is restricted. This will cause the tendon to show more negative values of half-cell potential. Potentials in the range -600 mV to -900 mV versus an SSC reference electrode may be detected, but the associated risk of corrosion is very low as there is not enough oxygen for corrosion to proceed [80]. Positive readings, if obtained, generally indicate a poor connection with the steel, insufficient moisture in the concrete or the presence of stray currents and should not be considered valid [85].

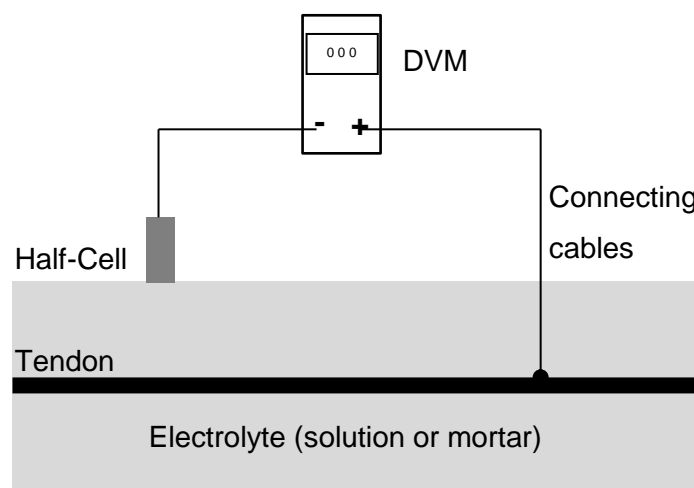
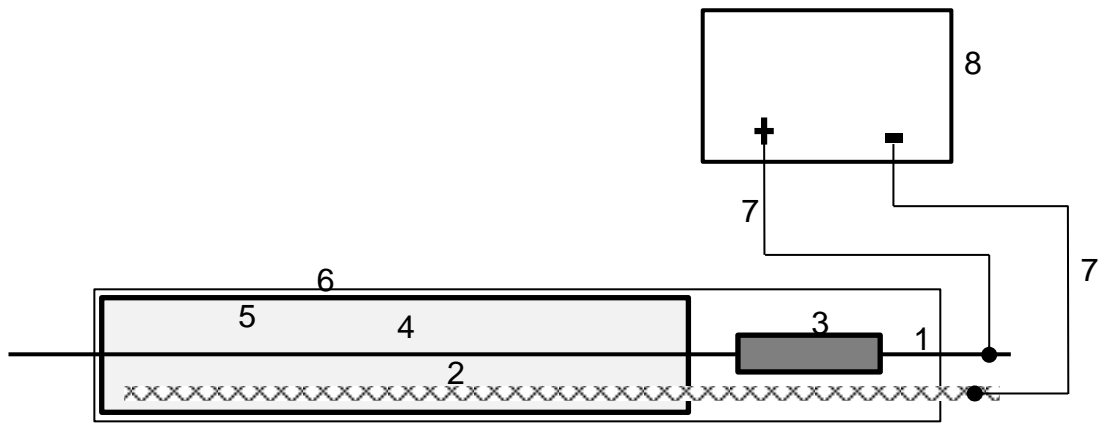


Figure 4.6 Schematic diagram of half-cell circuit

4.6.3 Experimental Procedure

Corrosion of steel in concrete usually takes several years to be initiated, which is too long for laboratory studies. Thus, laboratory acceleration of corrosion process is necessary [86]. There are some significant differences between accelerated corrosion by impressed anodic current and naturally occurring corrosion [87].

Impressed anodic current has been used widely to accelerate the corrosion of steel in concrete. This method has been selected for this study on the basis of being relatively fast and the amount of corrosion generated can be calculated from the current passed using Faraday's Law. A constant current density of 1 mA/cm^2 was adopted in this investigation. The total required current for each degree of corrosion was determined and applied to the pre-stressed tendon surface. The current density was kept constant throughout. This current density was previously adopted in earlier experiments and was found to provide an appropriate level of corrosion within a reasonable timescale. Using specialist equipment in the laboratory in order to verify the corrosion, the polarity of the current was such that the tendon served as the anode and mesh of titanium which was placed in the bottom of a plastic box retaining the electrolyte solution served as the cathode. The schematic drawing of the arrangement is shown in Figure 4.7. The electrolyte was a solution of water and 3% by weight Sodium Chloride (NaCl). Since there was no protective layer surrounding the tendon, there is no initiation time, i.e. corrosion occurred immediately after the current flow.



- | | | |
|---------------------------------|-----------------------------------|---------------------|
| (1) tendon (anode) | (4) electrolyte - solution/mortar | (7) DC cables |
| (2) titanium mesh (cathode) | (5) plastic box | (8) DC power supply |
| (3) vibrating wire strain gauge | (6) timber mould | |

Figure 4.7 The schematic diagram of acceleration corrosion test

4.6.3.1 Design of accelerated corrosion in the tendon

There are a number of techniques that may be used to accelerate the corrosion of steel in concrete. These include chloride diffusion, salt spray, wet-dry cycling in salt water and impressed anodic current. In this research work the impressed anodic current technique was selected and used on the basis of being relatively fast and quantifiable, based on the current passed. Despite this, the method offers the significant advantages of repeatability and control of the experimental procedure. After exposing the specimens to different levels of pre-stress according to the planned programme as shown in Table 4.1, the tendon specimens were immersed in either mortar or saline solution in a plastic container. The solution contained 1 litre of water with 3% NaCl for accelerated corrosion. Based on Faraday's Law, the degree of corrosion (as a percentage of reduction in reinforcing bar diameter) is defined by the expression $(2Rt'/D) \times 100$ percent, where R is the rate of corrosion in mm/year, D is the tendon bar diameter in mm, and t' is the time in years after corrosion initiation (see Section 3.9.1).

The tendon in each specimen was subjected to general corrosion by applying an anodic impressed current provided by a DC power supply. Three different percentages of corrosion were selected, Stage I (control), Stage II and Stage III.

Applying a unit degree of corrosion, $m = 1\%$, Equation 3.8 was used to determine the time taken to achieve Stages II and III degree of corrosion:

$$\frac{2 \times R \times t'}{D} = \frac{m}{100} \rightarrow R = \frac{m \times D}{2(100)t'} = \frac{m \times D}{200 \times t'} = 1165i \rightarrow t' = \frac{m \times D}{200 (1165 \times i)}$$

Equation 4.1

Substituting, $m= 3\%$, $i=1\text{mA/cm}^2$ and $D=0.54\text{cm}$ into Equation 4.1 gives:

$$t' = \frac{3 \times 0.54}{200 (1.165)} = 0.00695 \text{ years} = 2.536 \text{ days} = 60.8 \text{ hours}$$

Equation 4.2

The length of tendon surrounded by the solution is 30.7cm. The total surface area, a , of the tendon is: $a = \pi \times D \times L = 16.578 \pi \text{ cm}^2$

Therefore, the current required for 3% degree of corrosion per tendon is obtained from:

$$I = i \times a = 1 \times 16.578 \pi = 52.08 \text{ per specimen}$$

Equation 4.3

Applying the same procedure above for 6% degree of corrosion, the time required to achieve 6% degree of corrosion is 0.0139 years, 5.08 days or 121.81 hours. The current remains constant at 52.08 mA.

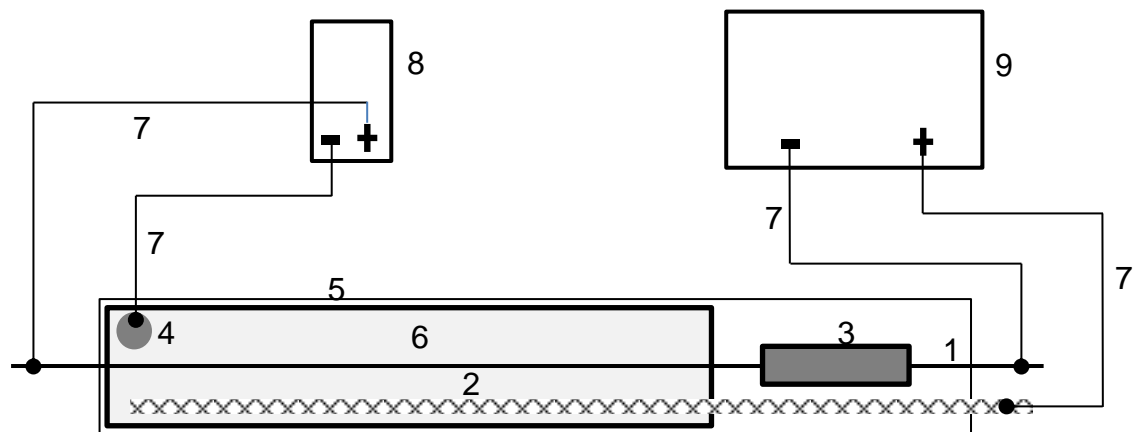
The degree of corrosion was measured both as gravimetric weight loss and reduction in the diameter of the tendons. With regards to the gravimetric weight loss method, the tendon was weighted before the specimens were corroded. A predefined degree of corrosion was applied to the tendons over a specified period of time. Upon completion of the corrosion period, the tendons were removed from the solution or mortar, cleaned by di-Ammonium hydrogen citrate and with a wire brush and re-weighted. The percentage loss in weight was subsequently calculated which present the actual degree of corrosion. The

second method to determine the percentage of corrosion was similarly performed, except that the average rebar diameter both before and after corrosion was measured and the loss was determined from a reduction in the diameter.

4.7 Impressed Current Cathodic Protection (ICCP)

A cathodic protection system comprises a number of basic components which include the following and a schematic illustration of the cathodic protection system is given in Figure 4.8:

- Titanium mesh acts as the anode
- Tendon acts as the cathode
- DC Power supply and rectifier
- Solution or gunite as the electrolyte
- Cabling to carry the system power and the monitoring signals
- Reference electrode (SSC)
- Digital voltage meter (DVM)
- Data Logger to record the strain readings
- Data logger software and laptop



- | | | |
|---------------------------------|-----------------------------------|---------------------|
| (1) tendon (cathode) | (4) reference electrode | (7) DC cables |
| (2) titanium mesh (anode) | (5) timber mould | (8) DVM |
| (3) vibrating wire strain gauge | (6) electrolyte - solution/mortar | (9) DC power supply |

Figure 4.8 Schematic diagram of ICCP set-up

The positive terminal of a direct current power source is connected to a conductive material of titanium mesh (anode). The negative terminal is connected to the tendon (cathode) and a DC power supply is applied. This

causes a flow of electrons from the anode through the solution/gunite to the tendon. The ICCP system was operated in the Construction Materials Laboratory with a relatively stable environment of average 20°C temperature and humidity of 60% ±5% (Figure 4.9).

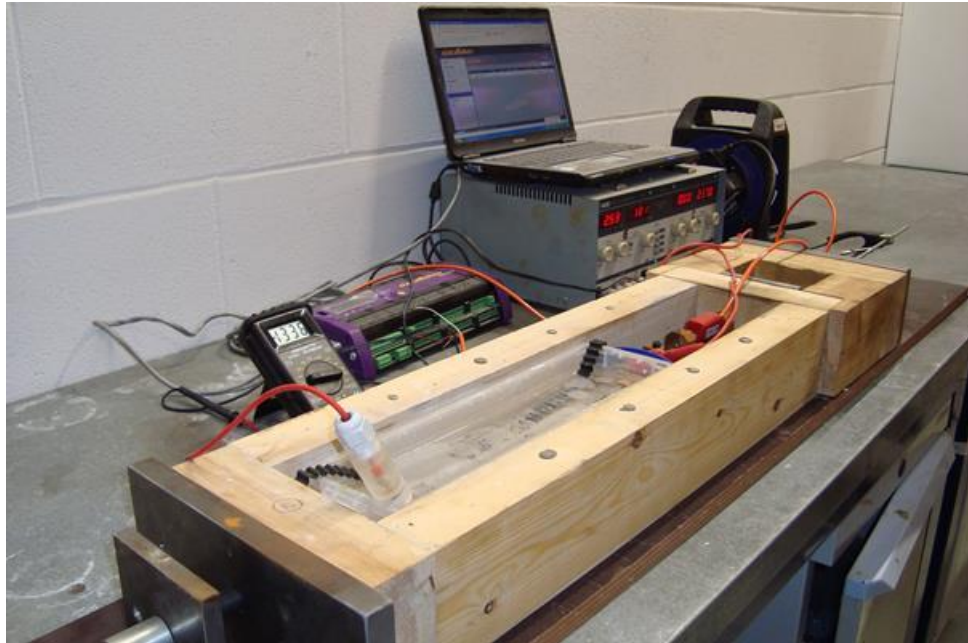


Figure 4.9 ICCP Components

4.7.1 Design of ICCP for corrosion control

Preliminary tests were carried out before commencing the formal research programme to confirm the reliability of the ICCP technique. The aim of ICCP is not only to protect the steel, but also determine if and when hydrogen is generated and its effect on the tendon. For this purpose, a high potential (-1.4V) was applied which exceeds the normal potential of -950mV. After completing the accelerated corrosion process by achieving the required period to reach to the target degree of corrosion, the ICCP process is commenced. Constituents comprising of one litre of water, 3% of sodium chloride (NaCl) and 3gm of calcium hydroxide ($\text{Ca}(\text{OH})_2$) were added to the plastic box to act as the electrolyte (Figure 4.10). The purpose of adding the calcium hydroxide is to maintain the pH at about 12 and this level of pH was recorded and maintained during the period of the test. The temperature was also recorded throughout the ICCP period. The tendon was connected to the negative terminal of the DC to act as a cathode and the titanium mesh connected to the positive terminal of the DC to act as an anode. Before starting the test, a datum reading of potential

was taken. The voltage and the current were adjusted so hydrogen was generated and once reached, the voltage is kept constantly at 2.54 V giving an instant-off potential of -812 mV. The test process and monitoring is conducted in accordance with BS EN ISO 12696:2016 [77] and with the Concrete Society Technical Report No.73 [48], including instant-off to confirm that ICCP was being achieved. The strain of the galvanised tendon was taken from the beginning of the test until the completion of ICCP test. After completion of ICCP, the galvanised tendon was removed, reweighed and the percentage of metal lost was calculated.

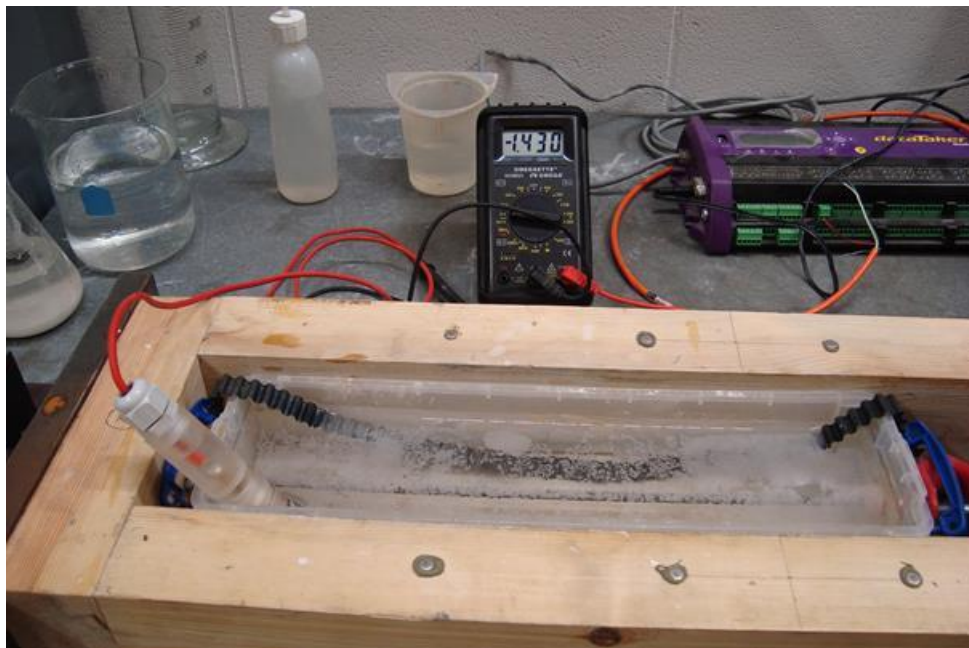


Figure 4.10 ICCP test in progress

4.8 Hydrogen test

The inert gas fusion and thermal conductivity methods are widely used for quantitative determination of hydrogen (H) in metals. A portion of sample is heated to 3000°C in an electrode furnace. Firstly, the sample is placed in a gas inert environment (He) and current is passed through the graphite crucible producing enough heat to melt the sample. The different gases produced are separated in the separation column and H₂ is measured by a thermal conductivity cell by comparing the conductivity of a pure inert gas with the sample conductivity (Figure 4.11)



Figure 4.11 Hydrogen test machine

4.9 Materials

4.9.1 Tendon

Galvanised and un-galvanised smooth pre-stressing tendons, with a length of 1.4 m and 5.4 mm in diameter are used in this research. Tendons were obtained from Bridon International Ltd, UK. According to the technical information provided by the supplier, the tendon supplied was the king wire of a seven wire strand. The method of manufacture for the galvanised version is 12.0mm drawn to 7.9mm, hot dip galvanised and then drawn to 5.4mm. The uncoated tendon is 12.0mm drawn direct down to 5.4mm. The ultimate tensile strength (UTS) is approximately 1800MPa. The chemical composition of the tendon, for both galvanised and ungalvanised (V micro alloyed rod) is given in Table 4.2.

Table 4.2 Composition of galvanised and ungalvanised tendons

<i>Material</i>	<i>Galvanised (%)</i>	<i>Un-Galvanised (%)</i>
Carbon	0.89	0.88
Silicon	0.24	0.26
Manganese	0.68	0.66
Phosphorous	0.009	0.013
Sulphur	0.015	0.014
Chromium	0.016	0.11
Molybdenum	0.003	0.01
Nickel	0.018	0.04
Aluminium	0.001	0.002
Copper	0.012	0.05
Nitrogen	0.006	0.004
Lead	0.001	
Tin	0.002	0.004
Vanadium	0.077	0.002
Titanium	0.00	

4.9.2 MMO Titanium Mesh

The Mixed Metal Oxide (MMO) titanium mesh type 170 Anode Ribbon Mesh was obtained from CORRPRO Companies Europe Limited, Adam Street, Bowesfield Lane, Stockton-on-Tees, UK. The titanium mesh is used as the cathode to induce corrosion and as an anode, its intended purpose, in ICCP applications. The specification of the MMO titanium mesh is shown in Table 4.3. For the purpose of this research the short term current density applied to the anode exceeded the recommended limits but did not have a detrimental effect on its ability to achieve overprotection of the tendons.

4.9.3 Cement

CEM II/A-L 32.5 N Portland -limestone cement which conforms to BS EN 197-1:2011 was used for gunite specimens. It was manufactured by Castle and supplied by The Builders Centre Ltd, Sheffield.

4.9.4 Aggregates

Coarse sharp sand (50% passing a 600 μm sieve) was used for mortar specimens. It was supplied by The Builders Centre Ltd, Sheffield.

4.9.5 Sodium Chloride

Sodium chloride was obtained from Fisher Scientific UK. It was added to the solution and gunite mix at 3.5% by weight of both solution and cement.

Table 4.3 Specification of MMO titanium mesh

<i>Performance specifications</i>	
Current Rating @ 110 mA/sq.m	5.3mA/m (1.61 mA/ft) (10mA/sq.ft)
Expected life (NACE standard TM02944-94)	75 years
Catalyst	Mixed Metal Oxide
Maximum anode concrete interface current density	
FHWA limit	110mA/sq.m (10mA/sq.ft)
Short-term limit	220mA/sq.m (20 mA/sq.ft)
<i>Dimensions</i>	
Width	20mm (0.79")
Coil length	76m (250ft)
Actual anode surface per unit length of anode	0.050sq.m/m(0.165sq.ft/ft)
Expanded thickness	1.30 mm (0.051")
Diamond dimensions	2.5mmx4.6mmx0.6mm
Shipping weight per coil	2.8 kg (6.1 lbs)
<i>Substrate</i>	
Composition	Titanium, Grade 1 per ASTM B265
Coefficient of thermal expansion	8.7 x 10 ⁻⁵ /Deg K (0.000048/in/in/Deg K)
Thermal conductivity @ 20 Deg C	15.6 W/sq.m-DegK (9.0) BTU/hr/sq.ft/Deg F./ft
Electrical resistivity	0.000056 ohm-cm (0.000022 ohm-in)
Modulus of elasticity	105 GPa (14,900,000 PSI) minimum
Tensile strength	245 MPa (35,000 PSI) minimum
Yield strength	175 MPa (25,000 PSI) minimum
Elongation	24% minimum
Resistance lengthwise	0.25 ohm/m (0.076 ohm/ft)
Current distributor resistance lengthwise	0.049 ohm/m (0.015 ohm/ft)

4.9.6 Calcium Hydroxide

Calcium hydroxide was obtained from Fisher Scientific UK. It was added to the solution to eliminate the generation of chlorine gas as a result of the electrochemical reactions and to maintain a pH of 12 and above.

4.9.7 Di-ammonium Hydrogen Citrate

Di-Ammonium hydrogen citrate, extra pure, was obtained from Fisher Scientific UK. It was used to clean the tendon before and after completion of corrosion and ICCP process from the rust. Cleaning the tendon after testing is to allow the actual degree of corrosion to be established. A 5% solution was used.

4.10 Apparatus

4.10.1 DC Power Supply

A DC power supply system (Figure 4.12), has been used to accelerate corrosion on the tendon and apply ICCP. The positive terminal is connected to the anode (tendon) and negative to the cathode for corrosion. This is reversed for the ICCP, the tendon is the cathode and the MMO titanium the anode.



Figure 4.12 DC Multi-Channel Power Supply

4.10.2 Reference Electrode (half-cell)

Different reference electrodes are available for measuring the potential and it is important to know which are being used as the type has a huge bearing on results. Table 4.4 shows the different types with comments.

Table 4.4 Reference electrodes for measurement and calibration

<i>Reference electrode</i>	<i>Comments</i>	<i>Potential (mV vs SHE)</i>
Standard hydrogen electrode (SHE)	Absolute standard for potentials against which all electrodes are quoted. Specialist laboratory only.	0
Saturated copper/copper sulfate (CSE)	Traditional and robust but liable to leakage that could stain and damage concrete.	-320
Silver/silver chloride (1M KCl) (SSC)	Originally for laboratory use, newer polymer body gel-filled version popular for site use.	-220
Saturated mercury/mercury chloride (calomel) (SCE)	Practical laboratory standard for calibrating electrodes before use on site. Potential mercury hazard.	-200

In this research, reference electrode types Silver/Silver Chloride Ag/AgCl/ 0.5M KCl Type WE100 (Figure 4.13) were used to measure the potential of the tendon in both solution and mortar. It was inserted in the solution or applied to the mortar face. It was supplied by Silvion Limited, UK.



Figure 4.13 Reference electrode

4.10.3 Digital Voltage Meter

The digital voltmeter (DVM) used in the investigation (Figure 4.14) has high input impedance so that current flowing through the reference electrode does not cause disturbance or affect its potential. It is manufactured by Omegaette.



Figure 4.14 Digital voltmeter

The voltmeter has a different range of resolution. The potential drop along the cable from the reinforcing steel to the voltmeter was less than 0.1 mV when measured between two previously calibrated reference electrodes.

4.10.4 Data Logger

A dataTaker DT85 is used to record the test results. The dataTaker DT85's dual channel configuration allows up to 32 isolated channel inputs to be used in many combinations (Figure 4.15).



Figure 4.15 Data logger Type 85D

4.10.5 Strain Gauges

Different strain gauges were used to measure the strain in the pre-stressing system during the tensioning process. A digital DEMEC with 300mm gauge length was used to measure the strain (compression) in the timber pre-stressing moulds during tensioning of the tendon. This would enable any losses in pre-stress to be attributed to the tendon and not a contraction of the mould. Two types of vibrating wires gauges were used and supplied by Geosense to continuously measure the strain in the tendon in the stressed state. Strain gauge with a gauge length of 89mm and a strain range of 3000 microstrain was used where lower strains were expected (low level of pre-stress). Where higher strains were expected (High level of pre-stress), a vibrating wire strain gauge with a gauge length of 150mm was used, this had a capacity of 6000 microstrain ($\mu\epsilon$) (Figure 4.16). Specifications of both 89mm and 150mm strain gauges are given in Table 4.5.



Figure 4.16 (a) Demec digital strain gauge, (b) Digital vibrating wire strain gauge

Table 4.5 Geosense VW Strain Gauges Specifications

<i>Model</i>	<i>VWS-2000</i>	<i>VWS-2010</i>
Gauge length (mm)	150	89
Overall Length (mm)	156	95
Resolution ($\mu\epsilon$)	1	1
Strain range ($\mu\epsilon$)	6000	3000
Accuracy	± 0.1 to $\pm 0.5\%$ FS	± 0.1 to $\pm 0.5\%$ FS
Nonlinearity	$< 0.5\%$ FS	$< 0.5\%$ FS
Temperature ($^{\circ}\text{C}$)	-20°C to $+80^{\circ}\text{C}$	-20°C to $+80^{\circ}\text{C}$
Frequency Range ($\mu\epsilon$)	850-1550	900-2000

4.10.6 Hydraulic Jack

A hydraulic jack RCH-121 with 12 tons capacity was supplied by Apex Hydraulic in the UK. It was used to apply different pre-determined tensioning loads to the tendons. It has a hollow centre allowing the tendon to pass through it, thereby enabling a load to be applied. A hand-pump was used to pressurise the cylinder (Figure 4.17).



Figure 4.17 Hydraulic hollow cylinder Jack

4.10.7 Load Cell

Load measurements were taken by means of a 10Te (100 kN) load cell connected to a signal amplifier with low pass filter which in turn was connected to a load cell power supply and laptop (See Figure 4.5 (a)). The amplifier was calibrated to ensure a direct reading of the applied load on the laptop, with an accuracy of 0.1 kN.

4.11 Analytical Methodology

4.11.1 Scanning Electronic Microscopy (SEM)

Fracture surface of the galvanised and ungalvanised specimens was investigated using the scanning electron microscope (SEM) type Quanta 650 (Figure 4.18). The system is equipped with FEI's "MAPS" software which allows for the automated acquisition of large area high-resolution images, and the Oxford Instruments. The Quanta FEG Scanning Electron Microscope (SEM) produces enlarged images of a variety of specimens, achieving magnifications

of over 100000x providing high resolution imaging in a digital format. This analytical tool provides exceptional depth of field, minimal specimen preparation and the ability to combine the technique with X-ray microanalysis. The Quanta FEG has 3 operating vacuum modes to deal with different types of sample. High Vacuum (HiVac) is the conventional operating mode associated with all scanning electron microscopes. The two other application modes are Low Vacuum (LowVac) and ESEM. In these modes the column is under high vacuum and the specimen chamber is at a high pressure range of 0.1 to 30 Torr (15 to 4000 Pa) [88].

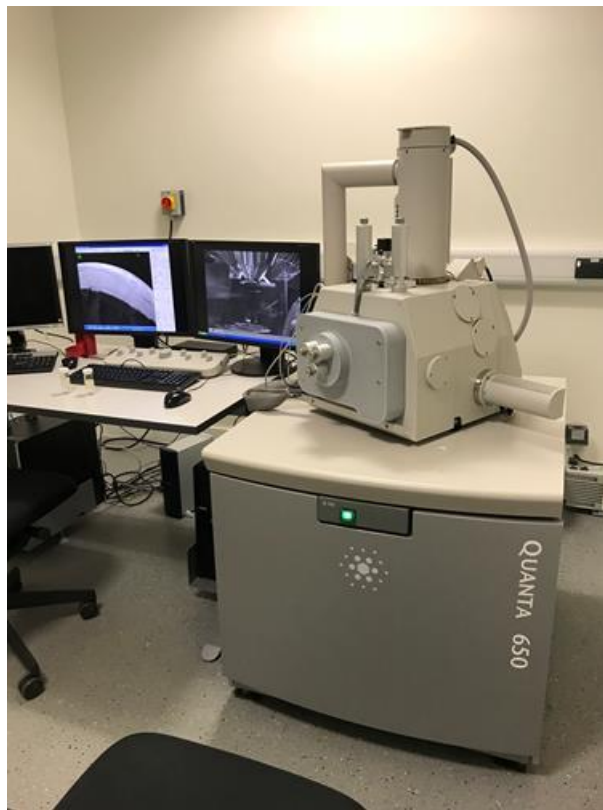


Figure 4.18 Scanning Electronic Microscopy (SEM)

4.11.1.1 Principle of SEM

Four main components combine to produce the images from the sample: an electron gun, a demagnification unit, a scan unit and a detection unit (Figure 4.19). The electron gun, which is the source emitter, produces electrons within a small spatial volume with a small angular spread and a selectable energy. This beam enters the demagnification unit, consisting of several electron lenses, and exits to arrive at the specimen surface with a much smaller diameter than that produced by the gun.

Electrons striking the specimen react with the atoms of the sample surface and produce three types of signals: X-rays, electrons, and photons. The main detector system picks up the electrons, amplifies them and converts them into electrical voltage, which is sent to the Monitor to control the intensity of the scanning spot. The scan generator signal, fed to the deflection system of the Monitor, moves the beam in a raster pattern over the specimen area. The electrical voltage changes as it rasters, which provides serial information of the specimen surface. This signal, modulated by the one from the detection system, produces the onscreen image.

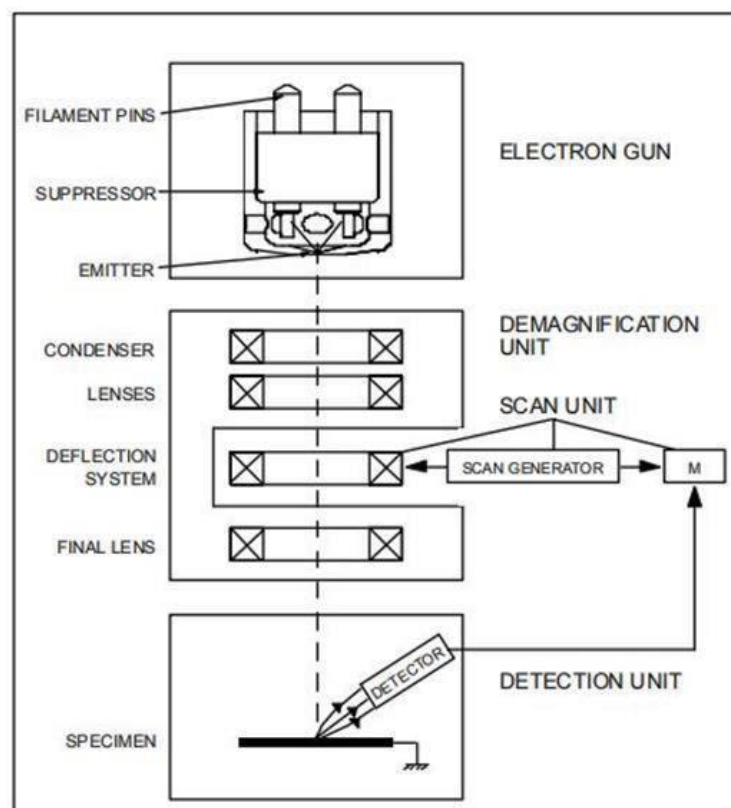


Figure 4.19 SEM principle schematic diagram [88]

The images obtained show the shape of the fracture after a tensile test was conducted to the tendons. The shape of fracture is compared to samples tested before and after the application of cathodic protection to study the effect of any hydrogen evolution or damage in the tendon.

Figure 4.20 (a) and (b) shows the cutting of the sample to fit with the sample holder and the SEM's chamber using the cutting machine type Delta Abrasimet made by Buehler.



(a) Cutting machine



(b) Cutting sample of tendon

Figure 4.20 Cutting SEM samples

Samples are subsequently cleaned from dust using Dust-Off and placed on the aluminum holder stub using a double sticky carbon film (Figure 4.21).

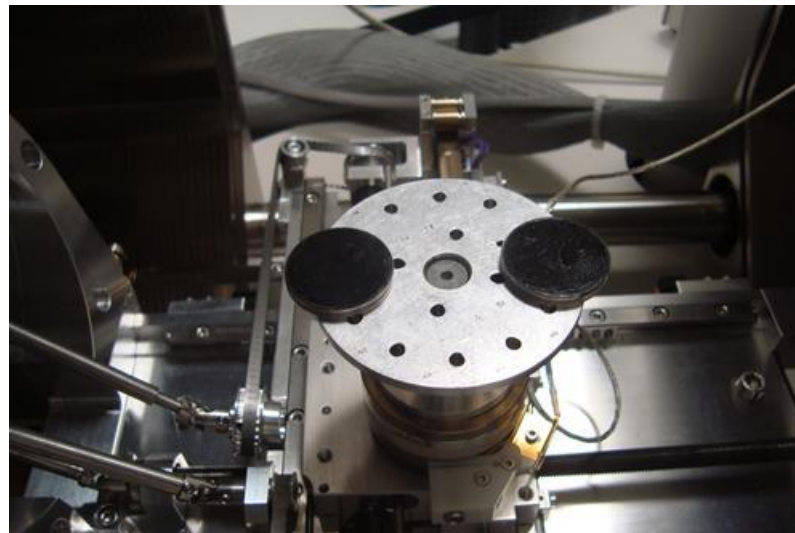


Figure 4.21 Aluminium holder with a double sticky carbon film

Several settings of SEM images trials were investigated to obtain the optimum resolution of the images and to standardize the setting for all images taken (Figure 4.6).

Table 4.6 Settings for SEM images

<i>Image</i>	<i>Spot</i>	<i>Det</i>	<i>HV</i> (<i>kV</i>)	<i>WD</i> (<i>mm</i>)	<i>Magnification</i>	<i>Scale</i> (μm)
Fracture	6	ETD	30	10mm	75	2000
Centre of fracture	6	ETD	30	10mm	500	400
Edge of fracture	4	ETD	30	10mm	1000	200

4.11.2 X-Ray Diffraction (XRD)

Sedimentation due to the reaction occurring during application of accelerated corrosion within the solution electrolyte on galvanised and ungalvanised specimens were investigated using the XRD as presented in Figure 4.22 (a) and (b). In addition, corrosion products on galvanised and ungalvanised specimens were investigated also using the XRD. This investigation applied when completing corrosion and ICCP tests, samples of corrosion products were taken and investigated.



(a) XRD Instrument



(b) Sample preparation

Figure 4.22 X-Ray Diffraction (XRD)

4.11.3 Infinite Focus Microscope (IFM)

Using a 3D micro coordinate measurement machine by Alicona, surface images before and after removing the corrosion products were taken. Surface integrity analysis is performed using Infinite Focus Microscope (IFM) Figure 4.23 (a) and (b). The Infinite Focus Microscope (IFM) is an optical 3D measurement device which allows the acquisition of datasets at a high depth of focus. First a stack of n images from the lowest to the highest plane of the surface features is acquired. Then the positions in the stack are determined where each image

point is best in focus. This leads to an overall sharp image and to a reconstruction of the surface, where a height value exists for each point on a ground plane. The IFM method allows capturing images with a lateral resolution down to 400 nm and a vertical resolution down to 20 nm [89]. The IFM 3.5 software version was used for the measurements. With a high magnification X50, roughness of the surface on both galvanised and ungalvanized tendons were measured. Corrosion pit widths were measured and comparisons with different stages of corrosion were made.



(a)



(b)

Figure 4.23 Infinite Focus Measurement (IFM) (a), taking image (b)

4.11.4 Tensile Test

Tensile Testing of tendons is a destructive test process that provides information about the mechanical properties including ultimate tensile strength, yield strength and ductility of the material. ESH600 Machine with load capacity 600 kN and an Epsilon Extensometer (50mm) were used. All tests were conducted in the Construction Materials Laboratory with a relatively stable environment of average 20°C temperature and humidity of 60% \pm 5%. Tensile tests were conducted in accordance with industry standards and specifications BS EN ISO 6892-1:2016, Metallic Materials-Tensile testing, tensile test methods [90].

Material strength testing, using the tensile or tension test method, involves applying two phases of an increasing load to a test specimen up to the point of failure. The process creates a stress/strain curve showing how the material reacts throughout the tensile test. The data generated during tensile testing is used to determine mechanical properties of tendons and provides elastic

modulus, percent elongation and includes the following quantitative measurements:

- Tensile strength, also known as Ultimate Tensile Strength (UTS), is the maximum tensile stress carried by the specimen, defined as the maximum load divided by the original cross-sectional area of the test sample.
- Yield strength is the stress at which time permanent (plastic) deformation or yielding is observed to begin.
- Ductility measurements are typically elongation, defined as the strain at, or after, the point of fracture, and reduction of area after the fracture of the test sample.

The test sample is securely held by top and bottom grips attached to the tensile or universal testing machine. During the tension test, the grips are moved apart at a constant rate to pull and stretch the specimen. The force on the specimen and its displacement is continuously monitored and plotted on a stress-strain curve until failure.

The measurements, tensile strength, proof strength and elongation, were calculated after the tensile test specimen has broken. The test specimen is put back together to measure the final length, then this measurement is compared to the pre-test or original length to obtain elongation. The original cross section measurement is also compared to the final cross section to obtain the reduction in area.

4.11.4.1 Procedure of Tensile Test

The following procedure was adopted in ensuring that the data recorded from tensile test specimens was taken in an organised and consistent manner.

1. Hold the sample in two developed clamps and securely held by top and bottom grips.
2. Before loading the specimens in the ESH600 machine, the computer system connected to the machine was set up by inputting the necessary information of gauge length, diameter and parallel length of the specimen. The computer system was then prepared to record data and output necessary load-deflection graphs.
3. The specimens were loaded into the ESH600 machine, and a tensile test was performed. The data was recorded electronically in text files and the stress-

strain curve was shown on the computer screen as a visual representation. Figure 4.24 shows both shield ESH600 tensile machine and extensometer used to conduct the tensile test.



(a) Tensile test machine

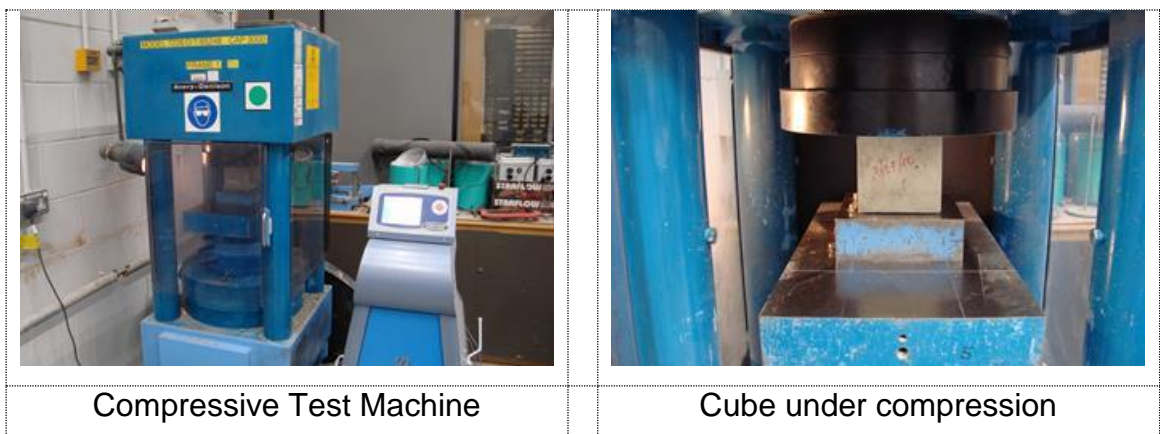


(b) Extensometer

Figure 4.24 Tensile test machine ESH600 and extensometer

4.11.5 Compressive strength

Compressive strength tests to BS 1881 Part 4: Section 2: 1970 "Tests for compressive strength of test cubes" were carried out to ensure that mortar specimens complied with the mix design parameters. Compression test machine type Avery-Denison, Model 7226/D/T/85248 CAP 3000 was used for this purpose. Three 100 mm standard test cubes were cast for each batch, demoulded at 24 hours and stored underwater before testing at 28 days. Each cube was surface dried, weighed and then tested to failure (Figure 4.25).



Compressive Test Machine

Cube under compression

Figure 4.25 Compressive test machine

4.11.6 Visual examination

Information regarding physical changes or signs of deterioration was obtained from visual examinations. Optical binocular microscopy was used to enhance observations and images were recorded using an attached camera. Greater depth of field and magnification were achieved by scanning electron microscopy.

5 Effect of accelerated corrosion on the applied service stress in tendons

5.1 Introduction

Reinforced and pre-stressed concrete represents a very successful combination of materials, not only from a mechanical point of view but also from a chemical perspective, because the hydrated cement is able to provide excellent protection against steel corrosion [91]. Corrosion occurs when metals react with their elements in their environment [92]. Corrosion in the presence of water occurs by an electrochemical mechanism [93].

One of the major causes of damage to reinforced concrete (RC) structures is the corrosion of steel in the concrete. There has been considerable research on the effect of corrosion on the performance of RC members. Corrosion of steel in concrete is an electrochemical process which can take a long time to develop naturally. Due to the protective nature of concrete, it takes a reasonably long time for initiation and progress of reinforcement corrosion even in the case of severe corrosive exposure conditions [94]. Due to time limitations in laboratory investigations, accelerated corrosion of steel in concrete has been used to simulate natural corrosion within a manageable timescale. There are different techniques such as wet and dry cycling and anodic impressed current, the latter is particularly used because of its relative speed. An impressed D.C. current is passed to the reinforcing steel acting as an anode [95], [96]. The reinforced steel is corroded, the extent being proportional to the quantity of current passed as defined by Faraday's Law [24], [82], [97]. The relationship between the applied D.C. current, time, and the degree of corrosion with the applied service stress in pretension tendons has not been fully investigated. This chapter will examine the effect of these variables on the performance of the pre-tensioned tendon.

5.2 The objectives of the tests

The test programme was selected to:

- investigate and measure the parameters of accelerated corrosion techniques

- investigate the loss of applied pre-stress during the corrosion period
- observe any change on the surface of the electrolyte

5.3 Anodic impressed current technique

An anodic impressed current technique has been selected for this study, to accelerate the corrosion of steel in mortar on the basis of reducing the duration to achieve the required level of corrosion [98]. This method was found to be extremely effective at rapidly initiating the corrosion of steel when compared to the natural corrosion initiation of steel in concrete which can be several years [99]. The other advantage of this technique is that the amount of corrosion generated can be calculated from the current passed using Faraday's Law. The principle of this technique has been described in Sections 3.5, 4.6.3 and 4.6.3.1. There are some differences that can be found between accelerated corrosion by impressed anodic current and naturally occurring corrosion. In terms of the latter, both the cathodic and anodic reactions take place at the reinforcement surface, while in the former, the reinforcement is forced to operate solely as an anode while an external steel electrode acts as the cathode, remote from the reinforcement. In the case of the mechanism of corrosion product formation, with natural corrosion, Fe^{2+} released from the anodic sites on the reinforcement, combines with OH^- from the cathodic reaction and corrosion products form at the steel/concrete interface. The volume of the corrosion products is greater than the original metal. The surrounding concrete, therefore, can develop cracks when the volume of corrosion products at the interface exceeds a critical value [87]. In the case of accelerated corrosion, Fe^{2+} from the reinforcement combines with free OH^- within the concrete pore solution to form the corrosion product $\text{Fe}(\text{OH})_2$, which may reduce the pH of the pore solution. Once all the free OH^- at the interface has combined with Fe^{2+} to form $\text{Fe}(\text{OH})_2$, this process will progress further within the concrete cover zone where alkalinity remains high. Consequently, the formation of the corrosion product $\text{Fe}(\text{OH})_2$ tends to move outward from the steel-concrete interface with rust staining occurring more quickly than for natural corrosion [87].

5.4 Experimental Works

5.4.1 Test programme

As shown in Table 4.1, the detailed experimental programme and to the research work, the specimens have been divided into 4 batches. Each batch has parameters in terms of type of the tendon, level of pre-stress, degree of corrosion and a control specimen representing Stage I corrosion as shown in Table 5.1. The objective of generating different degree of corrosion is to replicate the site problem and to investigate its effect on the applied service stress and to apply the cathodic protection.

Table 5.1 Tests programme

<i>Batch</i>	<i>Test code</i>	<i>Target degree of corrosion</i>
		<i>Stage</i>
1	S-U-L-I-1	I
	S-U-L-II-O-2	II
	S-U-L-III-O-3	III
	S-U-H-I-1	I
	S-U-H-II-O-2	II
	S-U-H-III-O-3	III
2	M-U-L-X-1	I
	M-U-L-II-N-2	II
	M-U-L-III-N-3	III
	M-U-H-X-1	I
	M-U-H-II-N-2	II
	M-U-H-III-N-3	III
3	M-U-L-X1-1	I
	M-U-L-II-O-2	II
	M-U-L-III-O-3	III
	M-U-H-X1-1	I
	M-U-H-II-O-2	II
	M-U-H-III-O-3	III
4	M-G-H-X-1	I
	M-G-H-II-N-1	II
	M-G-H-III-N-3	III
	M-G-H-X1-1	I
	M-G-H-II-O-2	II
	M-G-H-III-O-3	III

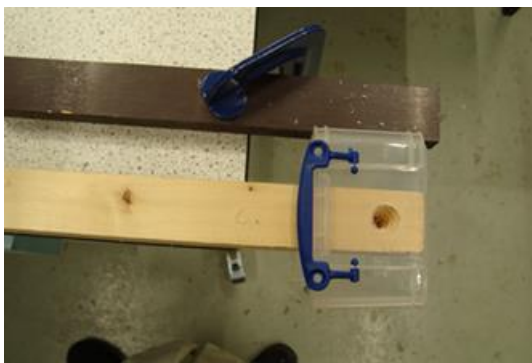
Key: U-Ungalvanised, G-Galvanised, M-Mortar electrolyte, S-Solution electrolyte, H-High level of pre-stress (800-1200MPa), L-Low level of pre-stress (300-400MPa), I-Degree of corrosion Stage I (0-1%), II-Degree of corrosion Stage II (2-4%), III-Degree of corrosion Stage III (4-7%), N-Normal protection, O-Overprotection, X and X1-no corrosion and no ICCP, R-As-received samples, 1, 2, 3-Sample numbers.

5.4.2 Tests in saline electrolyte

For the purpose of the test, batch one, plastic boxes with internal dimensions 320 mm length, 80 mm width and 60 mm depth were employed to contain the saline solution. Two holes were made in each end face of the box to allow the tendon to pass through with tight fitting bungs to prevent any leakage as shown in Figure 5.1. The saline solution consisted of water and 5 % by weight sodium chloride (NaCl) in order to promote the corrosion of the tendon.



Plastic box in a prestressing timber mould with test ongoing



Plastic box with drilled end to allow the tendon go through



Drilled Plastic box ready to use

Figure 5.1 Test set-up for saline electrolyte

5.4.3 Test in mortar electrolyte

When in service, preload pre-stressing tendons commonly protected with gunite (shotcrete). The gunite was replicated in the laboratory as a mortar and a number of trials were conducted to ensure that the mortar has similar performance criteria to that used on-site.

Figure 5.2 shows the design of specimens for the experimental work, each of 320mm length with a rectangular cross-section of 90 mm depth and 100 mm width. Each specimen was reinforced by a pre-stressed galvanised or ungalvanised tendon, 5.4mm diameter with UTS of around 1800MPa.

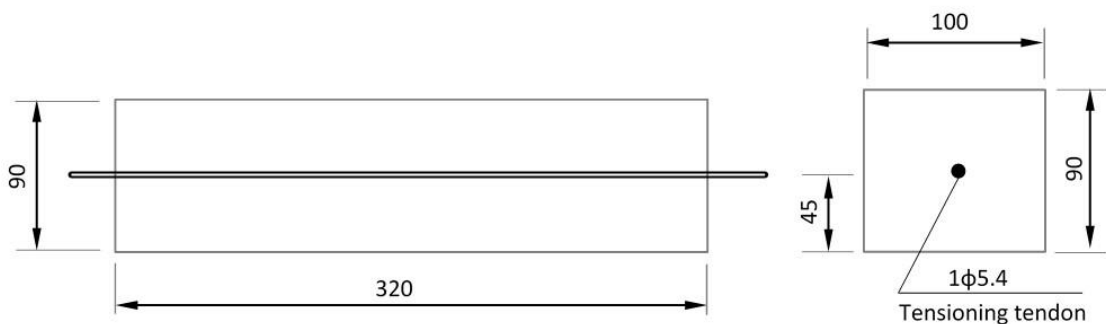


Figure 5.2 Specimens dimension (mm)

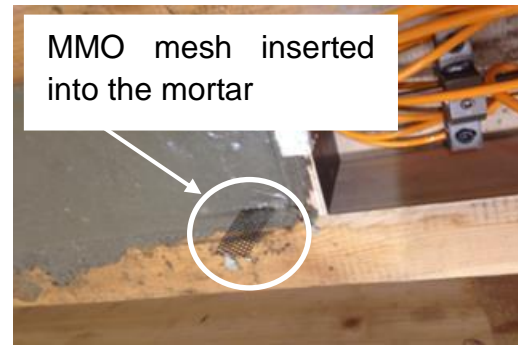
5.4.3.1 Mortar mix design and casting

It was determined that the mortar normally used in-situ is approximately Grade 35 N/mm² with a cement content of about 340 kg/m³. This mix was replicated in the laboratory to ensure it was appropriately moist to replicate the gunite applied mortar used on site. The mortar mix was designed to have high workability and achieve an average 28 day cube strength in accordance with BS EN 12390-3: 2009 of over 35 MPa. The mortar mix proportion was cement: sand: water of 1:3:0.4. The sand was oven dried at 100°C for 24 hours to eliminate the free water content and then maintained in a dry condition prior to use. The sand and cement were dry mixed in a mechanical mixer for about one minute before adding water gradually. In order to incorporate any residual dry material sticking to the mixer surface, a further hand mixing of the wet mix was carried out. The wet mix was then cast into the timber moulds in layers and each layer was carefully compacted by a vibrating poker, Figure 5.3 (a-c). After casting, the timber moulds were covered with polyethylene sheets and cured in the laboratory. The cast moulds were then kept moist by spraying water at 20°C

for a further 27 days (28 days in total). Cube specimens were cast for each mix and tested for compressive strength in accordance with BS EN 12390-3: 2009. Cubes were tested at 1, 14, and 28 days age as shown in Figure 5.3.



(a) Casting the mortar in the mould



(b) Placing MMO mesh



(c) Casting cubes



(d) Testing cubes

Figure 5.3 Casting the mortar and testing the cubes

The density of the concrete mixes and their compressive strengths at 28 days are given in Table 5.2.

It is important that all moulds in the same group were cast carefully to ensure the same quality and strength. Therefore, the procedure of drying aggregates, mixing, casting and curing was carried out with great care. Cubes were cast at the same time as casting of the moulds to ensure that they represented the compressive strength of the corresponding moulds.

Table 5.2 Compressive strength of mortar at 28 days

Sample ID	Cube ID	Weight	Crushing load	Density	Compressive strength	Mean compressive strength
		(g)	(kN)	(Kg/m ³)	(MPa)	(MPa)
M-U-L-X-1	A	2140	442	2140	44	46
M-U-L-II-N-2						
M-U-L-III-N-3						
M-U-L-X-1	B	2150	470	2150	47	
M-U-L-II-N-2						
M-U-L-III-N-3						
M-U-L-X1-1	A**	870	245	2062	44	45
M-U-L-II-O-2						
M-U-L-III-O-3						
M-U-H-X1-1	B**	870	260	2062	46	
M-U-H-II-O-2						
M-U-H-III-O-3						
M-G-H-X-1	100	2096	355	2096	35	35
M-G-H-II-N-2						
M-G-H-III-N-3						
M-G-H-X1-1						
M-G-H-II-O-2						
M-G-H-III-O-3						

* Key: U-Ungalvanised, G-Galvanised, M-Mortar electrolyte, S-Solution electrolyte, H-High level of pre-stress (800-1200MPa), L-Low level of pre-stress (300-400MPa), I-Degree of corrosion Stage I (0-1%), II-Degree of corrosion Stage II (2-4%), III-Degree of corrosion Stage III (4-7%), N-Normal protection, O-Overprotection, X and X1-no corrosion and no ICCP, R-As-received samples, 1, 2, 3-Sample numbers.

** Cube size 75 x 75 x75mm, the remainder is 100 x 100 x 100mm

5.4.4 Pre-tensioning and installing strain gauges

Twelve pre-stressing timber moulds were manufactured with external dimensions 675x200x100mm as shown in Figure 4.2. Six have been used for each batch. The timber mould was fastened to a plywood (WISA-Form) base and was used to pre-load the tendon, providing formwork for conducting accelerated corrosion and later applying ICCP in tendons immersed in a saline solution and embedded mortar electrolytes. A hollow cylinder/pre-stressing jack, hand pump, wedges, washers and anchorage were used for pre-stressing the tendon to different level of pre-stress, Figure 5.4.

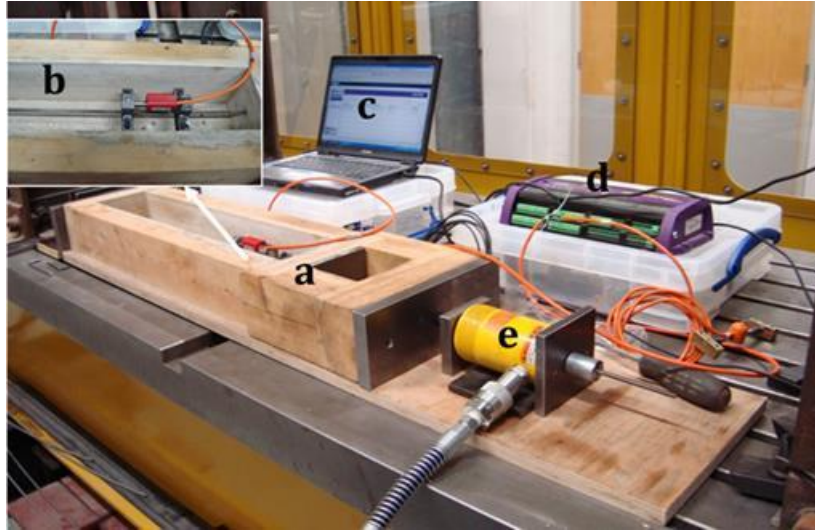


Figure 5.4 Pre-stressing System (a) mould; (b) strain gauge; (c) laptop; (d) data logger; (e) hydraulic jack connected to hand pump

Ungalvanised and galvanised tendons used were king wires from a 15.7mm, seven strand stay cable measured around 5.4mm diameter with a length of 1.4m. The ultimate strength is approximately 1800MPa.

The strain in the tendons was measured using vibrating wire strain gauges (VWSG) firmly attached to the tendons. The change in microstrain ($\Delta\mu\varepsilon$) was obtained by subtracting the initial strain from subsequent strains as shown in Eq. 5.1, then the applied service stress was obtained by multiplying the strain by the modulus of elasticity ($E=220$ GPa) as given in Table 5.3:

$$\Delta\mu\varepsilon = \left[\left(\frac{F_2^2}{1000} \right) - \left(\frac{F_1^2}{1000} \right) \right] (\text{Gauge Factor} \times \text{Batch Factor}) \quad \text{Equation 5.1}$$

where:

$\Delta\mu\varepsilon$ = the strain change in microstrain

F_1 = datum frequency of the VWSG (Hz).

F_2 = subsequent frequency of the VWSG (Hz).

The Gauge Factor and Batch Factors are constants provided by the supplier (if applicable).

Table 5.3 shows the applied service stress. This included tendons subjected to a low target pre-stress (300-400MPa) and high target pre-stress (800-

1200MPa) in a saline solution and mortar. The tendons are allowed to relax for up to two days before the mortar is cast. The set-up is shown in Figure 5.4.

Table 5.3 Convert obtained strain to applied service stress for tendons

Batch	Test Code	Strain	F1	Target	Actual	Strain	Actual
		gauge		F2	F2		stress
		mm	Hz	Hz	Hz	$\Delta\mu\epsilon$	MPa
1	S-U-L-I-1	89	1004	1599	1608	1894	407
	S-U-L-II-O-2	89	973	1580	1642	2100	452
	S-U-L-III-O-3	89	1163	1703	1751	2057	442
	S-U-H-I-1	150	952	1561	1597	5990	1289
	S-U-H-II-O-2	150	952	1586	1590	5626	1210
	S-U-H-III-O-3	150	952	1586	1590	5626	1210
2	M-U-L-X-1	150	974	1232	1217.29	1959	421
	M-U-L-II-N-2	89	1063	1613	1608.02	1747	376
	M-U-L-III-N-3	150	999	1238	1235.06	1921	413
	M-U-H-X-1	150	1020	1595	1577.99	5282	1136
	M-U-H-II-N-2	150	953	1568	1551.48	5461	1175
	M-U-H-III-N-3	150	981	1645	1584.71	5636	1213
3	M-U-L-X1-1	89	1029	1652	1565.04	1669	359
	M-U-L-II-O-2	89	1088	1670	1625.52	1751	377
	M-U-L-III-O-3	89	1042	1640	1637.36	1915	412
	M-U-H-X1-1	150	987	1640	1637.6	6222	1339
	M-U-H-II-O-2	150	975	1680	1678.24	6798	1463
	M-U-H-III-O-3	150	952	1610	1602.13	6050	1302
4	M-G-H-X-1	150	961	1440	1440	4225	882
	M-G-H-II-N-1	89	1073	2149	2149	4161	869
	M-G-H-III-N-3	150	979	1535	1535	5093	1063
	M-G-H-X1-1	150	1021	2117	2117	4128	862
	M-G-H-II-O-2	150	1029	2244	2244	4773	997
	M-G-H-III-O-3	150	1074	2173	2173	4283	894

Key: U-Ungalvanised, G-Galvanised, M-Mortar electrolyte, S-Solution electrolyte, H-High level of pre-stress (800-1200MPa), L-Low level of pre-stress (300-400MPa), I-Degree of corrosion Stage I (0-1%), II-Degree of corrosion Stage II (2-4%), III-Degree of corrosion Stage III (4-7%), N-Normal protection, O-Overprotection, X and X1-no corrosion and no ICCP, R-As-received samples, 1, 2, 3-Sample numbers.

5.5 Accelerated corrosion process

As discussed in Chapter 4, Section 4.6.3.1, the impressed anodic current technique was selected and used to accelerate the corrosion of the tendons in the samples. After installing the strain gauges and pre-tensioning of the tendons was done, the specimens were ready for exposure to the corrosion. For the purpose of the research work, the specimens have been divided into 4 batches. A constant current density of 1 mA/cm^2 was adopted based on the experience of previous research, and three different stages of corrosion Stage I (0-1%), Stage II (2-4%) and Stage III (4-7%) was conducted.

This method was selected for this study on the basis of being relatively fast and the amount of corrosion generated can be calculated from the current passed using Faraday's Law as discussed in Section 3.5.1.

Details are given in Table 5.4. Specimens of batches 1 to 4 were subjected to three different pre-degree of corrosion as is commonly used for inspection of actual structures, Stage I (0-1%), Stage II (2-4%) and Stage III (4-7%) respectively. Stage I (0-1%) was considered as a control specimen for each batch and was not corroded, therefore effectively 0%.

Table 5.4 Corrosion of tendon - test programme

Batch	Test Code	Length	Target	Corrosion	Applied	Corrosion
		of one tendon (cm)	degree of corrosion (%)	Rate (i) (mA/cm ²)	Current (I) (mA)	Duration (Hrs)
1	S-U-L-I-1	32	0	-	-	-
	S-U-L-II-O-2	32	3	1	54.28	60.90
	S-U-L-III-O-3	32	6	1	54.28	121.81
	S-U-H-I-1	32	0	-	-	-
	S-U-H-II-O-2	32	3	1	54.28	60.90
	S-U-H-III-O-3	32	6	1	54.28	121.81
2	M-U-L-X-1	32	0	-	-	-
	M-U-L-II-N-2	32	3	1	54.28	60.90
	M-U-L-III-N-3	32	6	1	54.28	121.81
	M-U-H-X-1	32	0	-	-	-
	M-U-H-II-N-2	32	3	1	54.28	60.90
	M-U-H-III-N-3	32	6	1	54.28	121.81
3	M-U-L-X1-1	32	0	-	-	-
	M-U-L-II-O-2	32	3	1	54.28	60.90
	M-U-L-III-O-3	32	6	1	54.28	121.81
	M-U-H-X1-1	32	0	-	-	-
	M-U-H-II-O-2	32	3	1	54.28	60.90
	M-U-H-III-O-3	32	6	1	54.28	121.81
4	M-G-H-X-1	32	0	-	-	-
	M-G-H-II-N-1	32	3	1	54.28	60.90
	M-G-H-III-N-3	32	6	1	54.28	121.81
	M-G-H-X1-1	32	0	-	-	-
	M-G-H-II-O-2	32	3		54.28	60.90
	M-G-H-III-O-3	32	6		54.28	121.81

Key: U-Ungalvanised, G-Galvanised, M-Mortar electrolyte, S-Solution electrolyte, H-High level of pre-stress (800-1200MPa), L-Low level of pre-stress (300-400MPa), I-Degree of corrosion Stage I (0-1%), II-Degree of corrosion Stage II (2-4%), III-Degree of corrosion Stage III (4-7%), N-Normal protection, O-Overprotection, X and X1-no corrosion and no ICCP, R-As-received samples, 1, 2, 3-Sample numbers.

5.5.1 Corrosion of tendons in saline solution

Figure 5.5 shows galvanised tendons in a saline solution ready for generating corrosion using the accelerated corrosion technique after completion of pre-stressing stage. Figure 5.6 shows Batch 1 of the specimens under accelerated

corrosion. MMO Ti mesh was connected to the negative terminal of a D.C power supply, working as the cathode, while the pre-stressed tendon was connected to the positive terminal of D.C power supply and corroded. The corrosion process took place in a plastic box containing 3.5% NaCl solution by weight. The solution level in the box was adjusted to ensure adequate submersion of the tendon, but to also allow sufficient oxygen availability for the corrosion processes to occur freely on the anodic tendon. Figure 5.7 shows Batch 1 under accelerated corrosion.

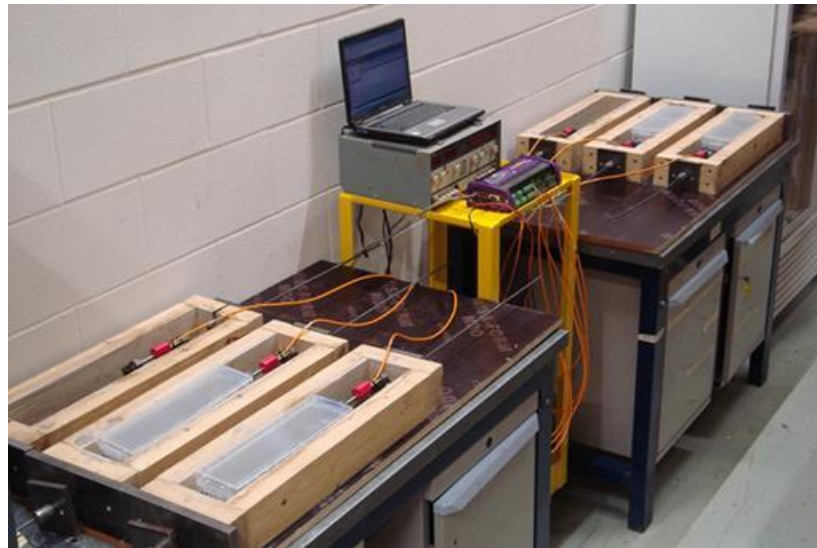


Figure 5.5 Batch 1 with pre-stressed tendons ready for accelerated corrosion

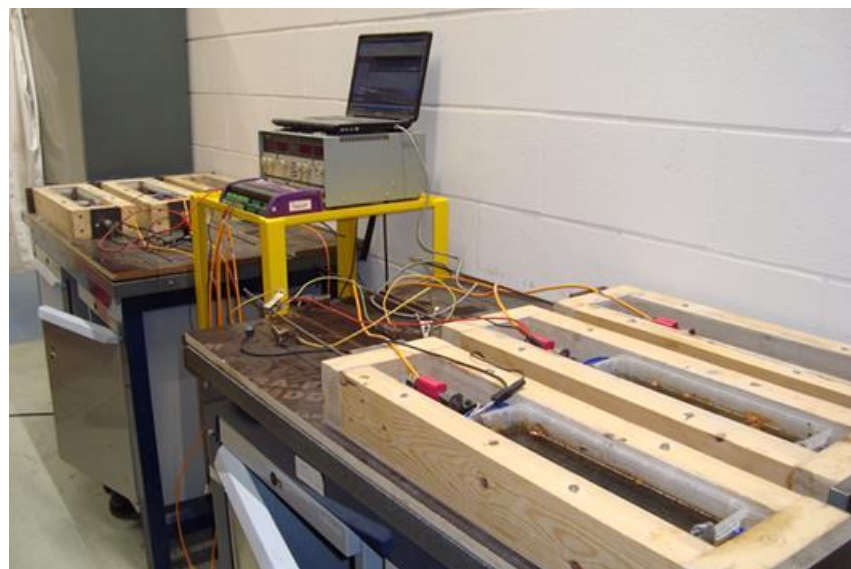


Figure 5.6 Batch 1 specimens under accelerated corrosion

The degree of corrosion was measured both as gravimetric weight loss and reduction in the diameter of the tendons. With regards to the gravimetric weight

loss method, the tendon was weighted before the specimens were corroded. Upon completion of the corrosion period, the tendons were removed from the solution, cleaned with a di-ammonium hydrogen citrate and re-weighted. The percentage loss in weight was subsequently calculated.

The tendon in each specimen was subjected to general corrosion by applying an anodic impressed current provided by the DC power supply to achieve a different corrosion degree as detailed in Section 5.4.1.



Batch 1



Specimens generating hydrogen during accelerated corrosion

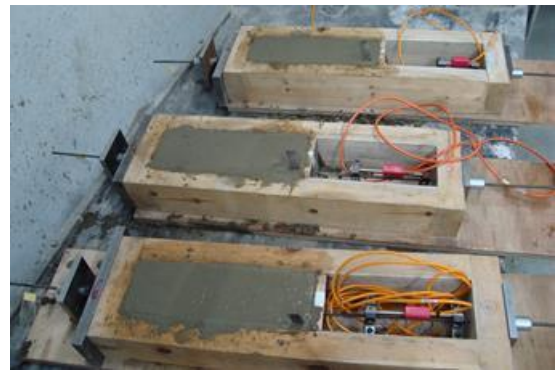
Figure 5.7 Batch 1 specimens under accelerated corrosion

5.5.2 Corrosion of tendons in mortar

After pre-stressing stage, the moulds were cast with mortar as shown in Figure 5.8 (a) & (b).



(a) Pre-stressing moulds and cubes ready for casting



(b) Specimens were casted with mortar

Figure 5.8 Specimens and cubes ready for casting

MMO Ti mesh was embedded into the mortar during casting to ensure a good conductivity and was connected to the negative terminal of a D.C power supply,

working as the cathode while the pre-stressed tendon was connected to the positive terminal of D.C power supply, Figure 5.9.

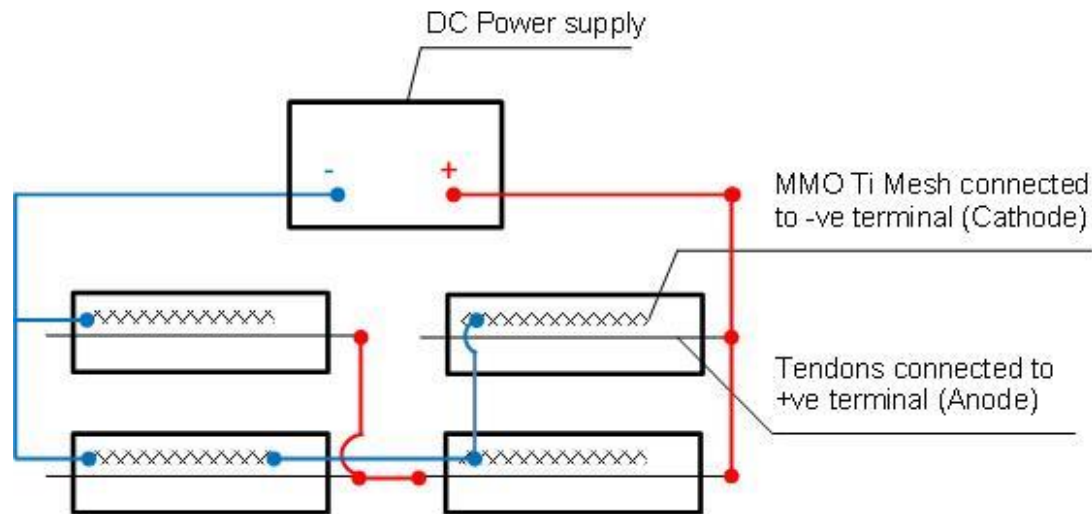


Figure 5.9 Schematic diagram shows the test set-up for one batch

The current density and corrosion period were adjusted for each specimen to give the required degree of corrosion. The current supplied to each beam was checked daily and any drift was corrected. A current density of 1 mA/cm^2 was used to simulate general corrosion. This current density has been successfully employed in Chapter 4 and in other previous research, and allows the required level of corrosion to be achieved within a reasonable timescale. This method produces a uniformly distributed or 'general' form of corrosion. Naturally occurring corrosion tends to be less uniform, therefore decreasing the likelihood of bond loss occurring along the entire anchorage length.

The duration of corrosion was calculated by Faraday's Law (Section 5.5). Three different stages of corrosion were selected Stage I (0-1 % control), Stage II (2-4 %) and Stage III (4-7 %). For all specimens, the applied current was fixed (54.28 mA, Equation 5.8) and corrosion period was adjusted (Equation 5.5) to give the required degree of corrosion (e.g. 20.23 hours for 1 %, 60.90 hours for 3 % and 121.81 hours for 6 %) Figure 5.10.



Figure 5.10 Set of specimens under accelerated corrosion - Batch 2

5.6 Results and discussion

5.6.1 Visual observation

5.6.1.1 Corrosion of tendons in a saline solution

Figure 5.11 shows Batch 1 specimen under accelerated corrosion and each sample was monitored daily during the test in terms of changes in applied service stress via the VWSG data logger and visual inspection for any change in the saline solution. The first sign of corrosion was yellow/brown (rust) staining on the surface of solution which was observed after a few hours (Figure 5.12 (a)). It was also observed after 24 hours that the colour of the corrosion on the solution surface changed first to a darker brown then to black (Figure 5.12 (b)). It was also observed that hydrogen on titanium was generated, as would be expected due to hydrolysis of water. Regarding the pre-stress in the tendon, it was observed that it reduced during the corrosion process; the next section will show this in more detail. Having achieved the required degree of corrosion, cathodic protection (CP) was applied to specimens and monitored. Upon completion of the CP, the tendons were removed and reweighed to determine the weight loss and hence, the actual degree of corrosion.

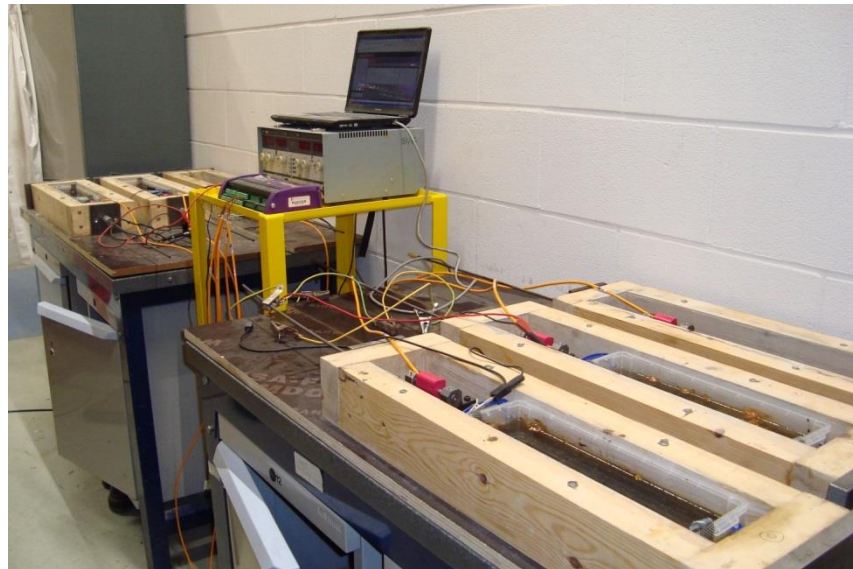


Figure 5.11 Specimens under accelerated corrosion



(a) Yellow to brown rust colour in the solution



(b) Dark brown and black colour in the solution

Figure 5.12 Corrosion of the tendons in the saline solution and colour changes

5.6.1.2 Corrosion of tendons in mortar

The progress of corrosion of each sample was monitored daily. As accelerated corrosion was induced in the tendons, most specimens in batches 2, 3, 4 and 5 a longitudinal crack was observed on the surface of the mortar where the stage III of corrosion was applied. It was observed that longitudinal cracks appeared on the surface of mortar along the pre-stressed tendon (Figure 5.13).



Figure 5.13 Cracks at each stage of corrosion during accelerated corrosion process

These cracks were located along the tendon. Table 5.5 shows the maximum crack width associated with each stage of corrosion, measured to the nearest 0.05 mm by means of a crack-measuring microscope. There is no cracking up to Stage II (2-4 %), while a clearly visible crack occurred when the degree of corrosion increased Stage III (4-7 %), indicating that a threshold stage had been passed.

Table 5.5 Maximum crack width at each stage of corrosion during accelerated corrosion process

	<i>Stage I (0-1%)</i>	<i>Stage II (2-4%)</i>	<i>Stage III (4-6%)</i>
<i>Corrosion stages</i>	<i>Along anode (tendon)</i>	<i>Along anode (tendon)</i>	<i>Along anode (tendon)</i>
Crack width (mm)	0.00	0.00	0.50

The first sign of corrosion was rust staining on the surface of mortar which was observed after a few days for the specimens with Stage III corrosion.

5.6.2 Surface condition of the corroded tendons

5.6.2.1 Visual inspection using digital camera

The corroded tendon was retrieved from each specimen after the accelerated corrosion test and application of ICCP were completed. Each tendon was cleaned to remove the corrosion products by immersing a 10 % diammonium hydrogen citrate solution for 48 hours, in order to remove the corrosion products Figure 5.14.

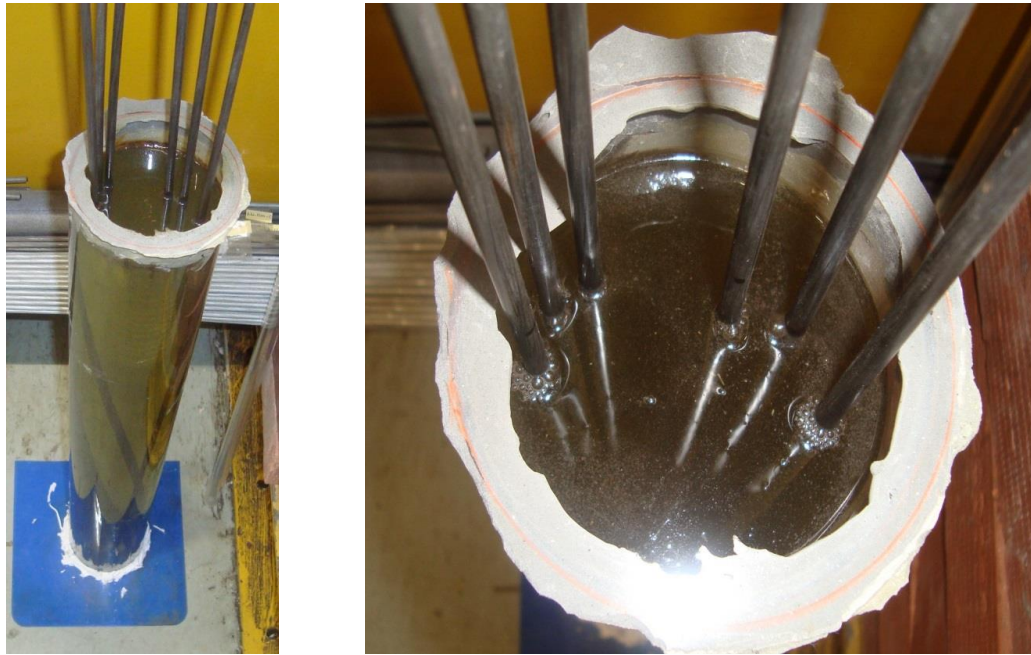


Figure 5.14 Removal of corrosion products with di-ammonium hydrogen citrate solution

After drying in the laboratory air, any remaining corrosion products were removed using a fine glass fibre brush. The surface of the corroded tendon was then examined to analyse the extent and type of corrosion. The corroded surface of the tendon after cleaning is shown in Figure 5.15 to Figure 5.18, images were taken by digital camera (Canon EOS 5D Mark2).



Figure 5.15 Surface of tendon after corrosion - Batch 1



Figure 5.16 Surface of tendon after corrosion - Batch 2

M-U-H-I-N-1 M-U-H-II-N-2 M-U-H-III-N-3 M-U-H-I-O-1 M-U-H-II-O-2 M-U-H-III-O-3



Figure 5.17 Surface of tendon after corrosion - Batch 3

M-G-H-I-N-1 M-G-H-II-N-2 M-G-H-III-N-3 M-G-H-I-O-1 M-G-H-II-O-2 M-G-H-III-O-3



Figure 5.18 Surface of tendon after corrosion - Batch 4

The visual inspection of the tendon surface condition indicates that localised corrosion appeared more clearly defined at higher degrees of pre-corrosion than for the lower degrees of pre-corrosion, as described in Table 5.6.

Table 5.6 Characteristics of tendon corrosion

<i>Batch</i>	<i>Test Code</i>	<i>Characteristics of Corrosion</i>
1	S-U-L-I-1	No corrosion was found.
	S-U-L-II-O-2	General corrosion, some small localised corrosion
	S-U-L-III-O-3	General corrosion, some localised corrosion
	S-U-H-I-1	No corrosion was found.
	S-U-H-II-O-2	General corrosion, some small localised corrosion
	S-U-H-III-O-3	General corrosion, some localised corrosion
2	M-U-L-X-1	No corrosion was found.
	M-U-L-II-N-2	General corrosion, some small localised corrosion
	M-U-L-III-N-3	General corrosion, some localised corrosion
	M-U-H-X-1	No corrosion was found.
	M-U-H-II-N-2	General corrosion, some small localised corrosion
	M-U-H-III-N-3	General corrosion, some localised corrosion
3	M-U-L-X1-1	No corrosion was found.
	M-U-L-II-O-2	General corrosion, some small localised corrosion
	M-U-L-III-O-3	General corrosion, some localised corrosion
	M-U-H-X1-1	No corrosion was found.
	M-U-H-II-O-2	General corrosion, some small localised corrosion
	M-U-H-III-O-3	General corrosion, some localised corrosion
4	M-G-H-X-1	No corrosion was found.
	M-G-H-II-N-1	General corrosion, some small localised corrosion
	M-G-H-III-N-3	General corrosion, some localised corrosion
	M-G-H-X1-1	No corrosion was found.
	M-G-H-II-O-2	General corrosion, some small localised corrosion
	M-G-H-III-O-3	General corrosion, some localised corrosion

Key: U-Ungalvanised, G-Galvanised, M-Mortar electrolyte, S-Solution electrolyte, H-High level of pre-stress (800-1200MPa), L-Low level of pre-stress (300-400MPa), I-Degree of corrosion Stage I (0-1%), II-Degree of corrosion Stage II (2-4%), III-Degree of corrosion Stage III (4-7%), N-Normal protection, O-Overprotection, X and X1-no corrosion and no ICCP, R-As-received samples, 1, 2, 3-Sample numbers.

5.6.2.2 Infinite focus microscope (IFM)

After completing both accelerated corrosion and the application of ICCP tests, the corroded surface of the tendons was examined by infinite focus microscope (IFM) as shown in Figure 5.19. The procedure is described in section 4.11.3.

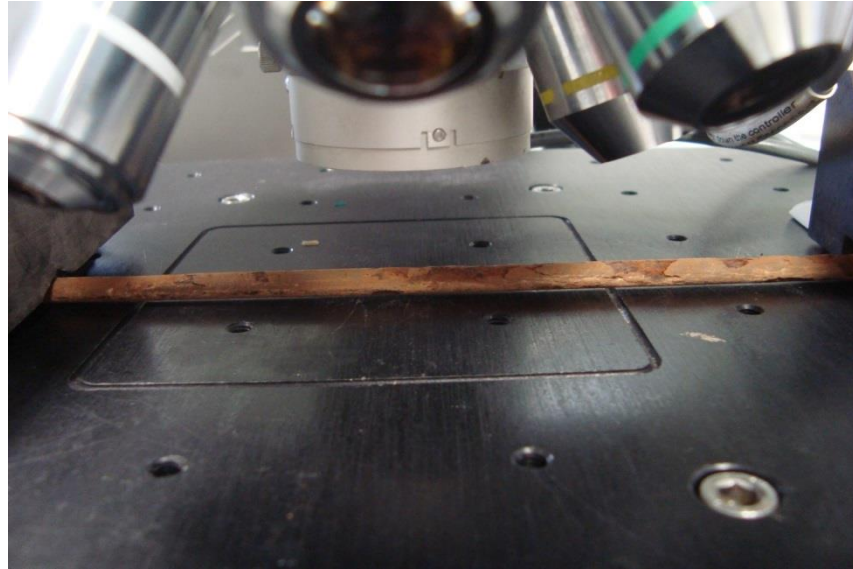


Figure 5.19 Specimen under surface investigation by IFM

The imaging of the surface of the tendon, together with measurement of the depth (Z), pit dimensions and roughness were carried out by an Alicona Infinite Focus Microscope. To determine the depth (Z), two different measurement points were selected from the surface profile data, one on the highest point on the surface and the other one on the lowest point on the bare surface of the tendon [100]. Random pits on the tendon were selected for pit dimension measurements. A profile path was drawn on the image of the pits to calculate the value of its diameter. Surface profile was derived from the same profile path to determine the depth of the pits. Profile roughness measurement of surfaces conforms to EN ISO 4387 and 4288. The images for specimens were taken with vertical resolution 10.18 μm and lateral resolution 7.82 μm .

Table 5.7 shows the depth of the corrosion products, pits depth and surface roughness.

Table 5.7 IFM results

Batch	Test Code	diameter	Depth Z	Pitting depth	Roughness
		before corrosion			Average (Ra)
		mm	μm	μm	μm
(1)	(2)	(3)	(4)	(5)	(6)
1	S-U-L-I-1	5.35	18.6	-	1.2
	S-U-L-II-O-2	5.35	23.9	18-20.1-22	3.9
	S-U-L-III-O-3	5.36	37.4	15-18-20-35	7.2
	S-U-H-I-1	5.35	16.4	-	1.6
	S-U-H-II-O-2	5.35	59.4	20-25	4.21
	S-U-H-III-O-3	5.33	57.3	15-27.23	5.3
2	M-U-L-I-1	5.28	14.41	-	1.4
	M-U-L-II-N-2	5.34	35.92	35-40-74.81	2.45
	M-U-L-III-N-3	5.34	30.47	24-30.84-45.81	3.24
	M-U-H-X-1	5.29	3.41	-	0.5
	M-U-H-II-N-2	5.34	114.36	84.04-93.72-100.99	1.67
	M-U-H-III-N-3	5.32	85.45	40-107.55	7.817
3	M-U-L-I-1	5.35	9.8	-	1.05
	M-U-L-II-O-2	5.35	55.34	62.84-56.421-30.98	4.56
	M-U-L-III-O-3	5.36	47.7	27.37-48.39-63.38	10.23
	M-U-H-X1-1	5.36	9.05	-	0.5
	M-U-H-II-O-2	5.36	46.15	5.92-25.46	1.0
	M-U-H-III-O-3	5.36	60.38	19.33-88.32-154.77-506.3	1.4
4	M-G-H-X-1	5.39	4.71	-	1.10
	M-G-H-II-N-1	5.40	68.79	93.03-62.95-50.38-77.45	6.98
	M-G-H-III-N-3	5.39	70.58	61.64-49.24-50.78-63.79-31.62	8.14
	M-G-H-X1-1	5.40	8.97	-	1.65
	M-G-H-II-O-2	5.39	56.47	62.79-61.22-53.05-56.96	1.53
	M-G-H-III-O-3	5.40	58.78		6.17

Key: U-Ungalvanised, G-Galvanised, M-Mortar electrolyte, S-Solution electrolyte, H-High level of pre-stress (800-1200MPa), L-Low level of pre-stress (300-400MPa), I-Degree of corrosion Stage I (0-1%), II-Degree of corrosion Stage II (2-4%), III-Degree of corrosion Stage III (4-7%), N-Normal protection, O-Overprotection, X and X1-no corrosion and no ICCP, R-As-received samples, 1, 2, 3-Sample numbers.

Batch 1

From Table 5.7, the original diameter of the tendons is shown in Column 3. The difference between high and low points in the profile (Z) is presented in Column 4. This difference is in the range 16.4 to 59.4 μm . It means that the surface of the tendons was affected by accelerated corrosion. The difference between in

pitting depth is in the range 15 to 27 μm . Moreover, the range of the average roughness (Ra) in this batch is between 1.78 to 4.72 μm .

Batch 2

The difference between high and low point in the profile (Z) is presented in Table 5.7- Column 4. This difference is in the range (Z) 3.416 to 85.45 μm . The difference between in pitting depth is in the range 30.84 to 107.55 μm . The range of the average roughness in this batch is between 0.5 to 7.817 μm .

Batch 3

The difference between high and low point in the profile (Z) is presented in Table 5.7 - Column 4. This difference is in the range (Z) 9.8 to 60.38 μm . The difference between in pitting depth is in the range 5.92 to 506.3 μm . The range of the average roughness in this batch is between 1.05 to 10.23 μm .

Batch 4

Table 5.7 - Column 4 shows the difference between measurement and reference lines in the profile (Z). This difference is in the range 4.71 to 70.58 μm . The pitting depth is in the range 31.62 to 93.03 μm . The range of the average roughness in this batch is between 1.10 to 8.14 μm .

From the above, the corrosion of the tendons in all batches were variable due to the combination of general corrosion (as assumed) and localised corrosion appearing along the surface of the tendon. The high measurements in both depth Z and roughness of the surface of tendon are related to the degree of corrosion; means more corrosion induced a high depth Z and roughness were measured.

5.6.3 X-ray Diffraction (XRD)

Corrosion products have been investigated using X-Ray Diffraction (XRD). XRD measures are performed on dry samples under Laboratory conditions ($T=20^{\circ}\text{C}$ and $\text{RH} = 50\%$). The results show that the main components of the corrosion products on the surface of tendons are Iron (III) oxide-hydroxide $\text{FeO}(\text{OH})$ which ranged between 35% to 75% and Iron (II,III) oxide Fe_3O_4 ranged between 25% to 65%.

5.6.4 Diameter and weight loss

Table 5.8 to Table 5.11 show the diameter and weight loss measured by both gravimetric weight loss and reduction in the diameter of the tendons as described in Section 4.6.3.1. The identification of tendon in each specimen is presented in Col. 1. The length of the corroded tendon was 320mm (Col. 2), three degrees of corrosion were investigated, Stage I (0-1 %), Stage II (2-4 %) and Stage III (4-7 %) as shown in Col. 3. Actual degree of corrosion is stipulated in Col. 4. Two reference methods were chosen to monitor the accelerated corrosion process and as described as follows:

Method I (reduction in tendon diameter) involved measuring the reduction in tendon diameter. The diameter of the tendon was measured before corrosion acceleration numerous locations along the bar and the average diameter was calculated (D1), Col. 5 (see appendix 1). At the end of the accelerated corrosion period, the tendons were removed from the electrolyte (Solution or Mortar), the corrosion products were cleaned using a solution of 10% diammonium hydrogen citrate and a soft wire brush. The diameter was re-measured as before and the average diameter was determined (D2), Col. 6 (see appendix 1). The reduction of corroded tendon diameter is the difference between the diameter of tendon before and after corrosion (Δd_1), Col.7. The reduction of the diameter of the corroded tendons was calculated as follows:

$$\Delta d_1 = D_1 - D_2 \quad \text{Equation 5.2}$$

The difference between measured diameter loss and theoretical diameter loss ($\% \Delta D$ Col. 9) is calculated as follows, in which Δd_2 , Col. 8, is the theoretical diameter loss, calculated by Faraday's Law.

$$\% \Delta d = \frac{\Delta D_1 - \Delta D_2}{\Delta D_1} \times 100\% \quad \text{Equation 5.3}$$

Method II (reduction weight loss - gravimetric method) takes into account the gravimetric weight loss from the bar after corrosion. The weight of tendon was measured before acceleration of corrosion (W1), Col. 10. After completing the accelerated corrosion, the tendons tendons were brushed, cleaned and

immersed in a 10% diammonium hydrogen citrate ($C_6H_{14}N_2O_7$) for 48 hours to remove the corrosion products. The tendons were dried and then re-weighed (W_2), Col. 11. The difference between measured weights (Δw_1), Col. 12, was calculated as follows:

$$\Delta w_1 = W_1 - W_2 \quad \text{Equation 5.4}$$

The difference between the measured weight loss and theoretical weight loss ($\% \Delta w$ Col.14) is calculated as follows:

$$\% \Delta w = \frac{\Delta w_1 - \Delta w_2}{\Delta w_2} \quad \text{Equation 5.5}$$

In which Δw_2 , Col. 13, is theoretical weight loss of tendon, calculated based on Faraday's Law (Equation 3.1).

The actual degree of corrosion is calculated as:

$$\frac{2 (RT)_1}{D} (\%). \quad \text{Equation 5.6}$$

In which $(RT)_1$ in cm, is actual metal loss after T(years):

$$(RT)_1 = \delta_1 \quad \text{Equation 5.7}$$

Referring to Equation 3.2, where δ_1 (cm) is actual metal section loss and Δw_1 is the measured weight loss, gives:

$$\delta_1 = \frac{\Delta w_1}{a \cdot \gamma} \quad \text{Equation 5.8}$$

Combination of Equation 5.13, 5.14 and 5.15, the actual degree of corrosion can be calculated as:

$$2 \times \frac{\Delta w_1}{a \cdot \gamma \cdot D} (\%) \quad \text{Equation 5.9}$$

Similarly, the theoretical degree of corrosion can be calculated as:

$$2 \times \frac{\Delta w_2}{a \cdot \gamma \cdot D} (\%) \quad \text{Equation 5.10}$$

The actual degree of corrosion of steel is calculated by its gravimetric weight loss. For Batch 1 (Table 5.8) shows the difference between measured diameter loss and theoretical diameter loss is calculated by Equation 5.10 and is in the range 123% to 259% (Table 5.8 - Col. 9). The very high difference is due to the theoretical calculation being for general corrosion whereas the experimental values include localised corrosion [101]. The actual degree of corrosion of steel is calculated by its gravimetric weight loss using Equation 5.16 (Col. 4). The difference between measured weight loss and theoretical weight loss is calculated by Equation 5.12 and presented in Table 5.8 (Col. 14). This difference is in the range 0.3% to 39%. It means that the measured weight loss was higher than the theoretical weight loss. This is attributed to the difference between experimental and theoretical weight loss basing on Faraday's Law. The theoretical weight loss calculated from Faraday's law is general corrosion while in practice there is some localised corrosion. Moreover, the current density in the theoretical calculation is constant while it fluctuates during the test, although it was monitored and adjusted to the constant value daily [101].

For Batch 2 (Table 5.9) the difference between measured diameter loss and theoretical diameter loss is in the range 22% to 165% (Table 5.9 - Col. 9). The reasons for these differences are the same as Batch 1. The difference between measured weight loss and theoretical weight loss is in the range -32% to 33% (Table 5.9 - Col. 9). The reason of negative percentage loss is the measured weight loss is smaller than the theoretical weight loss due the applied current dropping during the test whereas the calculation based on Faraday's law uses a higher value.

For Batch 3 (Table 5.10) the difference between measured diameter loss and theoretical diameter loss is in the range 9% to 172% (Table 5.10 - Col. 9). The reasons for these differences are the same as Batch 1. The difference between measured weight loss and theoretical weight loss is in the range -32% to 32%

(Table 5.10 - Col. 9). The reason for a negative percentage loss is the measured weight loss is smaller than the theoretical weight loss due the applied current dropping during the test whereas the calculation based on Faraday's Law uses a higher value.

For Batch 4 (Table 5.11) the difference between measured diameter loss and theoretical diameter loss is in the range 36% to 130% (Table 5.11 - Col. 9). The difference between measured weight loss and theoretical weight loss is in the range -32% to 16% (Table 5.11 - Col. 9). The reasons for these differences are the same as for Batch 1 and Batch 3.

Table 5.8 to Table 5.11 show that diameter loss is not a reliable method of measuring the actual degree of corrosion in practice because of the significant difference between the measured reduction in tendon bar diameters and the target degree of corrosion. This is due to the fact that it is difficult to measure accurately the diameter of the tendons both before, and especially after, the corrosion period. Also, the diameter of the steel bars is not perfectly circular hence this exaggerates the error even more. Furthermore, the reduction in diameter varied along the tendon due to the combination of general and localised corrosion appearing along the tendon bar. Method II (gravimetric weight loss) is a reliable method since the different between the target corrosion and the percentage of weight loss is not that significant. Therefore, in this research, the gravimetric weight loss method was employed as a means of monitoring the actual degree of corrosion.

Table 5.8 Mass and diameter loss of Batch 1

Test code	Tendon corroded length	Stage of Corrosion	Actual degree of corrosion	Method I					Method II				
				Reduction in tendon diameter					Weight loss				
				D1	D2	$\Delta d1$	$\Delta d2$	Difference % Δd	W1	W2	$\Delta w1$	$\Delta w2$	Difference % Δw
(mm)	Stage	(%)	(mm)	(mm)	(mm)	(mm)	(%)	(g)	(g)	(g)		(%)	
(1)	(2)	(3)	(4)	(5)	(6)	(7)	(8)	(9)	(10)	(11)	(12)	(13)	(14)
S-U-L-X-1	320	I	0.00	5.35	5.23	0.12	0.00	0	261.67	261.42	0.25	0.00	0
S-U-L-II-O-2	320	II	4.16	5.35	5.10	0.25	0.08	207	267.63	262.93	4.70	3.39	39
S-U-L-III-O-3	320	III	8.25	5.36	4.83	0.53	0.16	229	251.00	241.65	9.35	6.80	38
S-U-H-X1-1	320	I	0.00	5.35	5.27	0.08	0.00	0	266.62	266.26	0.36	0.00	0
S-U-H-II-O-2	320	II	3.85	5.35	5.06	0.29	0.08	257	259.29	254.94	4.35	3.39	28
S-U-H-III-O-3	320	III	6.23	5.33	4.98	0.36	0.16	123	260.06	253.06	7.00	6.74	3

- | | | | |
|-----|--|------|-----------------------------------|
| (5) | Mean diameter of tendon before corrosion | (10) | Weight of tendon before corrosion |
| (6) | Mean diameter of tendon before corrosion | (11) | Weight of tendon after corrosion |
| (7) | Actual diameter loss of tendon | (12) | Weight loss of tendon |
| (8) | Theoretical weight loss of tendon | (13) | Theoretical weight loss of tendon |
| (9) | Percent error in diameter reduction | (14) | Percent error in weight loss |

Key: U-Ungalvanised, G-Galvanised, M-Mortar electrolyte, S-Solution electrolyte, H-High level of pre-stress (800-1200MPa), L-Low level of pre-stress (300-400MPa), I-Degree of corrosion Stage I (0-1%), II-Degree of corrosion Stage II (2-4%), III-Degree of corrosion Stage III (4-7%), N-Normal protection, O-Overprotection, X and X1-no corrosion and no ICCP, R-As-received samples, 1, 2, 3-Sample numbers.

Table 5.9 Mass and diameter loss of Batch 2

Test code	Tendon corroded length	Stage of Corrosion	Actual degree of corrosion	Method I					Method II				
				Reduction in tendon diameter					Weight loss				
				D1	D2	$\Delta d1$	$\Delta d2$	Difference % Δd	W1	W2	$\Delta w1$	$\Delta w2$	Difference % Δw
(mm)	Stage	(%)	(mm)	(mm)	(mm)	(mm)	(%)	(g)	(g)	(g)	(g)	(%)	
(1)	(2)	(3)	(4)	(5)	(6)	(7)	(8)	(9)	(10)	(11)	(12)	(13)	(14)
M-U-L-X-1	320	I	0.00	5.28	5.29	-0.01	0.00	0	261.30	260.80	0.50	0.00	0
M-U-L-II-N-2	320	II	3.98	5.34	5.13	0.21	0.08	165	260.29	255.81	4.48	3.37	33
M-U-L-III-N-3	320	III	5.32	5.34	5.11	0.23	0.16	45	256.64	250.64	6.00	6.76	-11
M-U-H-X-1	320	I	0.00	5.35	5.30	0.05	0.00	0	262.10	261.88	0.22	0.00	0
M-U-H-II-N-2	320	II	2.25	5.35	5.19	0.16	0.08	97	265.80	263.25	2.55	3.39	-25
M-U-H-III-N-3	320	III	4.05	5.36	5.17	0.20	0.16	22	266.86	262.25	4.61	6.82	-32

- | | | | |
|-----|--|------|-----------------------------------|
| (5) | Mean diameter of tendon before corrosion | (10) | Weight of tendon before corrosion |
| (6) | Mean diameter of tendon before corrosion | (11) | Weight of tendon after corrosion |
| (7) | Actual diameter loss of tendon | (12) | Weight loss of tendon |
| (8) | Theoretical weight loss of tendon | (13) | Theoretical weight loss of tendon |
| (9) | Percent error in diameter reduction | (14) | Percent error in weight loss |

Key: U-Ungalvanised, G-Galvanised, M-Mortar electrolyte, S-Solution electrolyte, H-High level of pre-stress (800-1200MPa), L-Low level of pre-stress (300-400MPa), I-Degree of corrosion Stage I (0-1%), II-Degree of corrosion Stage II (2-4%), III-Degree of corrosion Stage III (4-7%), N-Normal protection, O-Overprotection, X and X1-no corrosion and no ICCP, R-As-received samples, 1, 2, 3-Sample numbers.

Table 5.10 Mass and diameter loss of Batch 3

Test code	Tendon corroded length	Stage of Corrosion	Actual degree of corrosion	Method I					Method II				
				Reduction in tendon diameter					Weight loss				
				D1	D2	$\Delta d1$	$\Delta d2$	Difference % Δd	W1	W2	$\Delta w1$	$\Delta w2$	Difference % Δw
(mm)	Stage	(%)	(mm)	(mm)	(mm)	(mm)	(%)	(g)	(g)	(g)	(g)	(%)	
(1)	(2)	(3)	(4)	(5)	(6)	(7)	(8)	(9)	(10)	(11)	(12)	(13)	(14)
M-U-L-X1-1	320	I	0.00	5.29	5.28	0.01	0.00	0	258.66	257.78	0.88	0.00	0
M-U-L-II-O-2	320	II	3.96	5.34	5.12	0.22	0.08	172	256.29	251.83	4.46	3.38	32
M-U-L-III-O-3	320	III	6.52	5.32	5.06	0.26	0.16	60	256.39	249.09	7.30	6.70	9
M-U-H-X1-1	320	I	0.00	5.36	5.33	0.03	0.00	0	257.23	256.99	0.24	0.00	0
M-U-H-II-O-2	320	II	2.06	5.36	5.19	0.17	0.08	106	252.35	250.01	2.34	3.40	-31
M-U-H-III-O-3	320	III	4.03	5.36	5.19	0.18	0.16	9	254.63	250.05	4.58	6.81	-32

- | | | | |
|-----|--|------|-----------------------------------|
| (5) | Mean diameter of tendon before corrosion | (10) | Weight of tendon before corrosion |
| (6) | Mean diameter of tendon before corrosion | (11) | Weight of tendon after corrosion |
| (7) | Actual diameter loss of tendon | (12) | Weight loss of tendon |
| (8) | Theoretical weight loss of tendon | (13) | Theoretical weight loss of tendon |
| (9) | Percent error in diameter reduction | (14) | Percent error in weight loss |

Key: U-Ungalvanised, G-Galvanised, M-Mortar electrolyte, S-Solution electrolyte, H-High level of pre-stress (800-1200MPa), L-Low level of pre-stress (300-400MPa), I-Degree of corrosion Stage I (0-1%), II-Degree of corrosion Stage II (2-4%), III-Degree of corrosion Stage III (4-7%), N-Normal protection, O-Overprotection, X and X1-no corrosion and no ICCP, R-As-received samples, 1, 2, 3-Sample numbers.

Table 5.11 Mass and diameter loss of Batch 4

Test code	Tendon corroded length	Stage of Corrosion	Actual degree of corrosion	Method I					Method II				
				Reduction in tendon diameter					Weight loss				
				D1	D2	$\Delta d1$	$\Delta d2$	Difference % Δd	W1	W2	$\Delta w1$	$\Delta w2$	Difference % Δw
(mm)	Stage	(%)	(mm)	(mm)	(mm)	(mm)	(%)	(g)	(g)	(g)	(g)	(%)	
(1)	(2)	(3)	(4)	(5)	(6)	(7)	(8)	(9)	(10)	(11)	(12)	(13)	(14)
M-G-H-X1-1	320	I	0.00	5.39	5.33	0.06	0.00	0	261.29	261.69	-0.40	0.00	0
M-G-H-II-N-1	320	II	3.48	5.40	5.21	0.19	0.08	130	263.85	259.85	4.00	3.45	16
M-G-H-III-N-3	320	III	4.36	5.39	5.16	0.23	0.16	41	267.51	262.5	5.01	6.88	-27
M-G-H-X1-1	320	I	0.00	5.40	5.31	0.09	0.00	0	271.53	271.94	-0.41	0.00	0
M-G-H-II-O-2	320	II	3.40	5.39	5.22	0.17	0.08	108	267.45	263.54	3.91	3.44	13
M-G-H-III-O-3	320	III	4.10	5.40	5.18	0.22	0.16	36	262.71	257.99	4.72	6.90	-32

- | | | | |
|-----|--|------|-----------------------------------|
| (5) | Mean diameter of tendon before corrosion | (10) | Weight of tendon before corrosion |
| (6) | Mean diameter of tendon before corrosion | (11) | Weight of tendon after corrosion |
| (7) | Actual diameter loss of tendon | (12) | Weight loss of tendon |
| (8) | Theoretical weight loss of tendon | (13) | Theoretical weight loss of tendon |
| (9) | Percent error in diameter reduction | (14) | Percent error in weight loss |

Key: U-Ungalvanised, G-Galvanised, M-Mortar electrolyte, S-Solution electrolyte, H-High level of pre-stress (800-1200MPa), L-Low level of pre-stress (300-400MPa), I-Degree of corrosion Stage I (0-1%), II-Degree of corrosion Stage II (2-4%), III-Degree of corrosion Stage III (4-7%), N-Normal protection, O-Overprotection, X and X1-no corrosion and no ICCP, R-As-received samples, 1, 2, 3-Sample numbers.

5.6.5 Loss in service stress

The arrangements for calculating the slippage and describing the tendon pre-tensioning technique was described in Sections 3.4 and 5.4.4 respectively. The accelerated corrosion technique is also described in Sections 3.5 and 5.5 for inducing corrosion in the tendons. Table 5.3 shows the actual applied stress on the tendons and Table 5.12 shows the corrosion design criteria for the same specimens.

Table 5.12 Corrosion design criteria

Batch	Test Code	Actual Stress	Target Degree of Corrosion	Applied Current	Corrosion Duration	Actual Degree of Corrosion
		(MPa)	Stage	(mA)	(Hrs)	(%)
1	S-U-L-X1-1	407	I	-	-	0
	S-U-L-II-O-2	452	II	54.28	60.90	4.16
	S-U-L-III-O-3	442	III	54.28	121.81	8.25
	S-U-H-X1-1	1289	I	-	-	0.32
	S-U-H-II-O-2	1210	II	54.28	60.90	3.85
	S-U-H-III-O-3	1210	III	54.28	121.81	6.23
2	M-U-L-X-1	421	I	-	-	0
	M-U-L-II-N-2	376	II	54.28	60.90	3.98
	M-U-L-III-N-3	413	III	54.28	121.81	5.32
	M-U-H-X-1	1136	I	-	-	0
	M-U-H-II-N-2	1175	II	54.28	60.90	2.25
	M-U-H-III-N-3	1213	III	54.28	121.81	4.05
3	M-U-L-X1-1	359	I	-	-	0
	M-U-L-II-O-2	377	II	54.28	60.90	3.96
	M-U-L-III-O-3	412	III	54.28	121.81	6.52
	M-U-H-X1-1	1339	I	-	-	0
	M-U-H-II-O-2	1463	II	54.28	60.90	2.06
	M-U-H-III-O-3	1302	III	54.28	121.81	4.03
4	M-G-H-X-1	882	I	-	-	0
	M-G-H-II-N-1	869	II	54.28	60.90	3.48
	M-G-H-III-N-3	1063	III	54.28	121.81	4.36
	M-G-H-X1-1	862	I	-	-	0
	M-G-H-II-O-2	997	II	54.28	60.90	3.40
	M-G-H-III-O-3	894	III	54.28	121.81	4.10

Key: U-Ungalvanised, G-Galvanised, M-Mortar electrolyte, S-Solution electrolyte, H-High level of pre-stress (800-1200MPa), L-Low level of pre-stress (300-400MPa), I-Degree of corrosion Stage I (0-1%), II-Degree of corrosion Stage II (2-4%), III-Degree of corrosion Stage III (4-7%), N-Normal protection, O-Overprotection, X and X1-no corrosion and no ICCP, R-As-received samples, 1, 2, 3-Sample numbers.

The reading from the strain gauges were recorded by a data logger every 15 minutes. The strains were converted to stresses by applying $\sigma = E \epsilon$, where $E = 220$ GPa. Table 5.13 shows the variation in stress during the accelerated corrosion period.

Table 5.13 Variation in stress in the tendons during accelerated corrosion

Batch	Test Code	Initial	Stress (MPa)					
		Stress (MPa)	Days					
			1	2	3	4	5	6
1	S-U-L-X1-1	407	376	373	368	362	358	354
	S-U-L-II-O-2	452	443	435	426	414	411	406
	S-U-L-III-O-3	443	433	423	412	396	388	377
	S-U-H-X1-1	1289	1254	1242	1232	1218	1208	1199
	S-U-H-II-O-2	1210	1126	1110	1096	1074	1066	1057
	S-U-H-III-O-3	1210	1120	1099	1082	1052	1040	1021
2	M-U-L-X-1	421	417	417	417	419	420	420
	M-U-L-II-N-2	376	332	332	331	331	331	331
	M-U-L-III-N-3	413	442	437	432	433	432	430
	M-U-H-X-1	1136	1126	1124	1119	1123	1127	1127
	M-U-H-II-N-2	1175	1174	1169	1161	1165	1169	1167
	M-U-H-III-N-3	1213	1211	1198	1186	1186	1178	1164
3	M-U-L-X1-1	359	340	340	339	339	339	340
	M-U-L-II-O-2	377	369	367	364	363	363	363
	M-U-L-III-O-3	412	430	428	424	419	407	407
	M-U-H-X1-1	1339	1192	1189	1186	1184	1185	1188
	M-U-H-II-O-2	1463	1339	1325	1318	1314	1314	1313
	M-U-H-III-O-3	1302	1024	1008	1003	996	994	997
4	M-G-H-X-1	882	699	705	702	702	702	704
	M-G-H-II-N-1	869	678	685	686	690	691	693
	M-G-H-III-N-3	1063	678	676	669	668	668	669
	M-G-H-X1-1	862	873	874	873	873	873	874
	M-G-H-II-O-2	997	850	836	835	834	833	833
	M-G-H-III-O-3	894	805	791	788	786	785	784

Key: U-Ungalvanised, G-Galvanised, M-Mortar electrolyte, S-Solution electrolyte, H-High level of pre-stress (800-1200MPa), L-Low level of pre-stress (300-400MPa), I-Degree of corrosion Stage I (0-1%), II-Degree of corrosion Stage II (2-4%), III-Degree of corrosion Stage III (4-7%), N-Normal protection, O-Overprotection, X and X1-no corrosion and no ICCP, R-As-received samples, 1, 2, 3-Sample numbers.

The data presented in Table 5.13 are shown graphically in Figure 5.20 to Figure 5.23 to illustrate the performance of the tendons during the corrosion period.

5.6.5.1 Influence of accelerated corrosion on pre-stress - Batch 1

Figure 5.20 compares the loss in pre-stress of the tendons with the different degrees of corrosion, Stage I (0-1 %), Stage II (2-4 %) and Stage III (4-7 %) at the low pre-stress level (300-400 N/mm², approximately 30% Ultimate Tensile Strength of the tendon, UTS). Figure 5.21 shows the net loss in pre-stress due to corrosion of Stage II and Stage III where the loss in pre-stress from the control Stage I specimen is subtracted from the corroded specimens with the same level of pre-stress, 30% UTS.

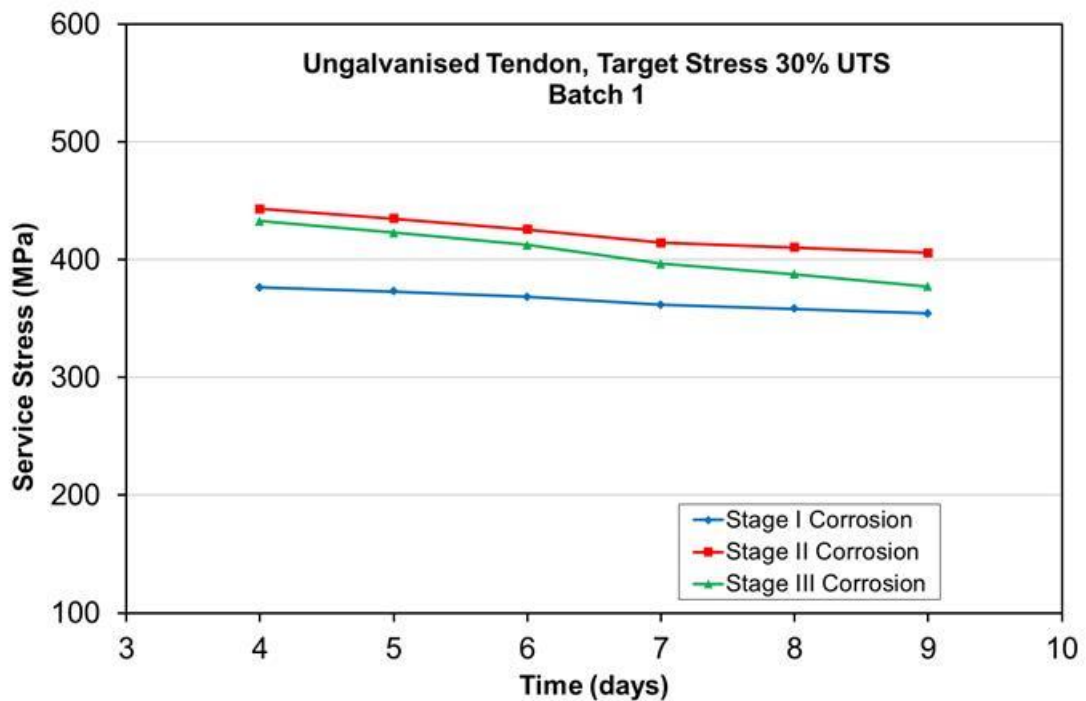


Figure 5.20 Gross loss in tendon pre-stress over corrosion period (30% UTS)

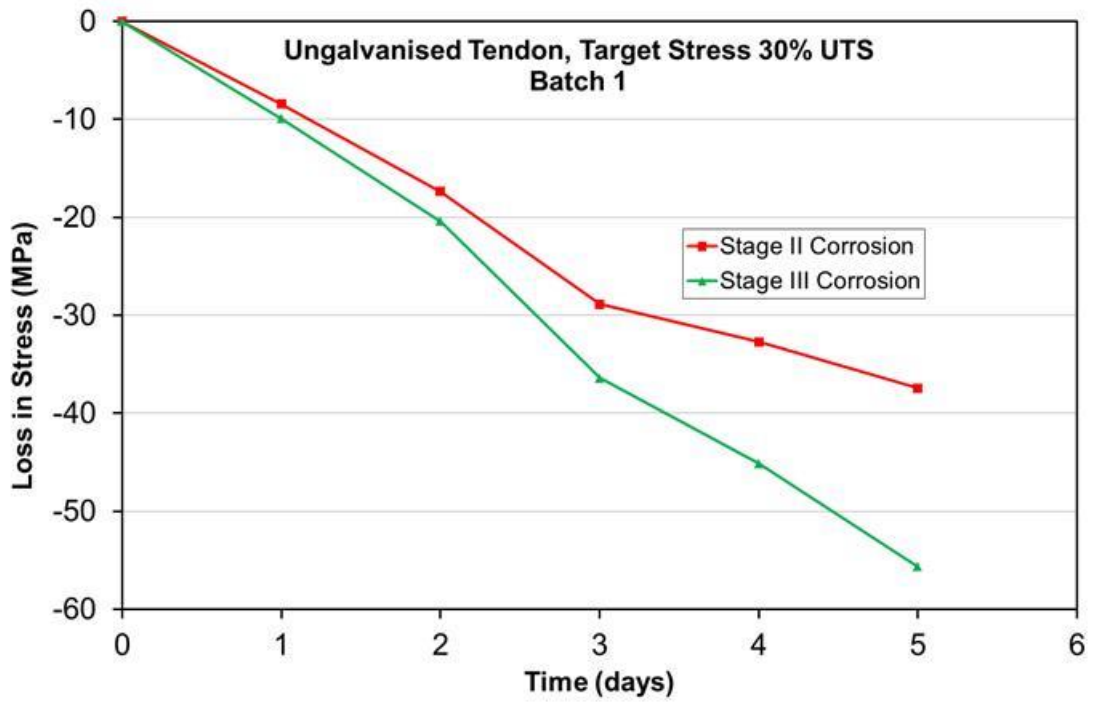


Figure 5.21 Net loss in tendon pre-stress over corrosion time (30% UTS)

Similarly for the target pre-stress, High Level (800-1200MPa), Figure 5.22 compares the loss in pre-stress of the tendons with the different degree of corrosion, Stage I, Stage II and Stage III over the corrosion period.

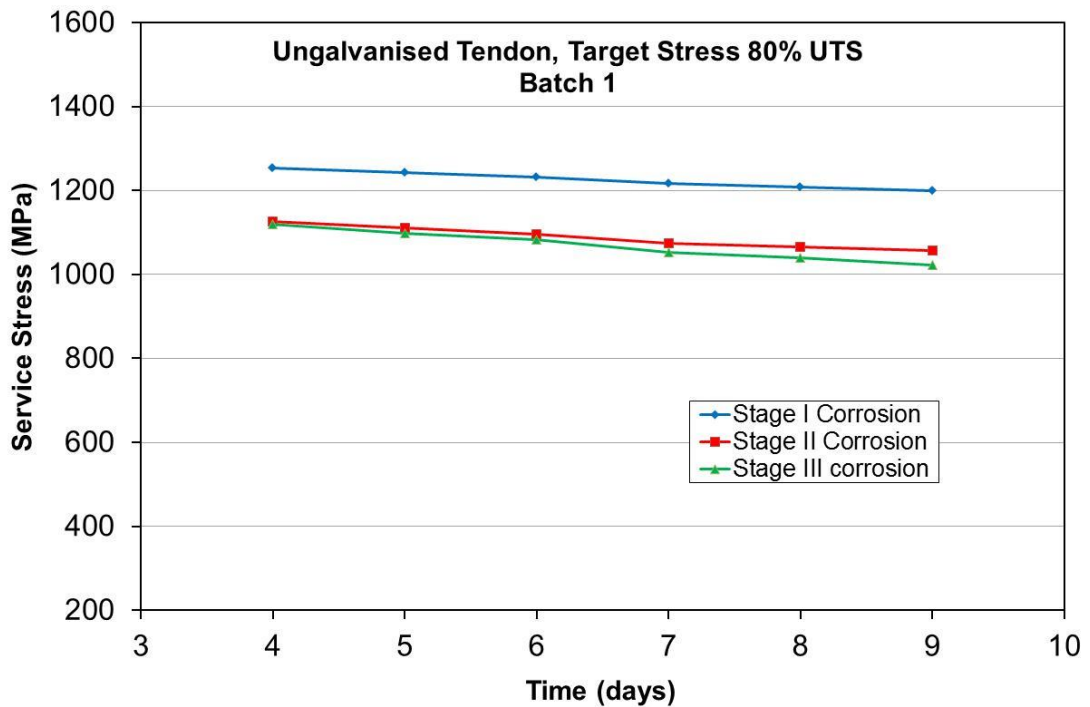


Figure 5.22 Gross loss in tendon pre-stress over corrosion time (80% UTS)

Figure 5.23 shows the net loss in pre-stress due to corrosion Stage II and Stage III. Again, the net losses in pre-stress are obtained by subtracting the control (Stage I) stress from the stress measured during the corrosion phase.

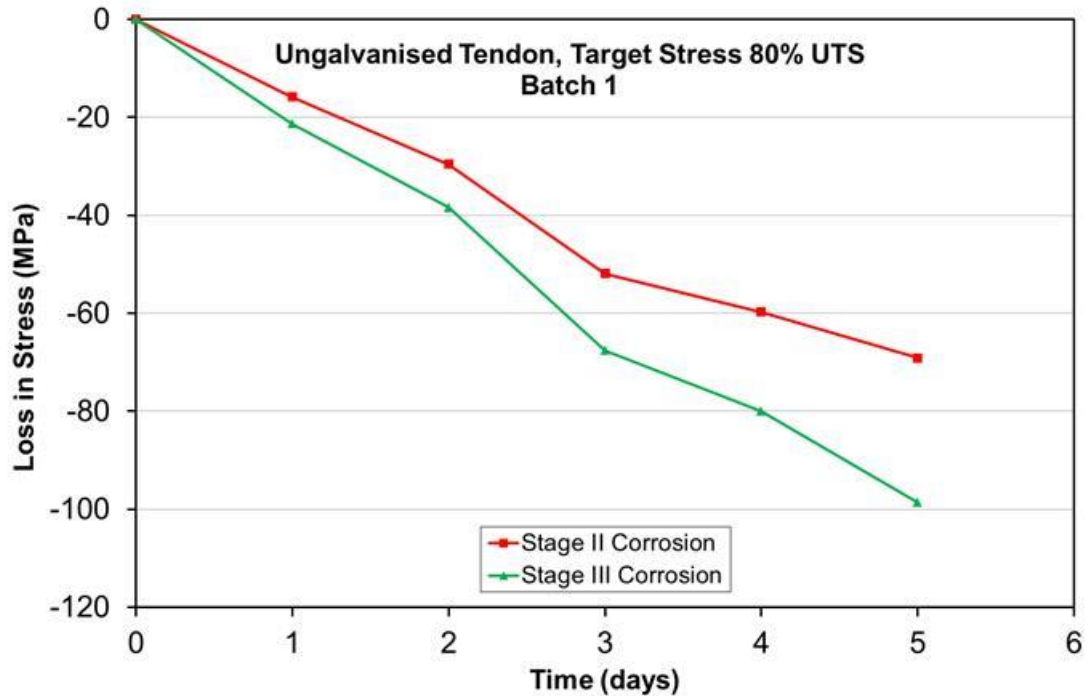


Figure 5.23 Net loss in tendon pre-stress over corrosion period (80% UTS)

5.6.4.1.1 Summary of loss in tendon service stress (Batch 1)

The results indicate that there is a loss in pre-stress due to corrosion as a result of the loss in cross sectional area of the tendons. In addition, the loss of pre-stress increased as the degree of corrosion increased. It is evident that there are smaller variations to the strain profiles for the 30% UTS pre-stressed tendons compared to the 80% UTS. This is particularly noticeable as the degree of corrosion increases from Stage I (control) to Stage II and Stage III.

Figure 5.24 shows losses in pre-stress in tendons with target pre-stress of 30% UTS and 80% UTS. At Stage II degree of corrosion, Stage II losses are very similar, while Figure 5.25 indicates that there is a greater difference in loss of pre-stress due corrosion Stage III. This indicates that the loss in pre-stress is more dependent on the degree of corrosion and less dependent on the initial pre-stress in the tendon.

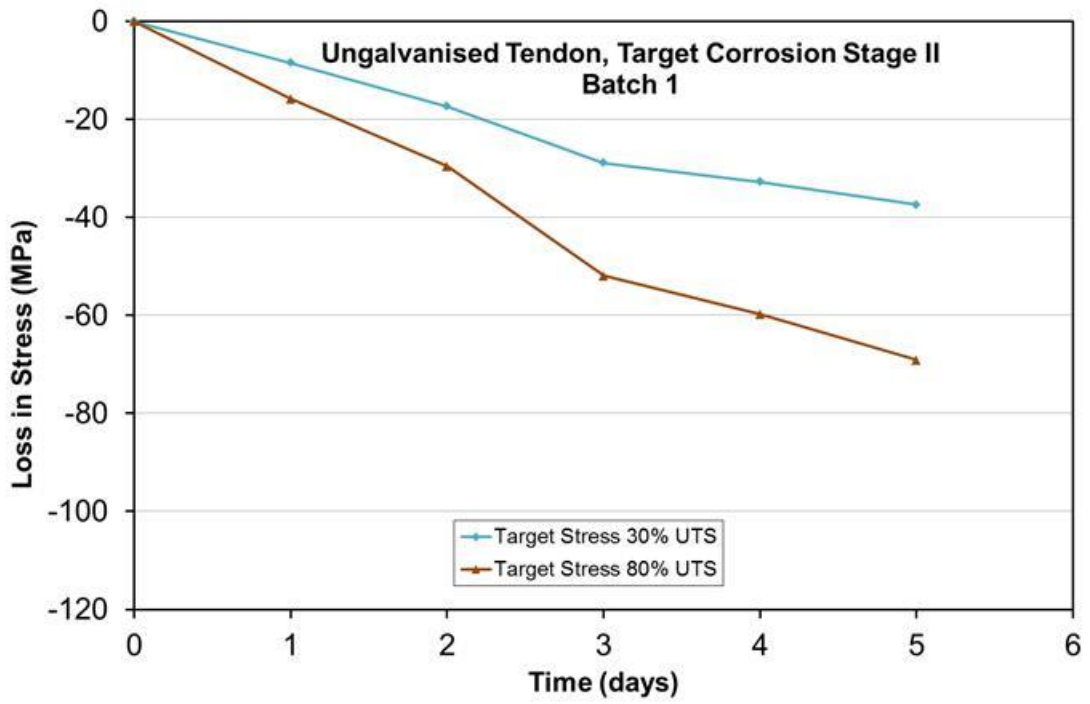


Figure 5.24 Loss in pre-stress due to corrosion Stage II

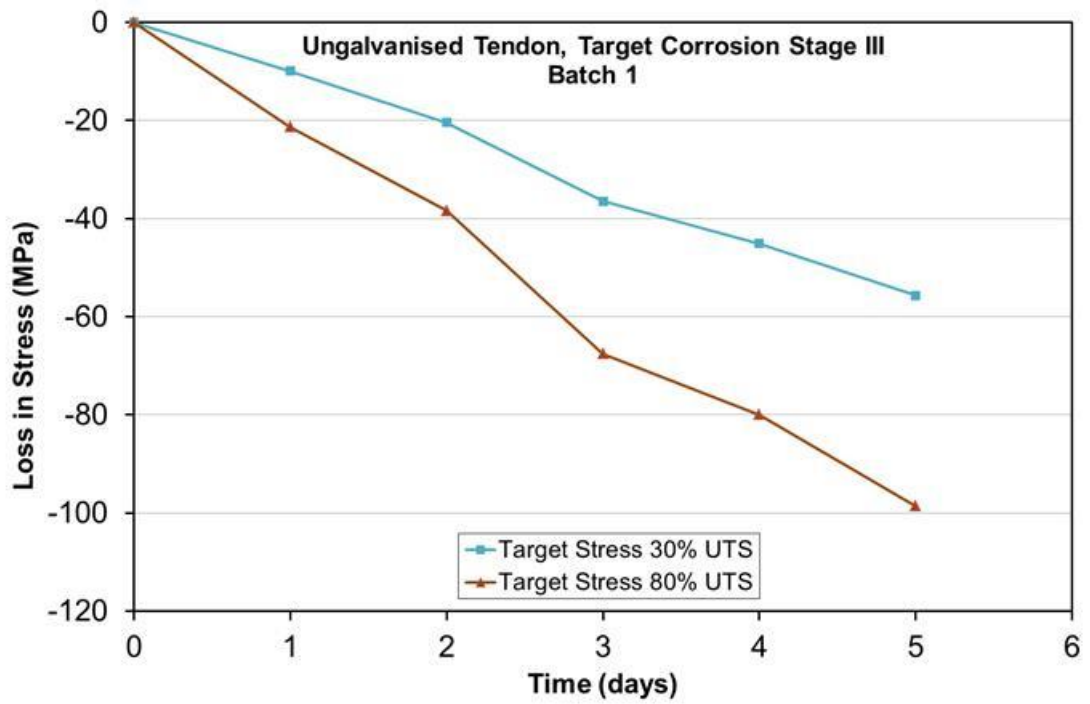


Figure 5.25 Loss in pre-stress due to corrosion Stage III

Table 5.14 Residual service stress due to corrosion

Corrosion Stage (%)	Residual Stress (MPa)	
	Target Service Stress 30% UTS (MPa)	Target Service Stress 80% UTS (MPa)
I	-22	-55
II	-37	-69
III	-56	-99

The results shown in Table 5.14 are plotted in Figure 5.26. It is apparent that as the degree of corrosion increases from Stage II through to Stage III, there is an increase in loss of pre-stress for both the highly stressed tendon (80% UTS) and the tendons exhibiting a pre-stress of 30% UTS. However, the decrease in loss in stress is slightly more pronounced for the 80% UTS specimens. This indicates that tendons subjected to higher degrees of corrosion will suffer higher losses which should be accounted for at the design stage as an additional loss. The tendons exposed to Stage I corrosion, although not subjected to corrosion, do suffer a reduction in pre-stress, perhaps as a result of compression in the timber moulds or relaxation (this has been accounted for in the net losses in Stage II and III).

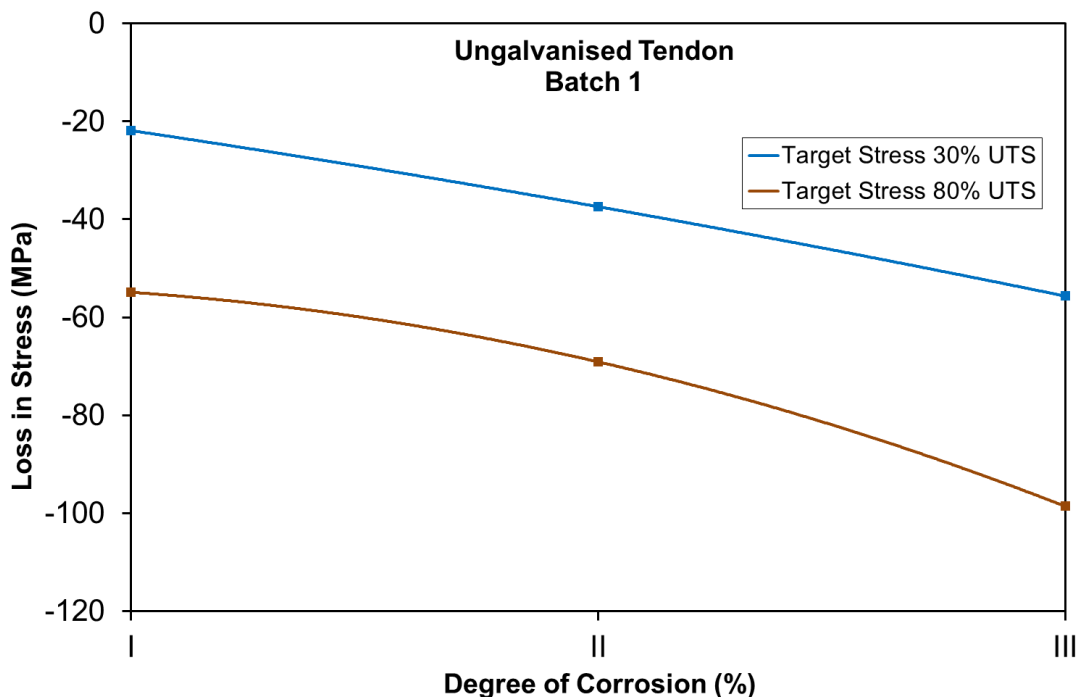


Figure 5.26 Relationship between degree of corrosion and different levels of pre-stress

5.6.5.2 Influence of accelerated corrosion on pre-stress - Batch 2 & 3

In this section, results of Batch 2 and Batch 3 are presented together as these two batches have the same parameters in terms of tendon type and corrosion criteria. The data presented in Table 5.13 are shown graphically in Figure 5.27 to Figure 5.33 to better understand the performance of the tendons. Figure 5.27 compares the gross loss in pre-stress of the tendons with the different degrees of corrosion, Stage I (0-1 %), Stage II (2-4 %) and Stage III (4-7 %) at a low level of applied pre-stress (300-400 N/mm²), 30% Ultimate Tensile Strength (UTS). Similarly, Figure 5.28 shows the gross loss in pre-stress due to corrosion of Stages I, II and III for Batch 3.

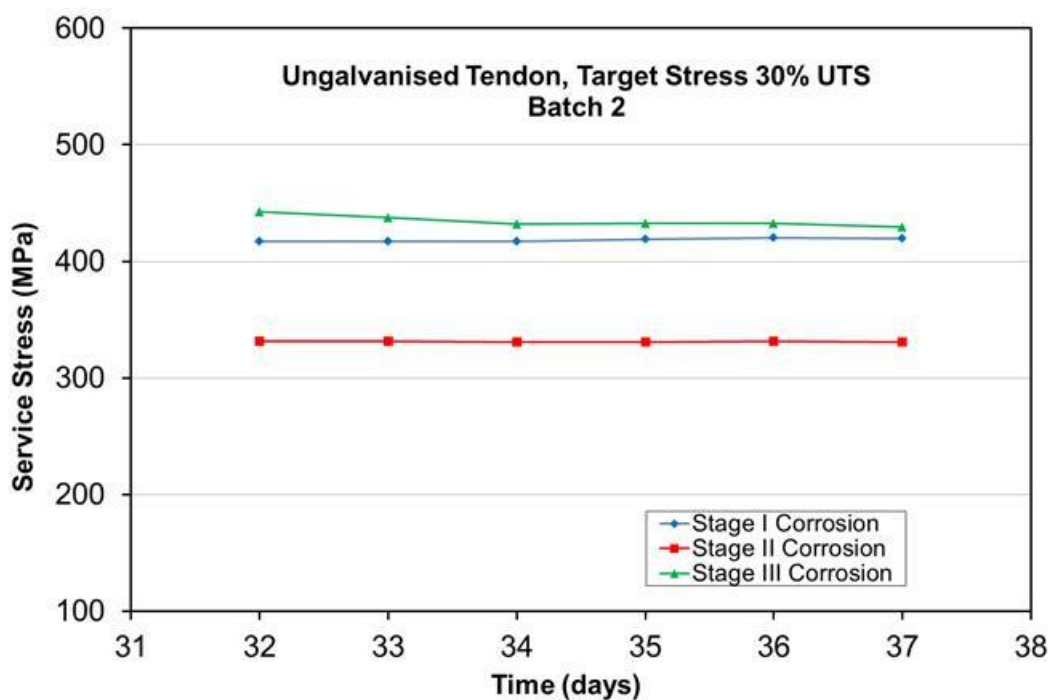


Figure 5.27 Gross loss in tendon pre-stress during corrosion period (30% UTS)
- Batch 2

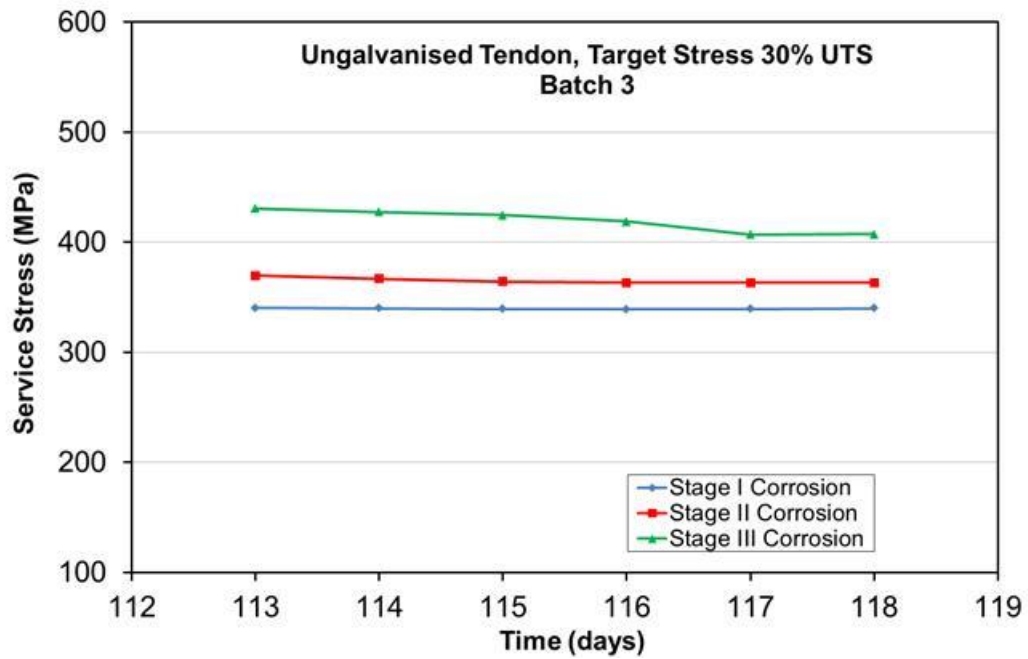


Figure 5.28 Gross loss in tendon pre-stress during corrosion period (30% UTS)
- Batch 3

Both Figure 5.29 and Figure 5.30 show the comparison in the gross loss in pre-stress of the tendons with the different degrees of corrosion Stage I (0-1 %), Stage II (2-4 %) and Stage III (4-7 %) at a High Level of pre-stress (800-1200 N/mm²), 80% Ultimate Tensile Strength (UTS).

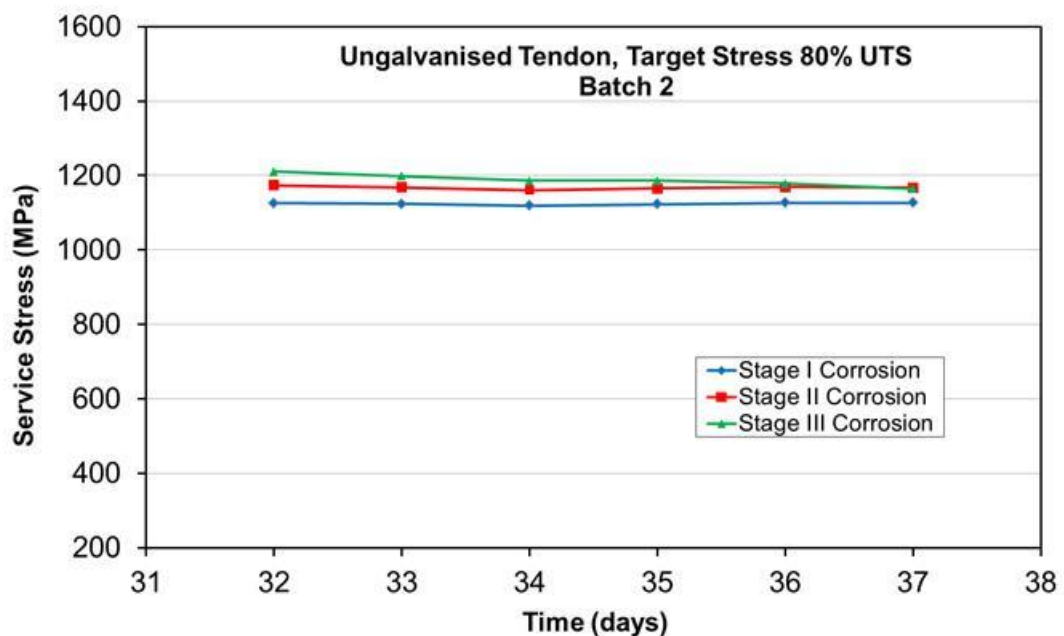


Figure 5.29 Gross loss in tendon pre-stress during corrosion period (80% UTS)
- Batch 2

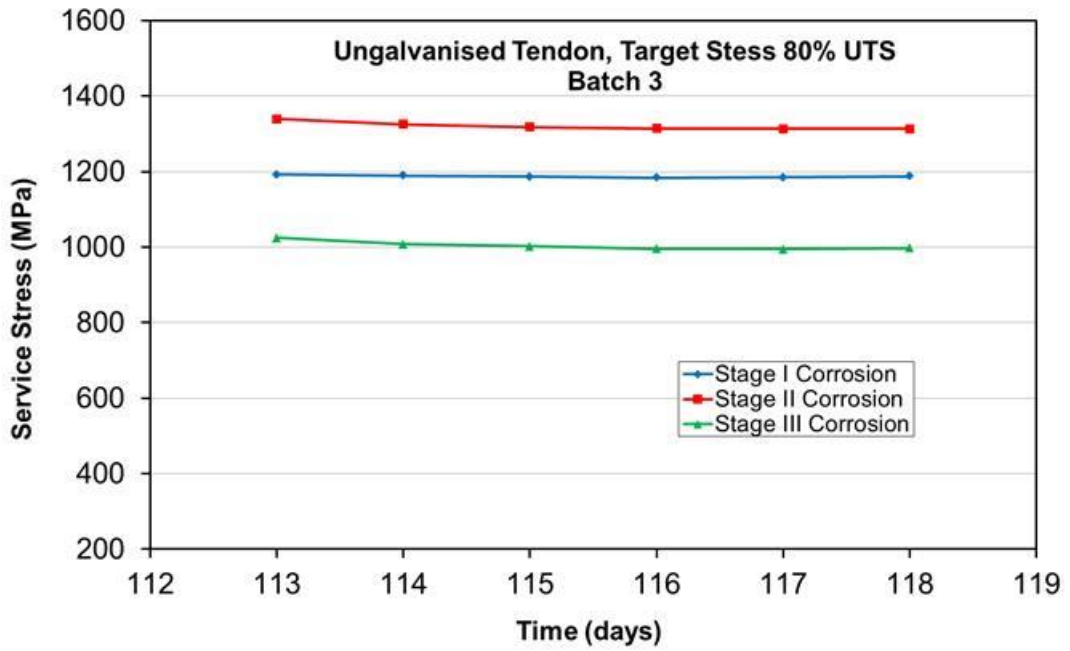


Figure 5.30 Gross loss in tendon pre-stress during corrosion period (80% UTS)
- Batch 3

Figure 5.31 shows the average loss in pre-stress due to corrosion Stages II and Stage III (Batches 2 & 3) for target stress 80% UTS.

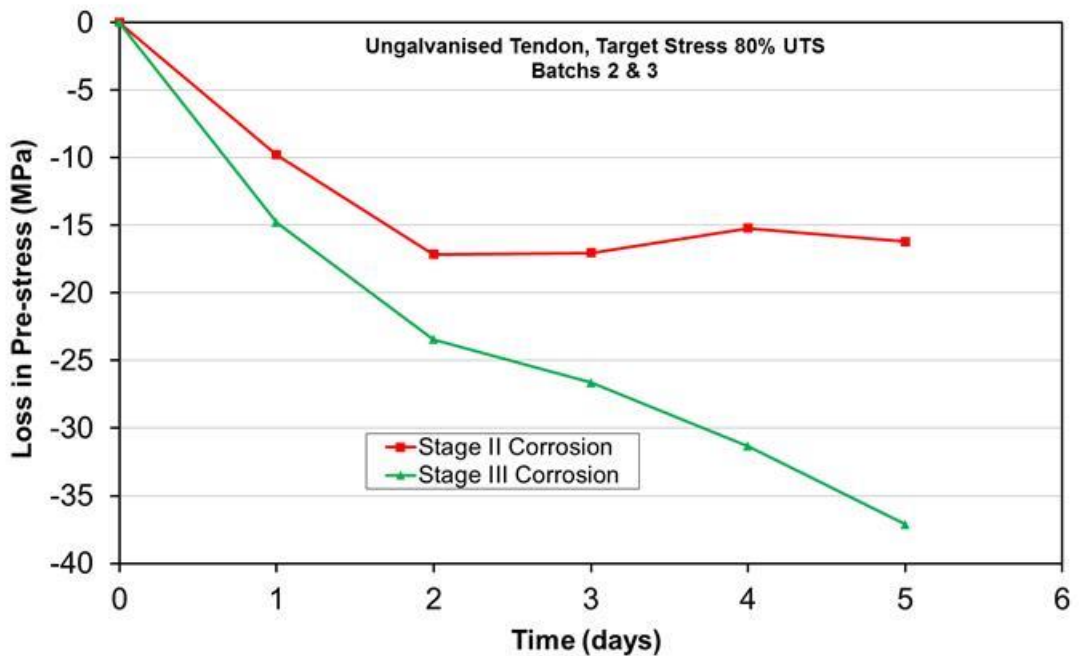


Figure 5.31 Average loss in tendon pre-stress during corrosion period (80% UTS) - Batch 2 & 3

5.6.4.2.1 Summary of loss in tendon service stress (Batches 2 & 3)

The results indicate that there is a loss in pre-stress due to corrosion. It is also evident that the loss of pre-stress increased as the degree of corrosion increased. Figure 5.32 shows the average losses in pre-stress in tendons with target pre-stress of 30% UTS and 80% UTS. At Stage II degree of corrosion, Stage II losses are not similar, the loss in stress in High Level (80%) is more than the loss in Low Level (30%), whereas Figure 5.33 indicates that there is a greater difference in loss of pre-stress due to corrosion Stage III. This indicates that the loss in pre-stress is more dependent on the degree of corrosion and less dependent on the initial pre-stress in the tendon. These results again show the same behaviour of the tendons in Batch 1 over the accelerated corrosion period.

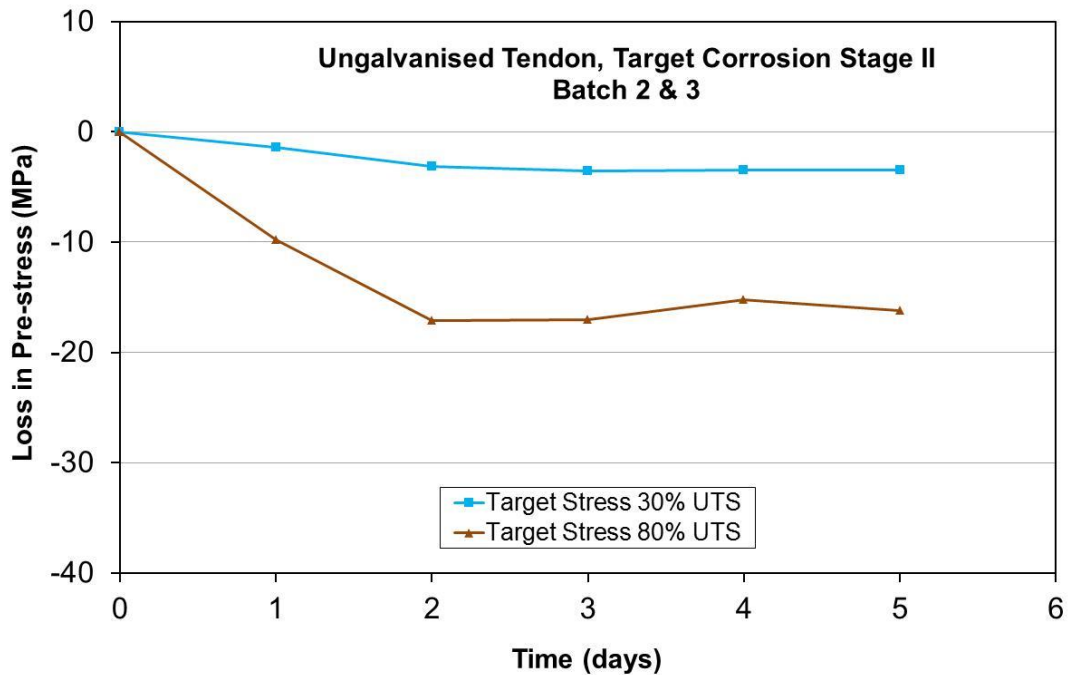


Figure 5.32 Average loss in pre-stress due to corrosion Stage II - Batch 2 & 3

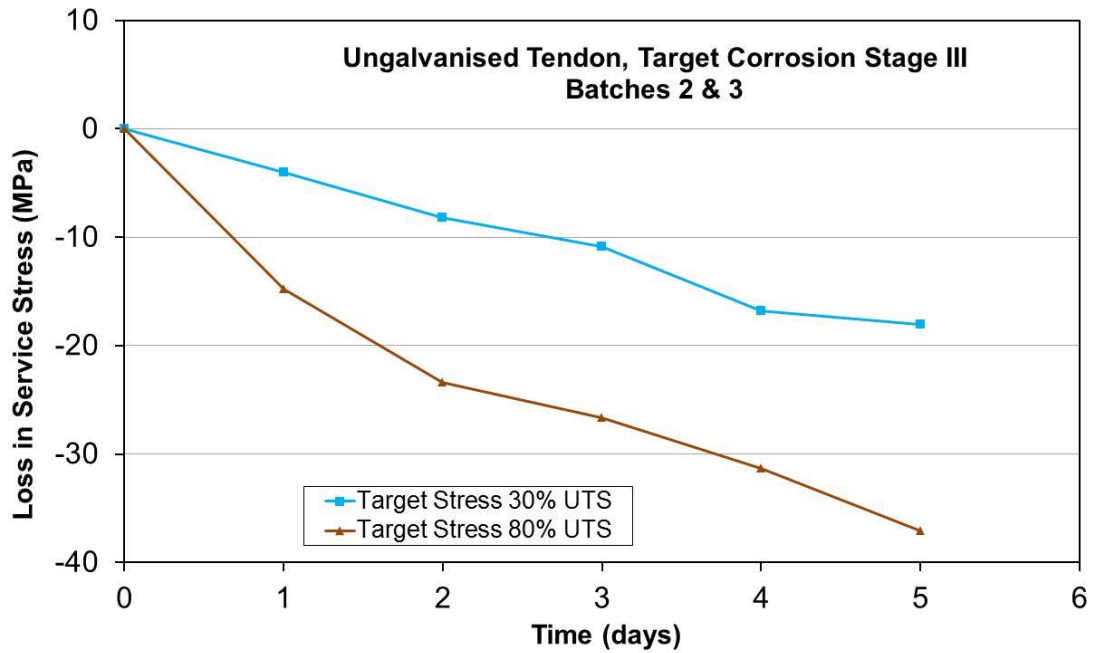


Figure 5.33 Average loss in pre-stress due to corrosion Stage III - Batches 2 & 3

Table 5.15 Residual service stress due to corrosion (Bath 2 & 3)

Corrosion stage		Residual stress (MPa)					
		Target Service Stress 30% UTS			Target Service Stress 80% UTS		
		Batch 2 (MPa)	Batch 3 (MPa)	Average (MPa)	Batch 2 (MPa)	Batch 3 (MPa)	Average (MPa)
Before	I	417	340	379	1126	1193	1159
Corrosion	II	332	370	351	1174	1339	1257
	III	442	431	437	1211	1024	1118
After	I	420	340	380	1127	1188	1157
Corrosion	II	331	363	347	1167	1313	1240
	III	430	407	418	1164	997	1081

The average results of the residual applied stress shown in Table 5.15 are plotted in Figure 5.34. The percentage of degree of corrosion represents the average of the each corrosion Stage, degree of corrosion 0 % represents Stage I, 3 % of corrosion represents Stage II and 6 % degree of corrosion represents Stage III. It is apparent that there is a greater decrease in pre-stress for 80% UTS than 30% UTS. There is also a larger divergence as the corrosion stage increases (Stage I-III) for 80% UTS compared to 30% UTS.

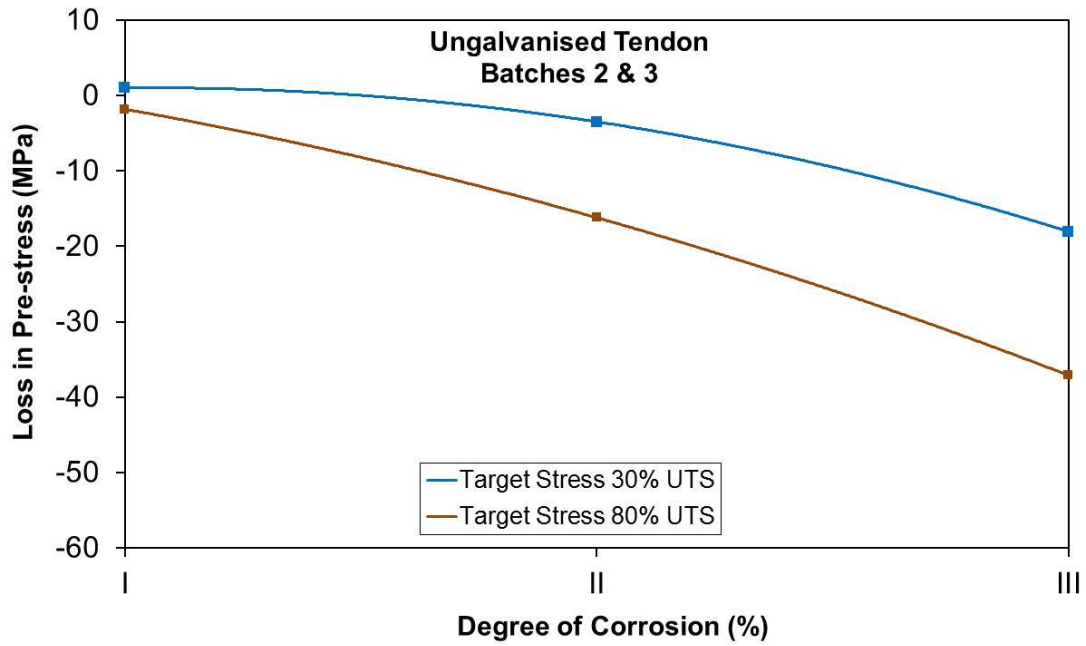


Figure 5.34 Relationship between degree of corrosion and different levels of pre-stress - Batches 2 & 3

5.6.5.3 Batch 4

In this section, Batch 4 is divided into two groups, Group 1 represents the three first specimens relating to Normal ICCP and the other three relate to Overprotection ICCP (Group 2). This division is due to the variation in the applied service stress and to give a better understanding of the behaviour of the tendons in each group (Table 5.16).

Table 5.16 Batch 4 galvanised tendons

Batch	Test Code	Group	Initial	Stress (MPa)					
			Stress (MPa)	Days					
				61	62	63	64	65	66
4	M-G-H-X-1	1	882	699	705	702	702	702	704
	M-G-H-II-N-1	1	869	678	685	686	690	691	693
	M-G-H-III-N-3	1	1063	678	676	669	668	668	669
	M-G-H-X1-1	2	862	873	874	873	873	873	874
	M-G-H-II-O-2	2	997	850	836	835	834	833	833
	M-G-H-III-O-3	2	894	805	791	788	786	785	784

Key: G-Galvanised, M-Mortar electrolyte, H-High level of pre-stress (800-1200MPa), I-Degree of corrosion Stage I (0-1%), II-Degree of corrosion Stage II (2-4%), III-Degree of corrosion Stage III (4-7%), O-Overprotection, X and X1-no corrosion and no ICCP, 1, 2, 3-Sample numbers.

The Batch 4 data presented in Table 5.16 are shown graphically in Figure 5.35 to Figure 5.38 to better understand the performance of the tendons. Figure 5.35 compares the gross loss in pre-stress for Group 1 tendons with the different degrees of corrosion Stage I (0-1 %), Stage II (2-4 %) and Stage III (2-3 %) at a High Level of pre-stress (800-1200 N/mm²), 80% (UTS). Similarly, Figure 5.36 shows the gross loss in pre-stress due to corrosion Stages I, II and III for Batch 4, Group 2.

Figure 5.37 and Figure 5.38 show the net loss in pre-stress due to corrosion of Stage II and Stage III (Batches 2 & 3) for target stress 80% UTS for Groups 1 and 2 respectively.

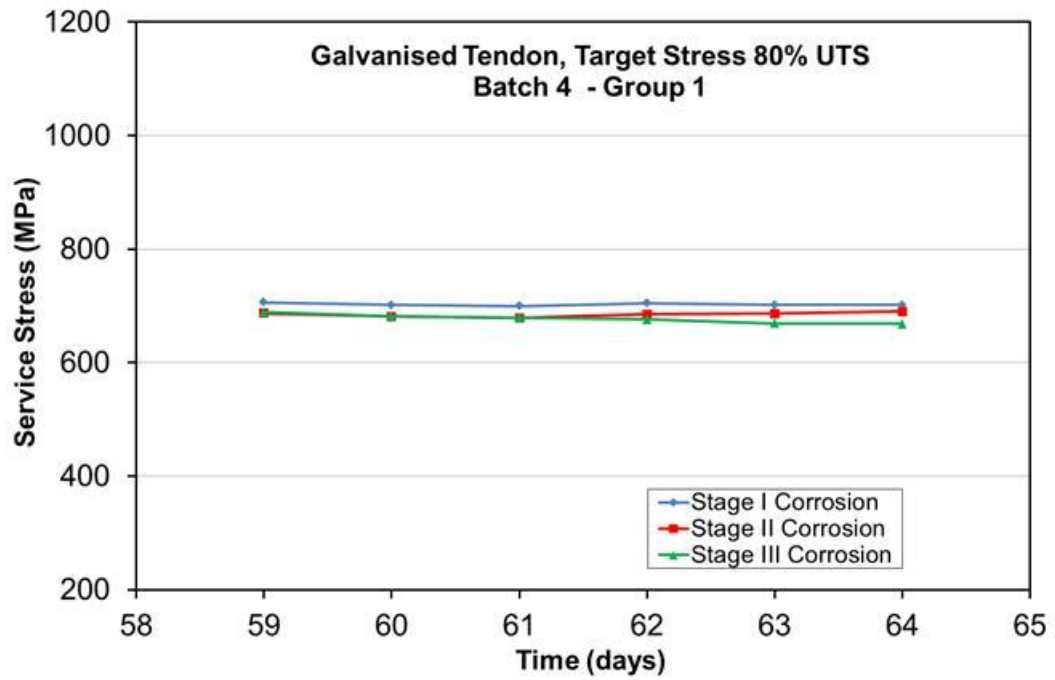


Figure 5.35 Gross loss in tendon pre-stress during corrosion period (80% UTS)
- Batch 4, Group 1

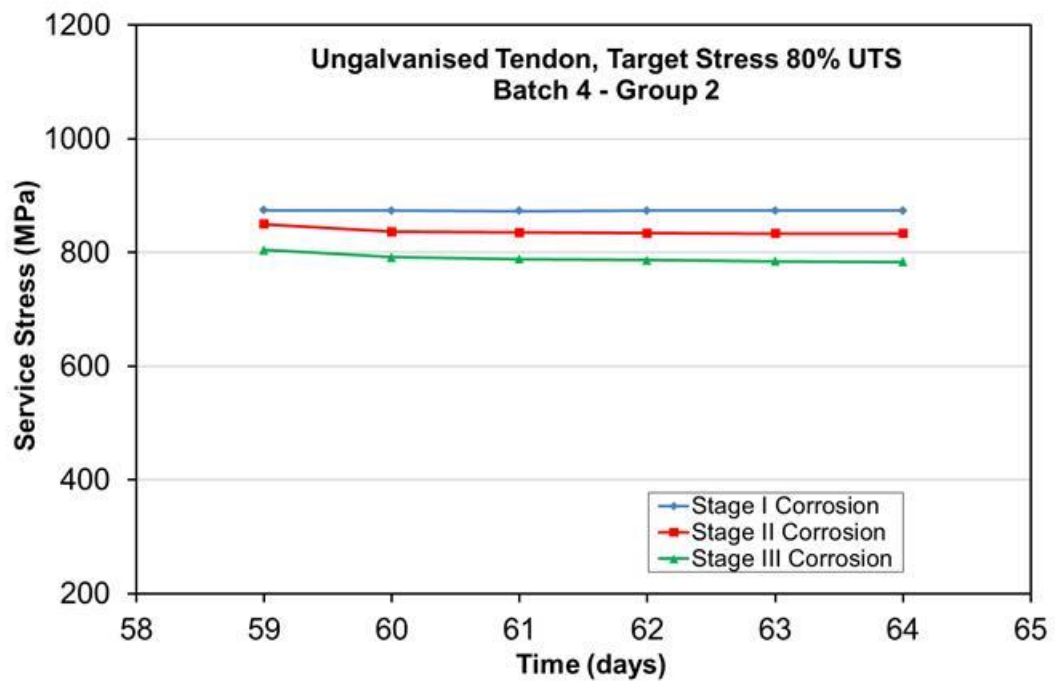


Figure 5.36 Gross loss in tendon pre-stress during corrosion period (80% UTS)
- Batch 4, Group 2

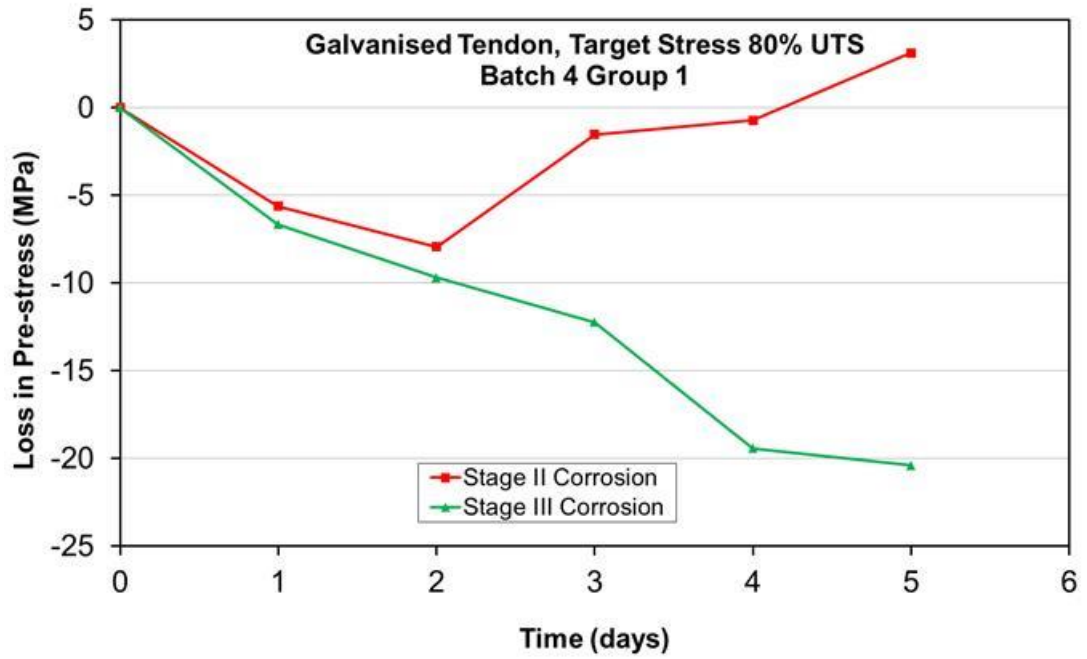


Figure 5.37 Net loss in tendon pre-stress during corrosion period (80% UTS) -
Batch 4, Group 1

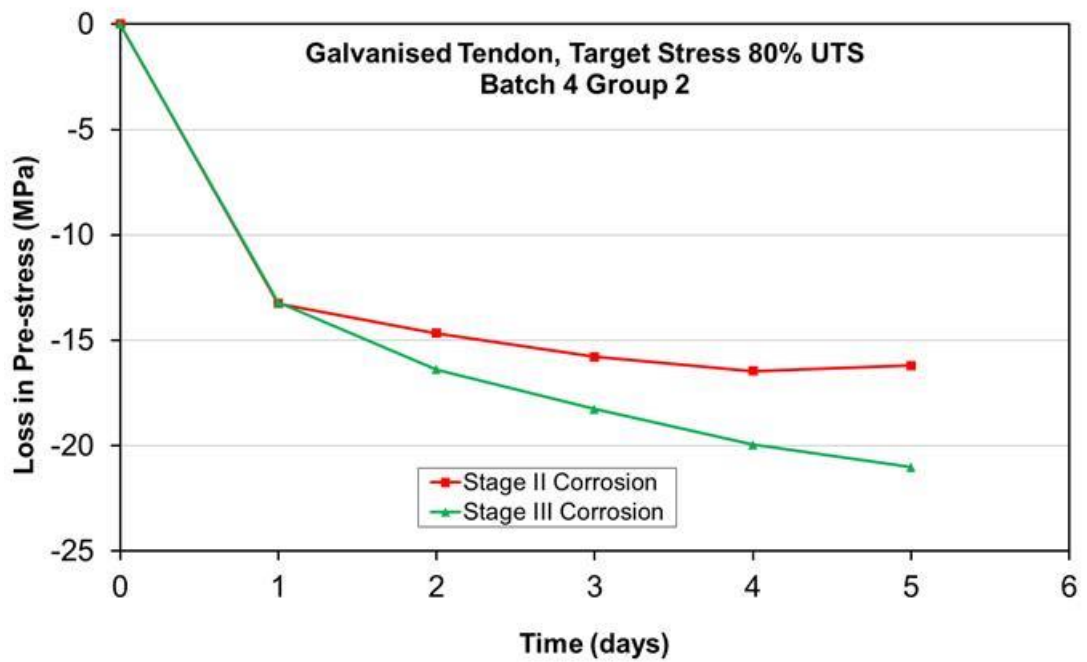


Figure 5.38 Net loss in tendon pre-stress during corrosion period (80% UTS) -
Batch 4, Group 2

5.6.4.3.1 Summary of loss in tendon service stress (Batch 4)

The results indicate that there is a loss in pre-stress due to corrosion and also the loss of pre-stress increased as the degree of corrosion increased. The results of residual applied stress shown in Table 5.17 were plotted in Figure 5.39 and show a loss in pre-stress increase as the degree of corrosion increases. This indicates that the loss in pre-stress is more dependent on the degree of corrosion and less dependent on the initial pre-stress in the tendon. These results again show the same behaviour of the tendons in Batch 1 over the corrosion process period.

Table 5.17 Residual service stress due to corrosion Batch 4

	<i>Corrosion stage</i>		<i>Residual stress (MPa)</i>	
	<i>(%)</i>		<i>Target Service Stress 80% UTS</i>	
			<i>(MPa)</i>	
Before	I		874	
Corrosion	II		850	
	III		805	
After	I		874	
Corrosion	II		833	
	III		784	

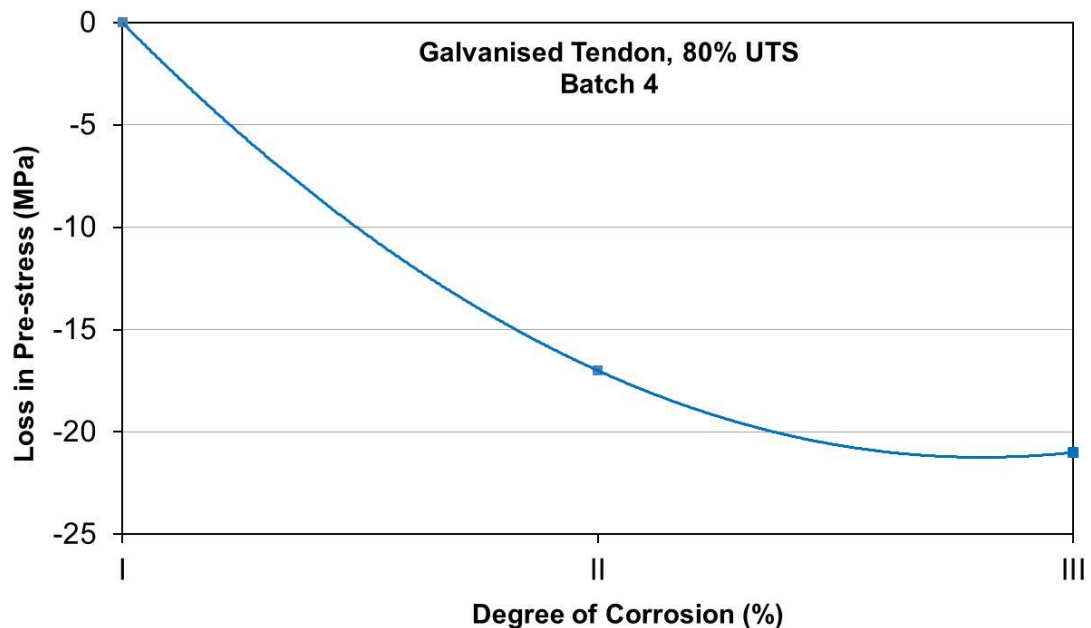


Figure 5.39 Relationship between degree of corrosion and the loss in pre-stress (80% UTS)

5.6.5.4 Comparison in loss of service stress between galvanised and ungalvanised tendons

From the above results of the loss in pre-stress over the corrosion test period for both galvanised and ungalvanised with the High Level of pre-stress, Figure 5.40 and Figure 5.41 show a comparison in the reduction in pre-stress of the ungalvanised and galvanised tendons with the different degree of corrosion Stage II and Stage III respectively. The loss in stress for both galvanised and ungalvanised with Stage I degree of corrosion exhibited a negligible change in pre-stress, therefore can be omitted. Both Figure 5.40 and Figure 5.41 show that the decline of ungalvanised pre-stress profile is more pronounced than the galvanised pre-stress profile. It can be seen that the loss in pre-stress in the ungalvanised tendons in both corrosion Stages II and III decline more than the loss in stress profile of the galvanised tendons. It is also noticeable that the different losses in pre-stress in galvanised and ungalvanised tendons with target stress 80 % UTS at Stage II degree of corrosion are broadly similar, while Figure 5.41 indicates that there is a large difference in loss of pre-stress resulting from Stage III corrosion. This indicates that the loss in pre-stress is more dependent on the degree of corrosion and less dependent on the initial pre-stress in the tendon.

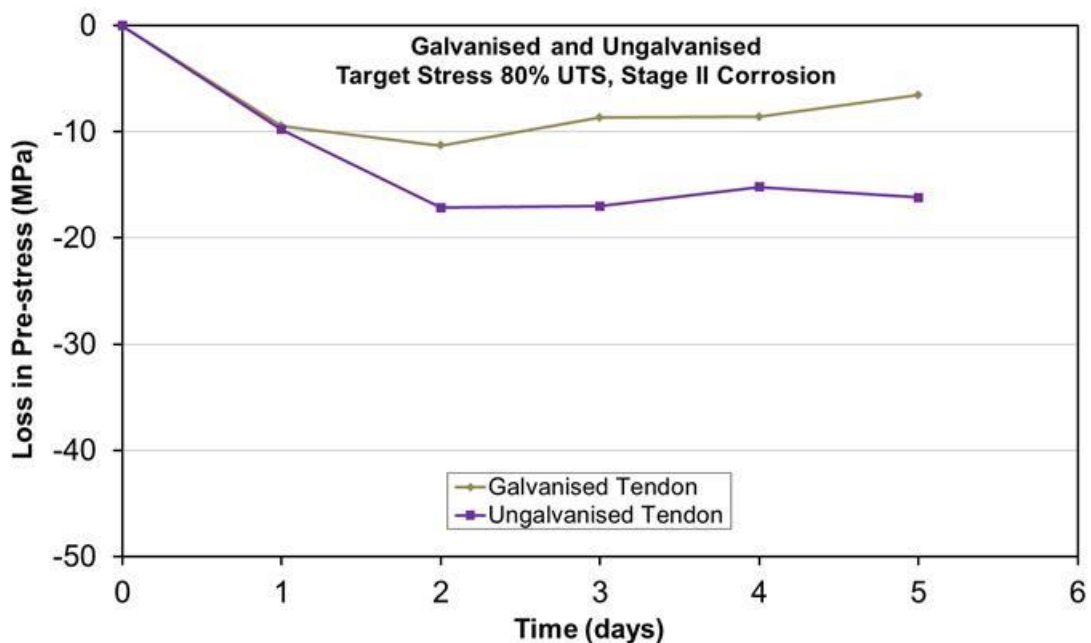


Figure 5.40 Net loss in galvanised and ungalvanised tendon pre-stress during corrosion period (Stage II)

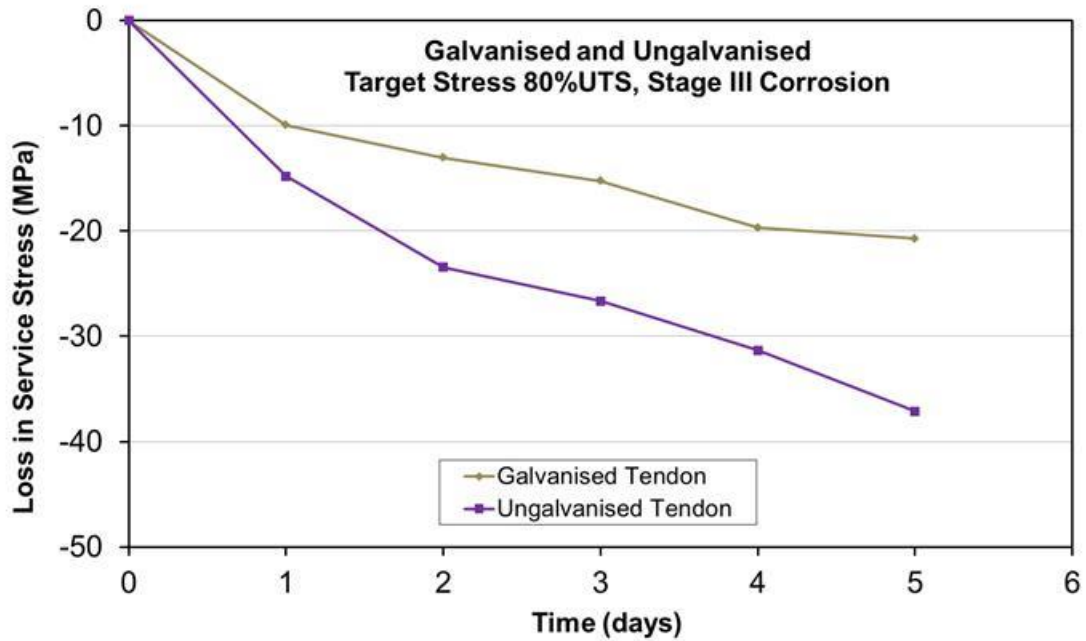


Figure 5.41 Net loss in galvanised and ungalvanised tendon pre-stress during corrosion period (Stage III)

The changes in pre-stress due to increasing corrosion are shown in Figure 5.42. The results show that the loss in pre-stress in the ungalvanised tendon with a High Level of pre-stress (80% UTS) declines more than the loss in pre-stress of the galvanised tendon. The decline in the loss in pre-stress for the galvanised tendon is recorded as 7MPa for Stage II corrosion and 21 MPa for Stage III corrosion. Similarly, a decline in the loss in pre-stress of ungalvanised tendon is recorded as 16 MPa for Stage II corrosion and 37 MPa for Stage III corrosion. Therefore, the change in the loss of pre-stress approximately doubles with the ungalvanised tendon compared with galvanised tendons.

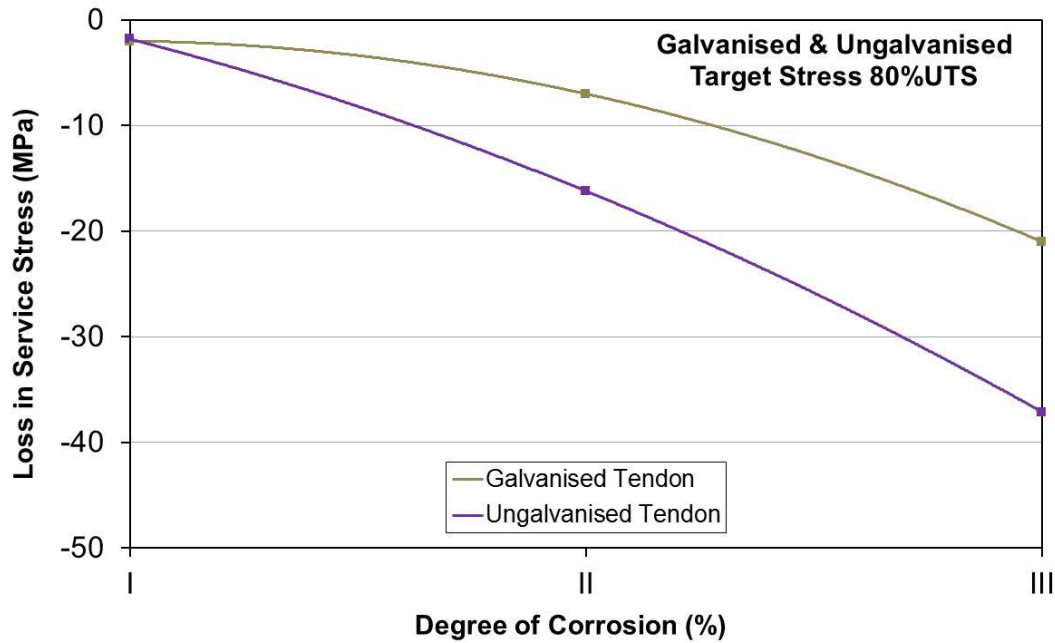


Figure 5.42 Relationship between degree of corrosion and the average loss in pre-stress in galvanised and ungalvanised tendon (80% UTS)

5.7 Conclusions

In light of the findings reported in this chapter, the following conclusions can be made:

- The anodic impressed current method was a practical method of generating and accelerating corrosion of both galvanised and ungalvanised pre-stressed tendons in the laboratory within a short timescale.
- The appearance of the corrosion products in a saline solution was yellow, brown and black. In mortar it was seen as rust staining, followed by longitudinal cracking in the mortar surface, especially when a high degree of corrosion was induced.
- For the galvanised tendons, the accelerated corrosion resulted in a loss of the zinc layer and the corrosion of the underlying steel.
- A corrosion current density of 1 mA/cm^2 was sufficient for inducing accelerated corrosion in all the specimens.
- Localised corrosion was observed on the corroded tendons along with general corrosion.

- The gravimetric (weight loss) method is preferable for measuring the actual degree of corrosion.
- Higher roughness characteristics were evident on the surface of the tendons at higher degrees of corrosion.
- A higher degree of corrosion leads to a higher loss in pre-stress in highly pre-stressed tendons which is an additional loss that should be considered for at the design stage.
- Loss in pre-stress in ungalvanised tendons with in both Stages I and II degree of corrosion is higher than the loss in pre-stressed galvanised tendon.

6 Effect of Cathodic protection on steel tendons

- Normal Protection

6.1 Introduction

Cathodic protection (CP) is a technique to control the corrosion of a metal surface by making it the cathode of an electrochemical cell. The simplest method to apply CP is by connecting the metal to be protected with another more easily corroded metal to act as the anode of the electrochemical cell [102]. Cathodic protection (CP) has been known for about 170 years. Primarily it has been used for protection of ordinary structural steel in soil and seawater, more seldom (and under special conditions) for steel exposed to fresh water. The application of this technology has increased considerably in recent decades and used for many reinforced concrete structures [103].

Cathodic protection can also reduce corrosion by minimizing the difference in potential between the anode and cathode. This is achieved by applying a current to the structure to be protected from some outside source. When enough current is applied, the whole structure will be at one potential; thus, anodic sites will not exist. Cathodic protection is commonly used on many types of structures, such as pipelines, underground storage tanks, locks, and ship hulls [103].

The protection potential and current density required to polarise any metal structure to this potential are the main factors affecting any cathodic protection system. Problems can occur in any cathodic protection system when the applied current density is not optimised. Too high an applied current density may be a problem because it can lead to cathodic over-protection which can be destructive to the protected metal structure, for example, due to hydrogen embrittlement of high strength steels; also the cost for running such a system is too high. Conversely, too low a value of applied current density can lead to corrosion [104].

Many corrosion engineers and technicians did not recognize that pre-stressing tendon, as a high tensile steel, was susceptible to hydrogen embrittlement (HE).

Unfortunately, HE of the pre-stressing wire from excessive CP appeared to have caused isolated ruptures. The most negative polarization (instant current-off) potential on one line was $-1,265$ mV CSE, with rupture adjacent to an anode bed 12 months after CP activation. On the other, it was $-1,330$ mV with rupture occurring 18 years after activation. This pipeline was in an area of frequent lightning [105].

The steel in pre-stressed concrete can corrode in a similar manner in conventionally reinforced concrete. Cathodic protection can provide a method of controlling the corrosion in pre-stressed concrete structures after appropriate system design consideration [35]. Several techniques have been used successfully to apply CP to reinforced concrete structures. These techniques include impressed-current CP (ICCP) systems and galvanic or 'sacrificial' anode systems [106]. However, the selection of an appropriate CP anode system is a major consideration, whether for galvanic or impressed current applications. A mixed metal oxide (MMO) coated titanium mesh ribbon is used as an anode in the ICCP systems in this research work.

In the light of the above and for the purpose of this research with taking the consideration of the effect of ICCP on high tensile steel with 1800MPa UTS, two scenarios for protection using impressed current were proposed and investigated, ICCP-Normal protection (ICCP-N) with an applied potential of -650 to -750 mV vs Ag/AgCl/KCl 0.5M (SSC) and ICCP-Overprotection (ICCP-O) with an applied potential of -850 to -1300 mV vs SSC. This chapter will investigate the effect of applying ICCP with Normal potential in both levels of pre-stressed galvanised and ungalvanised tendons, Low Level (300-400 MPa) and High Level (800-1200 MPa), exposed to three stages of corrosion I (0-1 %) , II (2-4 %) , and III (4-7 %).

6.2 The objectives of the tests

The objectives of this chapter are to investigate the following:

- Determine the loss of applied service stress during the period of the application of ICCP-N

- Apply ICCP-N and monitor its criteria in terms of the applied potential to the tendon, potential shift, instant off and potential decay according to the related standards
- Identify any effects of the application of ICCP-N on the surface of tendons
- Investigate the mechanical properties of the tendons
- Investigate the type and form of fracture of the tendons

6.3 Impressed Current Cathodic Protection (ICCP)

Traditionally, CP exist as two types: galvanic and impressed current, although a third (a combination of the two) known as a hybrid system is also occasionally employed. ICCP of atmospherically exposed steel reinforced concrete structures has been used since the 1970s and it is a proven technique which is able to arrest ongoing corrosion and induce and sustain steel passivity [60]. The main principle of cathodic protection is applying an impressed current to induce negative steel polarisation [77] and, drive the steel potentials more negative than -850 mV (SCE), where the anodic reactions are thermodynamically restrained. Under these conditions the steel will be immune to corrosion [60]. For conventional buried structures protected by this method the anodes are installed in the soil around the structure to be protected and the DC power is supplied to the anodes through buried wires [107].

The main difference between galvanic and impressed current systems is that the galvanic system relies on the difference in potential naturally generated between the anode and the structure; whereas the impressed current system uses an external power source to drive the currents shown in Figure 4.8. The external power source was traditionally a rectifier that converts ordinary AC power to DC although more efficient and reliable DC sources are now available. The current is carried in the external circuitry as electrons, free electrons do not exist in an electrolyte solution; therefore, the current must be carried by positively and negatively charged ions. The current flows through the electrolyte solution, equal to that in the external circuit (Figure 6.1).

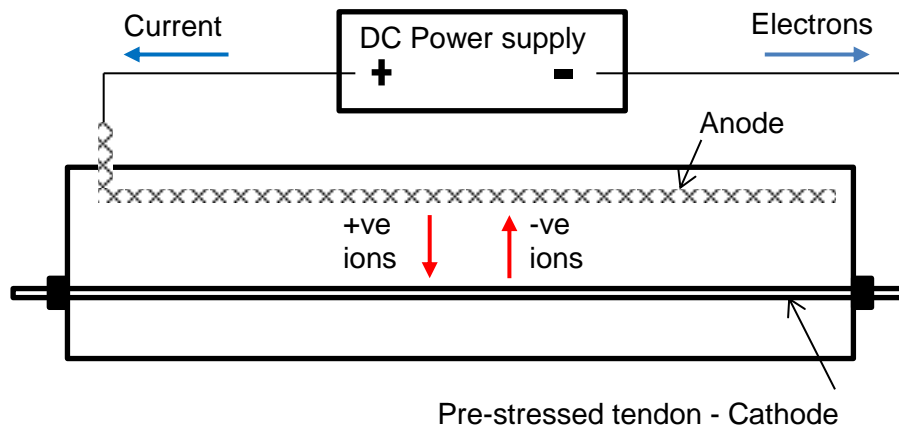


Figure 6.1 Schematic diagram of the principle of ICCP

Positively charged ions carrying the current electrochemical reactions at the electrodes are responsible for the mechanism of cathodic protection and for the transfer of charges from electron to ions at the electrode surface. Impressed current means that a current is impressed between the buried structure and an anode.

Concrete is a highly heterogeneous porous material consisting of coarse and fine aggregates bound by hydrated cement paste. The resistivity of concrete, which can reach up to 20,000 Ωcm is very high when compared to other media (for eg: seawater has a resistivity of 30 Ωcm) [108]. ICCP is widely used in concrete as it can deliver relatively high voltages compared to galvanic protection using, for example, surface-mounted anodes. As for any ICCP application, the protected metal and anode both need to be in contact through a common electrolytic medium to allow the passage and distribution of current and charges. Despite concrete having a high electrical resistance, it is able to pass charges through it due to the presence of pore solution which acts as the electrolyte. The basic components of an ICCP system in reinforced concrete has been described in Chapter 4 Section 4.7. The steel reinforcement is connected to the negative terminal of a power supply whereas the positive terminal is connected to the anode material. A real system in practical applications will normally include a number of other components such as electronic control units, junction boxes and monitoring equipment.

6.3.1 Anode

A number of different anode types are used for ICCP systems. The choice of the anode is made according to circumstances and requirements, keeping in mind factors such as performance, costs, operating life, resilience/durability and ease of installation. Anodic materials can be broadly divided into consumable (eg: zinc and aluminium), semi-consumable (eg: graphite and silicon cast iron) and inert (eg: platinized titanium and mixed metal oxide [MMO] Titanium) anodes, with each type differing in their consumption rates. The anode used for ICCP application was MMO titanium mesh type 170 Anode Ribbon Mesh, see Section 4.9.2 and Table 4.3. The anode was mechanically connected to an electrical wire and was positioned below the concrete surface while pouring concrete. For ICCP application, the anode was connected to the positive terminal of a DC power source, with the tendon connected to the negative terminal.

6.3.2 Current density requirement

The current required for cathodic protection depends upon the metal being protected and the environment and the potential required to achieve adequate protection as demonstrated by recognised criteria. To achieve the protection potentials, current must flow from the anode to the structure being protected. The amount of current required to protect a given structure is proportional to the area of the structure that is exposed to the electrolyte. Therefore, current requirements are usually given as current densities in units of amperes or milliamperes (0.001 amperes) per square meter (or foot) of the exposed surface [109]. However, typical values of current densities used in practical scenarios (10-30mA/m²) do not cause loss of bond-strength to an extent that would cause concern. The reduction in bond-strength is attributed to the softening effects of concrete caused by the formation of soluble silicates near the steel resulting from the interaction of alkali hydroxides formed by cations (such as K⁺ and Na⁺) with calcium silicate hydrate in cement [56].

6.3.3 ICCP with hydrogen embrittlement

ICCP can lead to hydrogen embrittlement of steel reinforcement in concrete, notably high strength pre-stressed steel, given that it is sufficiently cathodically polarized to very negative values. For steel in concrete, the predominant

cathodic reaction is normally the reduction of O₂, however, a second cathodic reaction may occur involving the reduction of water, provided the potential is lowered below the hydrogen potential [110]:



The adsorbed hydrogen atoms can further react to produce hydrogen gas or may dissolve into the metal:



Although the hydrogen potential is not fixed on account of its dependency on a number of variables, a potential more positive than -900mV is generally regarded to have a low risk of hydrogen embrittlement for pre-stressed steel in concrete [50]. The atomic hydrogen formed can either combine to form hydrogen gas or can ingress into the steel and can adversely influence its mechanical properties and lead to brittle fracture, with higher-strength steel being more susceptible to this form of failure [110]. The mechanism of hydrogen embrittlement was discussed in Section 2.6.3.2. In this chapter, the potential applied is less negative than -950mV vs Ag/AgCl/KCl 0.5M and, the purpose is to understand the behaviour of the tendon under normal protection.

6.4 Experimental Work

To have a better understanding of the behaviour of the pre-corroded tendons with two levels of pre-stress (Low and High), an extended period test approach was adopted. Four Batches were tested with ICCP after accelerated corrosion was applied and before demoulding the specimens. For the purpose of the research and in terms of the application of ICCP, the specimens were divided into two main categories for applying ICCP, one Normal-protection where the applied potential ranged between -650 to -750 mV (SSC), the other Over-protection where the applied potential ranged between -850 to -1300 mV (SSC). These ranges selected were based on the practical application of the ICCP. For this chapter, the performance of the pre-corroded tendons under ICCP-N were investigated (Table 6.1).

Table 6.1 Test programme

Batch	Test Code	Degree of	Actual	ICCP
		Corrosion (Stage)	Degree of Corrosion (%)	
2	M-U-L-X-1	I	0	None and uncorroded - Control
	M-U-L-II-N-2	II	3.98	ICCP (Normal-Protection)
	M-U-L-III-N-3	III	5.32	ICCP (Normal-Protection)
	M-U-H-X-1	I	0	None and uncorroded - Control
	M-U-H-II-N-2	II	2.25	ICCP (Normal-Protection)
	M-U-H-III-N-3	III	4.05	ICCP (Normal-Protection)
4	M-G-H-X-1	I	0	None and uncorroded - Control
	M-G-H-II-N-2	II	3.48	ICCP (Normal-Protection)
	M-G-H-III-N-3	III	4.36	ICCP (Normal-Protection)

Key: U-Ungalvanised, G-Galvanised, M-Mortar electrolyte, S-Solution electrolyte, H-High level of pre-stress (800-1200MPa), L-Low level of pre-stress (300-400MPa), I-Degree of corrosion Stage I (0-1%), II-Degree of corrosion Stage II (2-4%), III-Degree of corrosion Stage III (4-7%), N-Normal protection, O-Overprotection, X and X1-no corrosion and no ICCP, R-As-received samples, 1, 2, 3-Sample numbers.

Batch 2 investigated the effect of applying ICCP-N on ungalvanised tendons with low and high levels of pre-stress embedded in mortar, while Batch 4 investigated the effect of applying ICCP-N on galvanised tendons with high level of pre-stress embedded in mortar. Table 6.2 shows the overall period of the application of ICCP Normal-protection in the tendons.

Table 6.2 ICCP Normal-protection

Batch	Test Code	Degree of	Actual Degree	ICCP	
		Corrosion (Stage)	of Corrosion	Period	
			(%)	days	hours
2	M-U-L-X-1	I	0	367	8808
	M-U-L-II-N-2	II	3.98	367	8808
	M-U-L-III-N-3	III	5.32	367	8808
	M-U-X1-1	I	0	553	13272
	M-U-H-II-N-2	II	2.25	553	13272
	M-U-H-III-N-3	III	4.05	553	13272
4	M-G-X-1	I	0	137	3288
	M-G-H-II-N-2	II	3.48	137	3288
	M-G-H-III-N-3	III	4.36	137	3288

Key: U-Ungalvanised, G-Galvanised, M-Mortar electrolyte, S-Solution electrolyte, H-High level of pre-stress (800-1200MPa), L-Low level of pre-stress (300-400MPa), I-Degree of corrosion Stage I (0-1%), II-Degree of corrosion Stage II (2-4%), III-Degree of corrosion Stage III (4-7%), N-Normal protection, O-Overprotection, X and X1-no corrosion and no ICCP, R-As-received samples, 1, 2, 3-Sample numbers.

6.4.1 Specimen design, mortar mix, pre-tensioning and accelerated corrosion

ICCP-N was applied to the pre-corroded specimens shown in Table 6.2. The specimen dimensions and mortar mix are described in Section 5.4.3. The compressive strength of the mortar for each Batch is also presented in Table 5.2, in Section 5.4.3.1. The pre-tensioning procedures and different level of applied service stress are described in Section 5.4.4. The corrosion process has been described in Section 5.5, where MMO Ti mesh was connected to the negative terminal of a D.C power supply, working as the cathode while the tendons were connected to the positive terminal of the D.C power supply and corrosion took place in both a saline solution containing 3.5% NaCl and mortar. The moisture of the mortar was maintained by water spraying on a daily basis. The current and potential were also recorded on a daily basis. For the purpose of the research, two identical wooden supports were manufactured in order to store additional specimens, as shown in Figure 6.2.

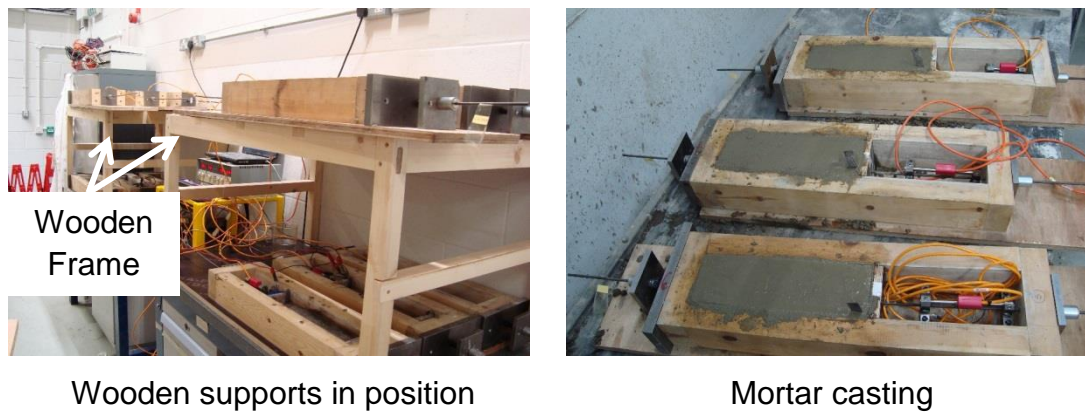


Figure 6.2 Wooden supports to facilitate storage of specimens

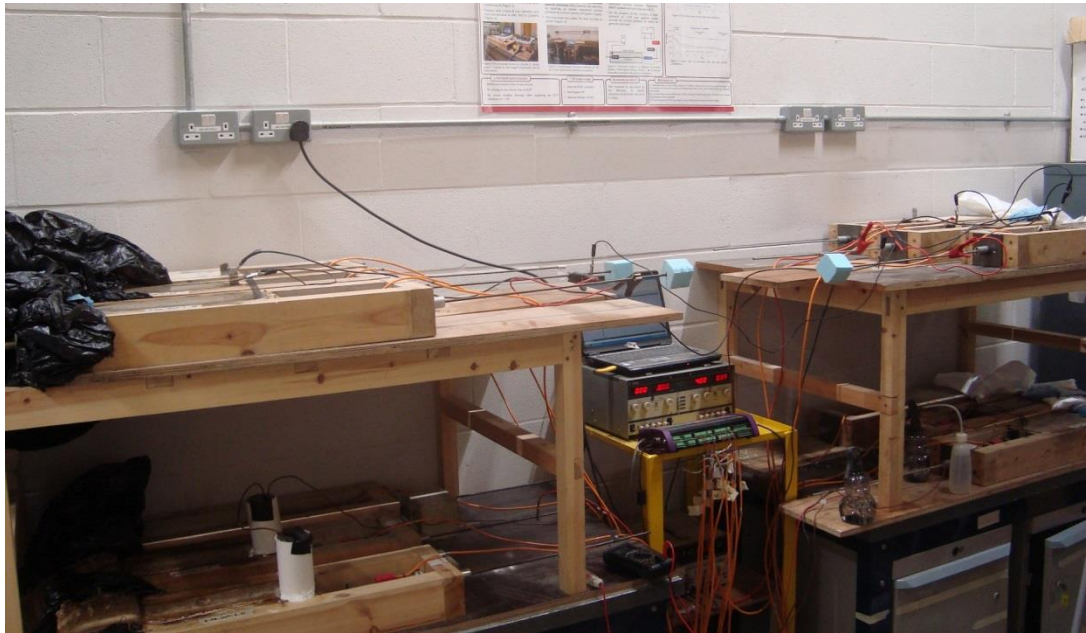
6.4.2 Application of impressed current cathodic protection (ICCP)

ICCP was applied for each specimen by connecting the pre-stressed tendon to the negative terminal and the mixed metal oxide (MMO) titanium mesh ribbon anode to the positive terminal of a D.C power supply. The length of each tendon exposed to ICCP-N is 32 cm. The principle of ICCP systems for reinforced concrete structures has previously been described in Chapter 4, Section 4.7. The system includes the following components:

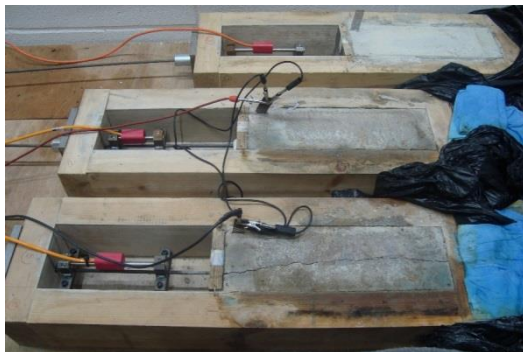
- DC power supply (traditionally a transformer rectifier system)
- Inert anode (MMO Ti mesh ribbon)
- Cathode system - the tendon bars
- Electrolyte - the mortar
- DC wiring between the anode, tendon (cathode), power supply and fitting
- Monitoring probes, reference electrode type Ag/AgCl/KCl 0.5M
- Digital voltage meter (DVM)
- Data Logger - to record the strain readings during the application of ICCP
- Monitoring and control system, often remotely operable

An ICCP system for reinforced mortar has been established for analysing the distribution of protective potential and current. In this study, the DC power supply was a CPI manual power system, supplied by Cathodic Protection International Aps. The ICCP system was operated in the Construction Materials Laboratory, which ensured a stable environment of average 20°C and humidity of 60% \pm 5% (Figure 6.3) (a-c). Following installation of all the components of the ICCP, each system was connected to the power and monitoring equipment and powered up. In general there are two methods of controlling ICCP systems. One is that the output voltage is kept constant and the current is allowed to alter

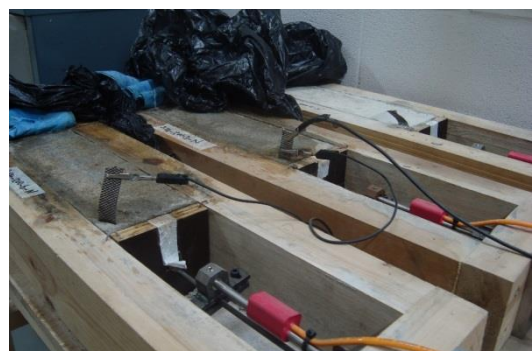
in order to maintain the set potential. The other method is to fix the current and allow the potential to float. In this research, the commonly employed former system of fixed potential was employed.



(a) General view



(b) Normal protection with low level of pre-stressed tendons



(c) Normal protection with high level of pre-stresses tendons

Figure 6.3 Setup of specimens under application of ICCP-Normal protection

6.4.3 Design criteria

As discussed in Section 6.4.2, the first method, where the potential is kept constant and the current is allowed to float, was adopted. It is recommended that commissioning of the ICCP system should start at a low level of current density for the initial part of the commissioning period to avoid any adverse effects on the anode durability. Tests can be then carried out to determine what adjustments are needed to satisfy the operating criteria. The topic of using a standard criterion to assess the achievement of adequate protection by ICCP has been the subject of considerable debate. A number of different criteria have been proposed, various criteria for ensuring satisfactory protection of the reinforcement have been considered for reinforced structures. The major international institutions and standards including National Association of Corrosion Engineers (NACE) [111], [112], International Standard Organisation (ISO) [113], British Standards and European Standards [114], [115] and Australian Standards [116] publish criteria to be used for ensuring cathodic protection of metallic structures. Companies working in the oil, gas and water industries also publish their own standards (e.g. Shell). The degree of complexity between the standards varies considerably from a blanket approach of specifying the minimum protection potential to detailing minimum and maximum protection potentials and corrosion potentials under particular environmental conditions. The NACE recommended criteria are:

- Polarization to a potential of -850 mV vs copper/copper sulfate reference electrode
- A minimum of 100 mV polarization (determined by depolarisation/decay)
- Voltage shift by 300 mV
- A voltage at least equal to that corresponding to the beginning of the linear segment (Tafel segment) of an E-Logi curve
- Measurement of a net protective current (ensuring current flow in single direction from electrolyte to structure)

The current NACE Standard SP 0169-2007 [117] Section 6 emphasizes the following CP criteria [118]:

- -850 mV vs. saturated copper/copper sulphate reference electrode (CSE) with CP current applied, or -850 mV on-potential considering voltage drops (IR)

- -850 mV off-potential or polarized potential
- 100 mV cathodic polarization.

Although the above criteria were applicable for steel buried in soil, similar criteria have been adopted for reinforced concrete. BS EN 12696 [77] for atmospherically exposed reinforced concrete structures has specified the following criteria:

- An instant-off potential (measured between 0.1s and 1s after switching the DC circuit open) more negative than -720mV with respect to Ag/AgCl/0.5MKCl.
- A potential decay over a maximum of 24h of at least 100mV from instant-off.
- A potential decay over an extended period (typically 24h or longer) of at least 150mV from the instant-off subject to a continuing decay and the use of reference electrodes (not potential decay sensors) for the measurement extended beyond 24 hours.

The criterion of (100 to 150 mV) potential shift is the most widely recognised criterion to ensure adequate protection from a CP system. This criterion specifies that when the CP system is switched off, the instant-off potential (E_{off}) measured at a time between 0.1 and 1 second and the potential after a certain period of time, e.g. 4 to 24 hours should be between -100 and -150mV. Therefore, in this research, this criterion was adopted as a means of monitoring and ensuring the effectiveness of the applied ICCP system.

6.4.4 Polarisation and Depolarisation Criteria

According to NACE SP0290, the requirement is for a minimum polarisation of 100 mV from native potentials, or 100 mV depolarisation from an “Instant Off” potential (E_{off}) reading. The term “Instant Off” reading is typically read between 0.1 and 1.0 seconds after the DC power supply is interrupted. Readings at times less than 0.1 seconds often include spurious components that have nothing to do with the CP. After more than one second, the apparent depolarisation will be understated. Figure 6.4 provides a stylised diagram. Starting on the left with the base potential before CP is applied the polarisation is shown, whereby the steel potential is polarised in a negative, cathodic direction. About midway, the power supply is turned off and the potential shifts in a positive direction. The area between ‘CP Off’ and ‘Instant Off’ include IR

error and reactive transients resulting from interrupting the CP current. A point between 0.1 and 1 second is the true start of the depolarisation [119] .

All normally encountered electrolytes are resistive. That being the case, Ohm's Law, $E = IR$, tells us that when CP current (I) passes through the electrolyte (R) a voltage is produced (E). When the CP system is turned off, there can be reactive transients that occur from the collapsing magnetic field that surrounds the wires and rebars carrying the CP current. There can also be capacitive transients. Errors from CP current-generated IR and interruption transient currents must be addressed when measuring the corrosion potentials of embedded rebar and when applying DC corrosion rate test methods such as LPR techniques.

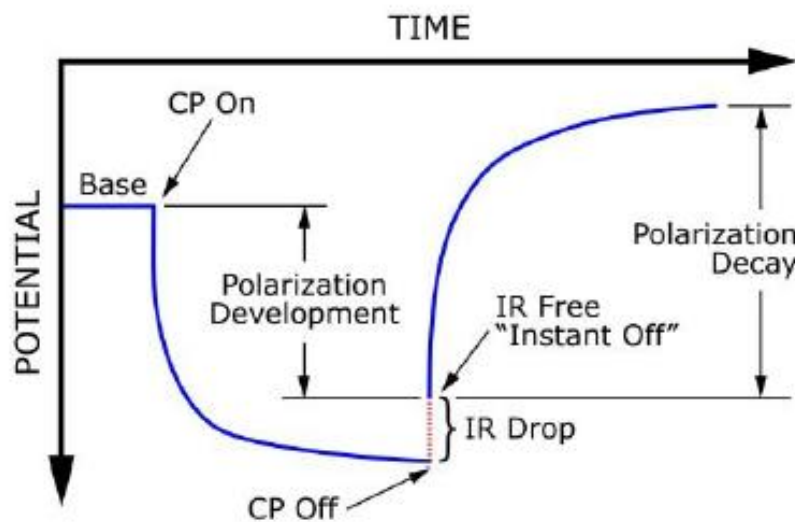


Figure 6.4 Polarization-Depolarisation [119]

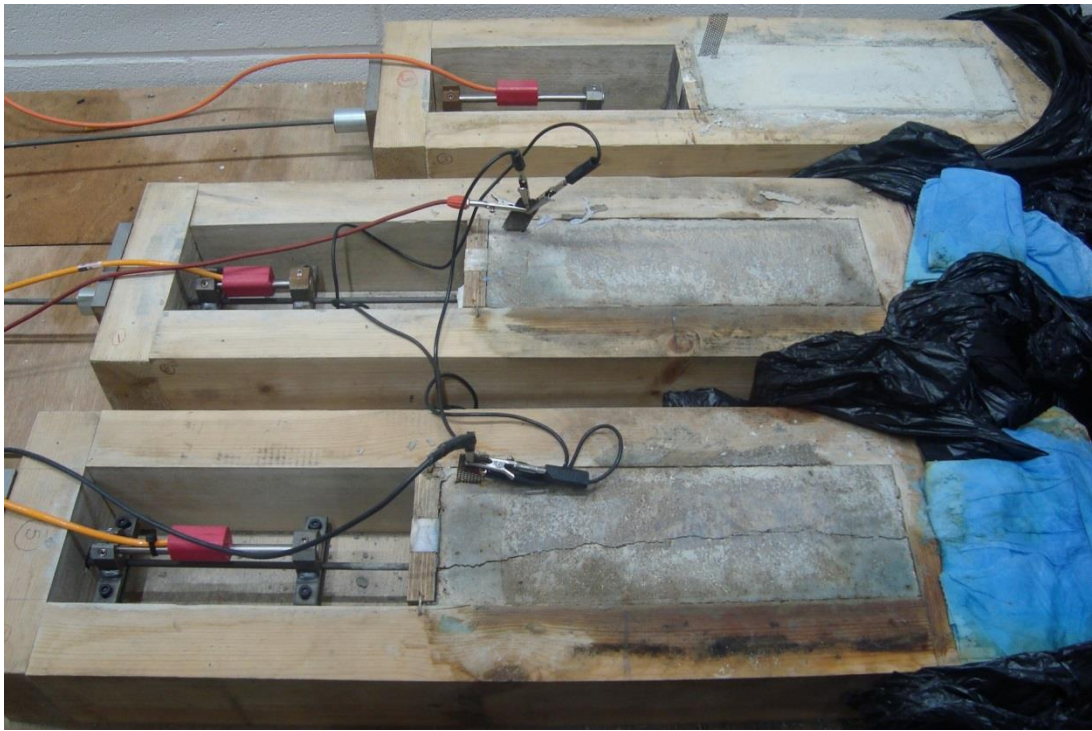
Accurate measurements of rebar corrosion potentials should only reflect the potential across the rebar-concrete interface and not include these transient voltages. For reinforced concrete structures the transients are no longer a factor after 0.1 to 1.0 seconds.

6.5 Results and discussion

6.5.1 Visual observation

Daily observation and data (Volts, Amps, Potential and 'Instant-off' steel potential) were recorded during the full period of applying ICCP-N. For ungalvanised tendons (Batch 2) for both Low and High levels of pre-stress, small yellow spots appeared on the surface of the mortar around the connection

of anode location as shown in Figure 6.5 (a-c) and Figure 6.6 (a-c). At the time corresponding to a current of 13mA applied to the MMO mesh anode, a gaseous and yellow liquid deposit appeared around the mesh. Concrete Society Technical Report No. 73 states that due to the electrochemical reactions, acid and oxygen is generated during operation at the surface of anodic commonly used for the cathodic protection of reinforced concrete. It has been stated that some anodes may also generate chloride depending on the environment [48]. Therefore, the yellow discharge observed at the MMO Ti anode and concrete interface is believed to result from acid generation [120]. In the case of the galvanised tendons (Batch 4), there was no sign of yellow spots (Figure 6.7).



(a) General view

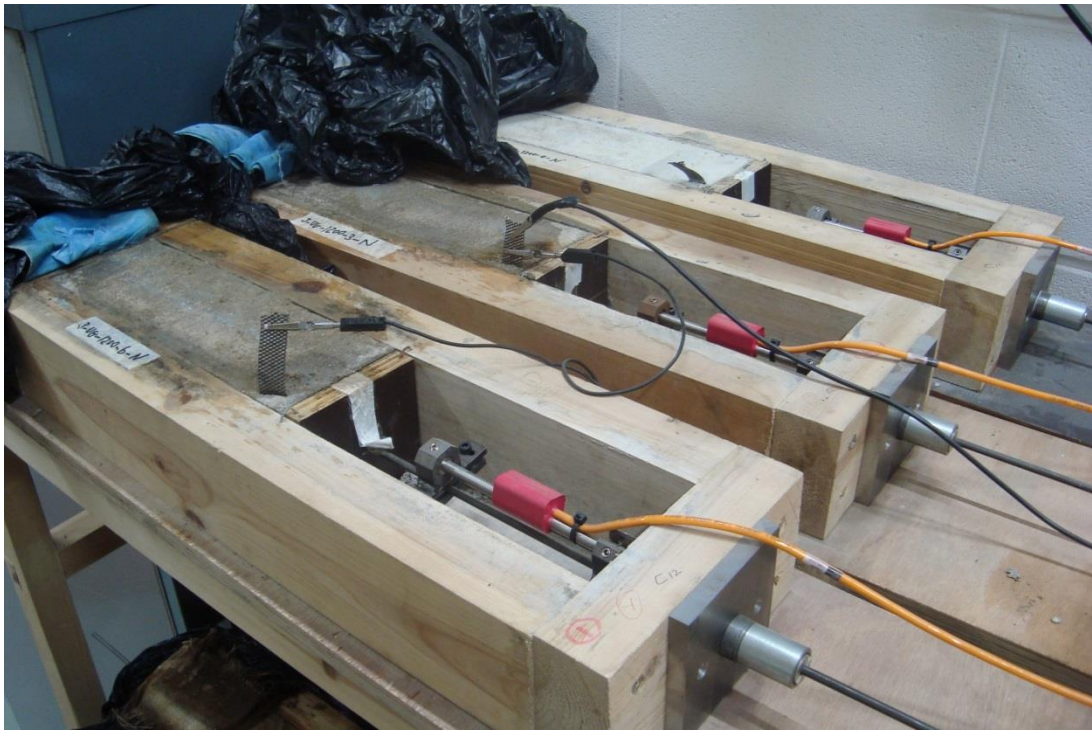


(b) Specimen M-U-L-II-N-2



(c) Specimen M-U-L-III-N-3

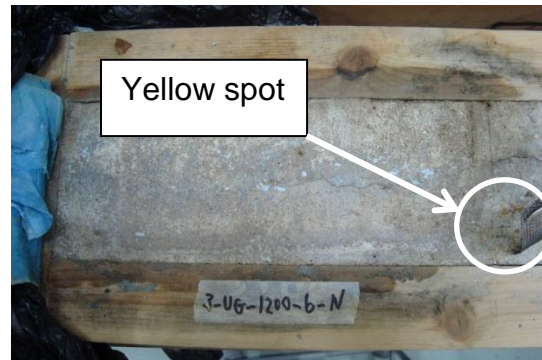
Figure 6.5 Yellow spots on the mortar surface for ungalvanised tendons with Low Level of pre-stress



(a) General view



(b) Specimen M-UG-H-II-N-2



(c) Specimen M-UG-H-III-N-3

Figure 6.6 Yellow spots on the mortar surface for ungalvanised tendons with High Level of pre-stress



(a) General view



(b) Specimen M-G-H-II-N-2



(c) Specimen M-G-H-III-N-3

Figure 6.7 No yellow spots on the mortar surface for galvanised tendons with High Level of pre-stress

6.5.2 Infinite Focus Microscope (IFM)

After completing the application of the cathodic protection, the pre-load was released at one end by turning the mild steel bolt and thereby relieving the stress in the tendon. The stress was released in a controlled manner by gripping the wedge with a vice-grip to prevent rotational bond failure of the tendon in the gunite and subsequently dis-engaging the bolt sufficiently to leave a gap (~10mm) between the head of the bolt and wedge.

The surface of the tendons was examined by Infinite Focus Microscope (IFM). The procedure is described in Chapter 4, Section 4.11.3. Figure 6.8 shows the

microstructure of the tendon surface using IFM with 5x magnification for ungalvanized tendons with Low Level of pre-stress with different degrees of corrosion. Figure 6.8 (a) represents the tendon before removing corrosion products and Figure 6.8 (b) shows the tendons after removing the corrosion products. It was found that the colour of the corrosion products on the surface of the tendons after applying ICCP-N was brown as shown in specimens M-U-L-II-N-2 (Figure 6.8 (a)) and M-U-L-III-N-3 (Figure 6.8 (a)). Specimen M-U-L-II-O-2 (Figure 6.8(b)) shows the damage to the steel caused by corrosion and this was assessed by profiling the pits on the surface of the tendon after the removal of the corrosion products. The presence of pitting corrosion indicates that the current was not distributed equally due to changes in the applied potential. The dimension of pitting was given in Chapter 5. On the other hand, pitting corrosion was virtually absent on the surface of specimen M-U-L-III-N-3 (Figure 6.8 (b)), showing that no apparent pitting was formed on the surface of the tendon. This damage is more related to the application of accelerated corrosion techniques rather than the application of ICCP-N.

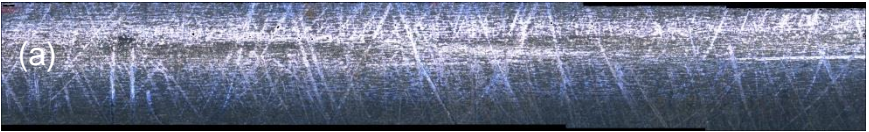
M-U-L- X-1	No Corr. No ICCP	
M-U-L-II-N-2	Before removing Corr. Products	
	After removing Corr. Products	
M-U-L-III-N-3	Before removing Corr. Products	
	After removing Corr. Products	

Figure 6.8 Microstructure of ungalvanized tendons surface

Figure 6.9 shows the microstructure of the tendon surface using IFM with 5x magnification for ungalvanised tendons with High Level of pre-stress and different degrees of corrosion. Figure 6.9 (a) represents the tendon before removing the corrosion products and Figure 6.9 (b) shows the tendons after removing the corrosion products. In this batch the colour of the corrosion products on the surface of the charged tendons after application of the ICCP-N appears pink due to the lighting used to illuminate the image. Specimens showed no apparent pitting was formed on the surface of the tendons and more uniform corrosion was observed. Again, there is no apparent effect on the surface of the tendons due to the application of ICCP-N.

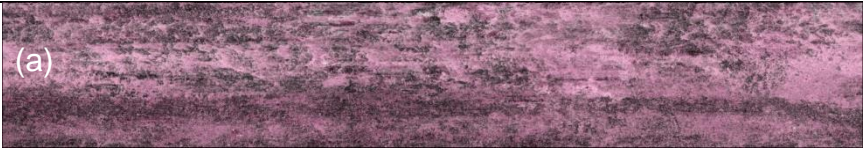
M-U-H-X-1	No Corr. No ICCP	
M-U-H-II-N-2	Before removing Corr. Products	(a) 
	After removing Corr. Products	(b) 
M-U-H-III-N-3	Before removing Corr. Products	(a) 
	After removing Corr. Products	(b) 

Figure 6.9 Microstructure of ungalvanized tendons surface with High Level of pre-stress

For the galvanised tendons with High Level of pre-stress, there is damage on the surface of the tendon caused by corrosion and there is pitting along the length as shown in Specimen M-G-H-II-N-2, (Figure 6.10 (b)) (shown by a red dashed area). Specimen M-G-H-III-N-3, (Figure 6.10 (b)) shows a damage on the surface of the tendon. This damage is caused by corrosion rather than the application of ICCP-N.

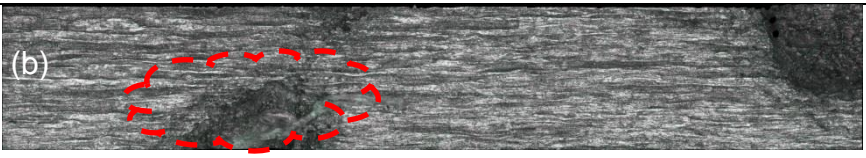
M-G-H-X-1	No Corr. No ICCP	
M-G-H-II-N-2	Before removing Corr. Products	(a) 
	After removing Corr. Products	(b) 
M-G-H-III-N-3	Before removing Corr. Products	(a) 
	After removing Corr. Products	(b) 

Figure 6.10 Microstructure of galvanised tendons surface with High Level of pre-stress

6.5.3 Potential

Table 6.3 shows the rest potential (E_{corr} vs Ag/AgCl) of the tendon when no cathodic protection was applied. The rest potential of the tendon ranged from -513mV to -670mV (Ag/AgCl).

Table 6.3 Potential before applying ICCP-N (Rest Potential)

<i>Batch</i>	<i>Test Code</i>	<i>Degree of Corrosion (Stage)</i>	<i>Actual Degree of Corrosion (%)</i>	<i>Rest Potential before applying ICCP (Ag/AgCl/KCl 0.5M) Negative (mV)</i>
2	M-U-L-I-N-1	I	0	–
	M-U-L-II-N-2	II	3.98	-602
	M-U-L-III-N-3	III	5.32	-581
	M-U-H-I-1	I	0	–
	M-U-H-II-N-2	II	2.25	-513
	M-U-H-III-N-3	III	4.05	-570
4	M-G-H-I-1	I	0	–
	M-G-H-II-N-2	II	3.48	-670
	M-G-H-III-N-3	III	4.36	-570

Key: U-Ungalvanised, G-Galvanised, M-Mortar electrolyte, S-Solution electrolyte, H-High level of pre-stress (800-1200MPa), L-Low level of pre-stress (300-400MPa), I-Degree of corrosion Stage I (0-1%), II-Degree of corrosion Stage II (2-4%), III-Degree of corrosion Stage III (4-7%), N-Normal protection, O-Overprotection, X and X1-no corrosion and no ICCP, R-As-received samples, 1, 2, 3-Sample numbers.

The power supply was switched on and the voltage adjusted until the steel potential reached the target negative potential -650 to -750mV for ICCP-N, then the "E_{on}" potentials were recorded as shown in Figure 6.11 and Figure 6.12 for ungalvanised tendons with Low Level and High Level of pre-stress respectively. As can be seen from these two figures, the potential started highly negative then decreased before stabilising at approximately 1000mV below the steel potential. This drop is due to the resistance of the mortar decreasing and also the cathode (pre-stressed tendon) becoming charged with more electrons. Figure 6.13 shows the 'ON' potential with time for galvanised tendons with High Level of pre-stress tendons. As can be seen, the initial potential is much more negative than for the ungalvanised due to the resistance of the galvanised tendons.

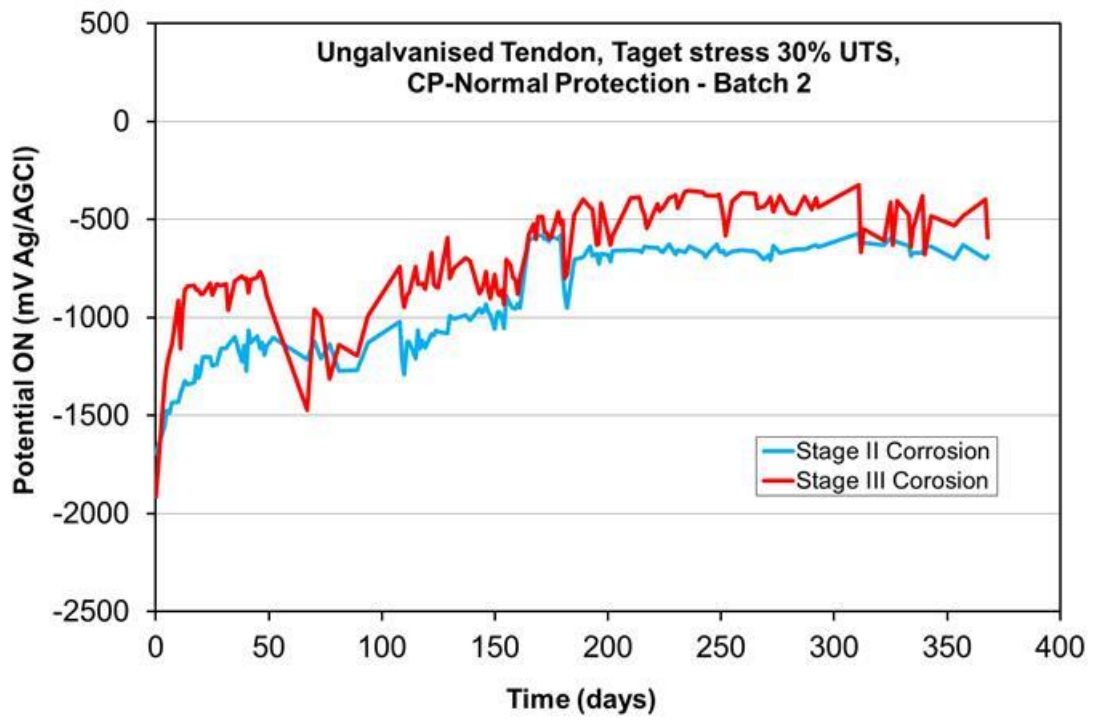


Figure 6.11 "ON" potential of ungalvanised tendons during applying ICCP- Normal Protection, 30% UTS

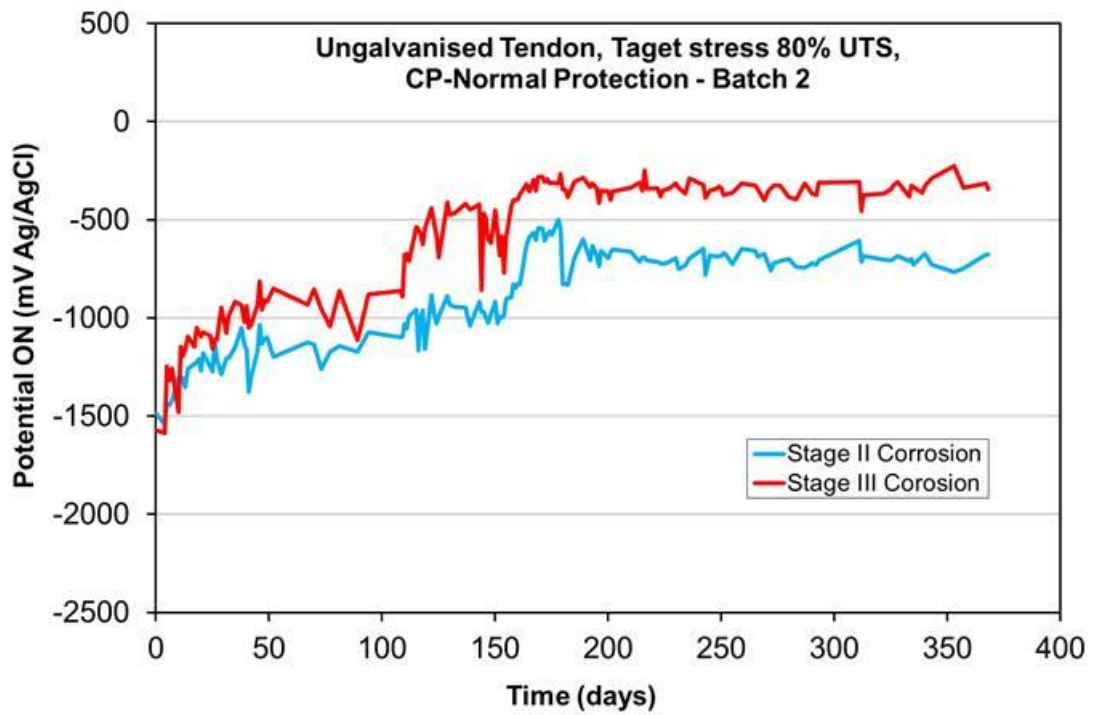


Figure 6.12 "ON" potential of ungalvanised tendons during applying ICCP- Normal Protection, 80% UTS

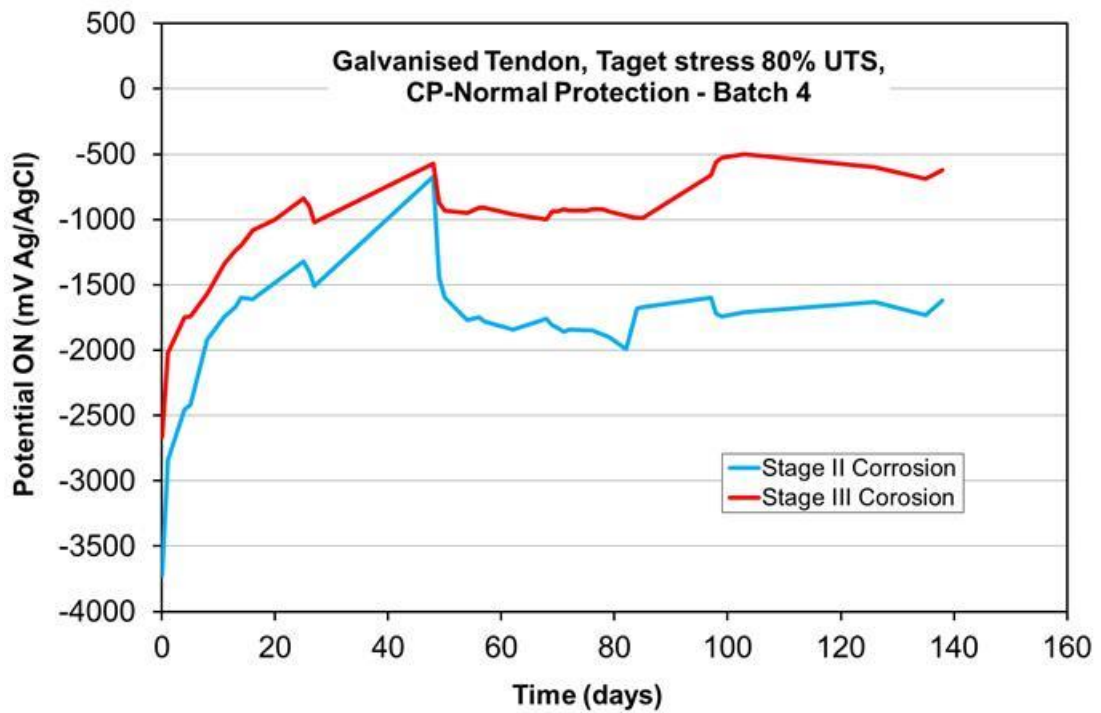


Figure 6.13 "ON" potential of galvanised tendons during applying ICCP-Normal Protection, 80% UTS

6.5.4 Monitoring of Condition and Performance

During the overall period of applying ICCP-N to the tendons, some specimens were protected for 553 days. The following routine investigations and monitoring were carried out and the surveys and results are recorded on suitably designed data sheets for each task:

- Monitoring and checking the wire connections of the ICCP system.
- Visual check of each DC power supply.
- Measuring of applied current (range 4 - 32 mA) and voltage (range 1.62 - 4 V).
- Recording potential using surface reference electrodes (Ag/AgCl/KCl 0.5M).
- Applying depolarisation (Instant-Off) for each reading and potential decay for 24 hours in two to three month intervals.
- Checking and taking readings of the applied service stress via a datalogger.
- Close visual inspection to the surface of the mortar and record any change.

6.5.4.1 Instant-Off (E_{off}) potential

The Instant-Off (E_{off}) which is the potential of the tendons during the application of ICCP-N was recorded. Figure 6.14 and Figure 6.15 show the potential of the ungalvanised tendons with Low and High levels of pre-stress. Figure 6.16 shows the potential of the galvanised tendons with High level of pre-stress.

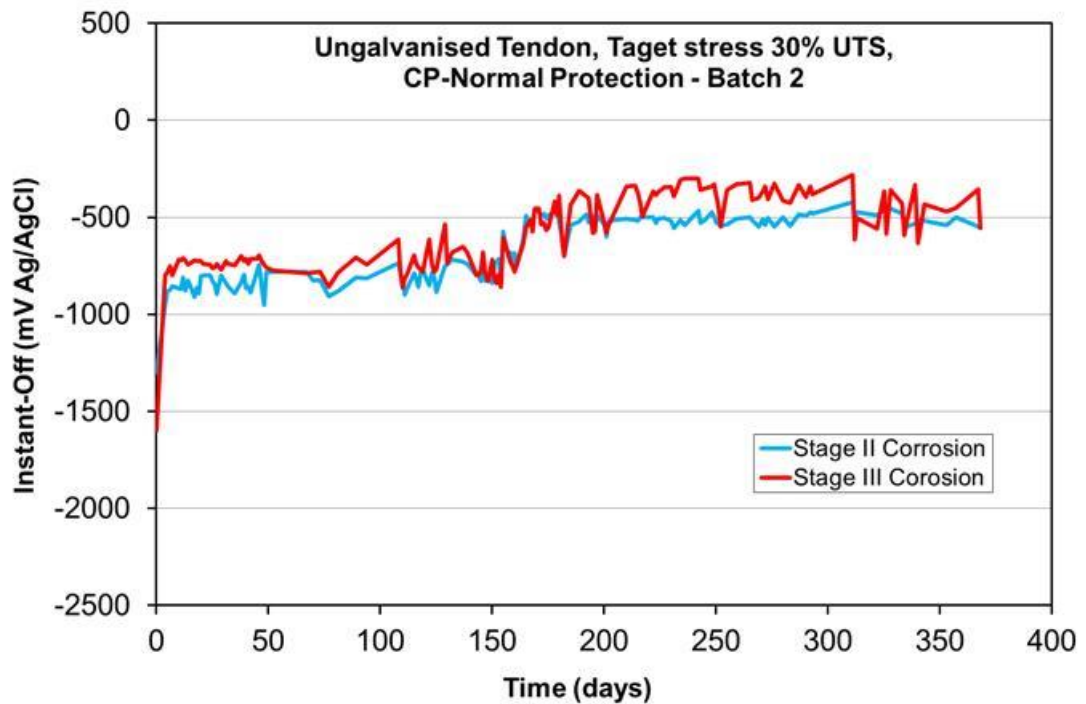


Figure 6.14 Instant-Off potential of ungalvanised tendons, 30% UTS

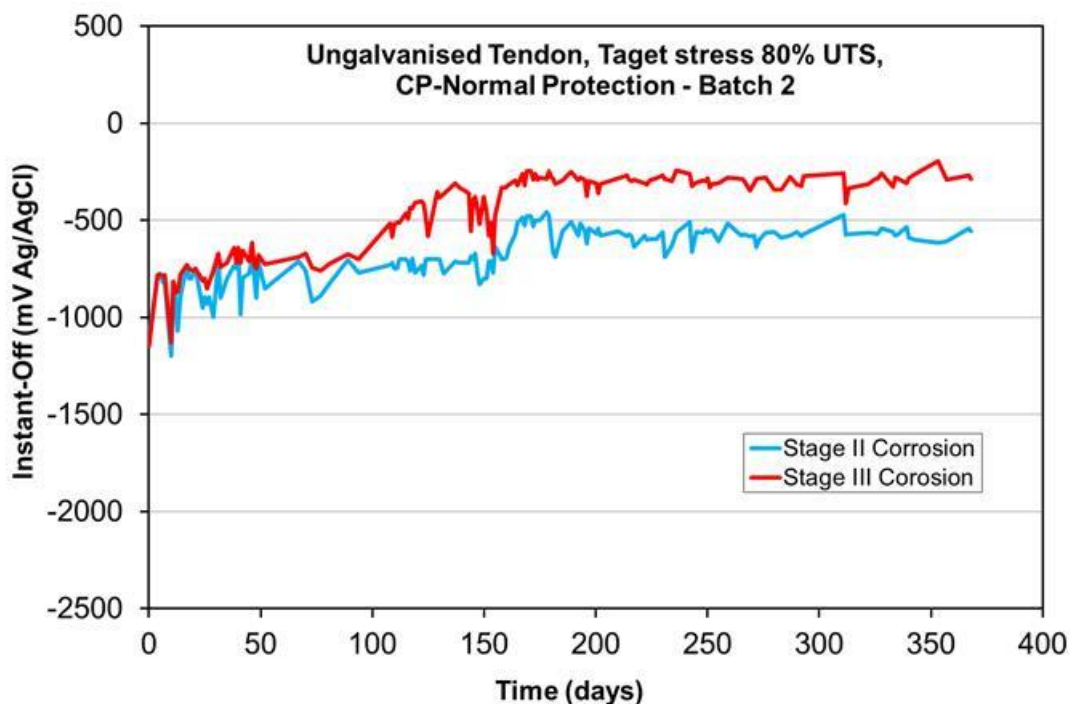


Figure 6.15 Instant-Off potential of ungalvanised tendons, 80% UTS

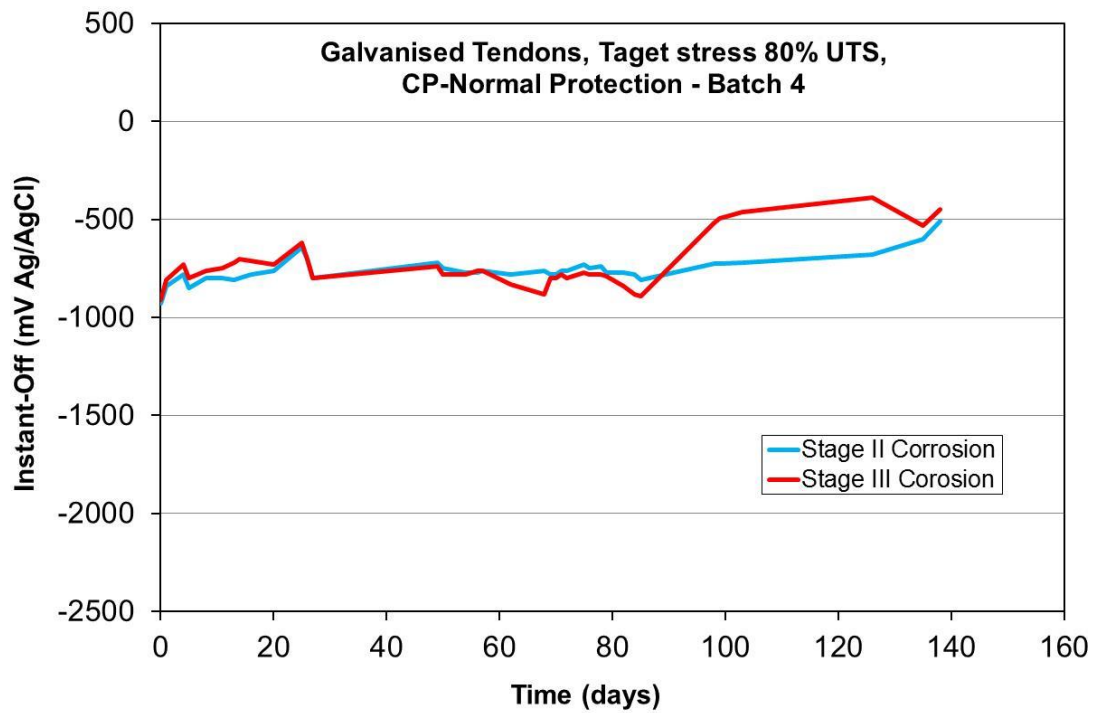


Figure 6.16 Instant-Off potential of galvanised tendon, 80% UTS

The ICCP-N was applied for a period of 8,808 hours for the ungalvanised tendon with Low Level pre-stress, 553 days for the ungalvanised tendons with High Level pre-stress tendons and 137 days for the galvanised tendons with High Level of pre-stress. The general trend of the ungalvanised tendon potential (Instant-Off) for both Low Level and High Level pre-stress with Stage I and II corrosion are the same. After around 150 days the potential became less negative and more steady as shown in Figure 6.14 and Figure 6.15. However, for the galvanised tendons, Figure 6.16, the potential stays at around the same level for 100 days and then becomes slightly less negative for the tendon with Stage II corrosion and more noble for the specimen with Stage III corrosion. This is due to less moisture in the specimen giving the mortar more resistance, thus the potential reached -530 mV vs SSC.

6.5.4.2 Effectiveness of ICCP-Potential decay (-100mV)

Based on CP criteria, the potential decay or the potential shift (ΔE_{off}) is the difference between instant-off (E_{off}) and the potential after 4 to 24 hours. This potential decay was monitored, recorded and plotted in Figure 6.17 for ungalvanised tendons and Figure 6.18 for galvanised tendons.

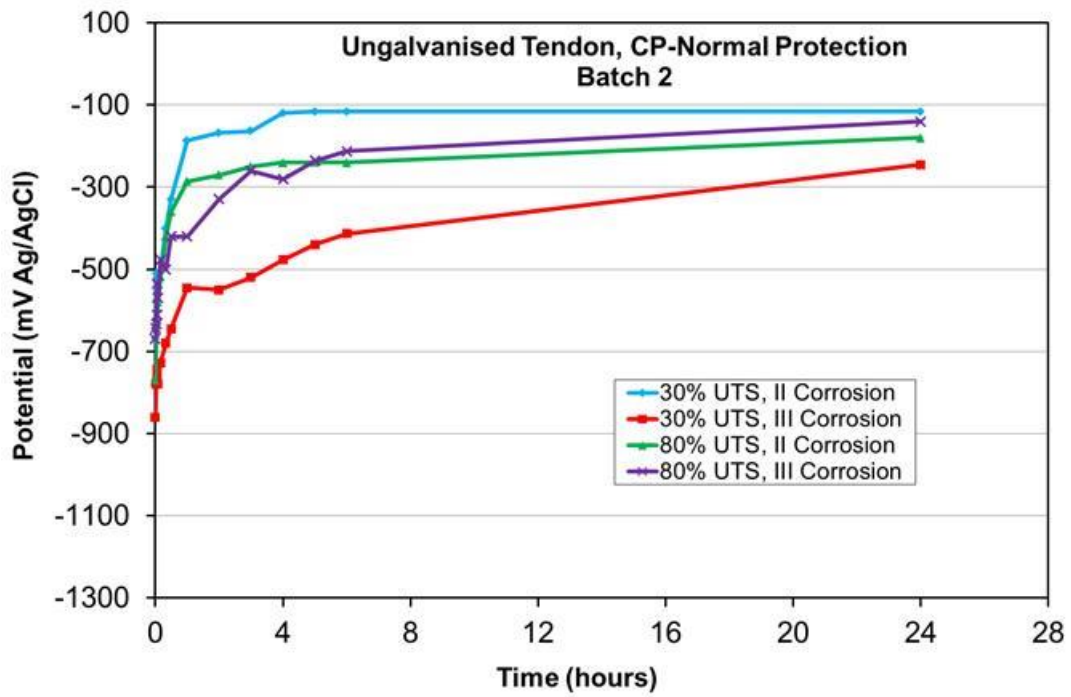


Figure 6.17 Potential decay of ungalvanised tendons

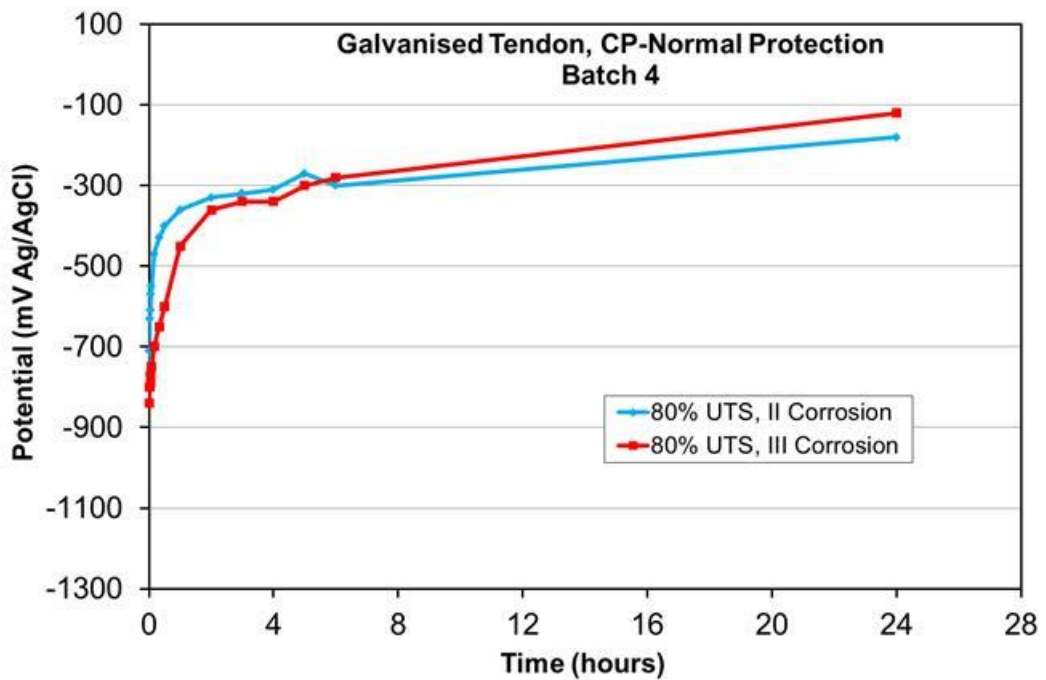


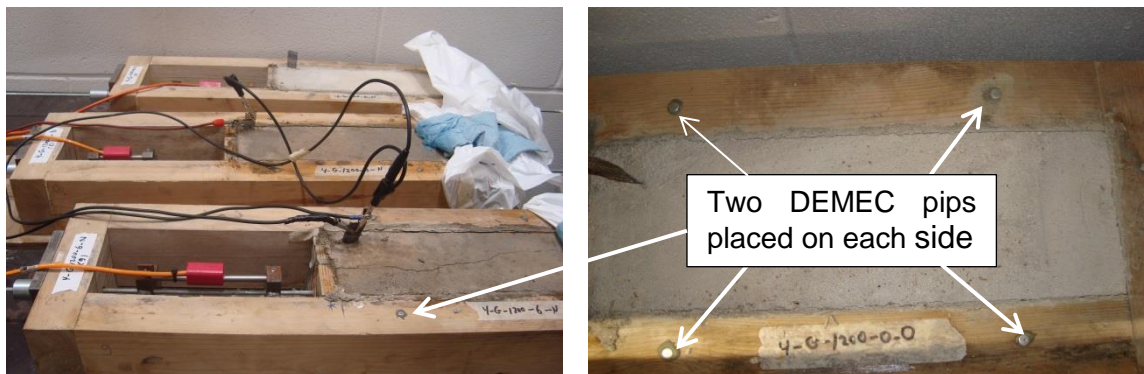
Figure 6.18 Potential decay of galvanised tendons

The effectiveness of ICCP-N was examined by conducting a potential decay test, with the ICCP-N interrupted for 24 hours before it was switched on again. Based on the data collected, the potential decays were more than 100mV after 4 hours for all monitoring events. According to the Concrete Society Technical

Report No 73, this demonstrates that an adequate level of cathodic protection has been achieved.

6.5.5 Effect of ICCP-N on the applied service stress

Surface wire vibrating strain gauges were installed on each tendon and changes in the applied service stress were monitored and recorded by a data logger. This is a long-term test to investigate the effect of ICCP-N on the performance of the tendons in terms of applied service stress and to measure any loss due to that effect. To calculate the contraction in the timber moulds for specimens with High Level of pre-stress, DEMEC pips were fixed to the top of the two-parallel longitudinal side faces (575x50x95 mm) at a gage length 200mm as shown in Figure 6.19, and the contraction in the timber mould was measured using a 200mm strain gauge and the average strain is determined (Table 6.4). This strain is considered in the calculation of the total loss of the service stress as shown in Table 6.5 which shows the service stress from the start of the ICCP-N to its completion.



Placing DEMEC pips at 200mm

Figure 6.19 DEMEC pips placing for contraction measurements

Table 6.4 Timber mould contraction (microstrain)

<i>Mould ID</i>	<i>Total Strain</i>	
	<i>Face 1</i>	<i>Face 2</i>
Mould 1	268	474
Mould 2	339	229
Mould 3	229	134
Mould 4	363	434
Mould 5	435	55
Mould 6	577	861
Overall Average		367

Table 6.5 Effect of ICCP-N on the applied service stress

Batch	Test code	Degree of Corrosion (Stage)	Actual Degree of Corrosion (%)	ICCP Period (hrs)	Service Stress			
					Start (MPa)	Finish (MPa)	Loss (MPa)	(%)
2	M-U-L-X-N-1	I	0	8808	424	366	58	14
	M-U-L-II-N-2	II	3.98	8808	330	319	11	3
	M-U-L-III-N-3	III	5.32	8808	436	424	12	3
	M-U-H-X-1	I	0	13272	1131	1000	131	12
	M-U-H-II-N-2	II	2.25	13272	1170	917	252	22
	M-U-H-III-N-3	III	4.05	13272	1163	881	283	24
4	M-G-H-X-1	I	0	3288	712	502	133	19
	M-G-H-II-N-2	II	3.48	3288	700	560	63	9
	M-G-H-III-N-3	III	4.36	3288	671	497	97	14

Key: U-Ungalvanised, G-Galvanised, M-Mortar electrolyte, S-Solution electrolyte, H-High level of pre-stress (800-1200MPa), L-Low level of pre-stress (300-400MPa), I-Degree of corrosion Stage I (0-1%), II-Degree of corrosion Stage II (2-4%), III-Degree of corrosion Stage III (4-7%), N-Normal protection, O-Overprotection, X and X1-no corrosion and no ICCP, R-As-received samples, 1, 2, 3-Sample numbers.

These data were plotted in Figure 6.20, Figure 6.21 and Figure 6.22 for the ungalvanised tendons and Figure 6.23 for the galvanised tendon. For the ungalvanised tendons, Figure 6.20 compares the gross loss in pre-stress of the tendons with the different corrosion Stages I (0-1 %), II (2-4 %) and III (4-7 %) and with Low Level of pre-stress over the period of ICCP-N application. Overall, the trend of the loss of stress of the tendon with Stage II degree of corrosion remains stable over the application of ICCP-N period with a total loss of just 3%, while the other gross loss for both tendons with Stages I and III degrees of corrosion have the same trend which started quite stable for 145 days then dropped gradually for 100 days to reach 350 MPa. Subsequently, both gross loss in tendons remain stable again to the end with a total stress loss 3 to 14 % for the tendons with Stage I and Stage II corrosion respectively.

For the ungalvanised tendons with High Level of pre-stress, shown in Figure 6.21, the gross loss has gradually decreased over the total period for all three tendons. The total loss ranged in between 12 to 24%, this loss is more than the loss in tendons with Low Level of pre-stress, a comparison is given in Figure 6.22. For galvanised tendons with High Level of pre-stress, Figure 6.23

compares the gross loss in pre-stress of the tendons with the different corrosion Stages I, II and III over time. The results clearly indicate that there is a loss in pre-stress of the galvanised tendon over the entire test period. This loss in the service stress of the tendons have the same trend, decreased gradually at the start and then remaining quite stable. The total loss ranged between 9 to 19%, this percentage of pre-stress loss is more than the percentage loss of ungalvanised pre-stressed tendon, which was 3 to 14%. The Stage I tendons, although not subjected to corrosion or ICCP-N, do suffer a reduction in pre-stress, perhaps as a result of compression in the timber moulds, relaxation or the laboratory environment.

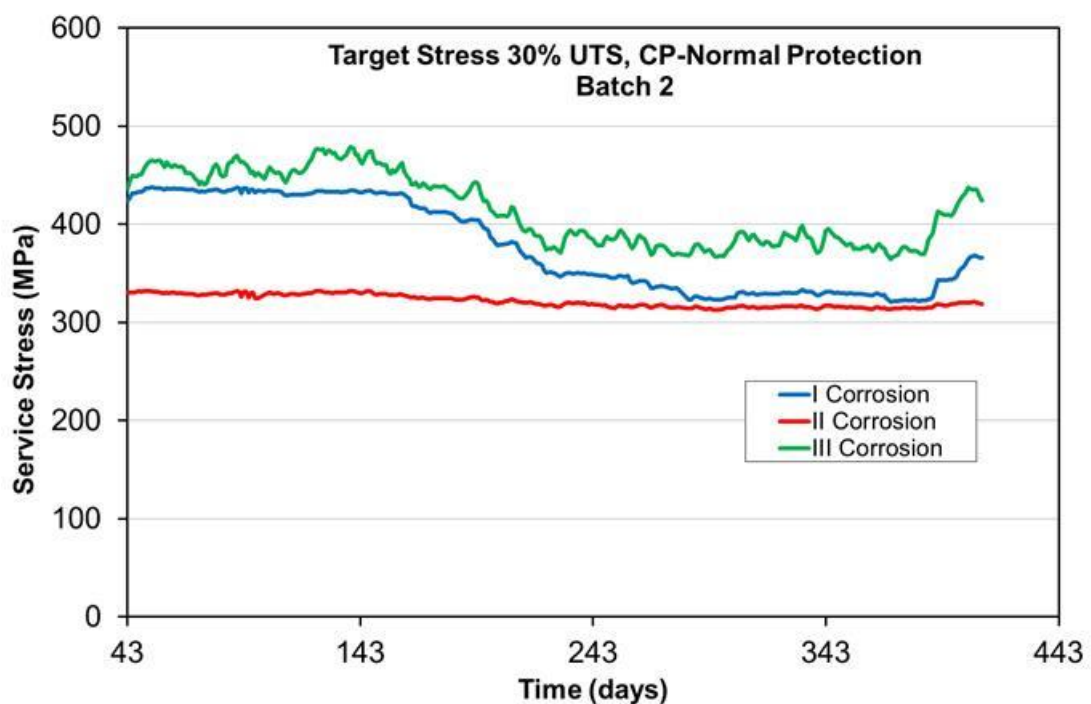


Figure 6.20 Service stress in the ungalvanised tendons over the ICCP-N period, Batch 2 (30% UTS)

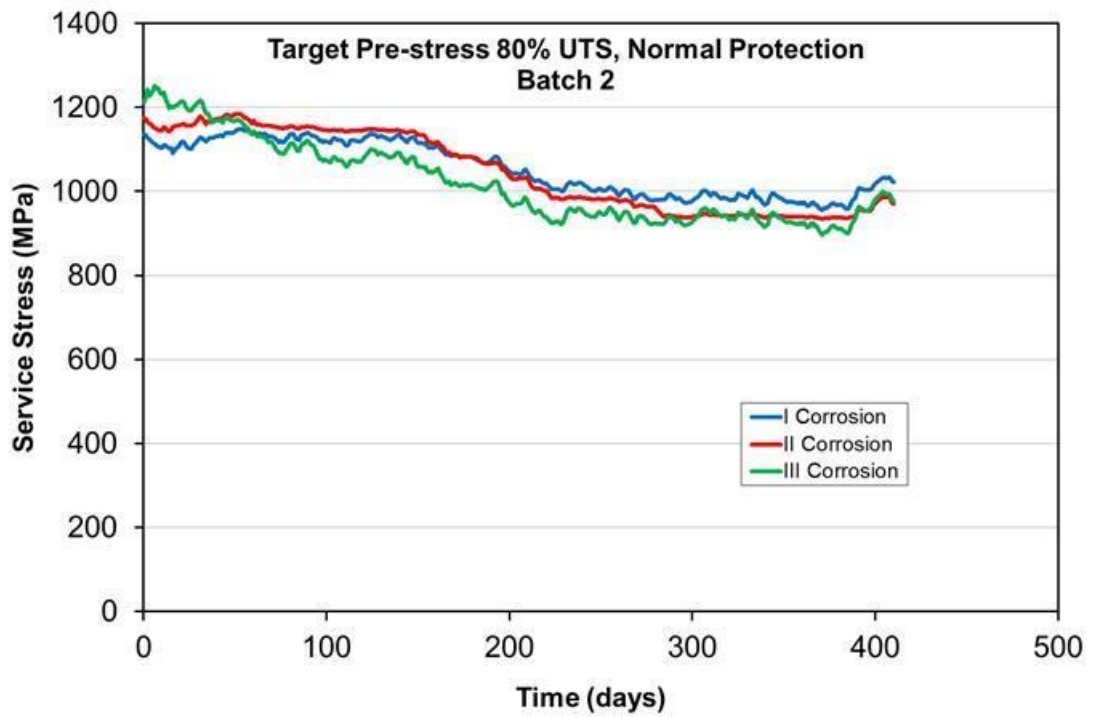


Figure 6.21 Service stress in the ungalvanised tendons over the ICCP-N period, Batch 2 (80% UTS)

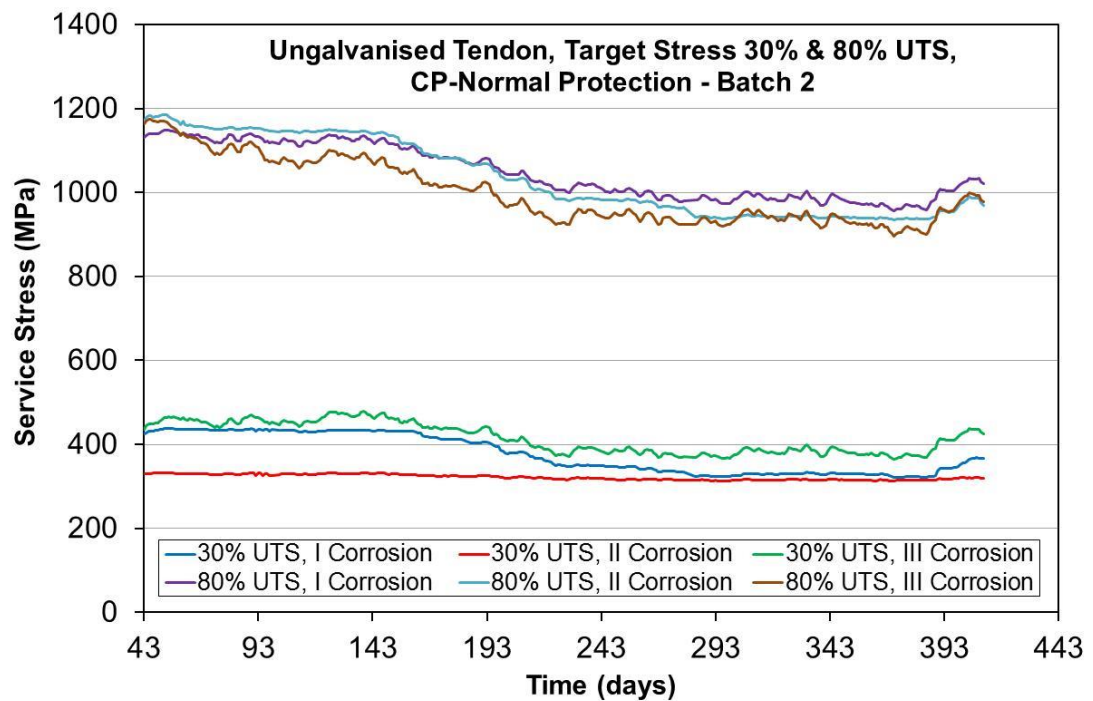


Figure 6.22 Service stress in the ungalvanised tendons over the ICCP-N period, Batch 2 (30% & 80% UTS)

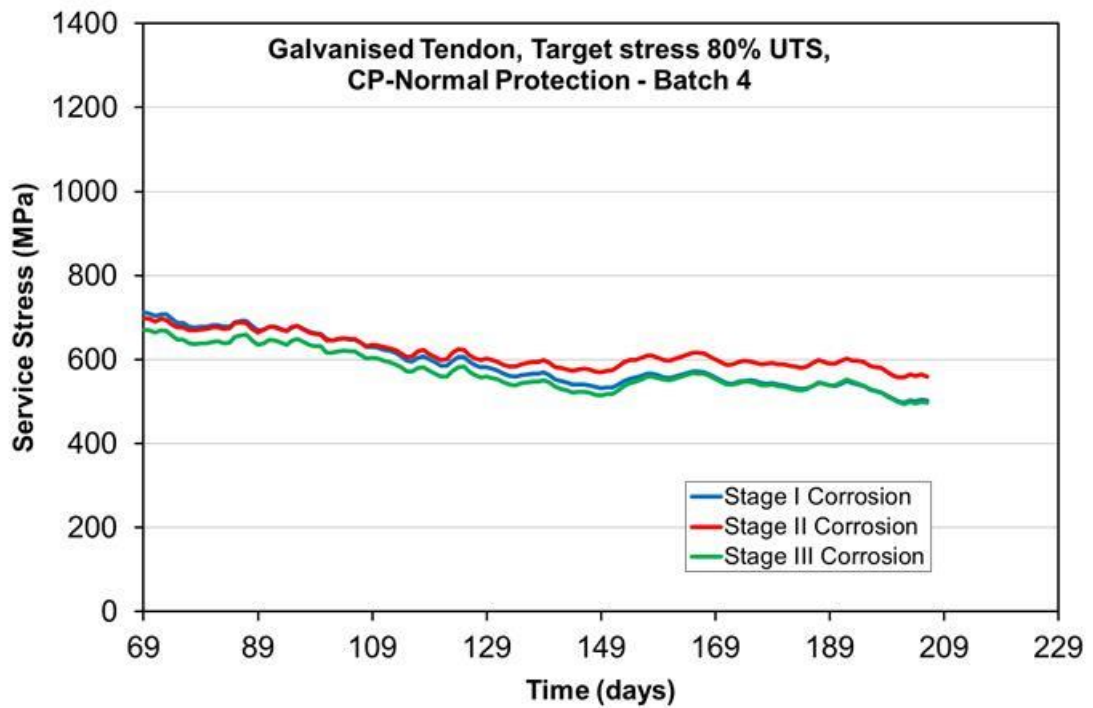


Figure 6.23 Service stress in pre-stressed galvanised tendon over the ICCP-N period, Batch 4 (80% UTS)

Table 5.6 shows the residual service stress in both the ungalvanised and galvanised tendons under the effect of ICCP-N. The loss of service stress is plotted in Figure 6.24. The results show that as the degree of corrosion increases from Stage I through to Stage II, there is a more rapid loss of pre-stress for the High Level stressed ungalvanised tendons from 131 MPa to 253 MPa. In the galvanised tendons the loss is not as a severe with only 60 MPa being lost during Stage II corrosion and 98 MPa during Stage III. This indicates that the galvanised tendons under ICCP-N application have a different behaviour than the ungalvanised tendons. Also it was noticed that the degree of corrosion has an impact on the loss of stress particularly in the ungalvanised tendon, this means that the tendons subjected to higher degrees of corrosion will suffer higher losses which should be accounted for at the design stage as an additional loss.

Table 6.6 Residual service stress in the pre-corroded tendons under the effect of ICCP

Corrosion Stage	Residual Stress (MPa)			
	Ungalvanised		Galvanised	
	Start ICCP	Finish ICCP	Start ICCP	Finish ICCP
	(MPa)	(MPa)	(MPa)	(MPa)
I	1131	1000	712	579
II	1170	917	700	637
III	1163	881	671	573

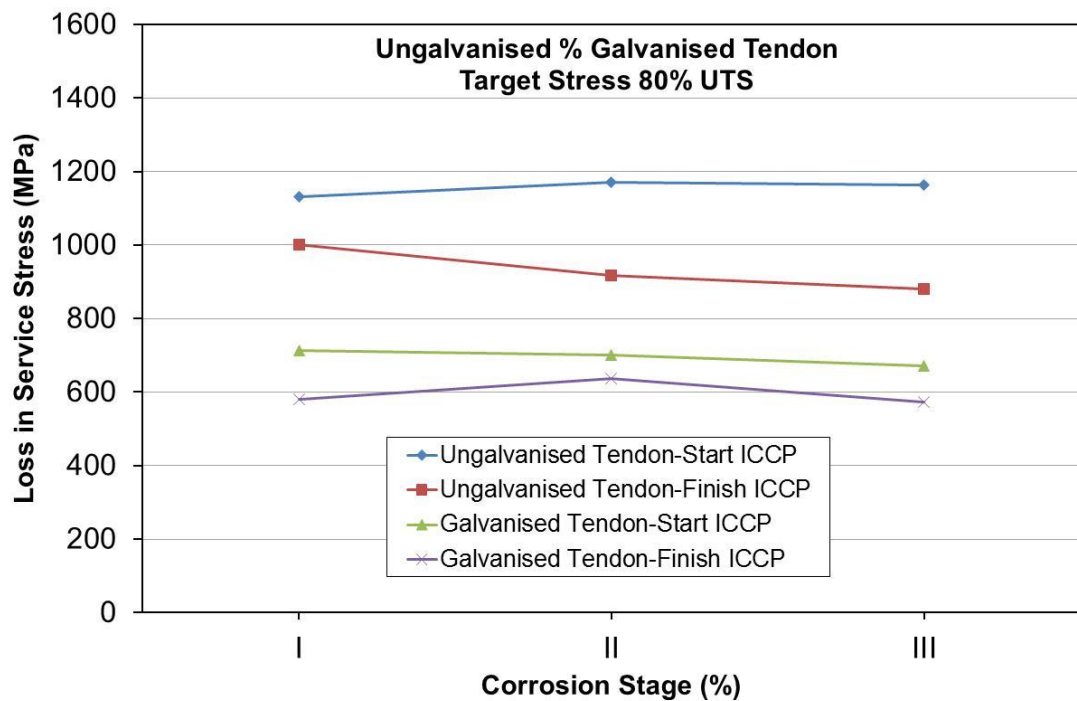


Figure 6.24 Relationship between Stages of corrosion and the loss in service stress in ungalvanised and galvanised tendons (80% UTS) during the ICCP-N period

6.5.6 Effect of ICCP-N on the mechanical properties of the tendon

Tensile tests were conducted on both the ungalvanised and galvanised tendons after ICCP-N was applied for 3288 and 13272 hours respectively. The chemical compositions of both the ungalvanised and galvanised tendons are presented in Table 4.2. Samples of the as-received tendons were randomly selected and tested using a tensile test machine (ESH600). The tensile tests were conducted

in accordance with BS EN ISO 6892-1:2016 [90]. Subsequently, the mechanical properties of the tendons were determined. The mechanical properties of the as-received tendons are presented in Table 6.7. These mechanical properties were used to compare with the properties of those tendons which were exposed to pre-corrosion and ICCP-N application. The mechanical properties of the tested tendons are described in Table 6.8.

Table 6.7 Tensile properties of the as-received tendons

Tendon Type	Test Code	Mean	Proof	Tensile	Young's	Elon-	Breaking
		Original diameter	Strength	Strength	Modulus	gation	Strength
		(mm)	(MPa)	(MPa)	(GPa)	(%)	(MPa)
Galvanised	U-R-1	5.33	1761	1990	214	2.22	1517
	U-R-2	5.31	1725	1978	212	1.10	1472
	U-R-3	5.32	1723	1982	217	2.20	1546
	U-R-4	5.32	1718	1970	216	4.90	1524
	U-R-5	5.30	1673	1978	216	2.50	1541
	Average	5.32	1720	1979	215	2.58	1520
Ungalvanised	G-R-1	5.34	1683	1941	208	2.00	1557
	G-R-2	5.35	1690	1946	211	2.00	1641
	G-R-3	5.34	1680	1952	207	3.00	1572
	G-R-4	5.38	1652	1939	212	3.00	1558
	Average	5.35	1676	1945	209	2.50	1582

Key: U-Ungalvanised, G-Galvanised, R- As-Received, 1-5 Sample Numbers

Stress-strain curves were determined from three samples for each type of tendon as shown in Figure 6.25 for ungalvanised as-received tendons and Figure 6.26 for galvanised as-received tendons. The elastic and plastic stages are clearly shown and the mechanical properties are almost identical for each type of tendon. These stress-strain curves indicate that the tendons are a ductile steel with high tensile strength.

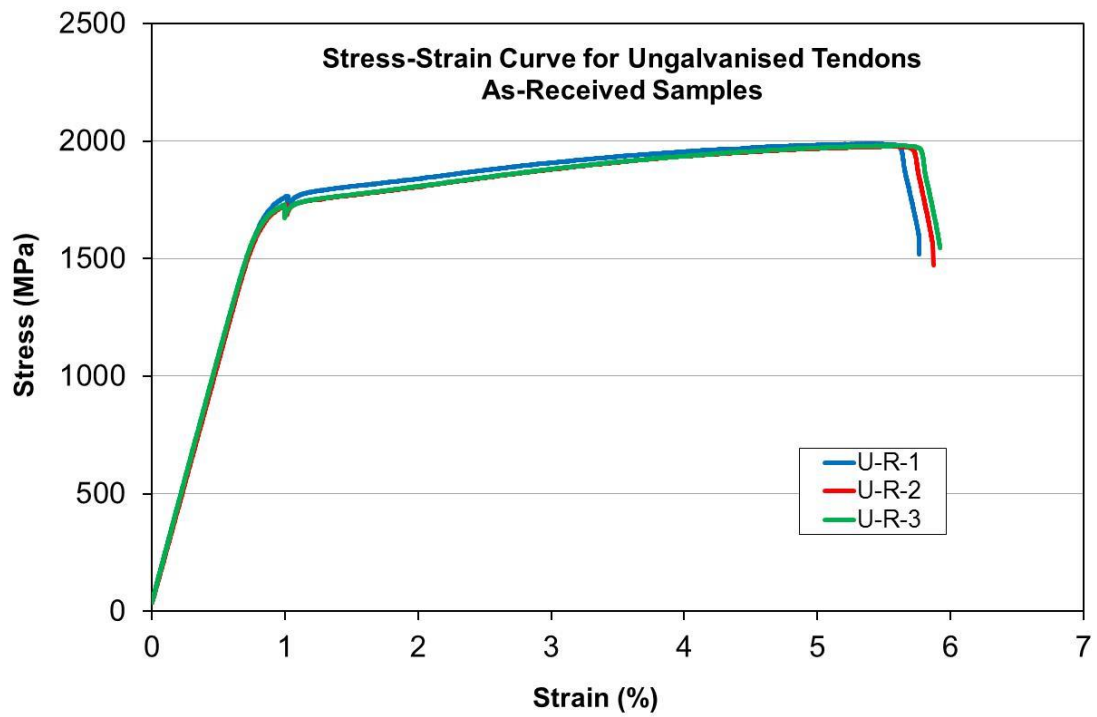


Figure 6.25 Stress-Strain curve for as-received ungalvanised tendons

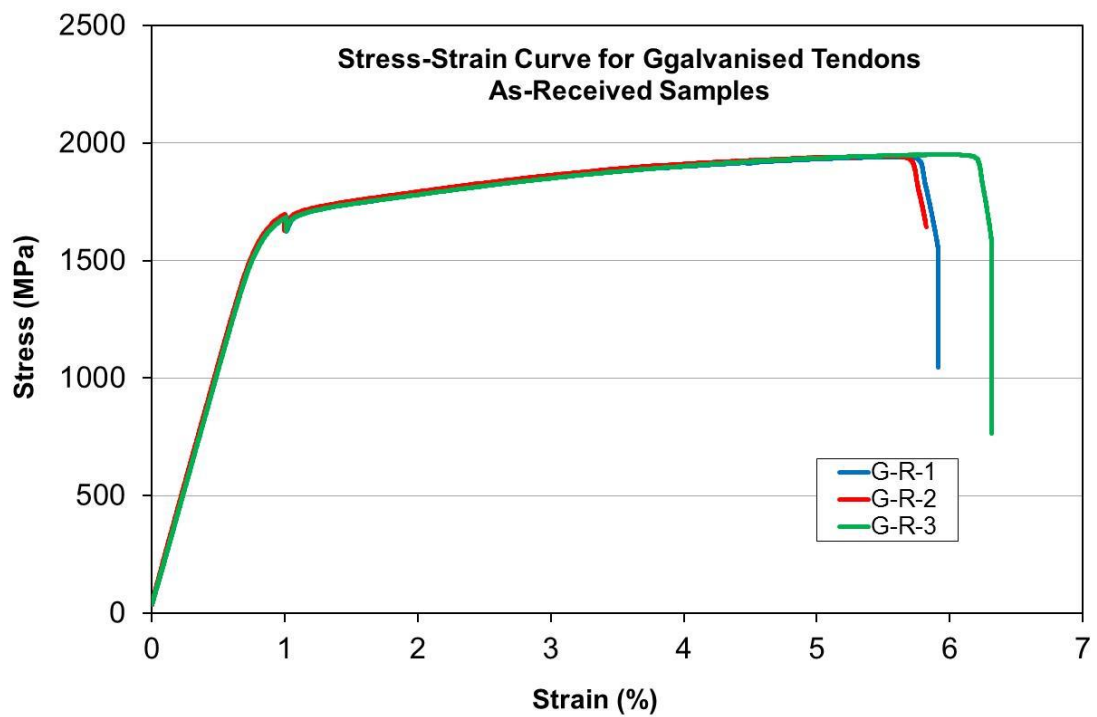


Figure 6.26 Stress-Strain curve for as-received galvanised tendons

After completing the tensile tests, all mechanical properties were recorded and images of the fracture modes were obtained as shown in Figure 6.27 (a-f). These images show a cup-cone failure mode which is characteristic of ductile steel.



(a) Ungalvanised tendon, UG-R-1



(b) Galvanised tendon, G-R-1



(c) Ungalvanised tendon, UG-R-2



(d) Galvanised Tendon, G-R-2



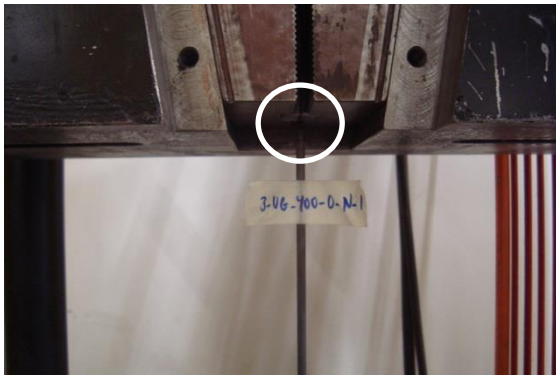
(e) Ungalvanised tendon, UG-R-3



(f) Galvanised Tendon, G-R-3

Figure 6.27 Fracture modes for ungalvanised and galvanised as-received tendons

Figure 6.28 (a-d) shows the different location of the tendon failures and was named Bottom Edge (close or at the grip), Upper middle (between top grip and the middle), Lower middle (between bottom edge and the middle) and Middle (within the gauge length).



(a) Edge failure



(b) Upper middle failure



(c) Bottom edge failure



(d) Middle failure

Figure 6.28 Location of failure mode

Table 6.8 Mechanical properties of the tendons after applying CP-Normal Protection

Batch	Test Code	Target Degree of Corrosion (Stage)	Actual Degree of Corrosion	ICCP Period	Mean original diameter	Ultimate Tensile Strength UTS	Proof Strength	Elongation	Necking	Young's Modulus	Toughness (X10 ⁶)	Failure location
			(%)	(hours)	(mm)	(MPa)	(MPa)	(%)	(mm ²)	(MPa)	J/m ³	
2	M-U-L-X-1	I	0	8808	5.28	1989	1733	2.50	33.00	213	125	T-edge
	M-U-L-II-N-2	II	3.98	8808	5.34	1968	1688	2.60	29.00	220	100	Middle
	M-U-L-III-N-3	III	5.32	8808	5.34	1963	1734	1.50	23.00	216	70	U-middle
	M-U-H-X-1	I	0	13272	5.35	1974	1745	2.00	27.00	212	95	B-edge
	M-U-H-II-N-2	II	2.25	13272	5.35	1989	1726	3.50	29.00	210	110	U-middle
	M-U-H-III-N-3	III	4.05	13272	5.36	1937	1747	2.50	32.00	205	69	U-middle
4	M-G-H-X-1	I	0	3288	5.39	1930	1668	2.74	31.00	208	100	Middle
	M-G-H-II-N-2	II	3.48	3288	5.40	1953	1720	3.55	29.00	213	75	U-middle
	M-G-H-III-N-3	III	4.36	3288	5.39	1952	1693	3.50	30.00	212	74	Middle

Key: U-Ungalvanised, G-Galvanised, M-Mortar electrolyte, S-Solution electrolyte, H-High level of pre-stress (800-1200MPa), L-Low level of pre-stress (300-400MPa), I-Degree of corrosion Stage I (0-1%), II-Degree of corrosion Stage II (2-4%), III-Degree of corrosion Stage III (4-7%), N-Normal protection, O-Overprotection, X and X1-no corrosion and no ICCP, R-As-received samples, 1, 2, 3-Sample numbers, T-edge - Top edge, B-edge - Bottom edge, U-middle - Upper middle, L-middle - Lower middle.

6.5.6.1 Summary and Discussion

Table 6.9 provides a summary for Young's Modulus and 0.2% proof strength, while Table 6.10 compares the UTS and elongation. As can be seen from the obtained results, there is no significant difference in mechanical properties for either type of tendon. However, the elongation in both types of tendon (Table 6.10) has been affected by ICCP-N as there is difference compared with the as-received specimens as will be discussed as follows:

Stress-Strain Curves

According to the obtained results and associated figures (Figure 6.29 to Figure 6.35), the stress–strain curve of both the ungalvanised and galvanised tendons show elasto-plastic deformation before fracture. This is a typically ductile steel failure. The stress-strain relationship for the as-received ungalvanised and galvanised tendons are given in Figure 6.25 and Figure 6.26 respectively. As seen in these figures, the stress-strain relationship is similar for both ungalvanised and galvanised tendons. The modulus of elasticity, yield strength and ultimate tensile strengths were similar. However, the stress-strain relationship for the tendons exposed to pre-corrosion and ICCP-Normal protection show slightly different behaviour in terms of elongation and toughness. These stress–strain curves of the tendon show a decrease in ductility (Figure 6.29 to Figure 6.32). The calculations of Young's modulus, 0.2% proof strength, ultimate tensile strength, elongation and toughness based on the BS EN ISO 6892-1:2016 [90].

Young's Modulus

It can be seen in the figures relating to stress-strain (Figure 6.25 to Figure 6.35) for the as-received and tested tendons that the Young's Modulus is similar. For Batch 2, Young's Modules ranged between 210 to 220 MPa and for Batch 4 was ranged between 208 to 213 MPa. ICCP-N appears to have no effect in the elastic stage properties of these tendons.

0.2% Proof Strength

Proof strength of both the ungalvanised and galvanised tendons was not affected by ICCP-Normal application. As can be seen from Figure 6.29, there is

a slight decrease in yield strength with the ungalvanised tendon with Low Level pre-stress and Stage II corrosion by 2% (32 MPa) but there is no significant variation in the proof strength for the remaining ungalvanised tendons exposed to ICCP-N. For galvanised tendons there is a slight increase in proof strength with High Level pre-stress and Stage II corrosion by 3% (44 MPa). There is no significant variation in the proof strength for the remaining the galvanised tendons exposed to ICCP-N, as shown in Figure 6.32.

Ultimate Tensile Strength

The tensile strength variation between ungalvanised and galvanised tendons exposed to the ICCP-N is very limited. There was no significant reduction in tensile strength for either type of tendon. The tensile strength losses for both types did not exceed 1% for all tendons except a single ungalvanised specimen with High Level pre-stress and Stage III corrosion where decreased by 2 % UTS (42 MPa).

Elongation

Based on the results obtained, the elongation ratio is shown in Figure 6.29 to Figure 6.34. These figures demonstrated that both ungalvanised and galvanised tendons exposed to pre-corrosion show a variation in elongation behaviour under ICCP-N. The elongation ratios difference for ungalvanised tendons are in the range 1.5 to 3.5 % but comparing to the as-received tendons the range is increases to between 3.3 to 42 %. However, for galvanised tendons, the elongation ratios are higher. It is in the range 2.7 to 3.6 % compared with the as-received galvanised tendons where the range is increased by between 10 to 42 %. According to these results, elongation capacity of ungalvanised tendons is lower than galvanised tendons .

Toughness

The ability of a metal to deform plastically and to absorb energy in the process before fracture is termed toughness. The fracture energy of materials is defined by the toughness concept [121]. The toughness values of the ungalvanised and galvanised tendons used in these experimental studies are given in Table 6.10. According to the test results, the toughness values of both types of tendons decreased after ICCP-N application in the range 69 to 95 x 10⁶ J/m³ for

ungalvanised and 75×10^6 J/m³ for galvanised. This decrease is in the range 3 to 9% and between 26 to 0% for ungalvanised and galvanised tendons respectively compared with the toughness of the as-received tendons. Although, the toughness values decreased in both type of tendons, both types still behave as ductile steels.

Table 6.9 Summary of mechanical properties (Young's modulus, 0.2% Proof strength and Ultimate tensile strength)

Batch	Test code	Young's Modulus				0.2% Proof Strength				Ultimate Tensile Strength (UTS)			
		Tested Tendons	As-received Ave. *	Difference		Tested Tendons	As-received Ave. *	Difference		Tested Tendons	As-received Ave. *	Difference	
		(MPa)	(MPa)	(MPa)	(%)	(MPa)	(MPa)	(MPa)	(%)	(MPa)	(MPa)	(MPa)	(%)
2	M-U-L-X-1	213	215	-2	-1	1733	1720	13	1	1989	1980	9	0
	M-U-L-II-N-2	220	215	5	2	1688	1720	-32	-2	1968	1980	-12	-1
	M-U-L-III-N-3	216	215	1	0	1734	1720	14	1	1964	1980	-16	-1
	M-U-H-X-1	212	215	-3	-1	1745	1720	25	1	1974	1980	-6	0
	M-U-H-II-N-2	210	215	-5	-2	1726	1720	6	0	1990	1980	10	1
	M-U-H-III-N-3	205	215	-10	-5	1747	1720	27	2	1937	1980	-42	-2
4	M-G-H-X-1	208	210	-1	-1	1668	1676	-8	0	1930	1945	-15	-1
	M-G-H-II-N-2	213	210	3	2	1720	1676	44	3	1953	1945	9	0
	M-G-H-III-N-3	213	210	3	1	1693	1676	17	1	1952	1945	7	0

Key: U-Ungalvanised, G-Galvanised, M-Mortar electrolyte, H-High level of pre-stress (800-1200MPa), L-Low level of pre-stress (300-400MPa), I-Degree of corrosion Stage I (0-1%), II-Degree of corrosion Stage I (2%), III-Degree of corrosion Stage I (2-3%), N-Normal protection, O-Overprotection, X&X1-No corrosion and NO CP, 1, 2, 3-Sample numbers.

* Average of as-received tendons results

Table 6.10 Summary of mechanical properties (Elongation, Toughness and Ductility)

Batch	Test code	Elongation				Toughness				Ductility			
		Tested Tendons	As-received Ave. *	Difference		Tested Tendons	As-received Ave. *	Difference		Tested Tendons	As-received Ave. *	Difference	
		(%)	(%)	(%)	(%)	(J/m ³) x10 ⁶	(J/m ³) x10 ⁶	(J/m ³) x10 ⁶	(%)	(%)	(%)	(%)	(%)
2	M-U-L-X-1	2.5	2.6	-0.1	-3.3	125	98	28	28	6.0	4.73	1.3	27.0
	M-U-L-II-N-2	2.6	2.6	0.0	0	100	98	3	3	4.7	4.73	0.0	-0.5
	M-U-L-III-N-3	1.5	2.6	-1.1	-42.0	70	98	-28	-28	3.3	4.73	-1.4	-30.2
	M-U-H-X-1	2.0	2.6	-0.6	-22.6	95	98	-3	-3	4.5	4.73	-0.2	-4.8
	M-U-H-II-N-2	3.5	2.6	0.9	35.4	110	98	13	13	5.3	4.73	0.5	11.1
	M-U-H-III-N-3	2.5	2.6	-0.1	-3.3	69	98	-29	-29	3.2	4.73	-1.5	-32.3
4	M-G-H-X-1	2.7	2.5	0.2	9.6	100	100	0	0	4.8	5.41	-0.7	-12.2
	M-G-H-II-N-2	3.6	2.5	1.1	42.0	75	100	-25	-25	3.6	5.41	-1.9	-34.4
	M-G-H-III-N-3	3.5	2.5	1.0	40.0	74	100	-26	-26	3.5	5.41	-1.9	-35.3

Key: U-Ungalvanised, G-Galvanised, M-Mortar electrolyte, H-High level of pre-stress (800-1200MPa), L-Low level of pre-stress (300-400MPa), I-Degree of corrosion Stage I (0-1%), II-Degree of corrosion Stage I (2%), III-Degree of corrosion Stage I (2-3%), N-Normal protection, O-Overprotection, X&X1-No corrosion and NO CP, 1, 2, 3-Sample numbers.

* Average of as-received tendons results

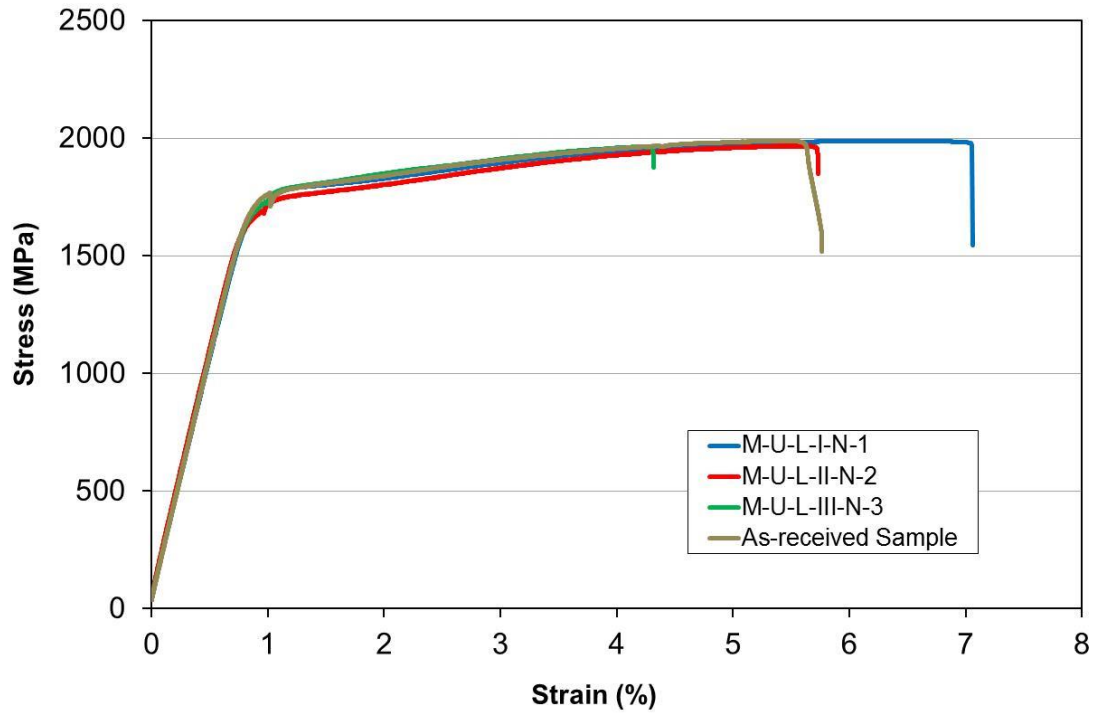


Figure 6.29 Stress-strain curves for the ungalvanised tendons, ICCP-N, 30% UTS

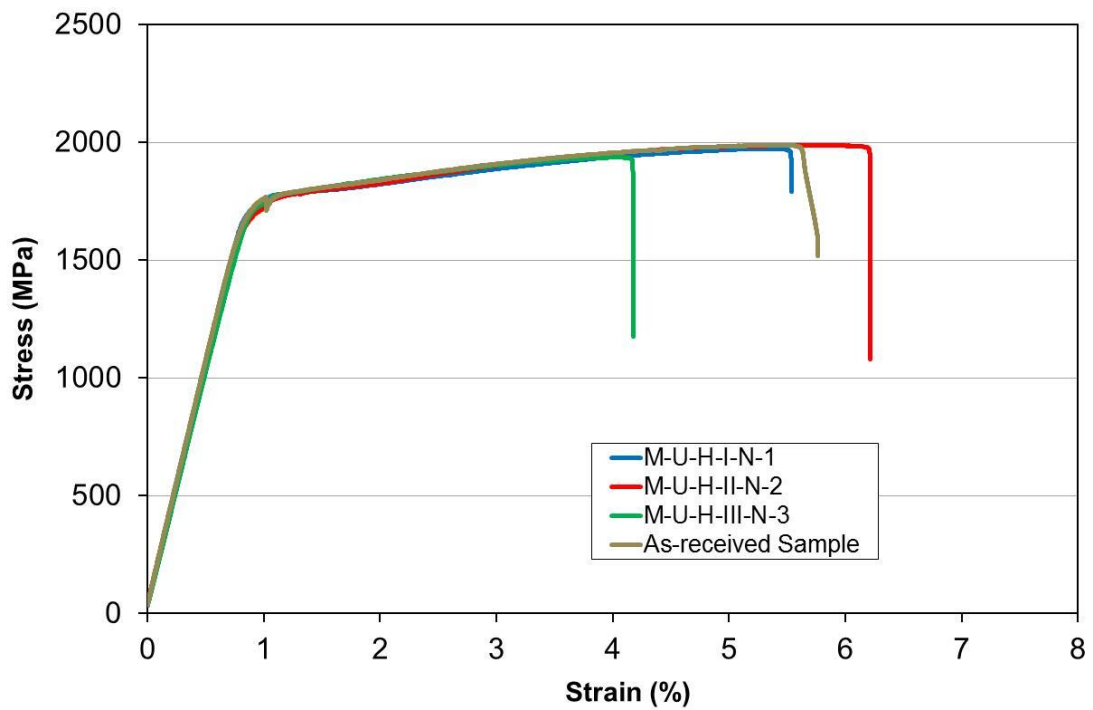


Figure 6.30 Stress-strain curves for the ungalvanised tendons, ICCP-N, 80% UTS

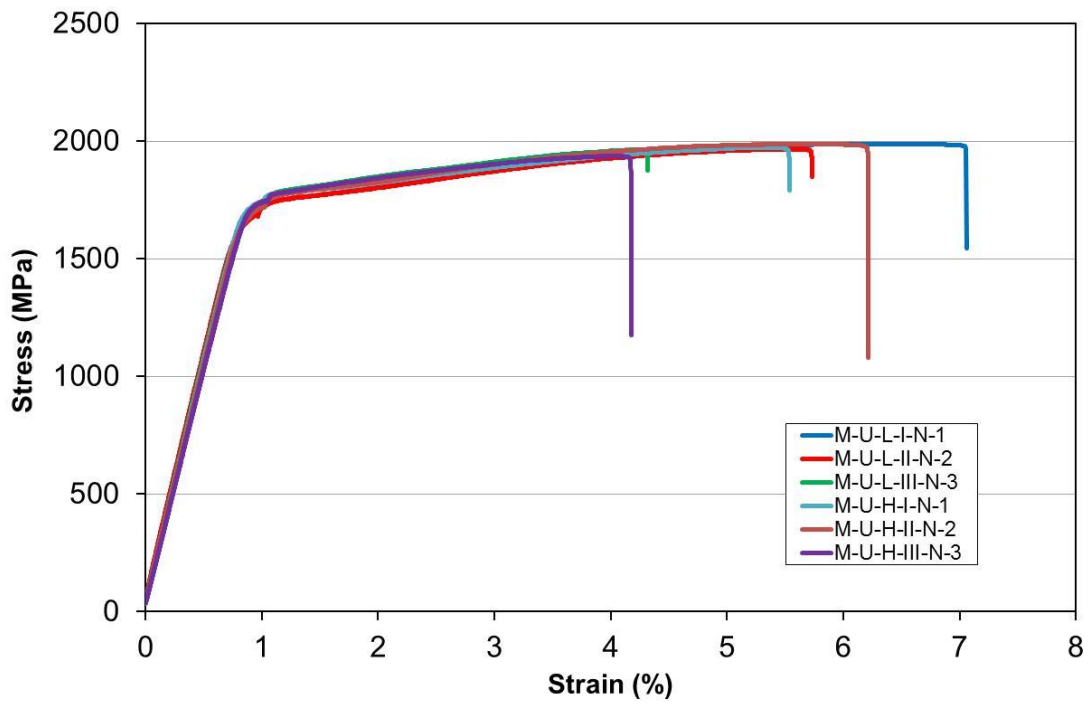


Figure 6.31 Comparison of stress-strain curves for all ungalvanised tendons, ICCP-N, 30% & 80% UTS

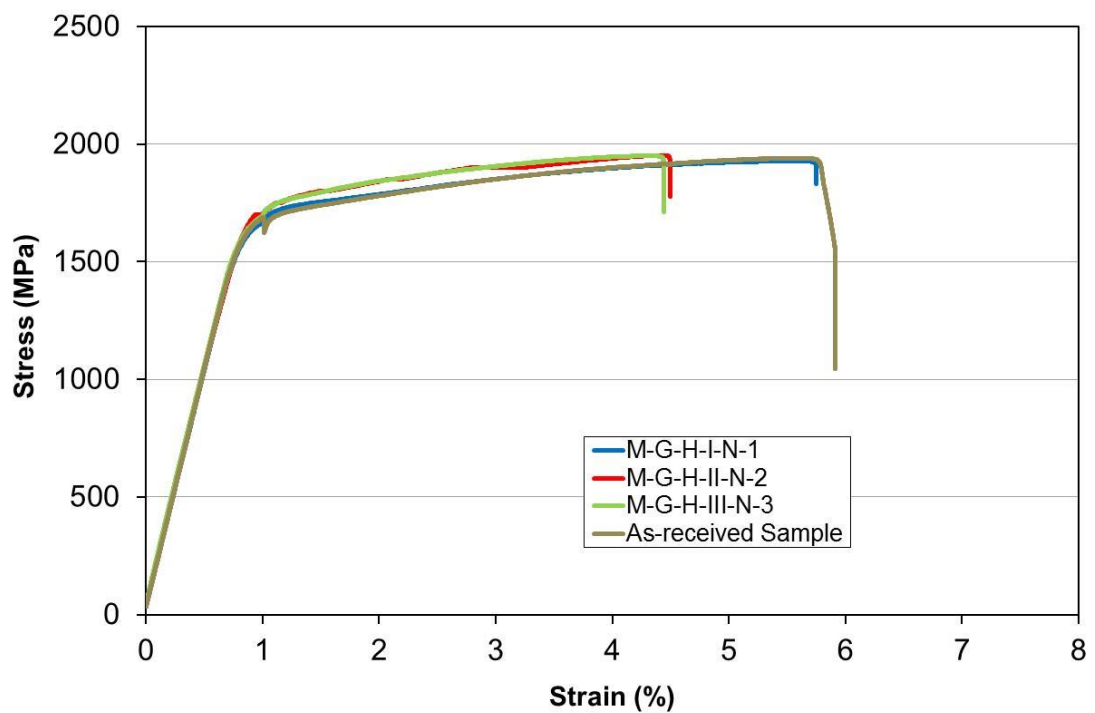


Figure 6.32 Comparison stress-strain curves for galvanised tendons, ICCP-N, 80% UTS

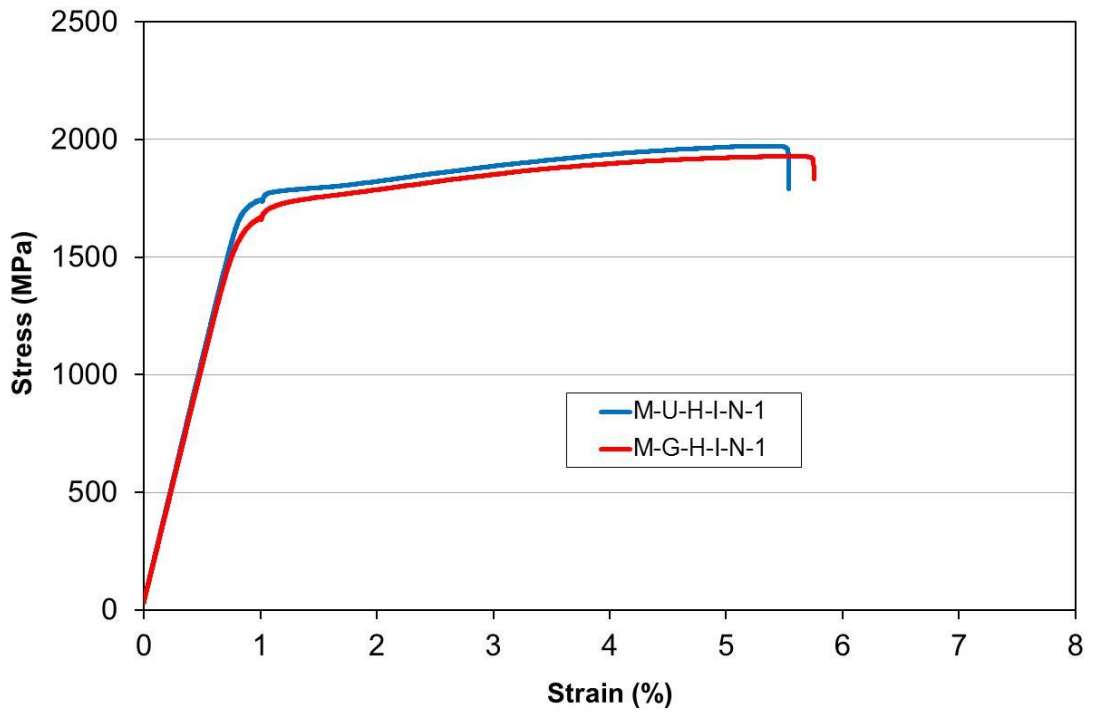


Figure 6.33 Comparison between ungalvanised and galvanised stress-strain curves, ICCP-N, 80% UTS, Stage I corrosion

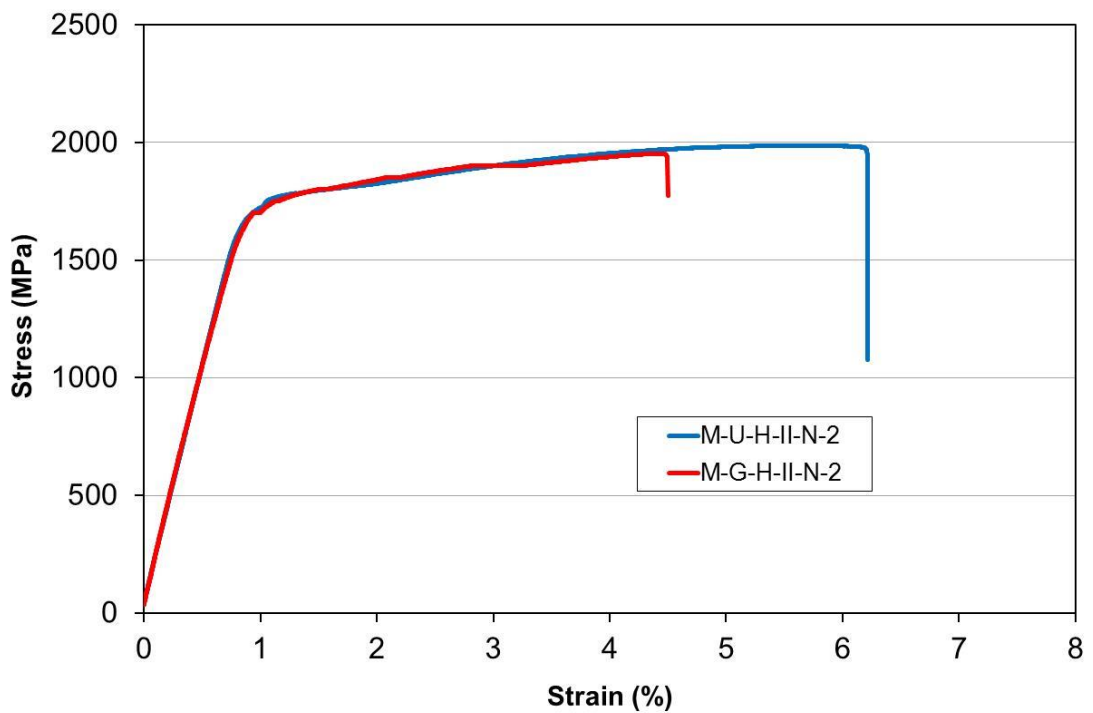


Figure 6.34 Comparison between ungalvanised and galvanised stress-strain curves, CP-N, 80% UTS, Stage II corrosion

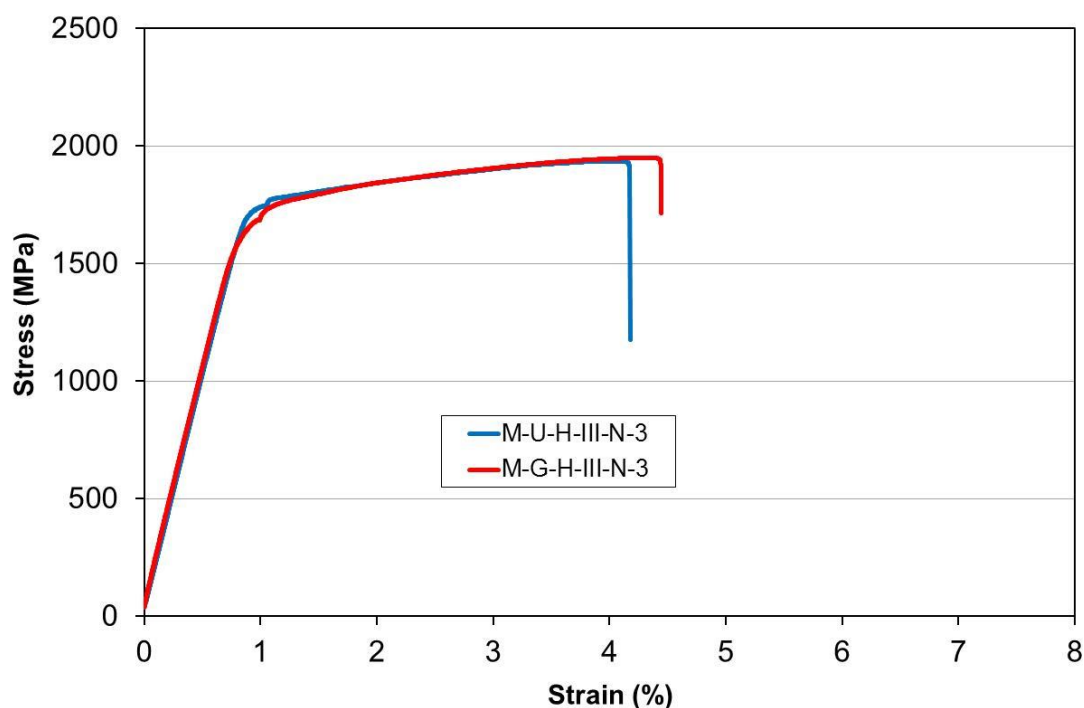


Figure 6.35 Comparison between ungalvanised and galvanised stress-strain curves, ICCP-N, 80% UTS, Stage III corrosion

Ductility

Ductility measures the amount of plastic deformation (strain) to the fracture. Figure 6.36 shows the measurement of the ductility, where a line parallel to the elastic slope is drawn from the fracture point to intersect the x-axis, thereby giving the value of ductility. Table 6.10 shows the values of ductility for different types of tendons with different level of stress and degree of corrosion. Comparison has been made with the ductility of the as-received samples to investigate the effect of ICCP-N. Results show that the ductility percentage decreased after applying the ICCP-N in the range 0.5 to 32 % for the ungalvanised tendons with Low Level and High Level of pre-stress and between 12 to 35 % for galvanised tendons with High Level of pre-stress. It was also observed that the decrease of ductility is greater with specimens exposed with Stage III corrosion for ungalvanised and galvanised tendons. This indicates that both types of tendon with Stage III corrosion were affected by the degree of corrosion and the application of ICCP-N. This reduction in ductility for both types of tendon appears to be caused by additional corrosion rather than the application of ICCP-N as previously observed elsewhere [122].

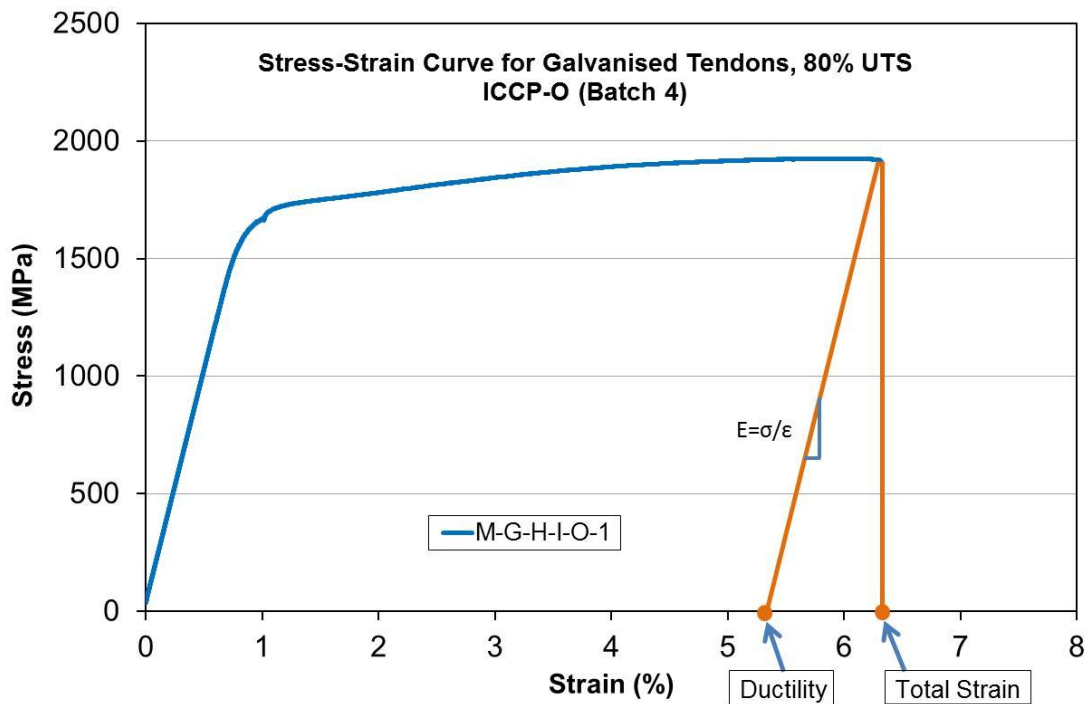


Figure 6.36 Ductility measurement

6.5.6.2 Fracture surface and hydrogen embrittlement

In order to evaluate the susceptibility to hydrogen embrittlement, embrittlement an ratio (I_x) was defined as follows [123]:

$$I_x = (X_{air} - X_{cathode}) / X_{air} \times 100 \quad \text{Equation 6.4}$$

Where:

X : mechanical property

I_x : embrittlement ratio of mechanical property " x "

air: mechanical property with no polarisation

cathode: mechanical property under polarisation

For Equation (6.4), a high embrittlement ratio indicates a high influence of hydrogen as previously determined elsewhere [123].

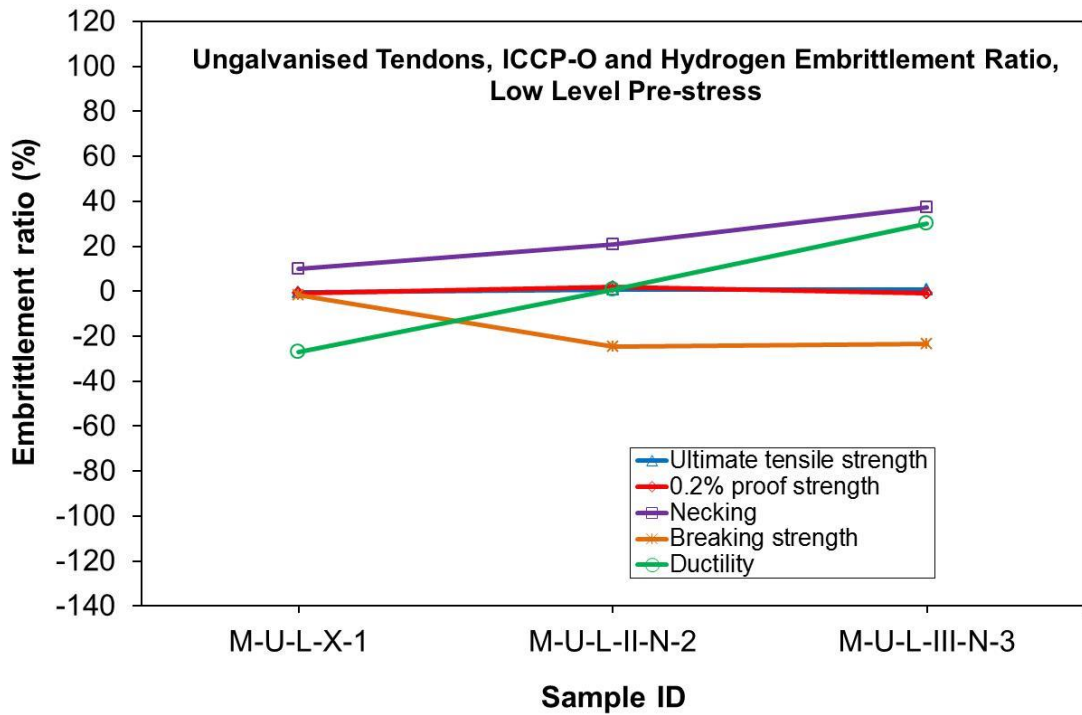


Figure 6.37 Relationship between normal CP potential and hydrogen embrittlement ratio, Low Level pre-stress and, ungalvanised tendons

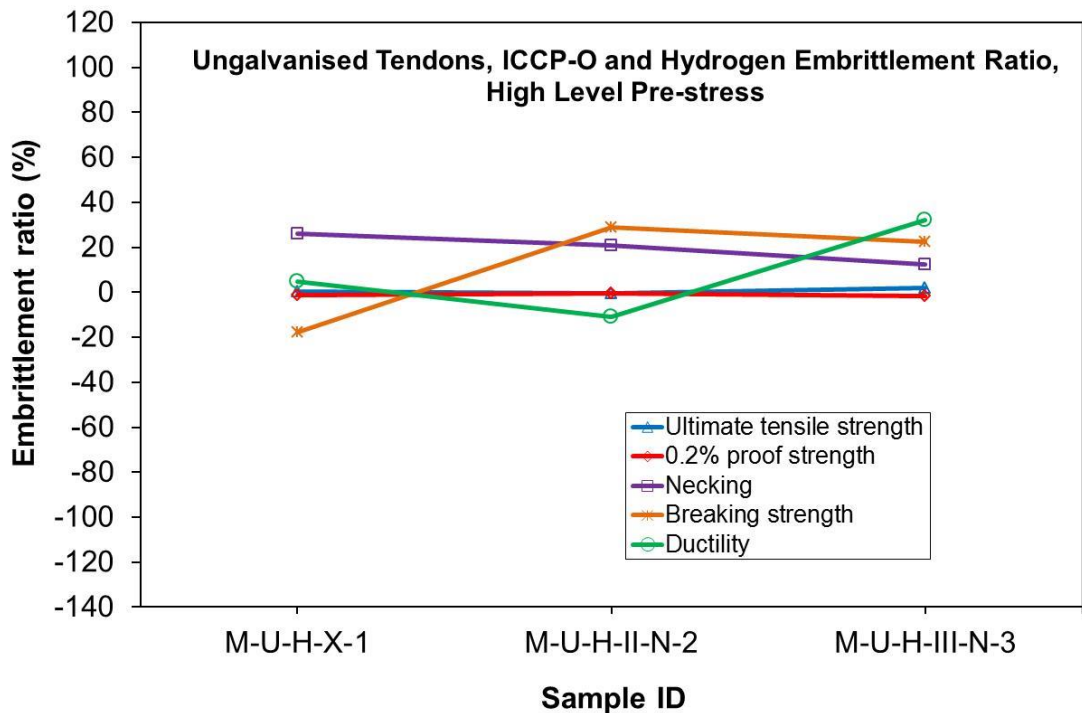


Figure 6.38 Relationship between normal CP potential and hydrogen embrittlement ratio, High Level pre-stress and, ungalvanised tendons

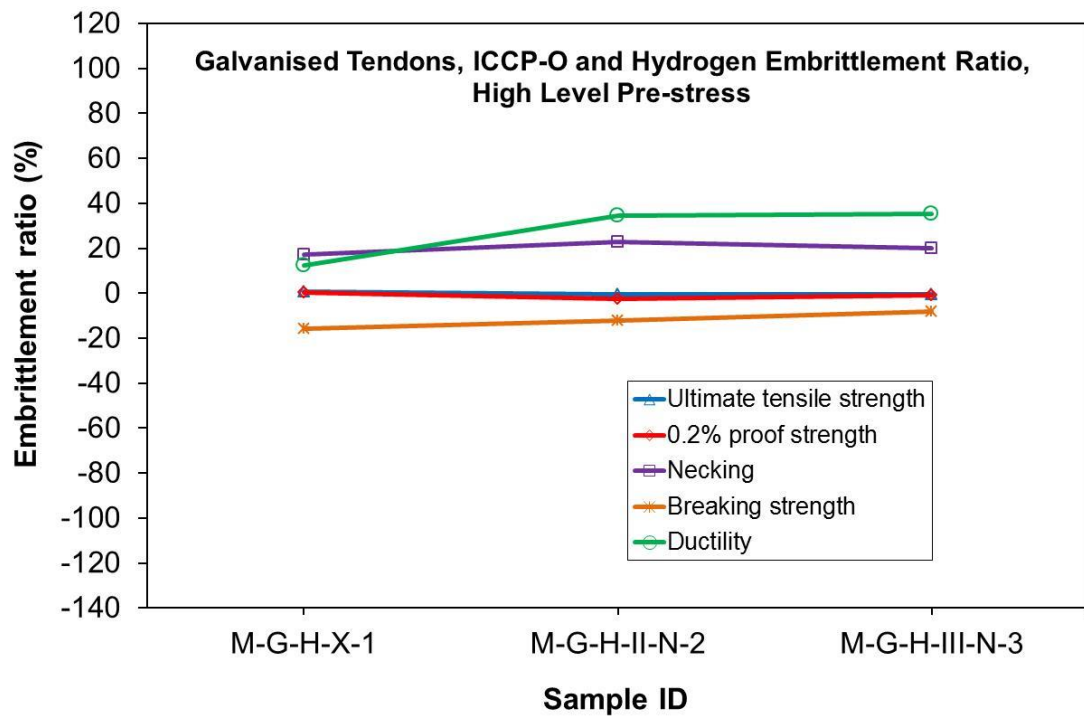


Figure 6.39 Relationship between normal CP potential and hydrogen embrittlement ratio, High Level pre-stress and, galvanised tendons

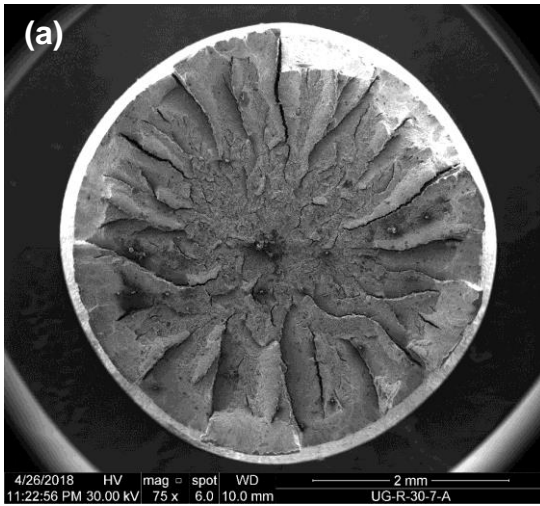
The embrittlement ratios of ultimate tensile strength and 0.2% proof strength in Figure 6.37 to Figure 6.39 have very similar trends. This indicates that hydrogen has little or no effect on both ultimate strength and proof strength. The embrittlement ratio of all mechanical properties was low for the ungalvanised tendon with Low Level of pre-stress and Stage I corrosion as shown in Figure 6.37. However, in both ungalvanised and galvanised tendons with High Level of pre-stress and Stage I corrosion, embrittlement ratios were slightly greater. At higher degrees of corrosion, the absolute ratio of elongation, reduction in area and breaking strength became high for ungalvanised tendons with Low Level of pre-stress, while with high degree of corrosion they were increased. However, for galvanised tendons with High Level of pre-stress the ratio was less for breaking strength and increased more for elongation. An increase in ratio of elongation indicates high susceptibility to hydrogen [124].

In order to investigate further, the fractured specimens were removed from the test machine and cleaned by dust removal to produce a clean fracture surface. Fracture surfaces were observed at different magnifications using the scanning electron microscope (SEM) to investigate the failure mechanism under tensile

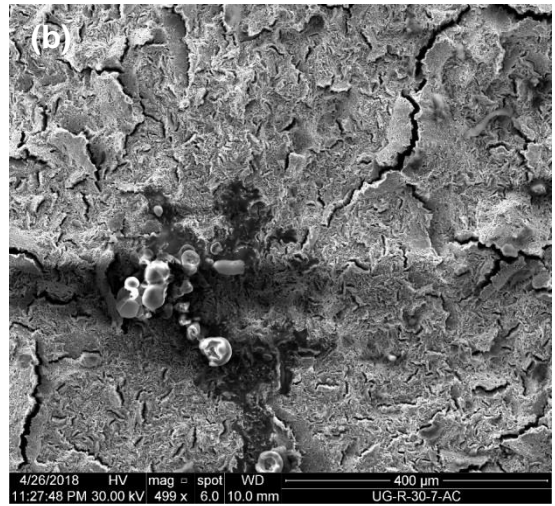
loading and to investigate any possible influence of hydrogen embrittlement. The SEM was used to examine the surface characteristics and evaluate the metallurgical information including the analysis of the phase microstructure. The SEM operating principle was described in Chapter 4 Section 4.11.1.1 and the settings, including magnifications for each type of images of the SEM is listed in Table 4.6. To investigate the hydrogen effect on the fracture mode, the microstructure and the fracture mode were compared between the Control tendon (As-received tendon with zero pre-stress, corrosion and ICCP) and pre-stressed tendons exposed to the three stages of corrosion (I, II and III) and to ICCP-Normal protection (ICCP-N) in the range of potential of -650 to -750mV vs SSC. Hydrogen was introduced in these tendons through cathodic charging by applying a current to the target potential (Normal protection -650 to -750mV SSC). Figure 6.40 (a-f) shows the fracture modes of the as-received ungalvanised tendons and Figure 6.41 (a-f) shows the fracture modes of the as-received galvanised tendons.

Referring to From Figure 6.40 (f) it is apparent that the tendons exhibited a failure resembling a partial cup and cone type fracture, which is a typical feature of ductile failure. Similarly, Figure 6.41 (f) shows the same fracture mechanism. For ungalvanised tendons, Figure 6.40 (d) obtained under powerful magnification, shows depressions or dimples, while Figure 6.40 (e) also shows small dimples (identified by yellow dashed circles). These fracture mechanisms are caused by a coalescence of pores, supporting that the fracture is ductile [125].

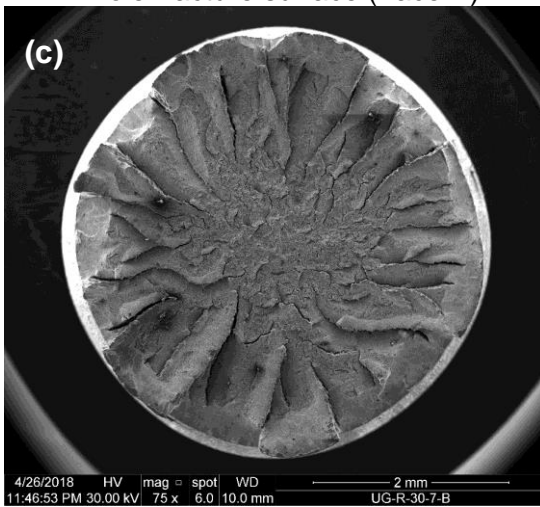
For the galvanised tendon, Figure 6.41 (d) shows dimples (identified by yellow dashed circles) and shows a quasi-cleavage fracture (identified by a red dashed circle) [126]. The microstructure in Figure 6.41 (e) shows dimples and small dimples. These fractures again indicate that the fracture mechanism is ductile [125], [126].



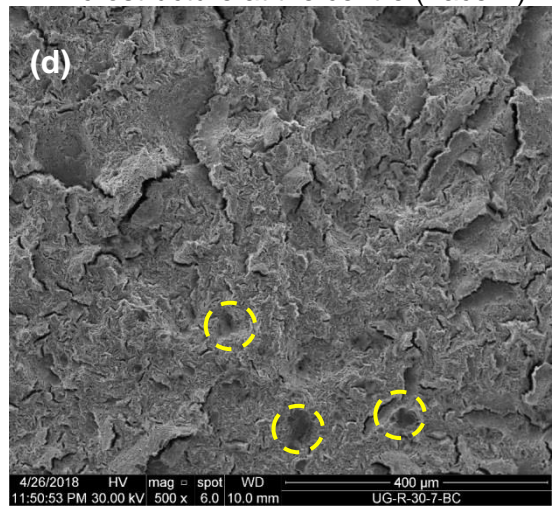
Ungalvanised as-received tendon - the whole fracture surface (Face A)



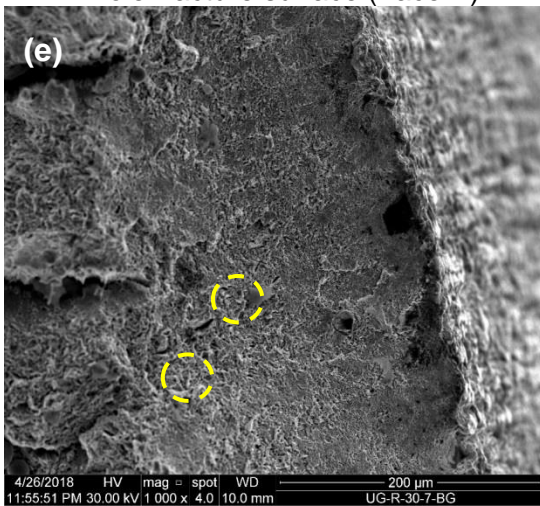
Ungalvanised as-received tendon - the microstructure at the centre (Face A)



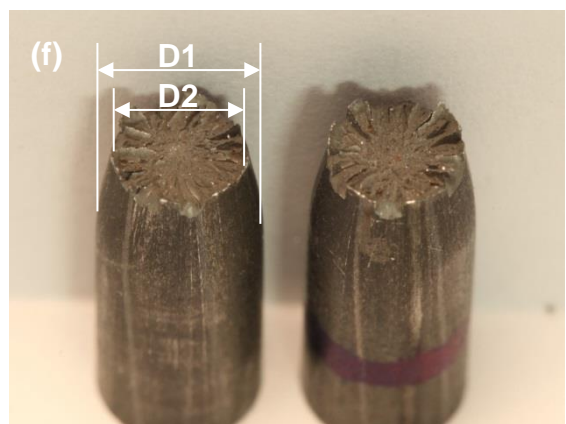
Ungalvanised as-received tendon - the whole fracture surface (Face A)



Ungalvanised as received tendon - the microstructure at the centre (Face B)

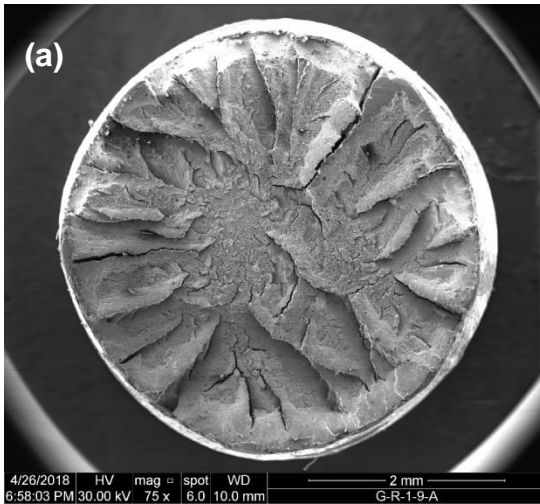


Ungalvanised as-received tendon - the microstructure at the edge of the tendon (Face B)

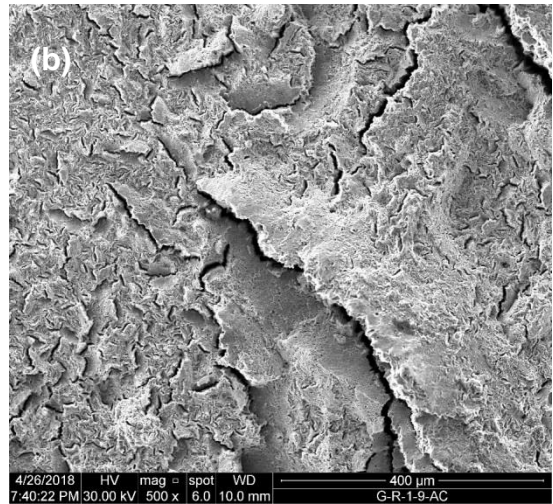


Fracture mode with necking stage

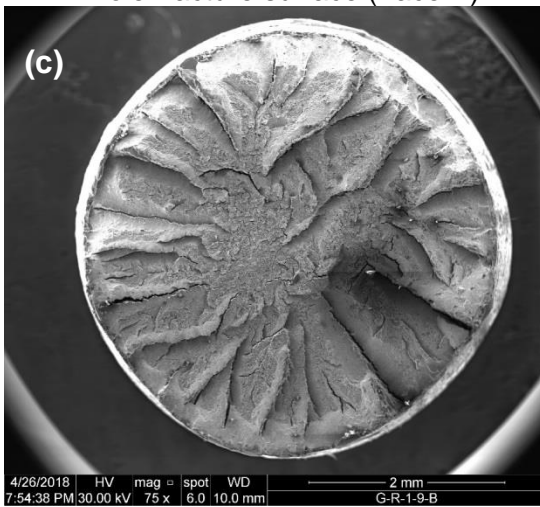
Figure 6.40 SEM micrographs and images showing the fracture mode of the as-received ungalvanised tendon



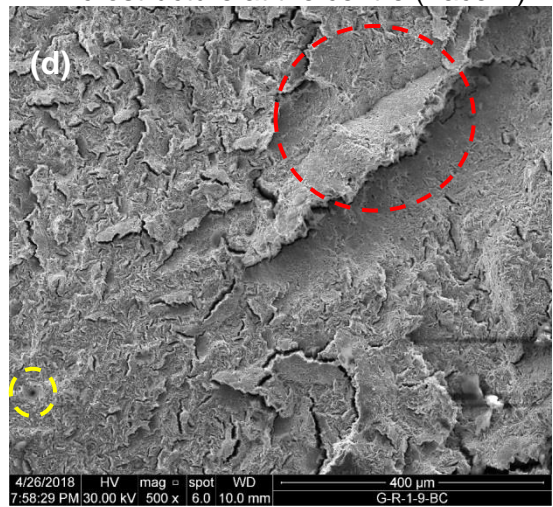
Galvanised as received tendon - the whole fracture surface (Face A)



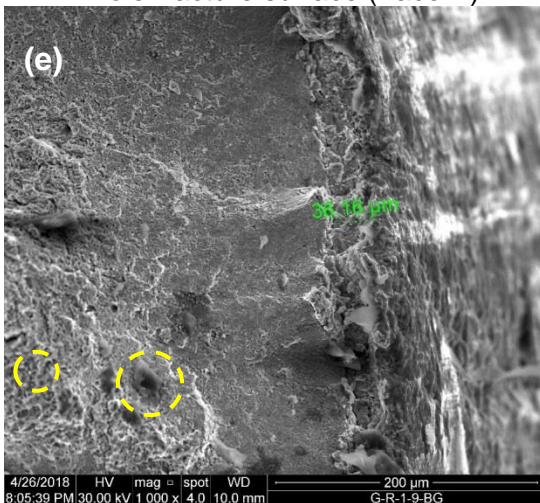
Galvanised as-received tendon - the microstructure at the centre (Face A)



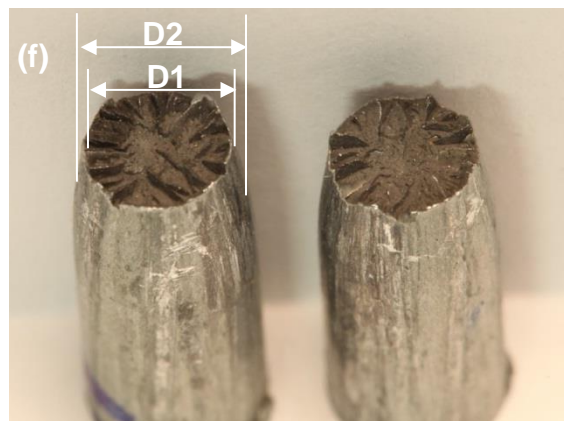
Galvanised as-received tendon - the whole fracture surface (Face B)



Galvanised as-received tendon - the microstructure at the centre (Face B)



Galvanised as-received tendon - the microstructure at the edge of the tendon (Face B)



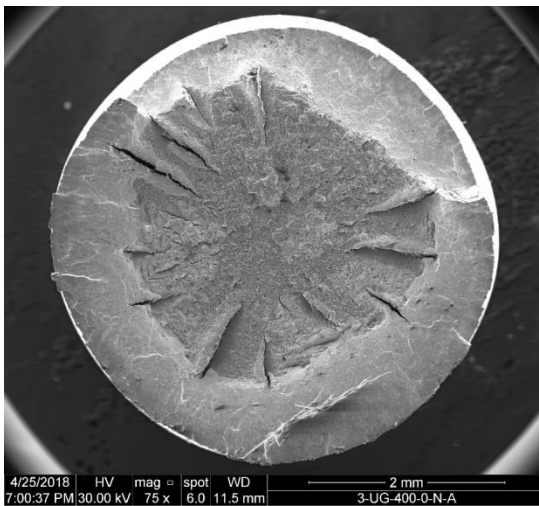
Fracture mode with necking stage

Figure 6.41 SEM micrographs and images showing the fracture mode of the as-received galvanised tendon

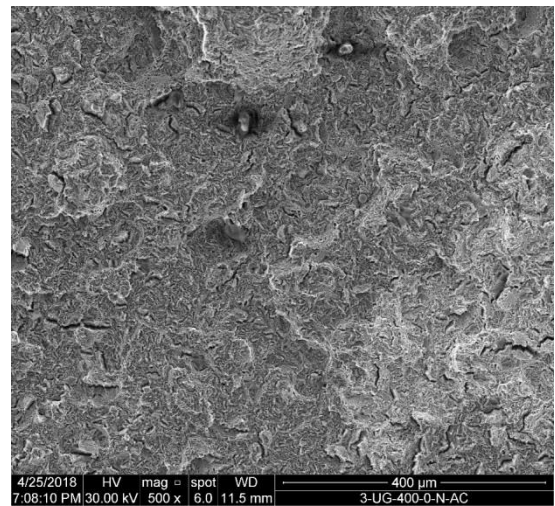
For the Batch 2, ungalvanised tendons with Low level of pre-stress as shown in Figure 6.42 (a-c), Figure 6.43 (a-c) and Figure 6.44 9 (a-c) all samples at different corrosion stages show cup-cone character and necking. Under powerful magnification, the dimples are present in the microstructure which indicates that the fracture surfaces were purely ductile.



(a) M-U-L-I-N-1
Fracture cup-cone type



(b) The whole fracture surface

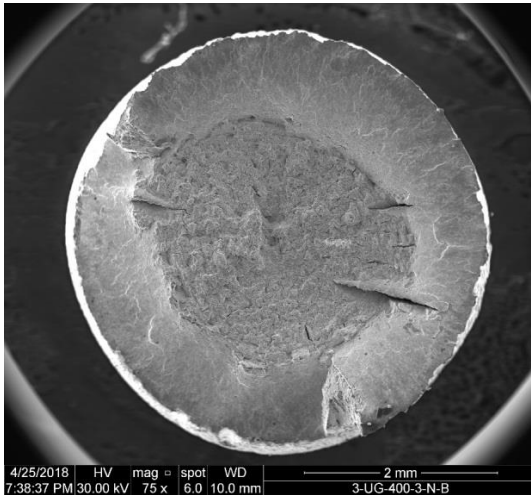


(c) The microstructure at centre

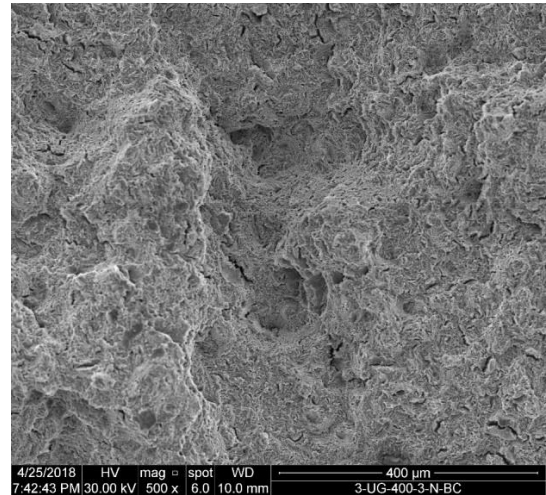
Figure 6.42 SEM images for ungalvanised tendon (M-U-L-I-N-1), 30% UTS



(a) M-U-L-II-N-2
Fracture with cup-cone type



(b) The whole fracture surface

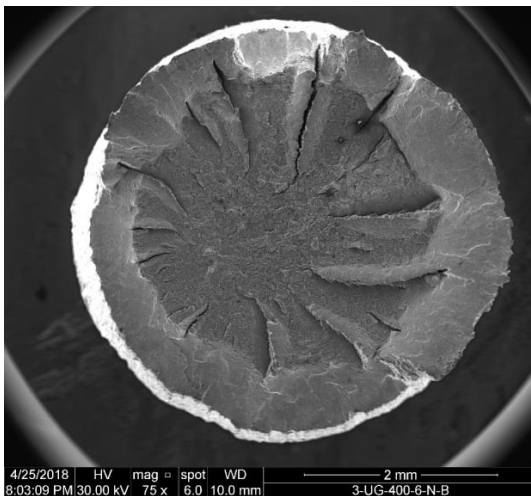


(c) The microstructure at centre

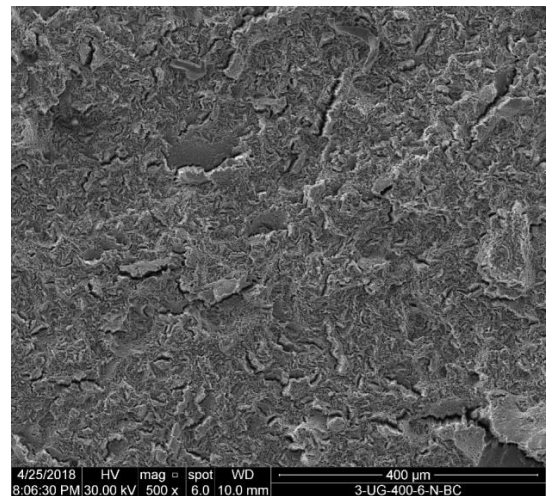
Figure 6.43 SEM images for ungalvanised tendon (M-U-L-I-N-2), 30% UTS



(a) M-U-L-III-N-3
Fracture with partial cup-cone type



(b) The whole fracture surface



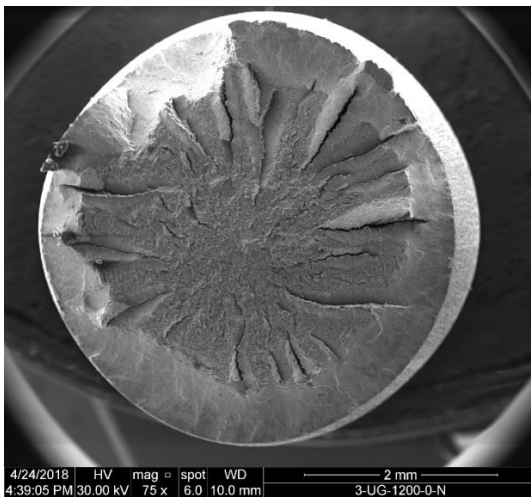
(c) The microstructure at centre

Figure 6.44 SEM images for ungalvanised tendon (M-U-L-III-N-3), 30% UTS

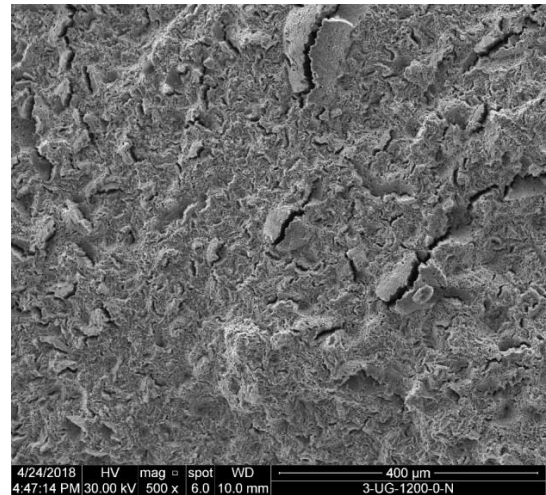
For Batch 2, ungalvanised with High Level of pre-stress, as shown in Figure 6.45 (a), Figure 6.46 (a) and Figure 6.47 (a) all fractures are cup-cone type. The microstructures show both small dimples and large, deep dimples (identified by red arrows) for specimen M-U-H-II-N-2 (Figure 6.46 (c)) and specimen SM-U-H-III-N-3 (Figure 6.47 (c)) and coalescence and connection of dimples on the fracture surface (red dashed area).



(a) M-U-H-I-N-1
Fracture cup-cone type



(b) The whole fracture surface

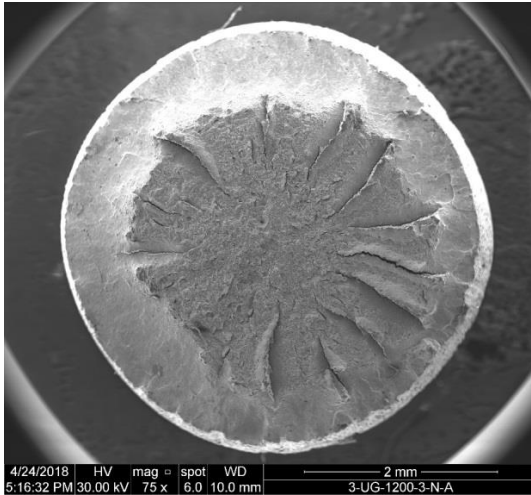


(c) The microstructure at centre

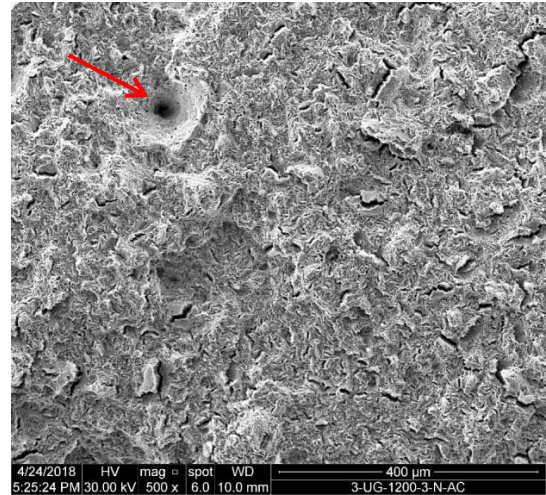
Figure 6.45 SEM images for ungalvanised tendon (M-U-H-I-N-1), 80% UTS



(a) M-U-H-II-N-2
Fracture cup-cone type



(b) The whole fracture surface



(c) The microstructure at centre

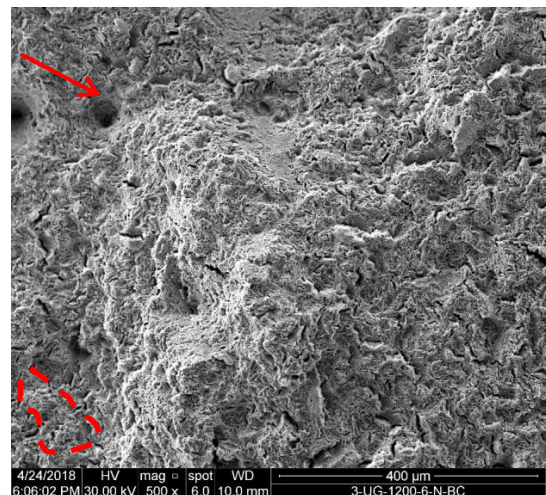
Figure 6.46 SEM images for ungalvanised tendon (M-U-H-II-N-2), 80% UTS



(a) M-U-H-III-N-3
Fracture with partial cup-cone type



(b) The whole fracture surface



(c) The microstructure at centre

Figure 6.47 SEM images for ungalvanised tendon (M-U-H-III-N-3), 80% UTS

For Batch 4, galvanised tendons with High Level of pre-stress, as shown in Figure 6.49, Figure 6.50 and Figure 6.51, the fracture modes for specimens M-G-H-I-N-1 (Figure 6.49 (a-c)) and M-G-H-II-N-2 (Figure 6.50 (a-c)) are cup-cone in character while specimen M-G-H-III-N-3 (Figure 6.51 (a)) exhibited brittle and shear (identified by white arrow) type fracture mode (Figure 6.51 (b) [127]). The microstructures show dimples in all of them and in addition specimen M-G-H-III-N-3 (Figure 6.51 (c)) shows a mixture of ductile (identified by yellow circle) and brittle (identified by red boxes) modes of fracture [125], [127].

In the light of the above, there is no damage to the steel due to the application of ICCP-N. This can be seen from the type of fracture modes. The only severe damage has been observed in specimen M-G-H-III-N-3 (Figure 6.51), but this damage is more likely caused by corrosion as shown in Figure 6.48, where the roughness (Ra) is $6.17 \mu\text{m}$ (Table 5.7) and mass loss is 4.1% (Table 5.11). Therefore, ICCP-N has had little or no effect on the pre-stresses tendons. Comparison is made between ICCP-N and ICCP-O in Chapter 7.

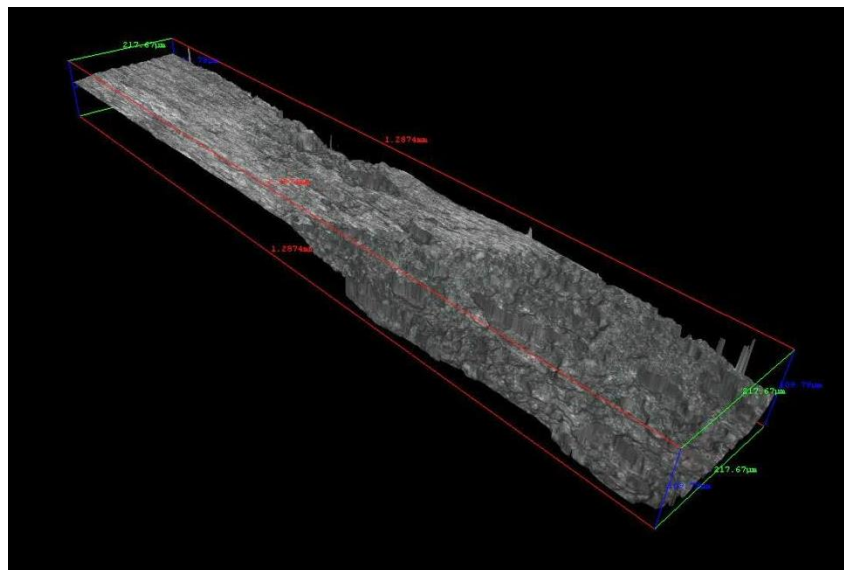
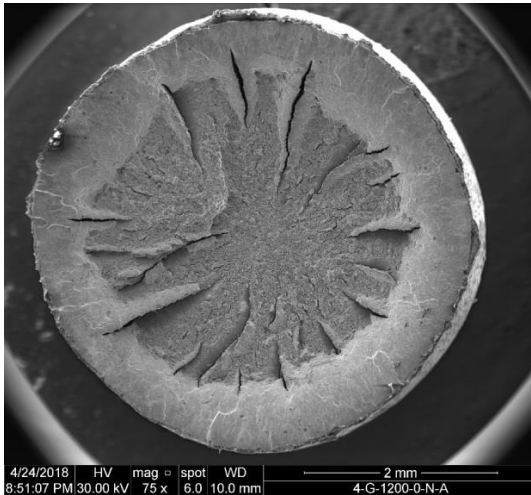


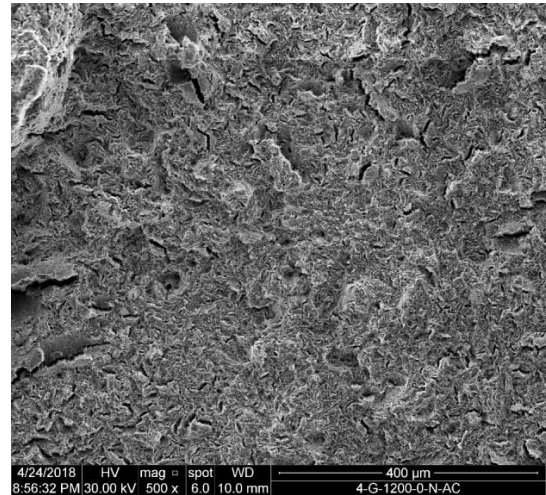
Figure 6.48 IFM image (50X magnification, 1mm length, 6x2 image) for specimen M-G-H-III-3



(a) M-G-H-I-N-1
Fracture cup-cone type



(b) The whole fracture surface

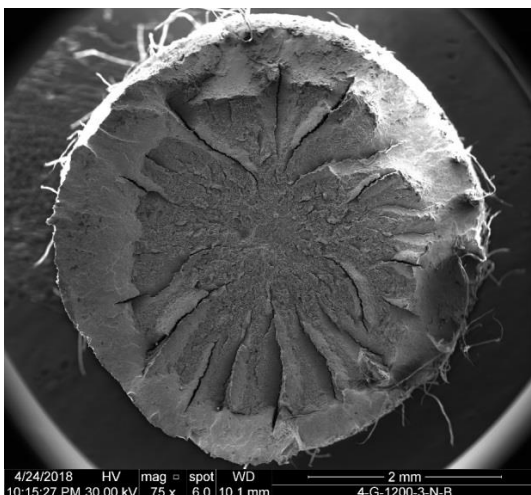


(c) The microstructure at centre

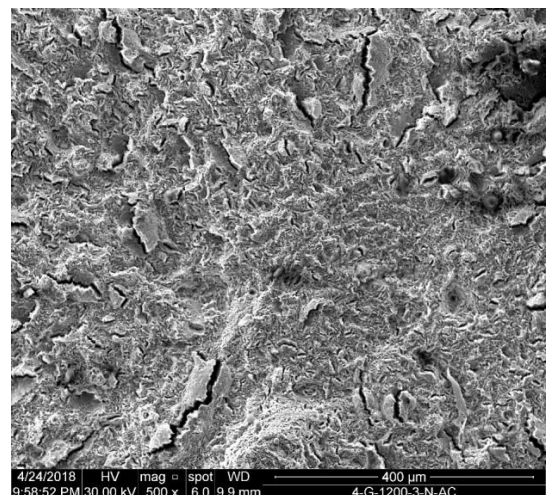
Figure 6.49 SEM images for galvanised tendon (M-G-H-I-N-1), 80% UTS



(a) M-G-H-II-N-2
Fracture of near cup-cone type



(b) The whole fracture surface

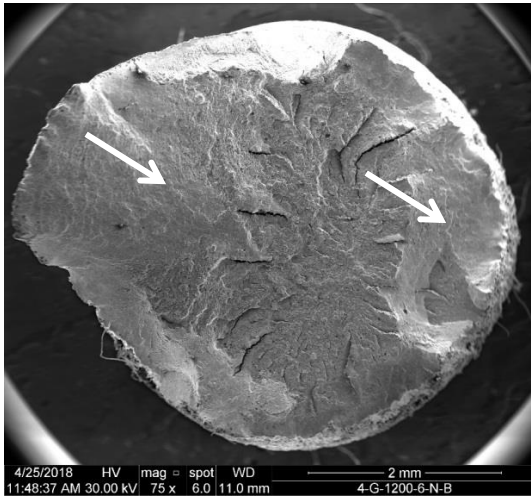


(c) The microstructure at centre

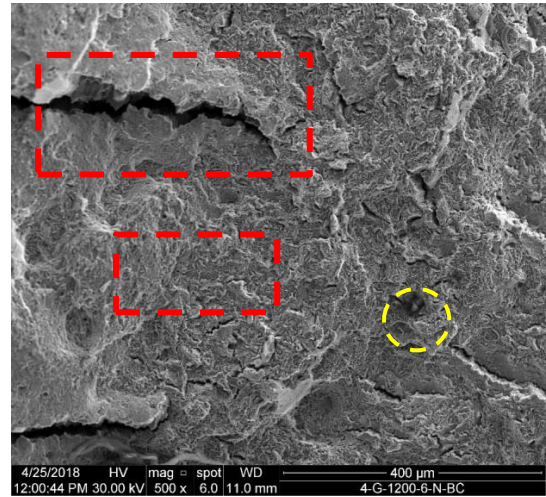
Figure 6.50 SEM images for galvanised tendon (M-G-H-II-N-2), 80% UTS



(a) M-G-H-III-N-3
Shear type fracture



(b) The whole fracture surface



(c) The microstructure at centre

Figure 6.51 SEM images for galvanised tendon (M-G-H-III-N-3), 80% UTS

6.5.7 Conclusion

- Small yellow spots appeared on the surface of the mortar around the connection of anode location in the ungalvanised tendon, while in the case of the galvanised tendons there is no sign of yellow spots.
- The ICCP was applied for an extended period of 13,272 hours for ungalvanised and 3,288 hours for galvanised tendons. When the application of the cathodic protection-Normal protection (ICCP-N) system was interrupted for 24 hours, the potential decays were more than 100mV after 4 hours for all tendons, demonstrating that an adequate level of protection has been achieved.
- The results clearly indicate that there is a loss in pre-stress in both the ungalvanised and galvanised tendons over the entire test period. It was also observed that the degree of corrosion has an impact on the loss of stress particularly in the ungalvanised tendons. This indicates that the ungalvanised tendons subjected to higher degrees of corrosion will suffer higher losses which should be accounted for as an additional loss which may be counteracted by adding more tendons at the design stage. This

loss of service stress can be from combination of degree of corrosion and the application of ICCP-N.

- Overall, there was no significant effect of ICCP-N on the strength of the tested tendons. The ultimate tensile strength and the 0.2% proof strength for all tendons in each type of tendon were similar. Typically the design safety factor is set to a maximum level of stress at approximately $\frac{2}{3}$ proof strength for structural engineering components. Although the ductility has been reduced by the application of the ICCP-N, the fracture occurred after reaching the ultimate strength in each type of tendon.
- The embrittlement ratio indicates that hydrogen generated by ICCP-N has no effect on either ultimate or proof strengths for either tendon types. However, for galvanised tendon with High Level of prestress, the ratio was less for breaking strength and increased more for elongation.
- All as-received specimens exhibited a ductile fracture with necking and cup and cone fracture surface. SEM images of the fracture surface of the ungalvanised tendons indicates that ductile mode failures occurred, while the galvanised tendon showed that two failures occurred with, one by a ductile mode and the other a combination of ductile and brittle.

7 Effect of Cathodic Protection on Steel Tendons - Over Protection

7.1 Introduction

In Chapter 6, Section 6.1, the importance of applying ICCP for controlling or mitigating the corrosion of the steel and improving the environment surrounding the steel has been discussed. Two regimes were introduced in this research work regarding the effect of ICCP in pre-stressed tendons. The first scenario applied ICCP with potentials as recommended by most of the standards, named normal protection (ICCP-N). The other scenario purposely applied ICCP over the threshold with a potential (Instant-Off) range between -850 to -1300mV vs SSC, named here as ICCP overprotection (ICCP-O), in order to have a better understanding of the effect of ICCP in pre-stressed tendons in terms of loss in service stress, mechanical properties and the concern of the risk of hydrogen embrittlement. Hydrogen can be electrochemically generated for a long period and, absorbed by the steel under a high level of stress. To get a better understanding of the behaviour of the tendon, this chapter will examine and discuss the effects of ICCP-O on the pre-stressed tendons. In addition, one batch of samples included unstressed tendons and non-corroded, both galvanised and ungalvanised, and were exposed to cathodic protection (CP) with a high potential ranging between -1000 to -1200mV vs SSC.

7.2 The objectives of the tests

The purpose of the planned tests is to investigate the following parameters as a result of applying ICCP overprotection (ICCP-O):

- Observe changes on the surface of the mortar
- Determine the loss of applied service stress
- Investigate the surface of the tendons
- Identify the criteria in terms of the applied potential, potential shift, instant off and potential decay in accordance with design criteria
- Investigate the mechanical properties of the tendons with regards to the strength and risk of Hydrogen embrittlement
- Analyse the type and form of fracture modes of the tendons

In addition, comparison between the application of ICCP-N and ICCP-O are made.

7.3 Impressed Current Cathodic Protection (ICCP)

The principle of the ICCP was described in Chapter 4, Section 4.7 and the components of the ICCP system was also described in Chapter 6, Section 6.3.

7.4 Experimental works

To have a better understanding of the effect of ICCP-O on the pre-corroded tendons with different degree of corrosion and with Low and High Level of pre-stress, a long period test approach was adopted. Three Batches were tested under ICCP-O after accelerated corrosion was applied and before dismantling the moulds. Batch 3 investigated the effect of ICCP-O on the ungalvanised tendon with both Low Level and High Level of pre-stressed embedded tendons and Batch 4 investigated the effect of ICCP-O on galvanised tendons with High Level of pre-stress. For the purpose of the research, an additional batch was introduced, Batch 5 for both types of tendons (galvanised and ungalvanised) which were neither stressed nor corroded and submerged in a saline solution of 3.5% NaCl. This was done to purposefully apply a high potential of ICCP-O in the range between -850 to -1300mV vs Ag/AgCl (Table 7.1).

Table 7.1 Test Programme

<i>Batch</i>	<i>Test Code</i>	<i>Degree of Corrosion (Stage)</i>	<i>Actual Degree of Corrosion (%)</i>	<i>ICCP Application</i>
3	M-U-L-X1-1	I	0.0	None and uncorroded - Control
	M-U-L-II-O-2	II	3.9	ICCP - Overprotection
	M-U-L-III-O-3	III	6.5	ICCP - Overprotection
	M-U-H-X1-1	I	0.0	None and uncorroded - Control
	M-U-H-II-O-2	II	2.0	ICCP - Overprotection
	M-U-H-III-O-3	III	4.0	ICCP - Overprotection
4	M-G-H-X1-1	I	0.0	None and uncorroded - Control
	M-G-H-II-O-2	II	3.4	ICCP - Overprotection
	M-G-H-III-O-3	III	4.1	ICCP - Overprotection

Key: U-Ungalvanised, G-Galvanised, M-Mortar electrolyte, S-Solution electrolyte, H-High level of pre-stress (800-1200MPa), L-Low level of pre-stress (300-400MPa), I-Degree of corrosion Stage I (0-1%), II-Degree of corrosion Stage II (2-4%), III-Degree of corrosion Stage III (4-7%), N-Normal protection, O-Overprotection, X and X1-no corrosion and no ICCP, R-As-received samples, 1, 2, 3-Sample numbers.

Table 7.1 (cont.) Test Programme

<i>Batch</i>	<i>Test Code</i>	<i>Degree of Corrosion (Stage)</i>	<i>Actual Degree of Corrosion (%)</i>	<i>ICCP Application</i>
5	5-UG-O-1	N/A	N/A	ICCP - Overprotection
	5-UG-O-2	N/A	N/A	ICCP - Overprotection
	5-UG-O-3	N/A	N/A	ICCP - Overprotection
	5-G-O-1	N/A	N/A	ICCP - Overprotection
	5-G-O-2	N/A	N/A	ICCP - Overprotection
	5-G-O-3	N/A	N/A	ICCP - Overprotection

Key: U-Ungalvanised, G-Galvanised, M-Mortar electrolyte, S-Solution electrolyte, H-High level of pre-stress (800-1200MPa), L-Low level of pre-stress (300-400MPa), I-Degree of corrosion Stage I (0-1%), II-Degree of corrosion Stage II (2-4%), III-Degree of corrosion Stage III (4-7%), N-Normal protection, O-Overprotection, X and X1-no corrosion and no ICCP, R-As-received samples, 1, 2, 3-Sample numbers.

Table 7.2 shows the overall period of the application of ICCP overprotection in tendons.

Table 7.2 ICCP Overprotection

<i>Batch</i>	<i>Test code</i>	<i>Degree of Corrosion (Stage)</i>	<i>Actual Degree of Corrosion (%)</i>	<i>ICCP Period (days)</i>	<i>(hours)</i>
3	M-U-L-X1-1	I	0.0	221	5304
	M-U-L-II-O-2	II	3.9	221	5304
	M-U-L-III-O-3	III	6.5	221	5304
	M-U-H-X1-1	I	0.0	221	5304
	M-U-H-II-O-2	II	2.0	221	5304
	M-U-H-III-O-3	III	4.0	221	5304
4	M-G-H-X1-1	I	0.0	137	3288
	M-G-H-II-O-2	II	3.4	137	3288
	M-G-H-III-O-3	III	4.1	137	3288
5	5-UG-O-1	N/A	N/A	488	11712
	5-UG-O-2	N/A	N/A	488	11712
	5-UG-O-3	N/A	N/A	488	11712
	5-G-O-1	N/A	N/A	488	11712
	5-G-O-2	N/A	N/A	488	11712
	5-G-O-3	N/A	N/A	488	11712

Key: U-Ungalvanised, G-Galvanised, M-Mortar electrolyte, S-Solution electrolyte, H-High level of pre-stress (800-1200MPa), L-Low level of pre-stress (300-400MPa), I-Degree of corrosion Stage I (0-1%), II-Degree of corrosion Stage II (2-4%), III-Degree of corrosion Stage III (4-7%), N-Normal protection, O-Overprotection, X and X1-no corrosion and no ICCP, R-As-received samples, 1, 2, 3-Sample numbers.

7.4.1 Specimens design, mortar mix, pre-tensioning and accelerated corrosion

ICCP-O was applied to the pre-corroded specimens as stipulated in Table 7.2. The specimen's dimensions and mortar mix are described in Section 5.4.3. The compressive strength of the mortar for each batch is also presented in Table 5.2 in Section 5.4.3.1. The pre-tensioning procedures and different levels of applied service stress are described in Section 5.4.4. The corrosion process has been described in Section 5.5, where mixed metal oxide (MMO) titanium mesh ribbon was connected to the negative terminal of a D.C power supply, working as the cathode while the tendons were connected to the positive terminal of a D.C power supply. Corrosion took place in both a saline solution containing 3.5% NaCl and mortar without adding sodium chloride. The samples were kept moist by spraying water on a daily basis. The current and potential were monitored and recorded on a daily basis.



(a) Specimens pre-stressed & ready for casting

(b) Specimens cast

Figure 7.1 ICCP-O specimens pre-stressed and cast

7.4.2 Application of impressed current cathodic protection (ICCP)

The application of ICCP has been previously described in Chapter 6, Section 6.4.2. A DC power supply with high DC Voltage (60V) was used to provide a high potential. Due to the requirements of the laboratory in terms of safety, the connections of the wires were protected by a plastic tube (Figure 7.3). Two types of DC power supply were provided to generate the necessary voltage for the target potential. One type was used for the pre-stressed tendons (Figure 7.2 (a)) and the other one was a CPI manual power

system, supplied by Cathodic Protection International Aps., for the non stressed tendons within the saline solution (Figure 7.2 (b)). The method used for applying ICCP-O is the same method used in applying ICCP-N, where the current is allowed to float until the target potential is obtained and then maintained at a constant value.



(a) DC power supply



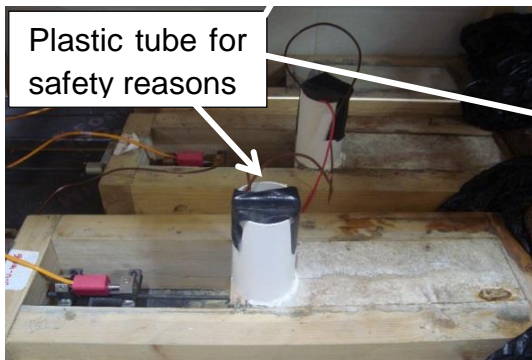
(b) CPI manual power system

Figure 7.2 Power supplies to generate the target potential

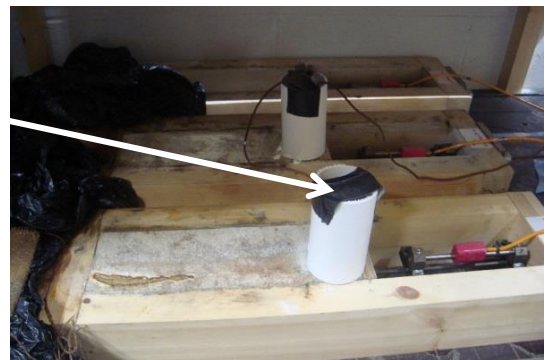
Figure 7.3 (a, b ,c, d and e) shows the test set-up for the pre-stressed and pre-corroded ungalvanised and galvanised specimens, while Figure 7.4 (a, b, and c) shows the test set-up for unstressed ungalvanised and galvanised specimens.



(a) Test set-up



(b) Ungalvanised with Low Level of pre-stress under ICCP-O



(c) Ungalvanised with High Level of pre-stress under ICCP-O

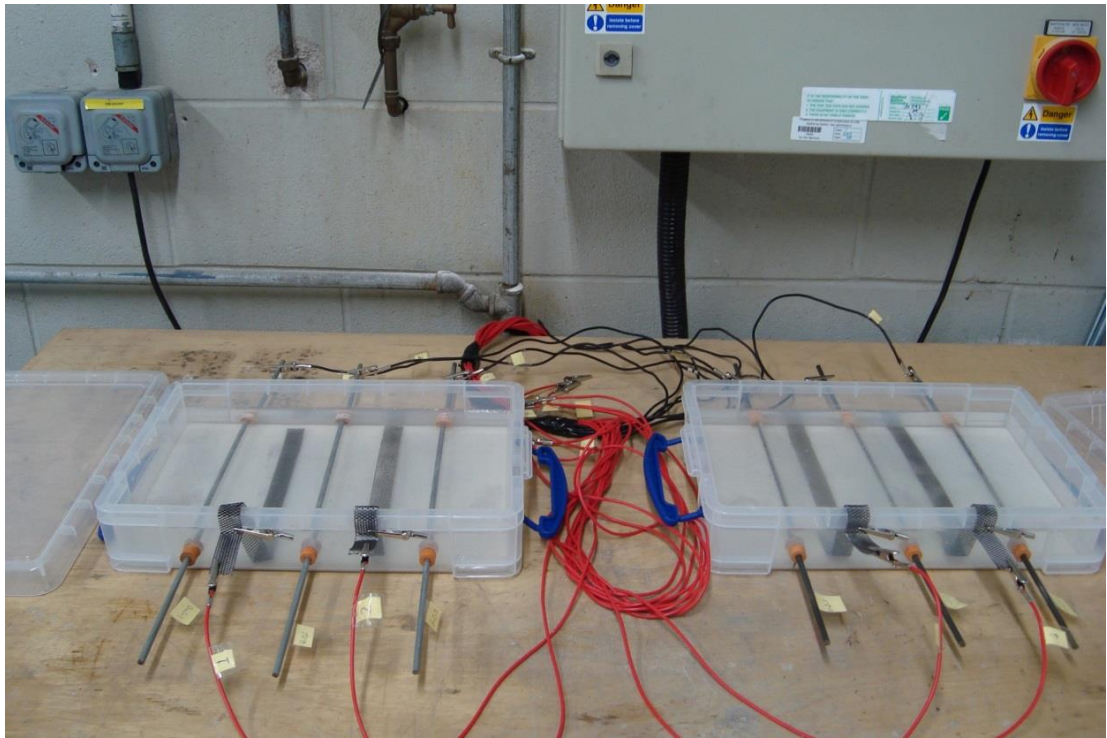


(d) Test set-up

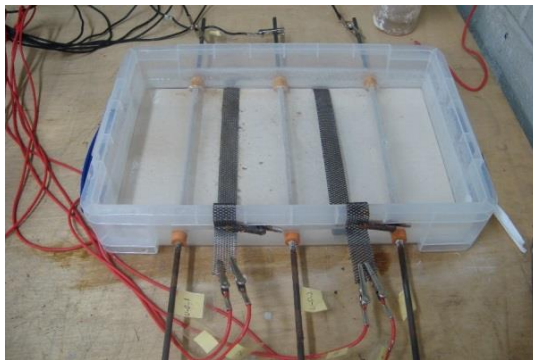


(e) Galvanised tendons with High Level of pre-stress under ICCP-O

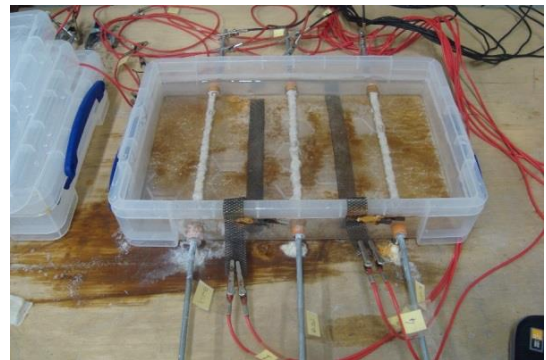
Figure 7.3 Set-up of specimens under the application of ICCP overprotection



(a) Test Set-up using CPI power supply system



(a) Unstressed ungalvanised tendons



(b) Unstressed galvanised tendons

Figure 7.4 Set-up of unstressed Ungalvanised & Galvanised tendons under application of ICCP-O

7.4.3 Design criteria

For the purpose of the test, the applied potential was more than the practical recommended limits and the criteria stated in Section 6.4.3 were adopted.

7.4.4 Polarization and Depolarization Criteria

The effectiveness of the application of ICCP-O was determined by interrupting the rectifier (DC) between 0.1 to 1.0 seconds to take 'Instant Off' readings. The polarisation and depolarisation principle and criteria were discussed in Section 6.4.4.

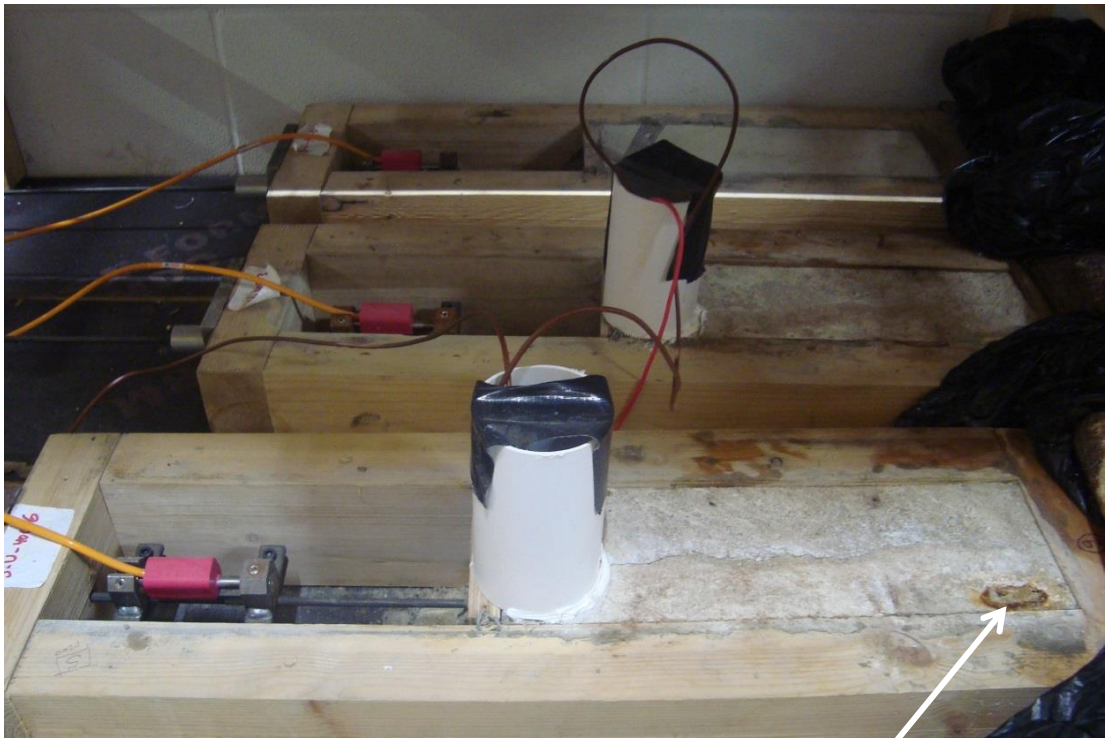
7.5 Results and discussion

7.5.1 Visual observation

Daily observation and data (Volts, Amps, Potential and Instant-Off steel potential) were recorded during the overall period of applying ICCP-O. For ungalvanised tendons (Batch 3) for Low Level of pre-stress with Stage II and Stage III corrosion, yellow spots appeared on the surface of the mortar on the opposite side to the connection, above the anode location. The spot size is about 5 cm long and 1.5 cm wide as shown in Figure 7.5 (a-c) The spot area remained as described until the end of the test.

For ungalvanised tendons (Batch 3) for High Level of pre-stress with Stage II corrosion, yellow spots appeared on the surface of the mortar along the anodic zone about 5 cm long and 1 cm wide, this spot increased in size, the length reached 10 cm long and 1.5 cm wide after 411 days of applying ICCP-O as shown in Figure 7.6 (b-e). For the tendon with Stage III corrosion, it was noticed that the spot increased in length to about 14 cm long and 1.5 cm wide after 165 days of applying ICCP-O. This spot further increased along the whole length of the anode after 411 days of applying ICCP-O. In general, the size of the yellow spot in the tendons with High Level of pre-stress is greater than in the tendons with Low Level of pre-stress. These yellow spots appear to have occurred due to acid generation from the lack of mortar cover for the experimental tests. In practice, the tendon is embedded within the concrete with sufficient cover to provide protection to the anode material.

Figure 7.7 (b-e) shows the yellow spots for the galvanised tendons (Batch 4). Overall, the size and shape of the yellow spot remained the same for both degrees of corrosion at Stage II and Stage III. For the tendon with Stage II corrosion, the spot was 3 cm long and 1 cm wide and for the tendon with Stage III corrosion, the spot was distributed along the anode in different sizes, (Figure 7.7 (b, e)). The area for both remained approximately the same until the end of the test.



(a) Test Set-up



(b) ICCP-O after 176 days, Stage II Corr.



(c) ICCP-O after 176 days, Stage III Corr.



(d) ICCP-O after 245 days, Stage II Corr.



(e) ICCP-O after 245 days, Stage III Corr.

Figure 7.5 Yellow spots on the mortar surface for ungalvanised tendons with Low Level of pre-stress



(a) Test Set-up



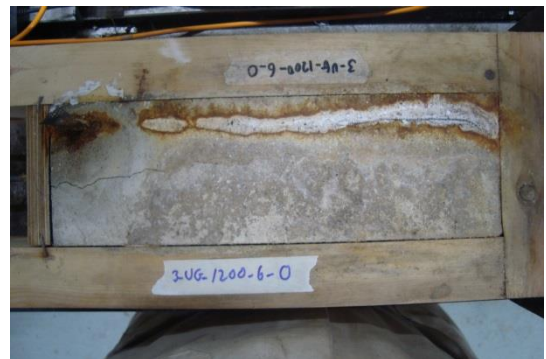
(b) ICCP-O after 165 days, Stage II Corr.



(c) CCP-O after 165 days, Stage III Corr.



(d) ICCP-O after 411 days, Stage II Corr.

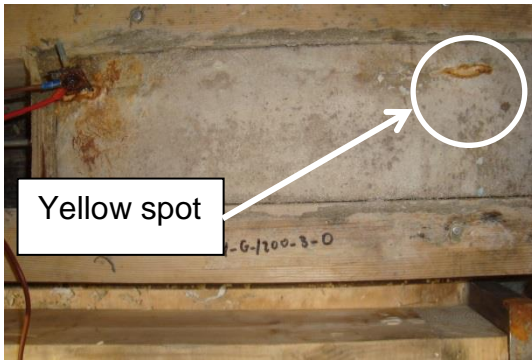


(e) CCP-O after 411 days, Stage III Corr.

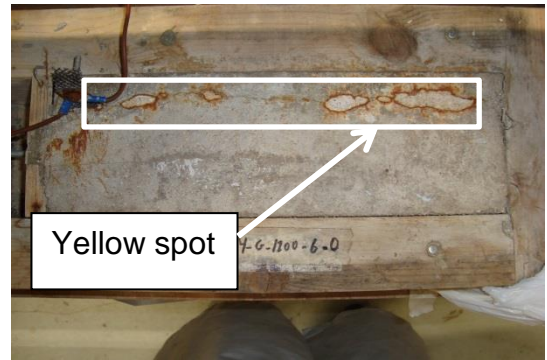
Figure 7.6 Yellow spots on the mortar surface for ungalvanised tendons with High Level of pre-stress



(a) Test Set-up



(b) ICCP-O after 132 days, Stage II Corr.



(c) ICCP-O after 132 days, Stage III Corr.



(d) ICCP-O after 154 days, Stage II Corr.



(e) ICCP-O after 154 days, Stage III Corr.

Figure 7.7 Yellow spots on the mortar surface for galvanised tendons with High Level of pre-stress

7.5.2 Infinite Focus Microscope (IFM)

After completing the application of ICCP-Overprotection, the surface of the tendons were examined using Infinite Focus Microscopy (IFM). The principle of the IFM was discussed in Chapter 4, Section 4.11.3. Figure 7.8 shows the microstructure of the tendon surface using IFM with magnification 5X for ungalvanized tendons with Low Level of pre-stress with different degrees of corrosion. The (a) samples is represents the tendon before removing corrosion products and (b) samples show the tendons after removing the corrosion products. It was found that the colour of the corrosion products on the surface of the charged tendons after applying ICCP-O was a black colour, this formed in the absence of oxygen with water providing the source of hydrogen as shown in specimens M-U-L-II-O-2 (Figure 7.8 (a)) and M-U-L-III-O-3 (Figure 7.8 (a)). Specimen M-U-L-II-O-2 (Figure 7.8 (b)) shows the damage to the steel caused by corrosion and this was assessed by profiling the pits on the surface of the tendon after the removal of the corrosion products. The presence of pitting corrosion indicates that the current was not distributed equally due to changes in the applied potential. The dimension of pitting was given in Chapter 5. On the other hand, pitting corrosion was virtually absent on the surface of specimen M-U-L-III-O-3 (Figure 7.8 (b)), showing that no apparent pitting was formed on the surface of the tendon.

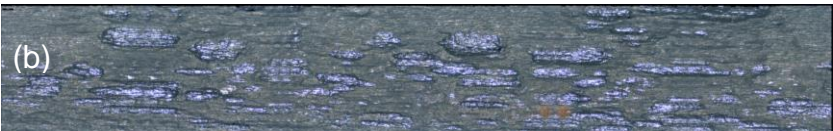
M-U-L-X1-1	No Corr. No ICCP	
M-U-L-II-O-2	Before removing Corr. Products	(a) 
	After removing Corr. Products	(b) 

Figure 7.8 Microstructure of ungalvanized tendon surface

M-U-L-III-O-3	Before removing Corr. Products	
	After removing Corr. Products	

Figure 7.8 (cont.) Microstructure of ungalvanized tendon surface

Figure 7.9 shows the microstructure of the tendon surface using IFM with magnification 5X for ungalvanized tendons with High Level of pre-stress with different degrees of corrosion. In this batch the colour of the corrosion products on the surface of the charged tendons after application of the ICCP-O was less black in colour. Specimens showed no apparent pitting on the surface of the tendons, more uniform corrosion was observed. Specimen M-U-L-III-O-3 (Figure 7.9 (b)), showed no apparent pitting but there is damage due to corrosion on the surface (identified by yellow dashed rectangle).

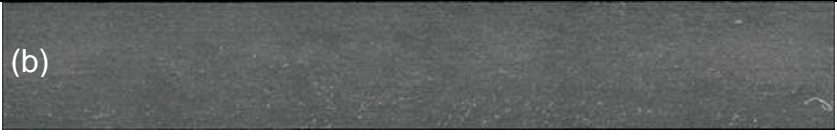
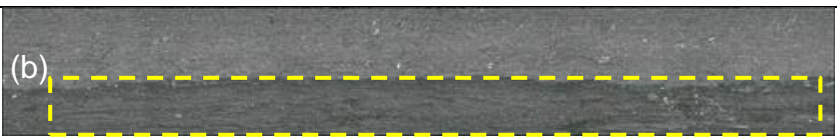
M-U-H-X1-1	No Corr. No ICCP	
M-U-H-II-O-2	Before removing Corr. Products	
	After removing Corr. Products	
M-U-H-III-O-3	Before removing Corr. Products	
	After removing Corr. Products	

Figure 7.9 Microstructure of ungalvanized tendon surface with High Level of pre-stress

For the galvanised tendons with High level of pre-stress, there is damage on the surface of the tendon caused by corrosion and there is pitting along the length

as shown in specimen M-G-H-II-O-2 (Figure 7.10 (b)). Specimen M-G-H-III-O-3 (Figure 7.10 (b)) shows a small group of pits (identified by red dashed area). This damage is either due to corrosion or application of ICCP-O or both.

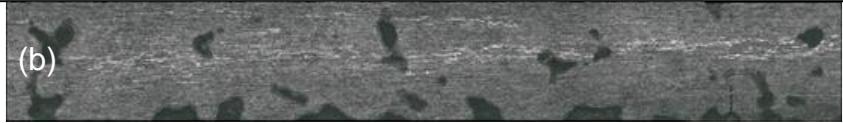
M-G-H-X1-1	No Corr. No ICCP	
M-G-H-II-O-2	Before removing Corr. Products	(a) 
	After removing Corr. Products	(b) 
M-G-H-III-O-3	Before removing Corr. Products	(a) 
	After removing Corr. Products	(b) 

Figure 7.10 Microstructure of galvanized tendon surface with High Level of pre-stress

For Batch 5 samples as shown in Figure 7.11, there is no visible damage on the surface of both type of tendons due to the application of ICCP-O only.

S-U-O-1	After Applying ICCP-O	
S-U-O-2	After Applying ICCP-O	

Figure 7.11 Microstructure of ungalvanised & galvanized tendon surface

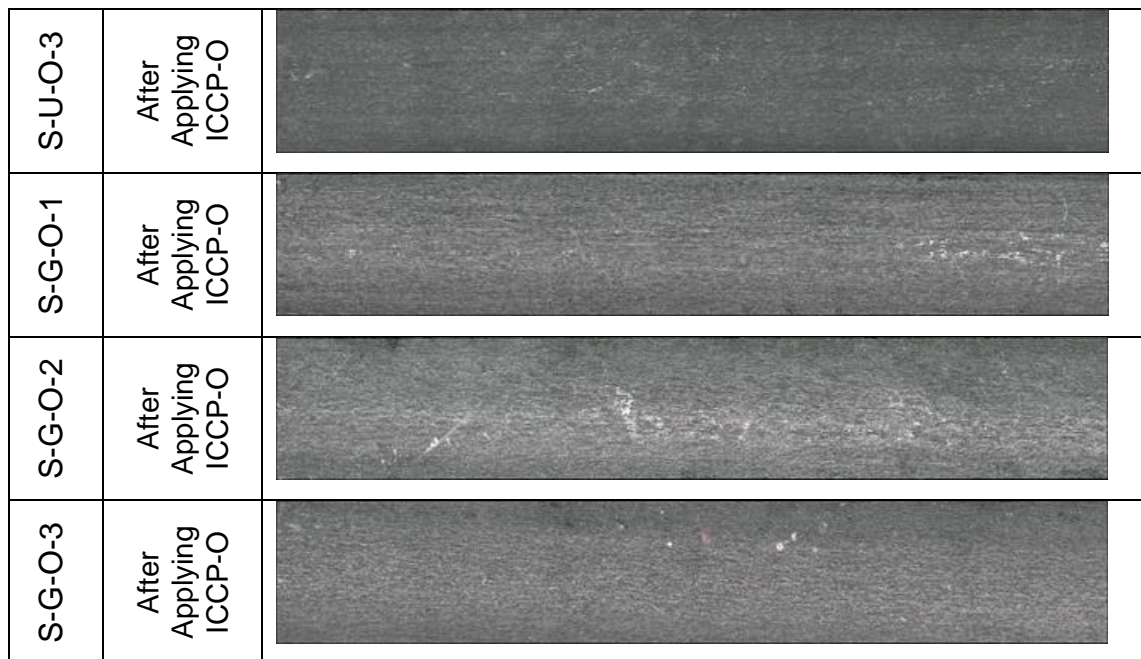


Figure 7.11 (cont.) Microstructure of ungalvanised & galvanized tendon surface

7.5.3 Potential

The rest potential E_{corr} vs SSC of the tendons when no cathodic protection was applied is shown in Table 7.3. Potential of the tendons ranged between -513mV to -670mV vs SSC.

Table 7.3 Potential before applying ICCP-O (Rest Potential)

<i>Batch</i>	<i>Test Code</i>	<i>Degree of Corrosion (Stage)</i>	<i>Actual Degree of Corrosion (%)</i>	<i>Rest Potential before applying ICCP-O (Ag/AgCl/KCl 0.5M) (-mV)</i>
3	M-U-L-X1-1	I	0.0	NA
	M-U-L-II-O-2	II	3.9	500
	M-U-L-III-O-3	III	6.5	580
	M-U-H-X1-1	I	0.0	NA
	M-U-H-II-O-2	II	2.0	470
	M-U-H-III-O-3	III	4.0	470
4	M-G-H-X1-1	I	0.0	NA
	M-G-H-II-O-2	II	3.4	450
	M-G-H-III-O-3	III	4.1	425
5	5-UG-O-1	N/A	N/A	525
	5-UG-O-2	N/A	N/A	525
	5-UG-O-3	N/A	N/A	525
	5-G-O-1	N/A	N/A	503
	5-G-O-2	N/A	N/A	503
	5-G-O-3	N/A	N/A	503

The aim was to generate more negative potentials than the recommended potential limit identified by various standards. The voltage was adjusted until the steel potential was somewhere between -850 to -1400mV. The voltage was then maintained constant at 60V for the specimens with mortar electrolyte and at 8V for unstressed specimens in the saline solution (3% NaCl) and the potentials " E_{on} " were recorded.

Overall, for pre-stressed ungalvanised and galvanised tendons, the required potential gradually becomes more negative throughout the period of the test. It was also noted that the required potential for tendons with Stage II corrosion was more negative than the potential for tendons with Stage III corrosion. It is shown in Figure 7.12 and Figure 7.13 for ungalvanised tendons with Low Level and High Level pre-stress respectively, that the potential shifts more negative up to about 100 days to reach the target steel potential, then becomes more stable giving a potential difference from the start in the range -4,000 to -15,000 mV for Low Level of pre-stress with Stage II and Stage III corrosion respectively. The potential in the ungalvanised tendons with High Level of pre-stress is more negative and ranged between 7,000 to 9,300mV for Stage II and Stage III corrosion respectively.

Figure 7.14 shows the required potential for the galvanised tendons. This required potential is more negative than the potential for ungalvanised tendons. This is because the zinc's natural potential is much more negative than the steel (Figure 7.15), in addition the mortar provides resistance as well. As can be seen in Figure 7.14, the start potential in the galvanised tendon is higher than the ungalvanised tendons due to the higher natural potential of the galvanising zinc. Figure 7.15 shows the different behaviour of the required potential for the unstressed tendon, which remain relatively stable over the test period. This is apparently due to the tendon not being exposed to both stress and corrosion, plus the electrolyte is a saline solution where the resistance is very low.

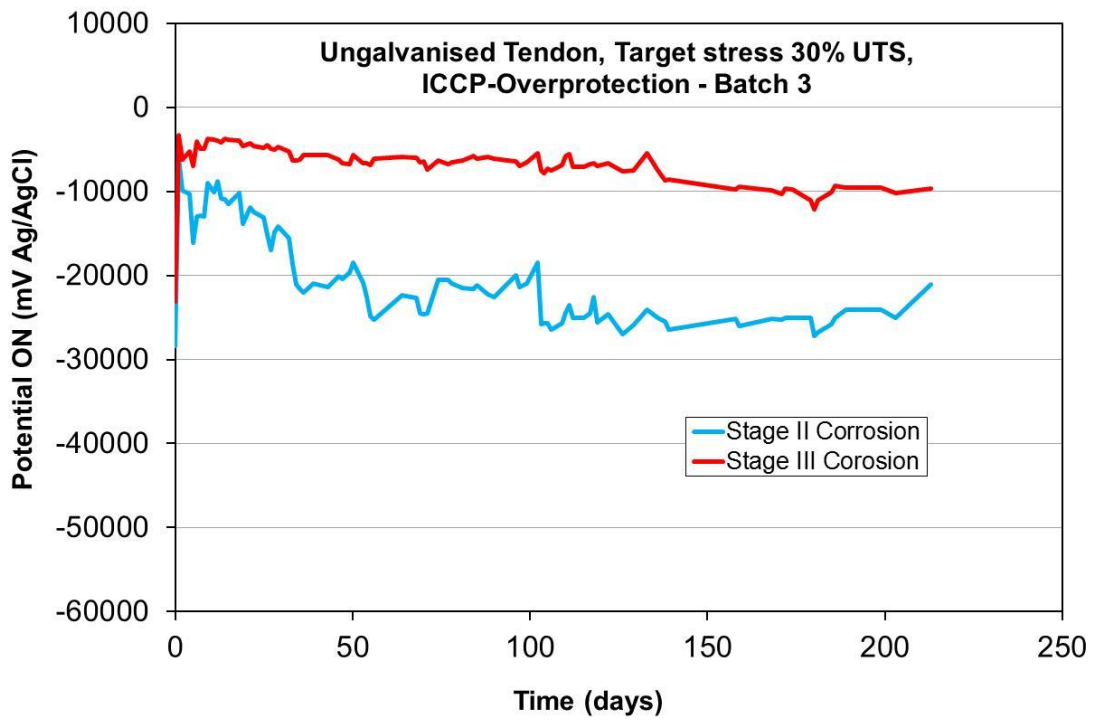


Figure 7.12 "ON" potential of ungalvanised tendon during application of ICCP-Overprotection, 30% UTS

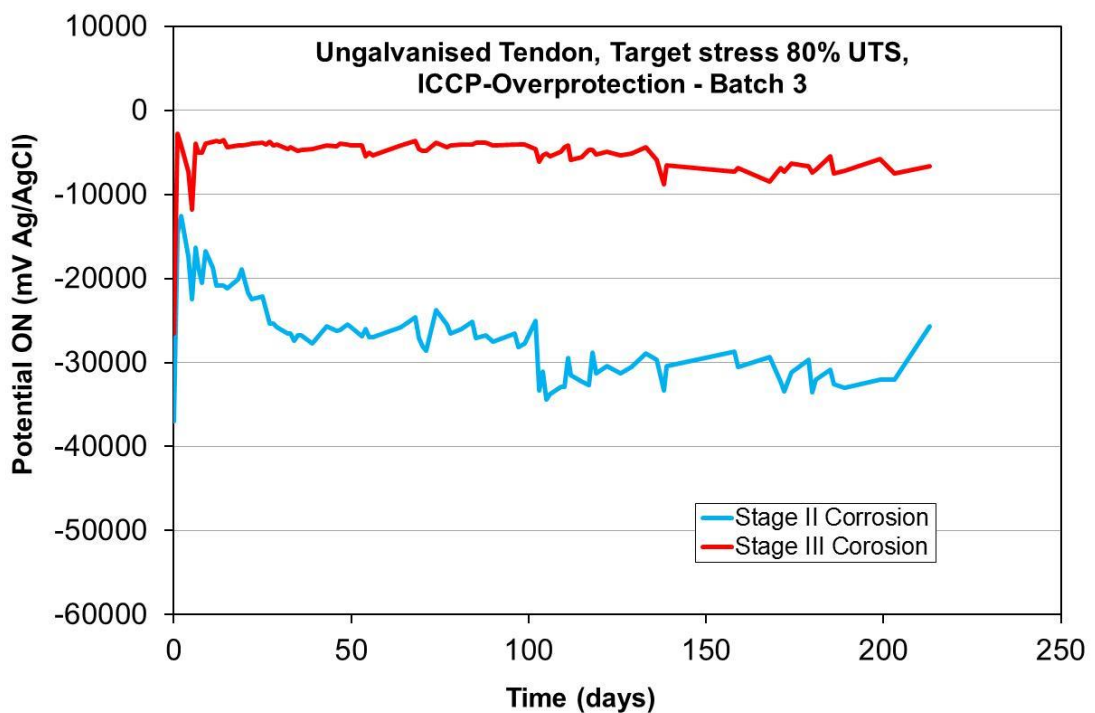


Figure 7.13 "ON" potential of ungalvanised tendon during application of ICCP-Overprotection, 80% UTS

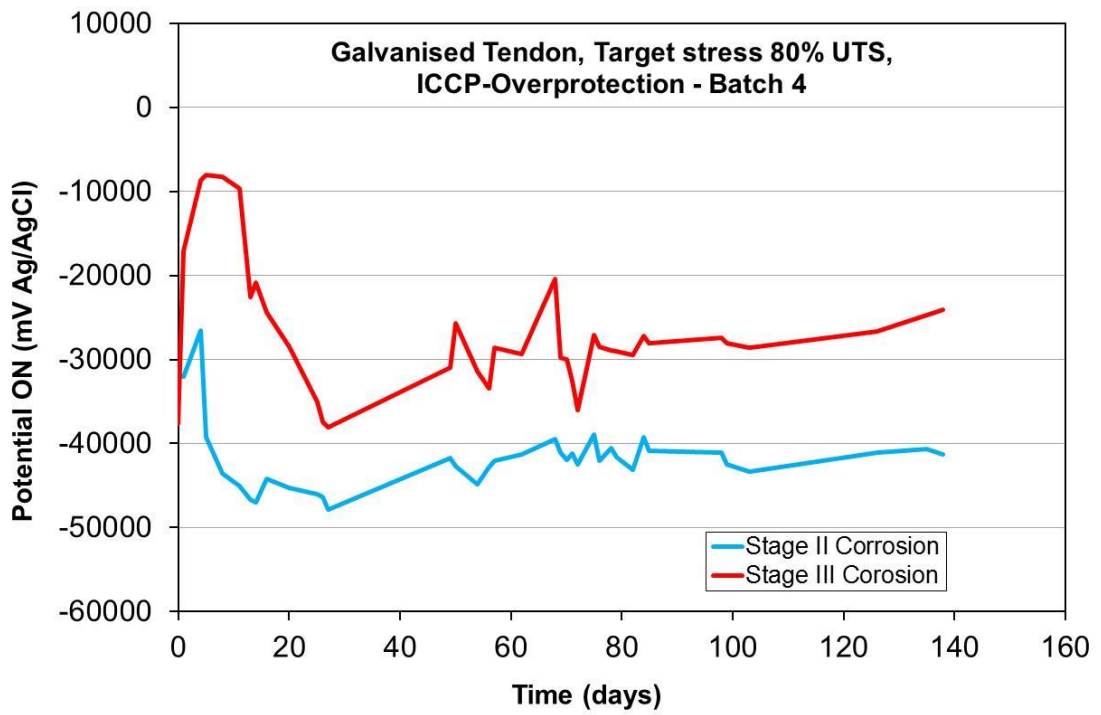


Figure 7.14 "ON" potential of galvanised tendon during application of ICCP-Overprotection, 80% UTS

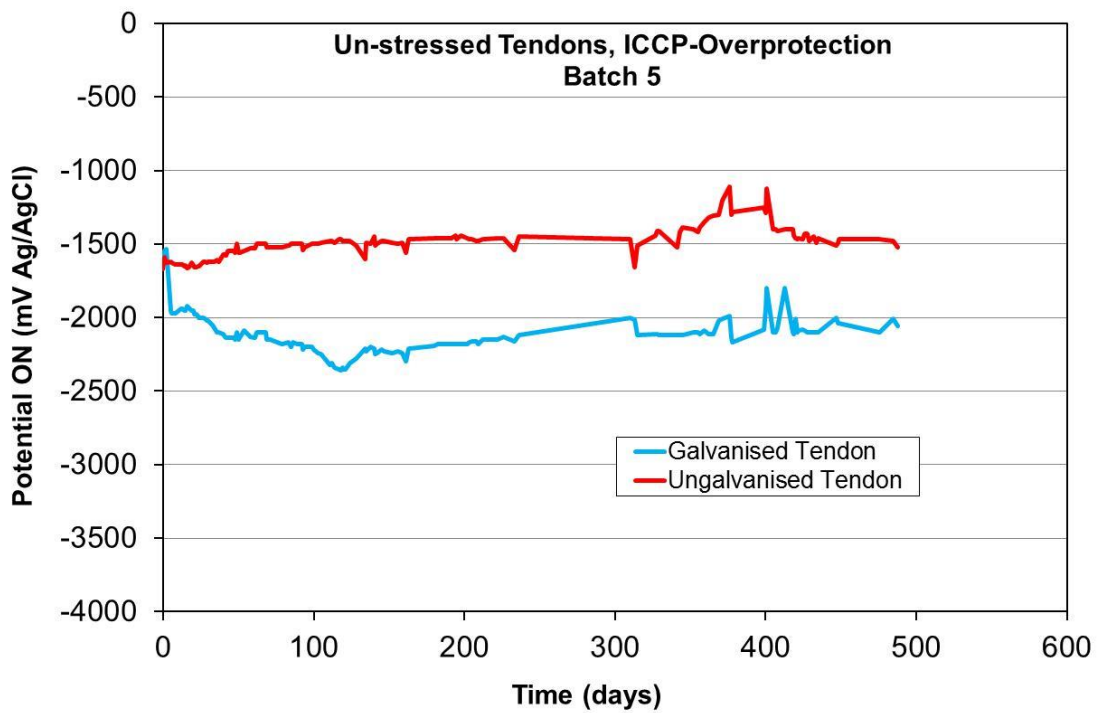


Figure 7.15 "ON" potential of un-stressed galvanised & ungalvanised tendons during application of ICCP-Overprotection

7.5.4 Monitoring of Condition and Performance

During the overall period of application of ICCP-O to the tendons, specimens had ICCP-O applied for up to 11,712 hours (488 days). The following monitoring was carried out and the results were recorded for each task:

- Monitoring and checking the wire connections of the ICCP system.
- Visually checking each DC power supply.
- Measuring of applied current (range 14 - 38 mA) and voltage (range 56 - 60mV).
- Recording potential using surface reference electrodes (Ag/AgCl/KCl 0.5M).
- Applying depolarisation (Instant-Off) for each reading and potential decay for 24 hours in two to three month intervals.
- Checking and taking reading of the applied service stress via strain gauges and a datalogger.
- Conducting close visual inspections of the surface of the mortar and recording any change.

7.5.4.1 Instant-Off (E_{off}) potential

The Instant-Off (E_{off}) value which provides the potential of the tendons during the application of ICCP were recorded. Figure 7.16 and Figure 7.17 show the potential of the ungalvanised tendons with Low Level and High Level of pre-stress respectively. Figure 7.18 shows the potential of the galvanised tendons with High Level of pre-stress, while Figure 7.19 shows the potential of unstressed galvanised and ungalvanised tendons.

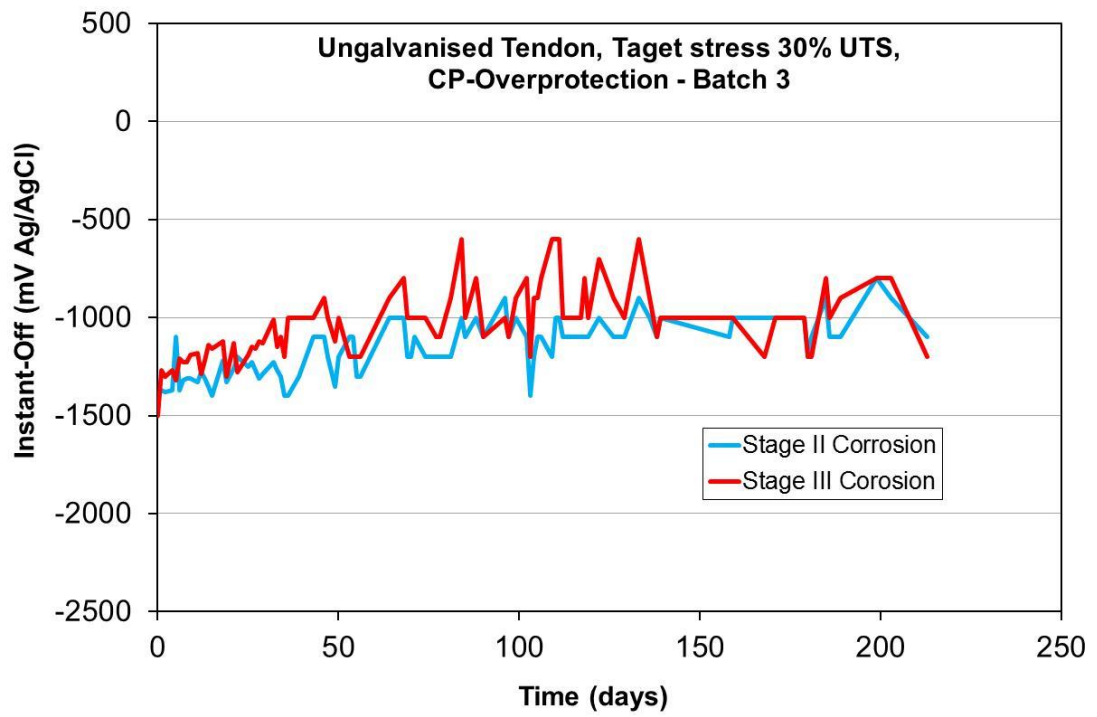


Figure 7.16 Instant-Off potential of ungalvanised tendons, 30% UTS

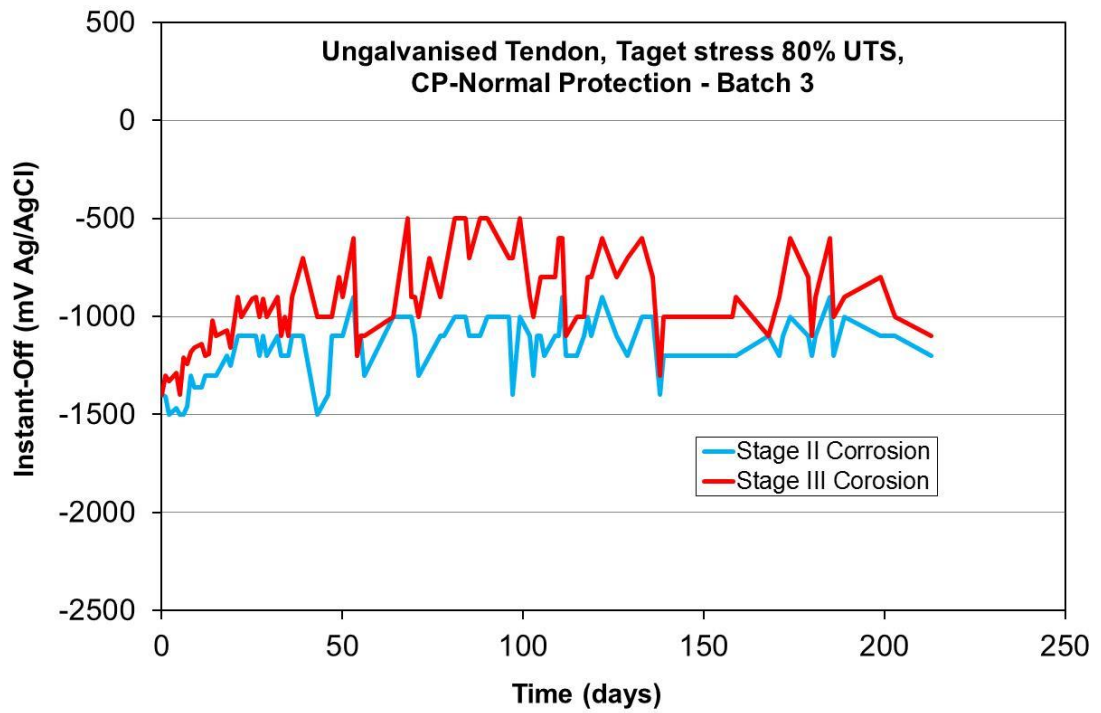


Figure 7.17 Instant-Off potential of ungalvanised tendons, 80% UTS

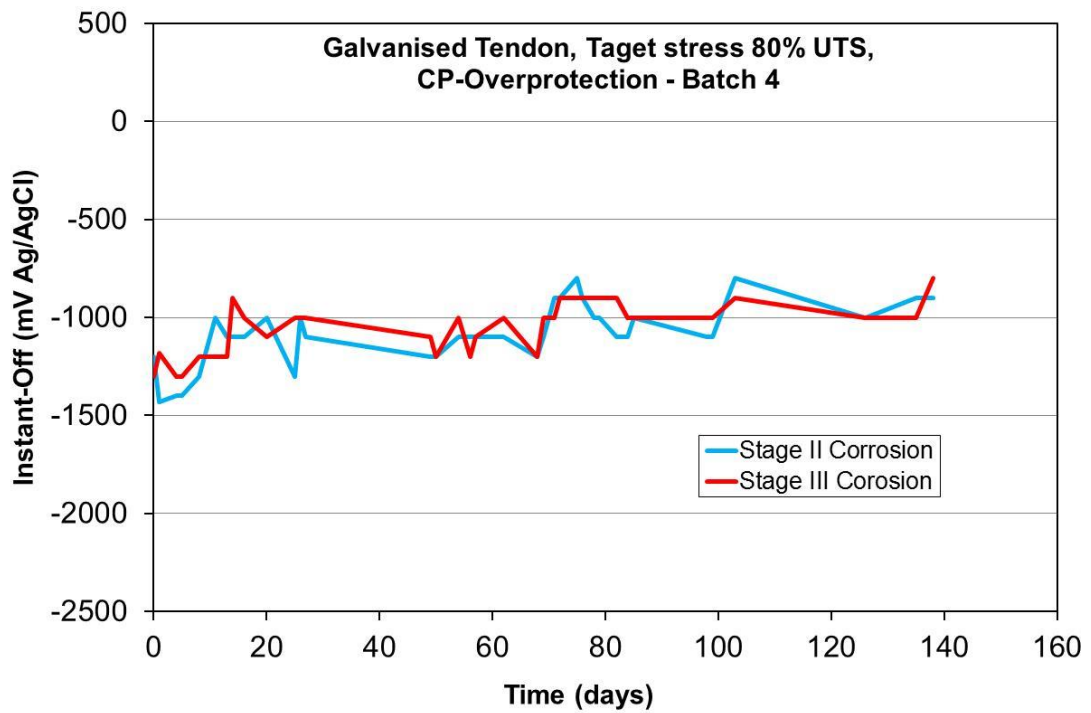


Figure 7.18 Instant-Off potential of galvanised tendons, 80% UTS

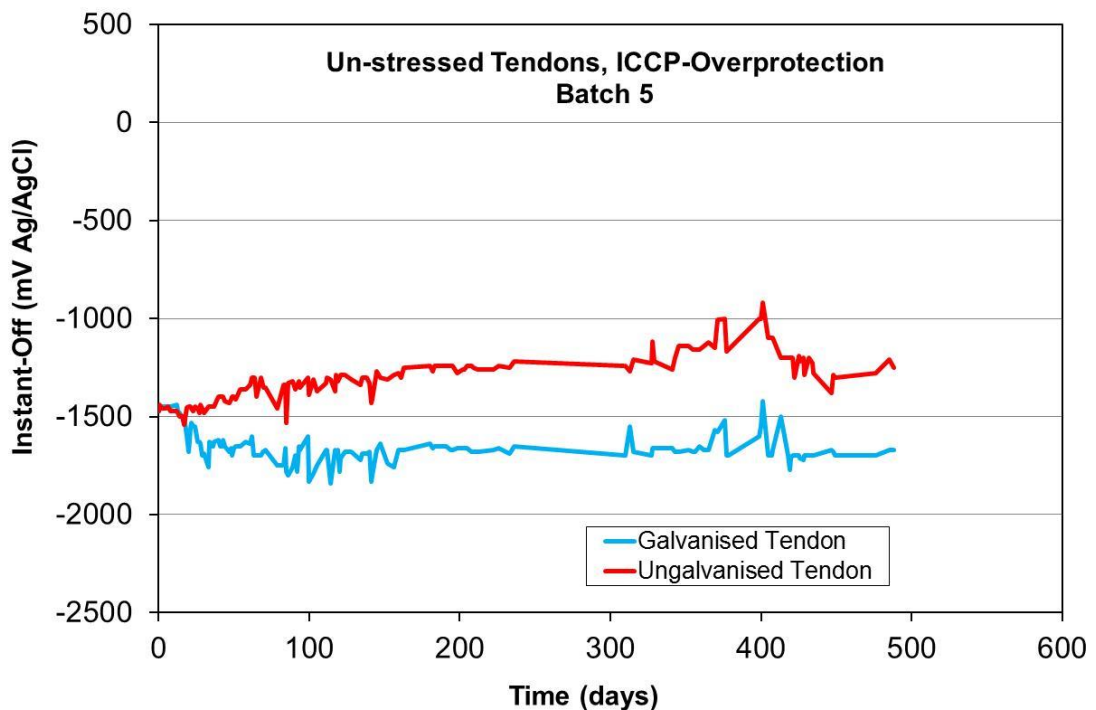


Figure 7.19 Instant-Off potential of Un-stressed galvanised tendons, 80% UTS

The ICCP-O was applied for a period of 5304 hrs (221 days) for the ungalvanised tendons with both Low Level and High Level of pre-stress, 3288 hrs (137 days) for the galvanised tendons with High Level of pre-stress and 11712 hrs (488 days) for unstressed galvanised tendons. The general trend of

the ungalvanised tendon potentials (Instant-Off) for both Low Level and High Level pre-stress with Stage I and II corrosion are similar. After 50 days the potential became less negative and relatively more steady as shown in Figure 7.16 and Figure 7.17. However, the potential for both levels of pre-stress is slightly less negative for the tendons with Stage II corrosion than for the potential of the tendons with Stage III corrosion. For galvanised tendons the potential remains steady for most of the test period as shown in Figure 7.18. For the unstressed tendons, although the potential of the galvanised tendon decreased negatively to about 30 days, the general trend for both types of tendon are the same. It was noticed that the potential of the unstressed galvanised tendon is more negative than ungalvanised tendon as shown in Figure 7.19.

7.5.4.2 Potential decay (-100mV)

Based on the CP criteria discussed in Section 6.4.3, the potential decay or the potential shift (ΔE_{off}) is the difference between instant-off (E_{off}) and the potential after 4 to 24 hours. This potential decay was monitored, recorded and as there was no significant variation with time, a representative example is plotted in Figure 7.20 for ungalvanised tendons, Figure 7.21 for galvanised tendons and Figure 7.22 for unstressed galvanised and ungalvanised tendons.

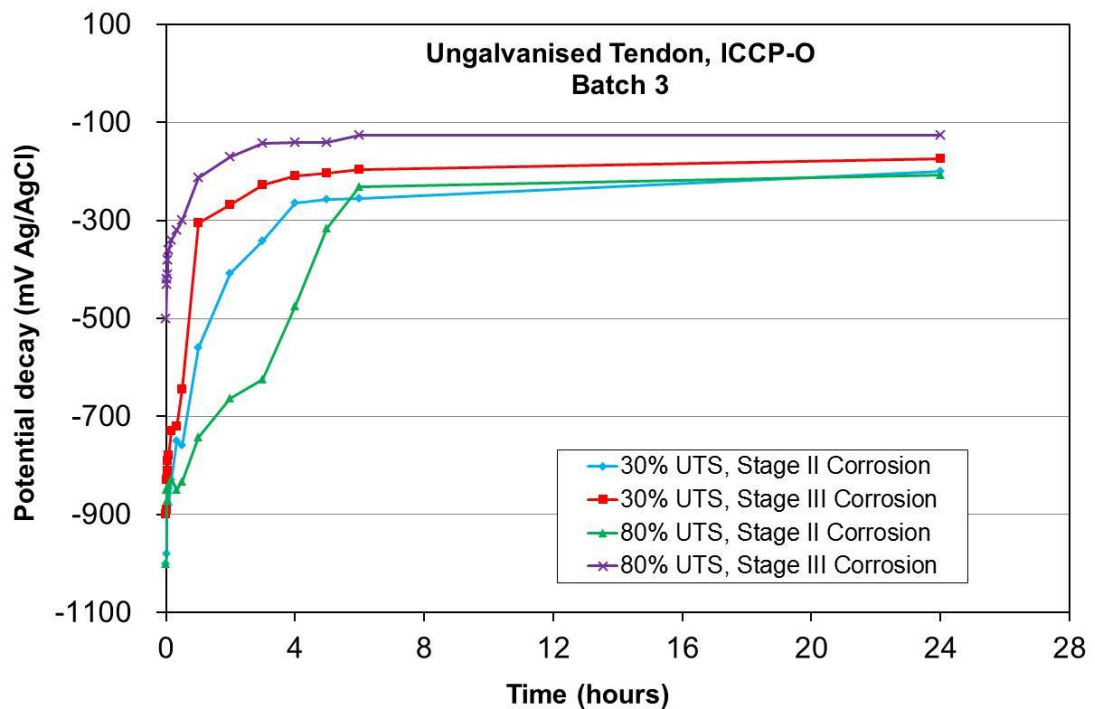


Figure 7.20 Potential decay of ungalvanised tendons

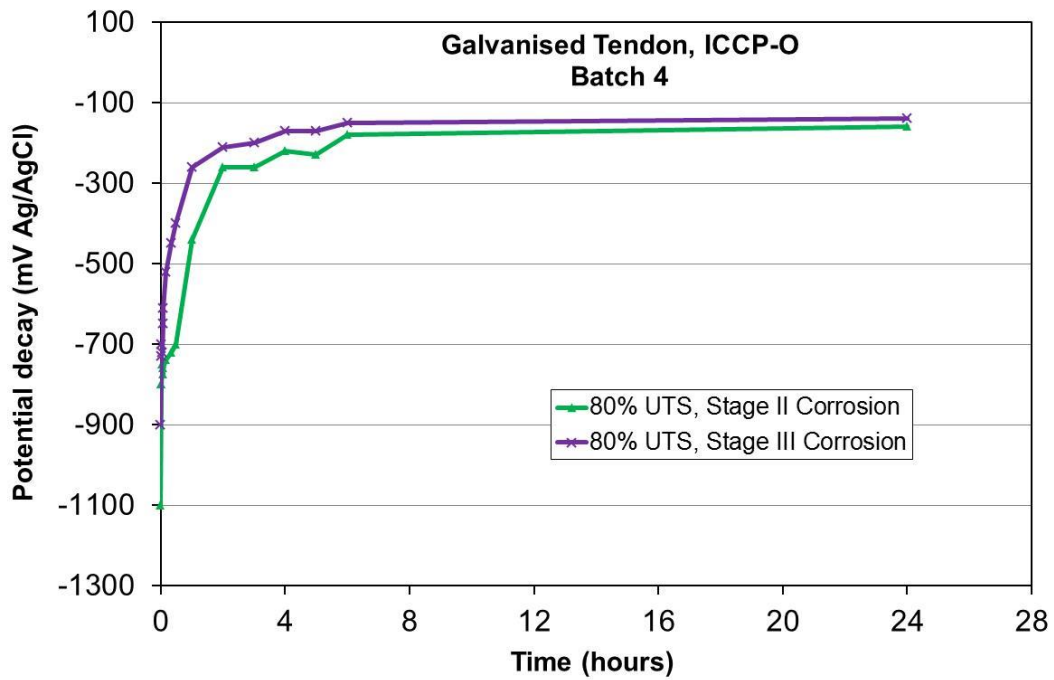


Figure 7.21 Potential decay of galvanised tendons

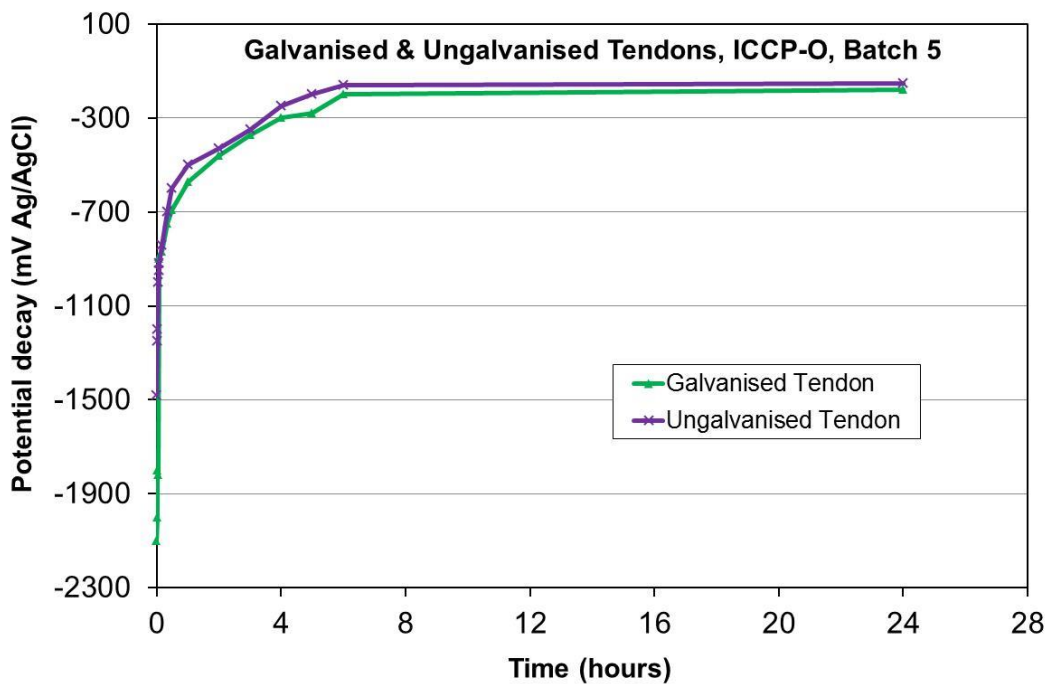


Figure 7.22 Potential decay of unstressed galvanised & ungalvanised tendons

The effectiveness of ICCP-O was confirmed by potential decay, the ICCP-O was interrupted for 24 hours before it was run again. Based on the data collected, the potential decays were greater than 100mV after 4 hours for all monitoring events (see Figure 7.20 to 7.22). According to the Concrete Society

Technical Report No.73, this demonstrates that an adequate level of protection has been achieved.

7.5.5 Effect of ICCP-O on the applied service stress

Chapter 5, Section 5.4.4 showed the setup of the vibrating wire strain gauges installed on each tendon to monitor changes in the applied service stress due to the application of ICCP-N. For this Chapter, the aim is to observe the behaviour of the tendons under the ICCP-O over a long period of time. To calculate the contraction in the timber moulds for specimens with High Level of pre-stress, DEMEC pins were placed on the top of the two-parallel longitudinal side faces (575x50x95 mm) at a gauge length 200mm as shown in Figure 7.23. The contraction in the timber mould was measured using a 200 mm strain gauge and the average strain determined (Table 7.4). This strain is taken into account in the calculation of the total loss of the service stress as shown in

Table 7.5 which shows the loss of service stress for ICCP-O throughout the monitoring period.

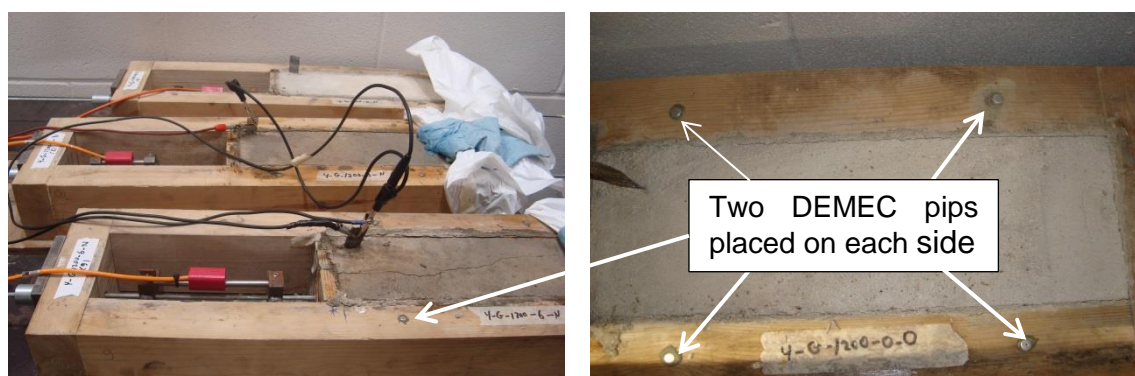


Figure 7.23 Monitoring contraction of timber moulds

Table 7.4 The average timber mould contraction (strain)

<i>Mould ID</i>	<i>Total microstrain</i>	
	<i>Face 1</i>	<i>Face 2</i>
Mould 1	268	474
Mould 2	339	229
Mould 3	229	134
Mould 4	363	434
Mould 5	435	55
Mould 6	577	861
Overall Average		367

Table 7.5 Effect of ICCP-O on the applied service stress

Batch	Test code	Degree of Corrosion (Stage)	Actual Degree of Corrosion (%)	ICCP Period (hrs)	Service Stress			
					Start (MPa)	Finish (MPa)	Loss (MPa)	(%)
3	M-U-L-X1-1	I	0.00	5304	340	329	12	2
	M-U-L-II-O-2	II	3.96	5304	362	338	24	7
	M-U-L-III-O-3	III	6.52	5304	404	377	27	7
	M-U-H-X1-1	I	0.00	5304	1192	1153	39	3
	M-U-H-II-O-2	II	2.06	5304	1305	989	316	24
	M-U-H-III-O-3	III	4.03	5304	991	863	128	13
4	M-G-H-X1-1	I	0.00	3288	875	842	33	4
	M-G-H-II-O-2	II	3.40	3288	832	718	114	14
	M-G-H-III-O-3	III	4.10	3288	783	694	89	11
5	5-UG-O-1	N/A	N/A	11712	N/A			
	5-UG-O-2	N/A	N/A	11712	N/A			
	5-UG-O-3	N/A	N/A	11712	N/A			
	5-G-O-1	N/A	N/A	11712	N/A			
	5-G-O-2	N/A	N/A	11712	N/A			
	5-G-O-3	N/A	N/A	11712	N/A			

Key: U-Ungalvanised, G-Galvanised, M-Mortar electrolyte, S-Solution electrolyte, H-High level of pre-stress (800-1200MPa), L-Low level of pre-stress (300-400MPa), I-Degree of corrosion Stage I (0-1%), II-Degree of corrosion Stage II (2-4%), III-Degree of corrosion Stage III (4-7%), N-Normal protection, O-Overprotection, X and X1-no corrosion and no ICCP, R-As-received samples, 1, 2, 3-Sample numbers.

These data are plotted in Figure 7.24, Figure 7.25 and Figure 7.26 for the ungalvanised tendons, Figure 7.27 for the galvanised tendon. For the ungalvanised tendons, and after 119 days from the completion of pre-stressing and accelerating corrosion, Figure 7.24 compares the gross loss in pre-stress of the tendons with the different stages of corrosion, Stage I (0-1%), II (2-4%) and III (4-7%) and with Low Level of pre-stress over the period of application of ICCP-O. The presented results is results presented after Overall, the gross loss trend of stress in the tendon with Stage I corrosion remains stable over the ICCP-O period with a total loss of just 2%, while the gross loss for tendons with Stages II and III degrees of corrosion have the same trend which started

relatively stable for the first 40 days or so and then dropped gradually for 10 days to reach 325 MPa. Following this, the gross loss in tendons remain roughly stable to the end of the monitoring period with a total stress loss of 7 % for the both tendons with Stage II and Stage III corrosion.

For the ungalvanised tendon with High Level of pre-stress, overall, the gross loss has gradually decreased over the total period for both tendons as shown in Figure 7.25. The total stress loss ranged between 3 to 24%, this loss is more than the loss in tendons with Low Level of pre-stress (Figure 7.26). However, the gross losses in stress for the tendon with Stage I degree of corrosion is less at 3% (39 MPa). For galvanised tendons with High Level of pre-stress, Figure 7.27 compares the gross loss in pre-stress with the different stages of corrosion Stages I, II and III over time. The results indicate that there is a loss in pre-stress of the galvanised tendons over the entire test period. These losses have the same trend, decreasing gradually over the whole test period and ranging between 4 to 14%. This percentage of pre-stress loss is less than the percentage loss for the ungalvanised pre-stressed tendons.

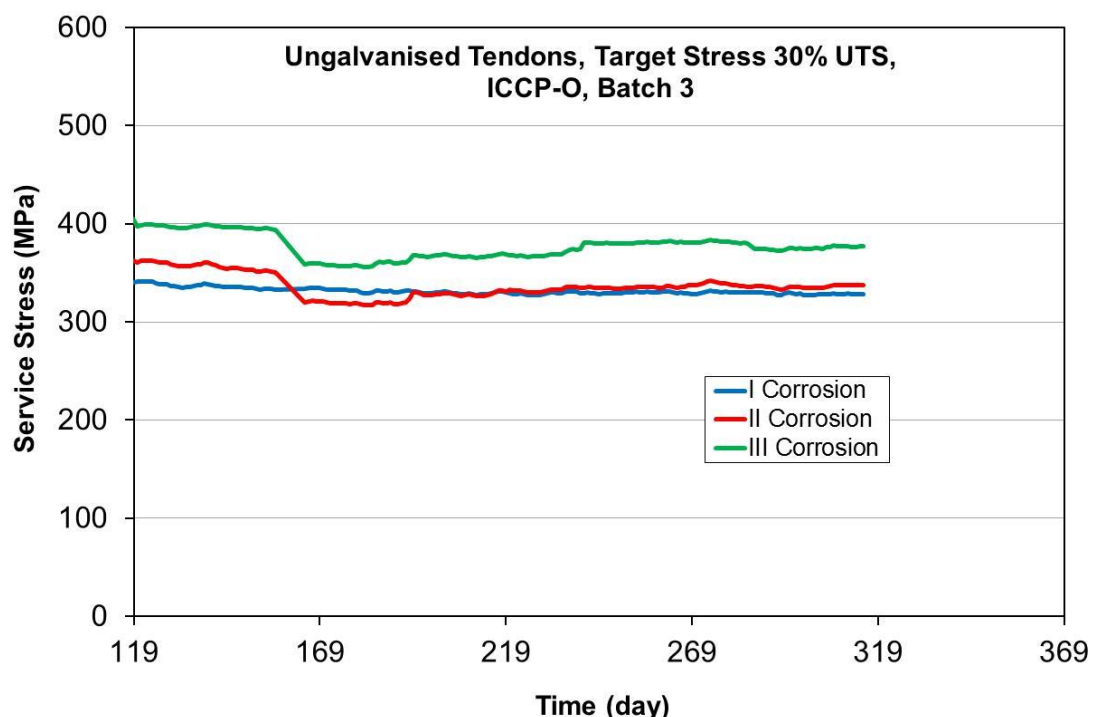


Figure 7.24 Service stress in pre-stressed ungalvanised tendon over the ICCP-O period, Batch 3 (30% UTS)

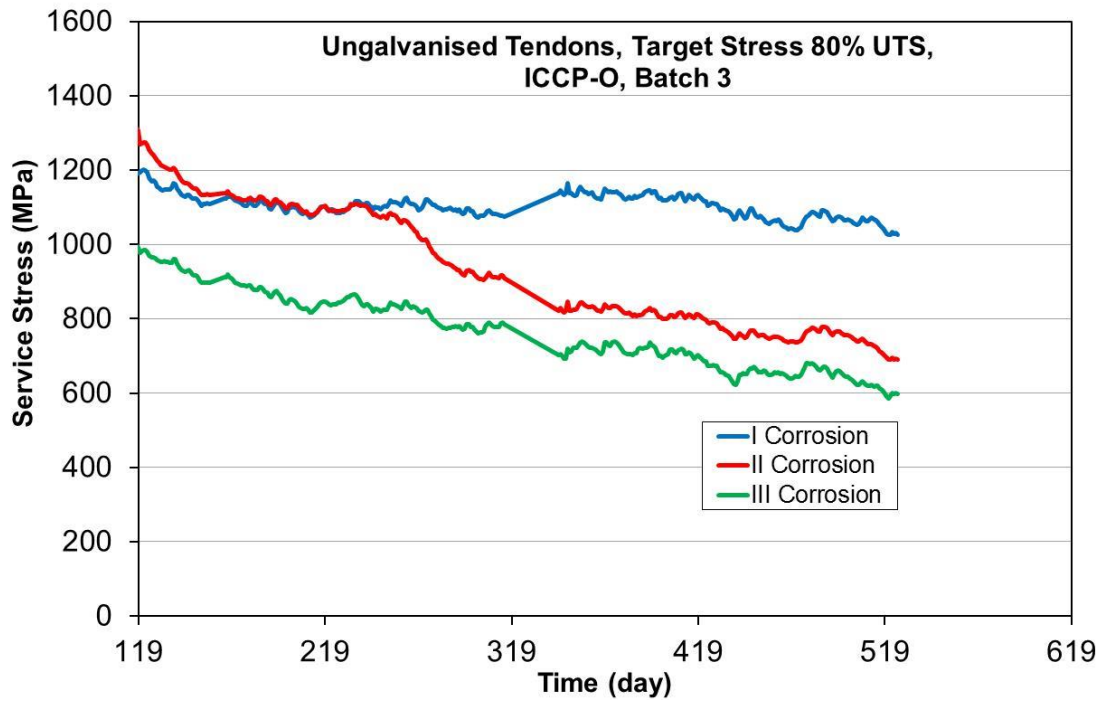


Figure 7.25 Service stress in pre-stressed ungalvanised tendon over the ICCP-O period, Batch 3 (80% UTS)

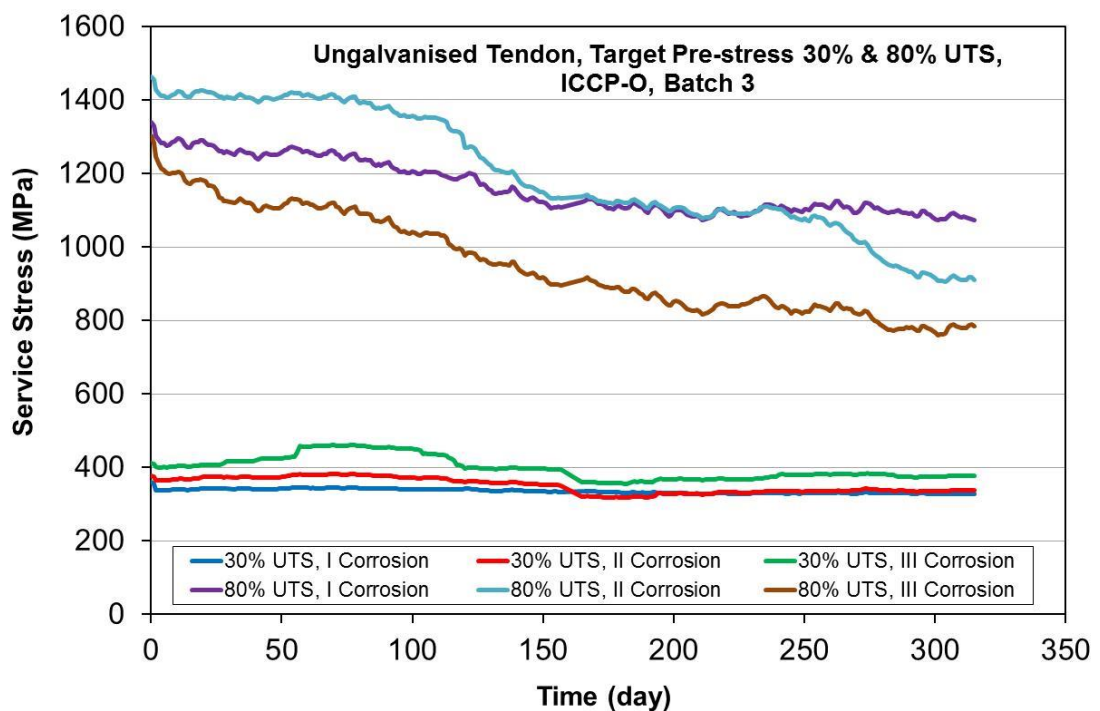


Figure 7.26 Service stress in pre-stressed ungalvanised tendons over the ICCP-O period, Batch 3 (30% & 80% UTS)

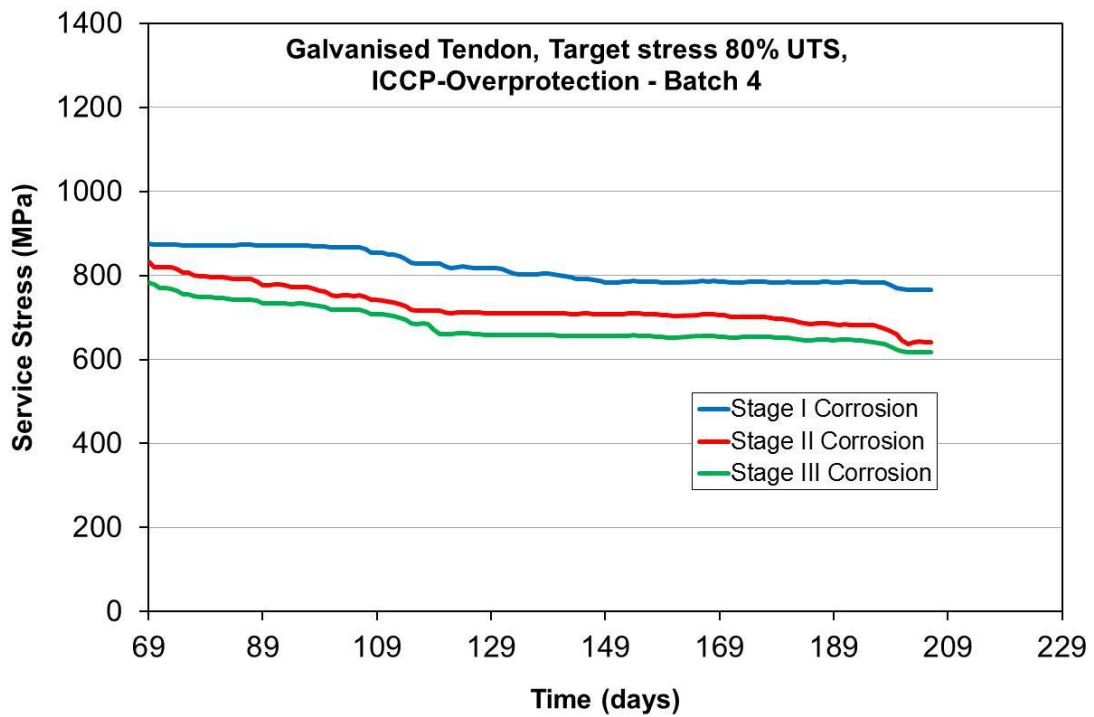


Figure 7.27 Service stress in pre-stressed galvanised tendons over the ICCP-O period, Batch 4 (80% UTS)

Table 7.6 shows a summary of the residual service stress in both the ungalvanised and galvanised tendons under the effect of ICCP-O and this is plotted in Figure 7.28. The results show that as the degree of corrosion increases from Stage I through to Stage II. There is a sharp increase in loss of pre-stress for the High Level pre-stressed ungalvanised tendon to 300 MPa, while in the galvanised tendon, in general, shows less loss than the ungalvanised tendon, the loss increasing to 50 MPa in Stage II of corrosion. This indicates that the galvanised tendon behaviour under ICCP-O application has a similar trend but lower magnitude compared to the ungalvanised tendon. Also it was noticed that the degree of corrosion has impacted in the loss of stress particularly in ungalvanised tendon. This means that the tendons subjected to higher degrees of corrosion will suffer higher losses which should be accounted for at the design stage as an additional loss.

Table 7.6 Residual service stress in the pre-corroded tendons under the effect of ICCP-O

Corrosion Stage	Residual Stress (MPa)			
	Target Service Stress 80% UTS			
	Ungalvanised		Galvanised	
	Start ICCP	Finish ICCP	Start ICCP	Finish ICCP
	(MPa)	(MPa)	(MPa)	(MPa)
I	1192	1153	875	842
II	1305	989	832	718
III	991	863	783	694

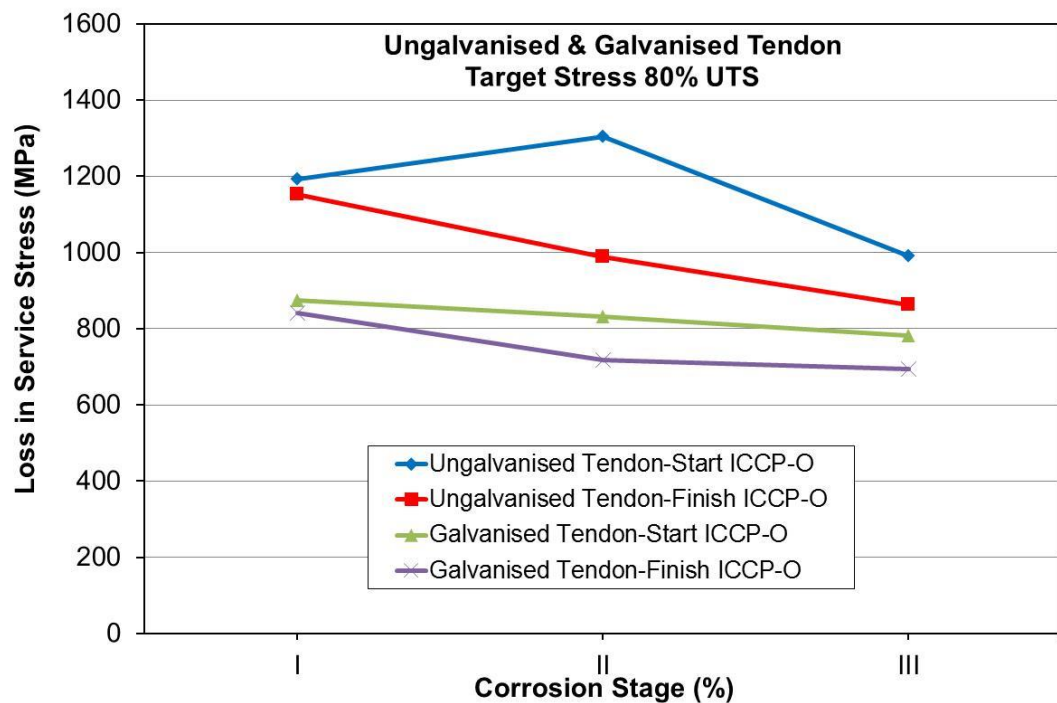


Figure 7.28 Relationship between stages of corrosion and the loss in service stress in the ungalvanised and galvanised tendons (80% UTS) over the ICCP-O period

7.5.6 Effect of ICCP-O on the mechanical properties of the tendon

Tensile tests were conducted for both the ungalvanised and galvanised tendons after ICCP-O was run for 3288 to 5304 hours and 11712 hours for the as-received samples. The chemical compositions of both ungalvanised and galvanised tendons are presented in Table 4.2. Samples of the as-received tendons were randomly selected and tested using a tensile test machine

(ESH600). The tensile tests were conducted in accordance to BS EN ISO 6892-1:2016 [63]. Subsequently, the mechanical properties of the tendons were determined. The mechanical properties of the as-received tendons are presented in Chapter 6, Table 6.6. These mechanical properties of the as-received tendons were used as a control to compare to those tendons exposed with pre-corrosion and ICCP-O application. Stress-Strain curves were plotted for three samples of each type of tendon as shown in Figure 6.25 for the ungalvanised as-received tendons and Figure 6.26 for the galvanised tendon. The mechanical properties of the as-received samples were also discussed in Chapter 6, Section 6.5.6. After completing the tensile tests, all mechanical properties were recorded and are listed as shown in

Table 7.7. Figure 7.29 shows the different location of the tendon failures and were named edge (close or at the grip), upper middle (between top grip and the middle), lower middle (between bottom edge and the middle) and middle (between the gauge length).

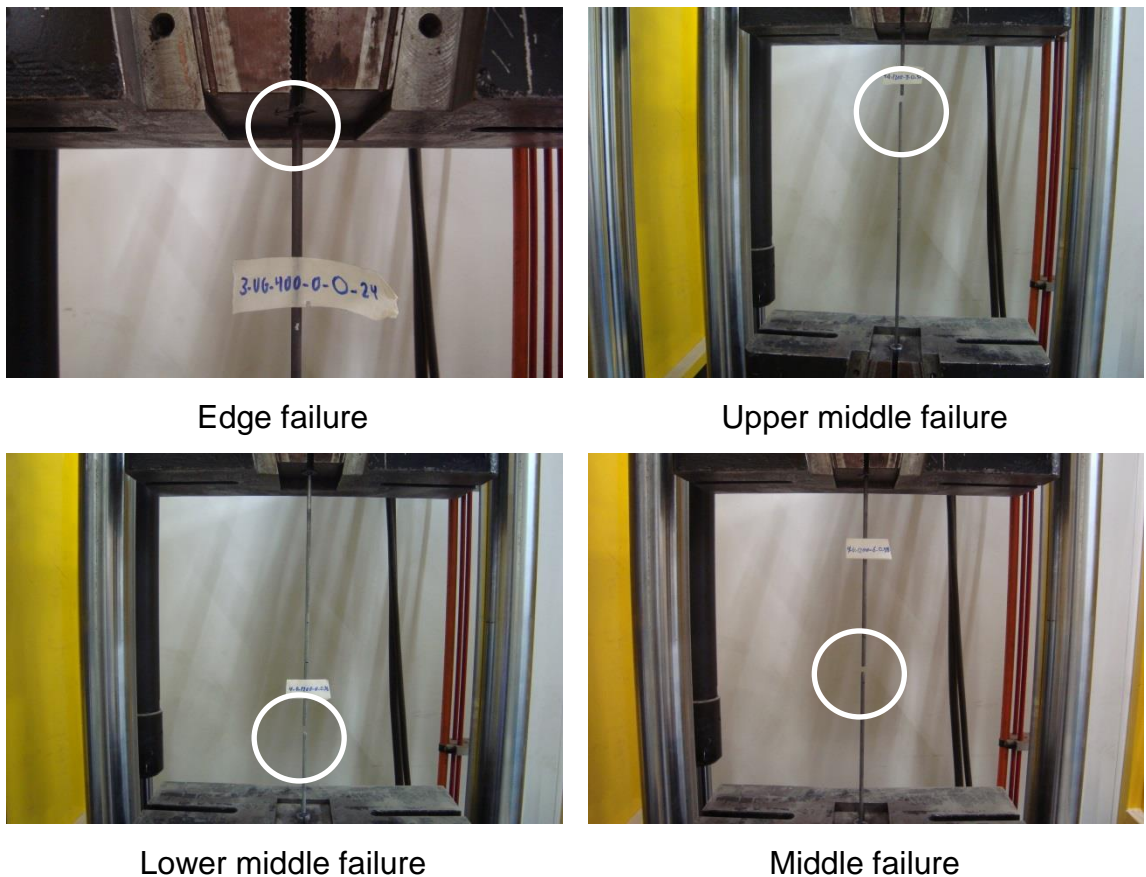


Figure 7.29 Location of failure

Table 7.7 Mechanical properties of the tendons after applying ICCP-O

Batch	Test Code	Degree of Corrosion (Stage)	Actual Degree of Corrosion	ICCP Period	Mean Original Diameter	Ultimate Tensile Strength UTS	Proof Strength	Elongation	Reduction in area	Young's Modulus	Toughness (x10 ⁶)	Failure Location
			(%)	(hours)	(mm)	(MPa)	(MPa)	(%)	(%)	(MPa)	J/m ³	
3	M-U-L-X1-1	I	0.8	5304	5.29	1956	1690	2.5	27	213	104	T-edge
	M-U-L-II-O-2	II	3.96	5304	5.34	1962	1720	3.5	24	214	80	L-middle
	M-U-L-III-O-3	III	6.52	5304	5.32	1850	1608	5.5	25	205	49	Middle
	M-U-H-X1-1	I	0.21	5304	5.36	1972	1750	5.0	21	210	90	B-edge
	M-U-H-II-O-2	II	2.06	5304	5.36	1998	1785	4.5	36	213	97	L-middle
	M-U-H-III-O-3	III	4.03	5304	5.36	1897	1736	3.4	29	210	50	U-middle
4	M-G-H-X1-1	I	0.36	3288	5.40	1926	1671	3.5	31	206	110	L-middle
	M-G-H-II-O-2	II	3.4	3288	5.39	1959	1733	3.0	23	215	72	T-middle
	M-G-H-III-O-3	III	4.1	3288	5.40	1857	1651	3.5	29	221	31	Middle
5	5-UG-O-1	N/A	N/A	11712	5.37	1976	1729	3.0	26	215	85	L-middle
	5-UG-O-2	N/A	N/A	11712	5.37	1968	1730	3.0	29	212	85	B-edge
	5-UG-O-3	N/A	N/A	11712	5.38	1997	1741	3.5	29	206	110	U-edge
	5-G-O-1	N/A	N/A	11712	5.33	1937	1665	2.0	19	213	85	L-middle
	5-G-O-2	N/A	N/A	11712	5.33	1966	1650	5.2	30	215	134	Middle
	5-G-O-3	N/A	N/A	11712	5.33	1975	1672.	5.0	31	216	130	L-middle

Key: U-Ungalvanised, G-Galvanised, M-Mortar electrolyte, S-Solution electrolyte, H-High level of pre-stress (800-1200MPa), L-Low level of pre-stress (300-400MPa), I-Degree of corrosion Stage I (0-1%), II-Degree of corrosion Stage II (2-4%), III-Degree of corrosion Stage III (4-7%), N-Normal protection, O-Overprotection, X and X1-no corrosion and no ICCP, R-As-received samples, 1, 2, 3-Sample numbers, T-edge - Top edge, B-edge - Bottom edge, U-middle - Upper middle, L-middle - Lower middle.

7.5.6.1 Summary and Discussion

Table 7.8 provides a summary of the mechanical properties of the investigated tendons in comparison to the mechanical properties of the as-received samples for Young's Modulus, 0.2% proof strength and ultimate tensile strength.

Table 7.9 compares the elongation, toughness and ductility for the same samples. As can be seen from the results, there is relatively little difference in the mechanical properties for either type of tendon. However, the elongation in both types of tendons (galvanised and ungalvanised) has been affected by ICCP-O. Further discussion is provided in the following sections.

Table 7.8 Summary of mechanical properties (Young's modulus, 0.2% Proof strength and Ultimate tensile strength)

Batch	Test Code	Young's Modulus			0.2% Proof Strength				Ultimate Tensile Strength (UTS)			
		Tendon	As-received Ave. *	Difference	Tendon	As-received Ave. *	Difference	Tendon	As-received Ave. *	Difference		
		(MPa)	(MPa)	(MPa) (%)	(MPa)	(MPa)	(MPa) (%)	(MPa)	(MPa)	(MPa) (%)		
3	M-U-L-X1-1	213	215	-2.5 -1.2	1690	1720	-30.0 -1.7	1956	1980	-23.4 -1.2		
	M-U-L-II-O-2	214	215	-1.4 -0.7	1720	1720	0.0 0.0	1963	1980	-17.0 -0.9		
	M-U-L-III-O-3	205	215	-10.7 -5.0	1608	1720	-112.0 -6.5	1850	1980	-129.5 -6.5		
	M-U-H-X1-1	210	215	-5.0 -2.3	1750	1720	30.0 1.7	1972	1980	-7.1 -0.4		
	M-U-H-II-O-2	213	215	-1.9 -0.9	1785	1720	65.0 3.8	1998	1980	18.9 1.0		
	M-U-H-III-O-3	210	215	-5.7 -2.7	1736	1720	16.0 0.9	1897	1980	-82.2 -4.2		
4	M-G-H-X1-1	206	210	-3.6 -1.7	1671	1676	-5.3 -0.3	1926	1945	-18.7 -1.0		
	M-G-H-II-O-2	215	210	5.0 2.4	1733	1676	56.8 3.4	1959	1945	14.6 0.8		
	M-G-H-III-O-3	221	210	11.9 5.7	1651	1676	-25.3 -1.5	1857	1945	-87.6 -4.5		
5	S-UG-O-1	215	215	-0.4 -0.2	1729	1720	9.0 0.5	1976	1980	-3.2 -0.2		
	S-UG-O-2	212	215	-3.7 -1.7	1730	1720	10.0 0.6	1968	1980	-11.6 -0.6		
	S-UG-O-3	206	215	-9.5 -4.4	1741	1720	21.0 1.2	1997	1980	17.6 0.9		
	S-G-O-1	213	210	3.5 1.7	1665	1676	-11.3 -0.7	1937	1945	-7.3 -0.4		
	S-G-O-2	215	210	5.1 2.5	1650	1676	-26.3 -1.6	1966	1945	21.2 1.1		
	S-G-O-3	216	21	6.4 3.1	1672	1676	-4.3 -0.3	1975	1945	30.4 1.6		

Key: U-Ungalvanised, G-Galvanised, M-Mortar electrolyte, S-Solution electrolyte, H-High level of pre-stress (800-1200MPa), L-Low level of pre-stress (300-400MPa), I-Degree of corrosion Stage I (0-1%), II-Degree of corrosion Stage II (2-4%), III-Degree of corrosion Stage III (4-7%), N-Normal protection, O-Overprotection, X and X1-no corrosion and no ICCP, R-As-received samples, 1, 2, 3-Sample numbers.

* Average of as-received tendons results.

Table 7.9 Summary of mechanical properties (Elongation, Toughness and Ductility)

Batch	Test Code	Elongation				Toughness				Ductility			
		Tendon	As-received Ave. *	Difference		Tendon	As-received Ave. *	Difference		Tendon	As-received Ave. *	Difference	
		(%)	(%)	(%)	(%)	(J/m ³) x10 ⁶	(J/m ³) x10 ⁶	(J/m ³) x10 ⁶	(%)	(%)	(%)	(%)	(%)
3	M-U-L-X1-1	2.5	2.6	-0.1	-3.3	104	98	6.5	6.7	4.90	4.7	0.2	3.7
	M-U-L-II-O-2	3.5	2.6	0.9	35.4	80	98	-17.5	-17.9	3.60	4.7	-1.1	-23.8
	M-U-L-III-O-3	5.5	2.6	2.9	112.8	49	98	-48.5	-49.7	2.10	4.7	-2.6	-55.6
	M-U-H-X1-1	5.0	2.6	2.4	93.5	90	98	-7.5	-7.7	4.20	4.7	-0.5	-11.1
	M-U-H-II-O-2	4.5	2.6	1.9	74.1	98	98	0.0	0.0	4.60	4.7	-0.1	-2.6
	M-U-H-III-O-3	3.4	2.6	0.8	31.6	50	98	-47.5	-48.7	2.25	4.7	-2.5	-52.4
4	M-G-H-X1-1	3.5	2.5	1.0	40.0	110	100	10.0	10.0	5.30	5.4	-0.1	-2.0
	M-G-H-II-O-2	3.0	2.5	0.5	20.0	73	100	-27.5	-27.5	3.40	5.4	-2.0	-37.2
	M-G-H-III-O-3	3.5	2.5	1.0	40.0	32	100	-68.5	-68.5	1.35	5.4	-4.1	-75.0
5	5-UG-O-1	3.0	2.6	0.4	16.1	85	98	-12.5	-12.8	3.90	4.7	-0.8	-17.5
	5-UG-O-2	3.0	2.6	0.4	16.1	85	98	-12.5	-12.8	4.00	4.7	-0.7	-15.3
	5-UG-O-3	3.5	2.6	0.9	35.4	110	98	12.5	12.8	5.25	4.7	0.5	11.1
	5-G-O-1	2.0	2.5	-0.5	-20.0	85	100	-15.0	-15.0	4.00	5.4	-1.4	-26.1
	5-G-O-2	5.21	2.5	2.7	108.4	134	100	33.8	33.8	6.40	5.4	1.0	18.3
	5-G-O-3	5.0	2.5	2.5	100.0	130	100	30.0	30.0	6.25	5.4	0.8	15.5

Key: U-Ungalvanised, G-Galvanised, M-Mortar electrolyte, S-Solution electrolyte, H-High level of pre-stress (800-1200MPa), L-Low level of pre-stress (300-400MPa), I-Degree of corrosion Stage I (0-1%), II-Degree of corrosion Stage II (2-4%), III-Degree of corrosion Stage III (4-7%), N-Normal protection, O-Overprotection, X and X1-no corrosion and no ICCP, R-As-received samples, 1, 2, 3-Sample numbers.

* Average of as-received tendons results

Stress-Strain Curve

Based on the results obtained and Figures 7.30 to 7.34, the stress–strain curve of both the ungalvanised and galvanised tendons show elasto-plastic deformation before fracture. This is typical of ductile steel failure. The stress-strain relationship for both types of tendons exposed to pre-corrosion and ICCP-O have shown no significant change on the mechanical properties in terms of modulus of elasticity, 0.2% proof strength and tensile strengths. However, there is a slight difference in behaviour in terms of elongation and toughness, where a decrease in ductility is evident. The calculations of Young's modulus, 0.2% proof strength, ultimate tensile strength, elongation and toughness based on the BS EN ISO 6892-1:2016 [90].

Young's Modulus

It can be seen in the figures relating to stress-strain (Figures 7.30 to 7.34) for the as-received and investigated tendons that the Young's modulus is similar. For Batch 3, Young's Modulus ranged between 210 to 214 MPa, for Batch 4 was ranged between 206 to 221 MPa, and for Batch 5 was ranged between 206 to 216 MPa. ICCP-O, therefore, has little or no effect in the elastic properties of these tendons.

0.2% Proof Strength

It can be seen in Figure 7.30, Figure 7.31, Figure 7.32 and Table 7.8 that there is a decrease in proof strength of the ungalvanised tendon with Low Level pre-stress and Stage II corrosion by 6.51% (112 MPa), while the proof strength with High Level pre-stress and Stage II corrosion increased slightly by 3.8 % (65 MPa) compared to the as-received sample. However, for the remainder of the ungalvanised tendons exposed to ICCP-O, there is no significant variation in the proof strength. Similarly, for the galvanised tendons there is a slight increase in proof strength with High Level pre-stress and Stage II corrosion by 3.4% (57 MPa) and there is no a significant variation in the proof strength for the rest of the galvanised tendons exposed to ICCP-O as shown in Figure 7.33. For the un-corroded samples, ICCP-O has no effect on the proof strength as shown in Figure 7.34.

Ultimate Tensile Strength

There is generally very little difference in the tensile strengths of the ungalvanised and galvanised tendons exposed to the ICCP-O. The tensile strength losses in both types of tendons did not exceed 1.2 % for all tendons except the ungalvanised specimens with Stage III corrosion with Low Level and High Level of pre-stress which decreased by 6.5 % (129 MPa) and 4.2% (82 MPa) as shown in Figure 7.31 and Figure 7.32 respectively. Similarly, for the galvanised tendon with Stage III degree of corrosion with High Level of pre-stress there is a decrease in ultimate strength. Its magnitude was similar to the ungalvanised tendon with the same degree of corrosion. Its loss was 4.5% (88 MPa).

Elongation

According to the results, the elongation ratio can be seen in Figures 7.30 to 7.34. These figures demonstrate that both the ungalvanised and galvanised tendons exposed to pre-corrosion show a variation in elongation behaviour under ICCP-O. The elongation ratios for ungalvanised tendons are in the range 2.5 to 4.5 % and compared to the as-received tendons, the range increased to between 35 to 74 %. However, for galvanised tendons, the elongation ratios are greater in the range 3.5 to 6.5 %. Comparing to the as-received galvanised tendons, the range increases to between 40 to 160 %. According to these results, the elongation capacity of the ungalvanised tendons is lower than the galvanised tendons.

Toughness

The principle of toughness was described in Chapter 6, Section 6.5.6.1. The toughness values of the ungalvanised and galvanised tendons used in the experimental studies are given in Table 7.9. According to these results, the toughness values of both types of tendons decreased after ICCP-O was applied in the range 6.5 to 48.5 x 10⁶ J/m³ for ungalvanised with Low Level and High Level of pre-stress and between 10 to 68.5 x 10⁶ J/m³ for galvanised with High Level of pre-stress compared with the toughness of as-received tendons.

This decrease was more noticeable with the specimens exposed to Stage III corrosion for both galvanised and ungalvanised. However, for Batch 5 where the tendon was exposed to ICCP-O alone, there is only slight variance in toughness. Therefore, toughness values decreased in both types of tendons

with slightly more in the galvanised tendon. This indicates that the behaviour of tendons with Stage III suffered from both degree of corrosion and the application of ICCP-O. In addition, the fracture changed from ductile behaviour to a mix of ductile and brittle fracture mode, as discussed in the next section.

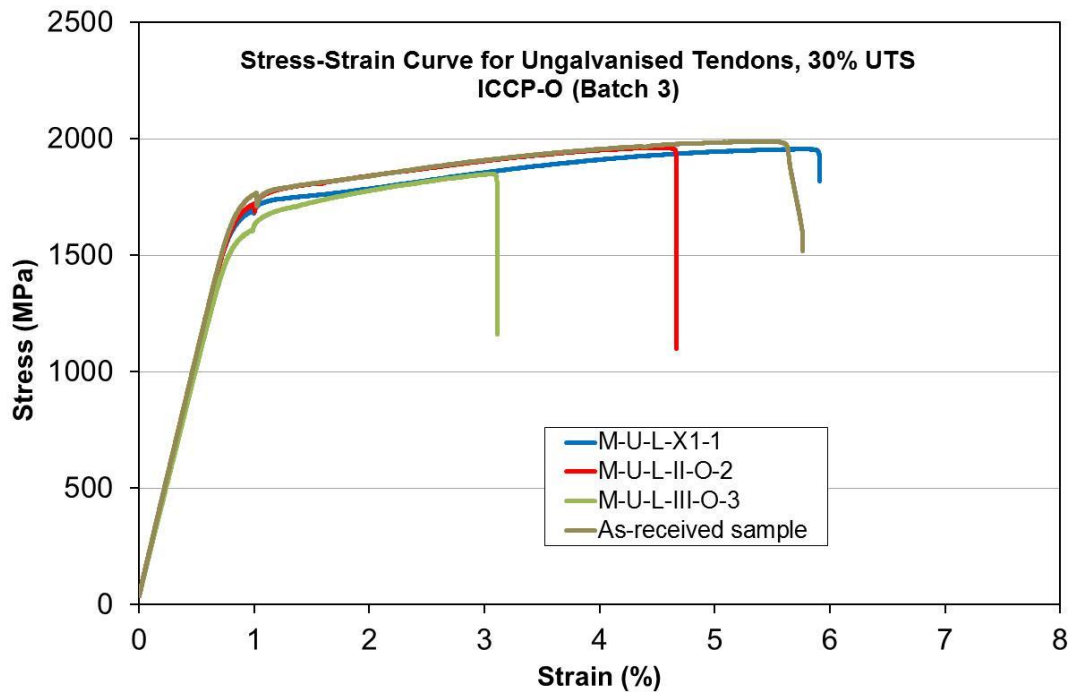


Figure 7.30 Stress-Strain curve for ungalvanised tendons, 30% UTS

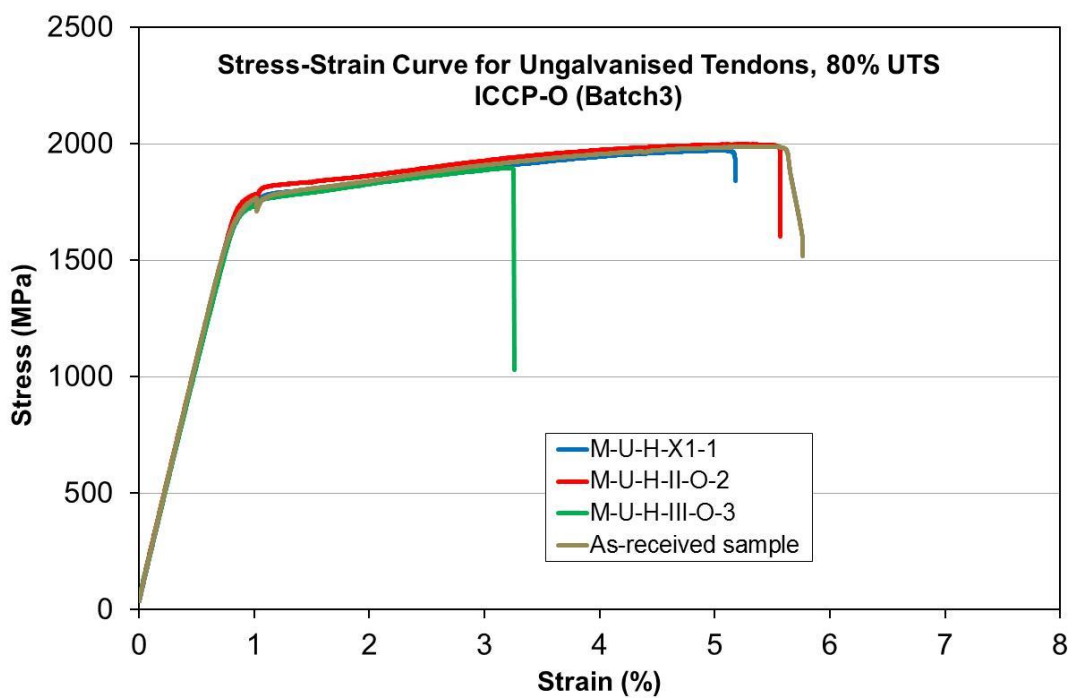


Figure 7.31 Stress-Strain curve for ungalvanised tendons, 80% UTS

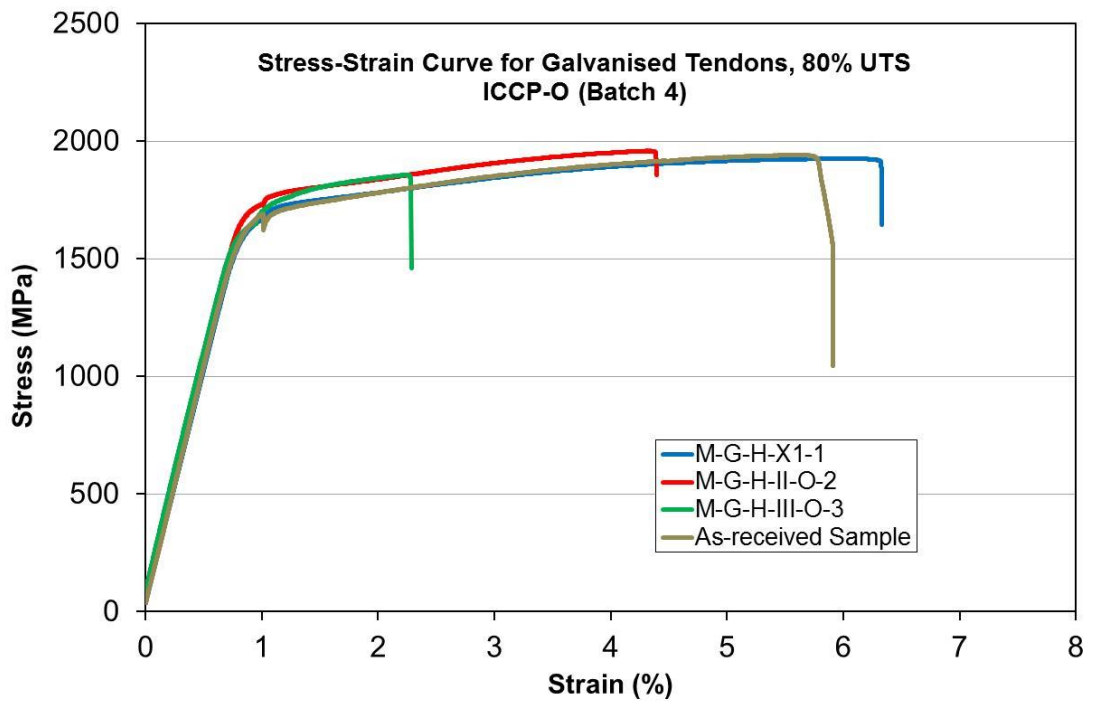


Figure 7.32 Stress-Strain curve for galvanised tendons, 80% UTS

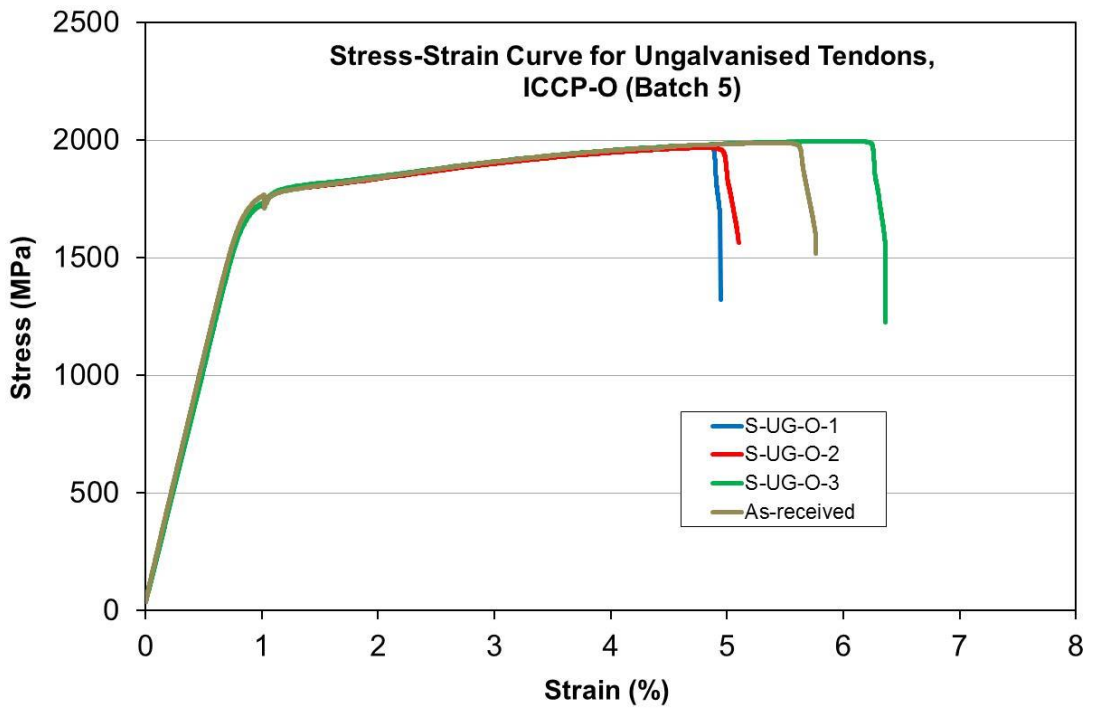


Figure 7.33 Stress-Strain curve for ungalvanised tendons (unstressed)

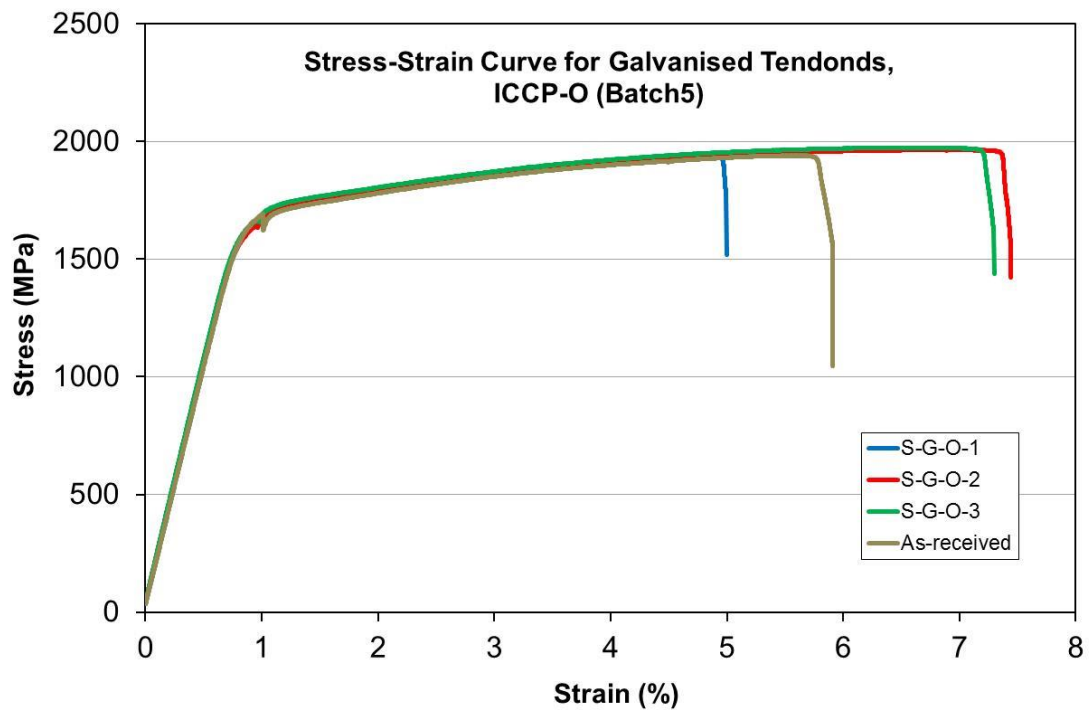


Figure 7.34 Stress-Strain curve for galvanised tendons (unstressed)

Ductility

Ductility definition and its measurement are given in Chapter 6, Section 6.5.6.1. Table 7.9 shows the values of ductility for different types of tendons with different level of stress and degree of corrosion. Comparison has been made with the ductility of the as-received samples to investigate the effect of ICCP-O. Results show that the ductility percentage decreased after applying the ICCP-O in the range 2.6 to 55.6 % for the ungalvanised tendons with Low Level and High Level pre-stress and between 2 to 75 % for galvanised tendons with High Level pre-stress. It was also observed that the decrease in ductility is greater for specimens exposed to Stage III corrosion for ungalvanised and galvanised tendons. For unstressed samples, the reduction in ductility is less than the pre-stressed with pre-corroded samples and the reduction was 7 % (average) for ungalvanised and no reduction in galvanised tendons. This indicates that the two types of tendons with Stage III corrosion suffered are affected by the degrees of corrosion and the application of ICCP-O. As the results of the application of ICCP-O in unstressed samples suggests, this reduction in ductility for both types of tendons was caused by more corrosion rather than the application of ICCP-O.

7.5.6.2 Fracture surface and hydrogen embrittlement

To assess the level of hydrogen in the tendons, some samples were investigated in Sheffield Assay Laboratory as shown in Table 7.10. The test involved slicing the tendons into smaller elements and analysing to establish if hydrogen was present. The test method used was inert gas fusion thermal conductivity detection. The downside to this test is that the quantity of surface area is very small, hence the likelihood of finding hydrogen is low even when present. In addition, the tests were carried out 7 days after the end of the ICCP application so any hydrogen present may have evaporated. The test results are given in Figure 7.10 and show that there is little difference between each sample indicating no significant difference between the samples. Further work is required to establish whether this approach can be used in practise to establish whether hydrogen is present in tendons exposed to ICCP.

Table 7.10 Hydrogen investigation

<i>Sample</i>	<i>Hydrogen</i> <i>(ppm)</i>	<i>Method</i>
As-received	19	Fusion & Thermal Conduct
Normal protection	20	Fusion & Thermal Conduct
Overprotection	18	Fusion & Thermal Conduct

To further investigate the effect of hydrogen in the tendons, embrittlement ratio (λ) was used in order to evaluate the susceptibility to hydrogen embrittlement as defined in Equation 6.4.

Overall, the embrittlement ratio at the UTS and 0.2% proof strength in Figures 7.36 to 7.38 have similar trends with relatively little difference between them. This indicates that hydrogen has no significant effect on ultimate strength and 0.2% proof strength under these conditions.

Necking

The embrittlement ratio at the necking stage was more for the ungalvanised tendon with the High Level of pre-stress and Stage I corrosion as shown in Figure 7.36 compared with the Low Level of pre-stress and galvanised tendon. This ratio reduces when the degree of corrosion increased to Stage II. This

behaviour is reversed for the galvanised tendon with a High Level of pre-stress as shown in Figure 7.37.

Breaking strength

The ratio of breaking strength for ungalvanised tendons is slightly more than in the galvanised tendons with a High Level of pre-stress, Figures 7.36 to 7.38.

Ductility

For ductility, the ratio for both types of tendons with a High Level of pre-stress increased as the degree of corrosion increased. This ratio in the galvanised tendon (Figure 7.37) is more than the ratio in ungalvanised tendons with a High Level of pre-stress (Figure 7.36). The reduction of ductility and the increase of the embrittlement ratio are increased as the degree of corrosion is increased. This indicates that there is an effect of hydrogen on ductility which is generated by ICCP-O and the increase of the degree of corrosion. The results from unstressed and uncorroded samples (Figure 7.38 and Figure 7.39) show less embrittlement ratio, this shows that the effect of degree of corrosion in this condition is more critical than the effect of hydrogen generated by ICCP-O.

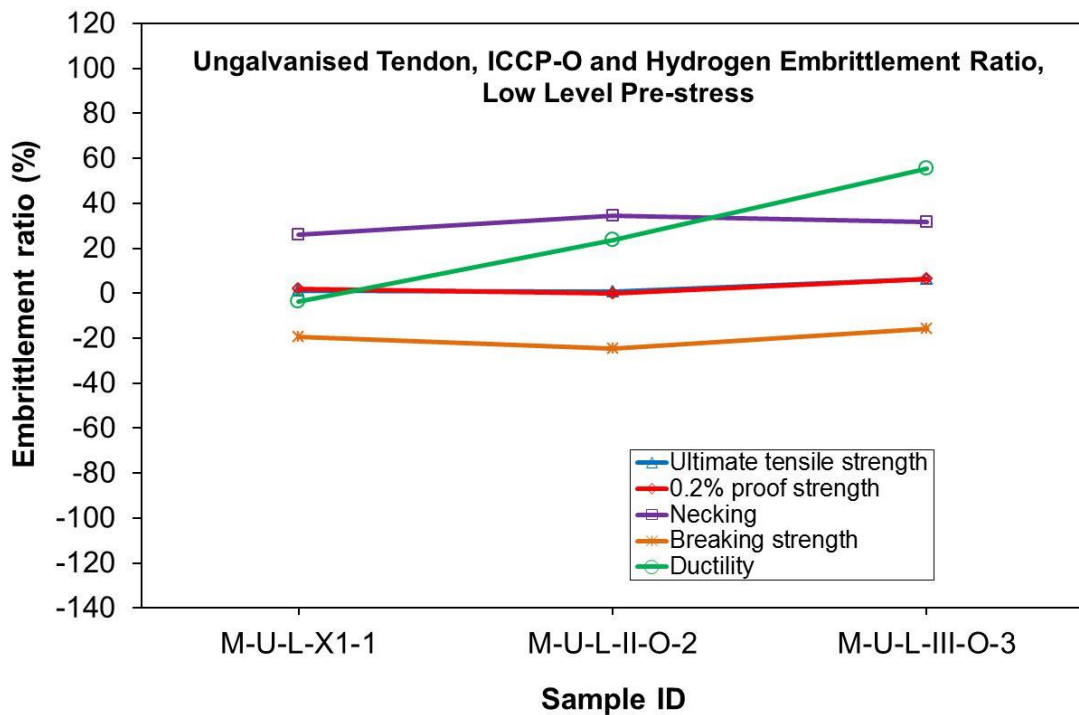


Figure 7.35 Relationship between overpotential and the hydrogen embrittlement ratio, Low Level pre-stress, ungalvanised tendon

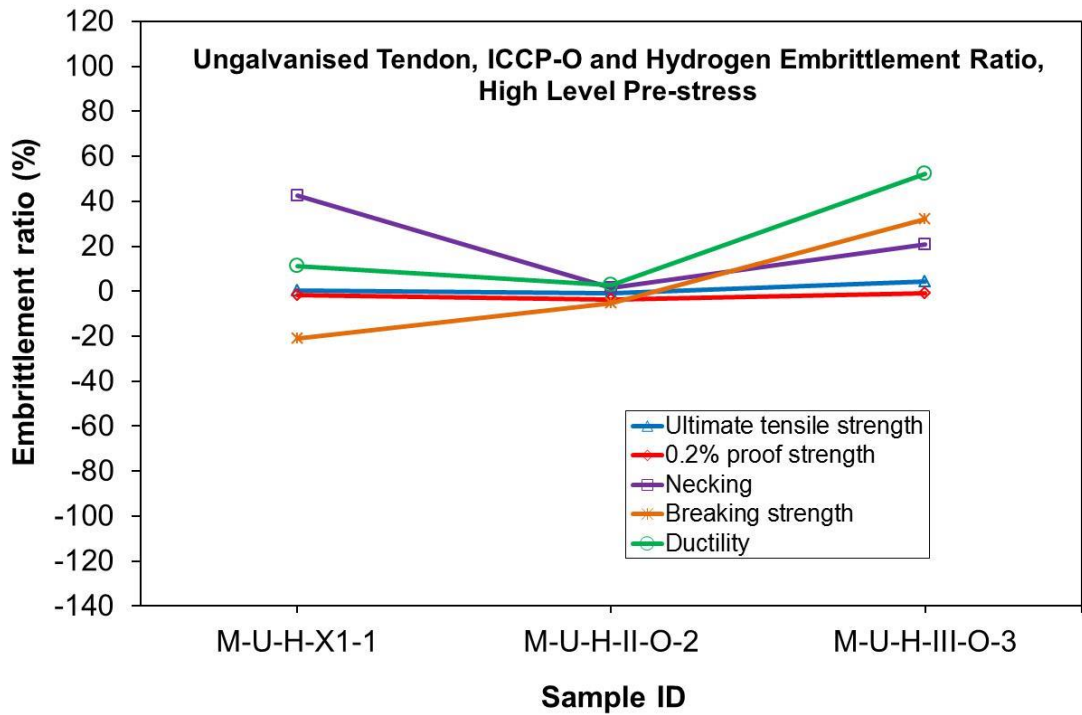


Figure 7.36 Relationship between over potential and the hydrogen embrittlement ratio, High Level pre-stress, ungalvanised tendon, 80% UTS

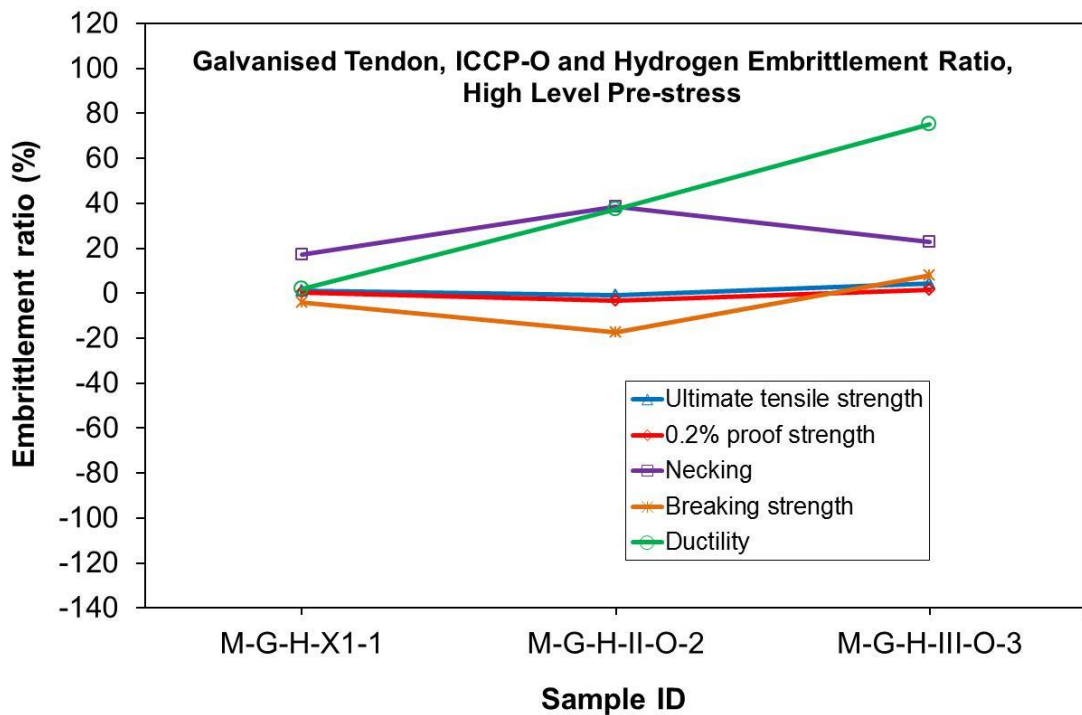


Figure 7.37 Relationship between over potential and the hydrogen embrittlement ratio, High Level pre-stress, galvanised tendon, 80% UTS

For both types of unstressed tendons, the embrittlement ratio for ultimate strength, 0.2% proof strength and breaking strength are very similar. The ratio

for necking in the galvanised tendons is more than in the ungalvanised tendons. For ductility, both types of tendons have the same behaviour.

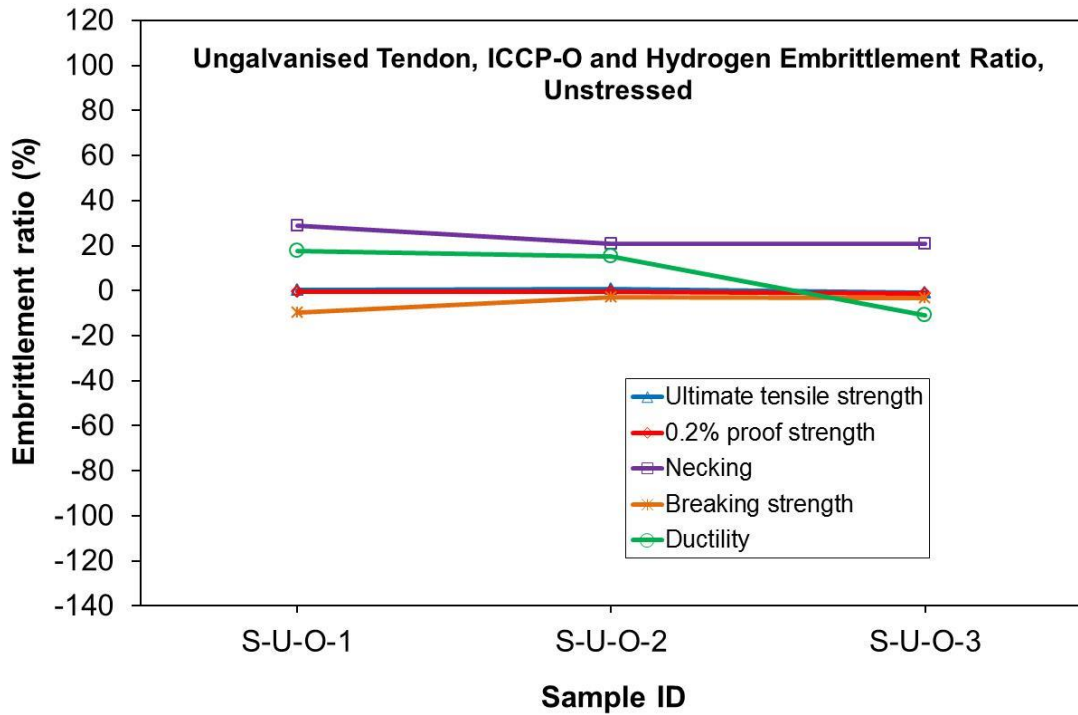


Figure 7.38 Relationship between overpotential and the hydrogen embrittlement ratio, ungalvanised tendon (Batch 5)

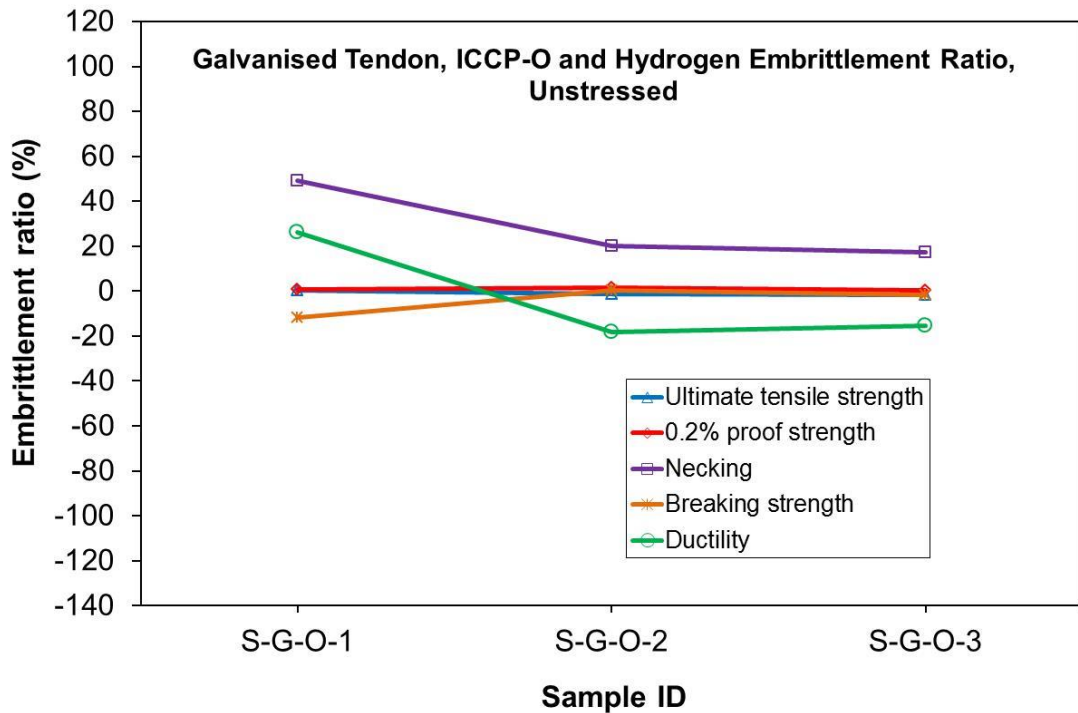


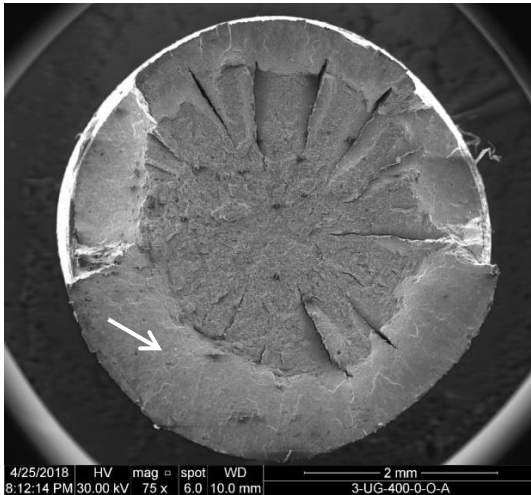
Figure 7.39 Relationship between overpotential and the hydrogen embrittlement ratio, galvanised tendon (Batch 5)

Employing the same approach adopted in Chapter 6 for ICCP-N, the SEM was used to examine the surface characteristics and evaluate the metallurgical information including the analysis of the phase microstructure. The principle of the SEM was described in Chapter 4, Section 4.11.1.1 and the settings, including magnifications of each type of images were listed in Table 4.6. To investigate the hydrogen effect on the fracture mode, the microstructure and the fracture mode was compared between a control tendon (as-received tendon with no pre-stress, corrosion or applied ICCP) and pre-stressed tendons exposed to the three stages of corrosion (I, II and III) and to ICCP-O in the range of potential -850 to -1300mV vs SSC. Hydrogen was introduced in these tendons through cathode charging by applying a current to the target potential. The fracture mode of the as-received samples was illustrated and discussed in Chapter 6, Figure 6.34 for the ungalvanised tendons and Figure 6.35 for the galvanised tendons.

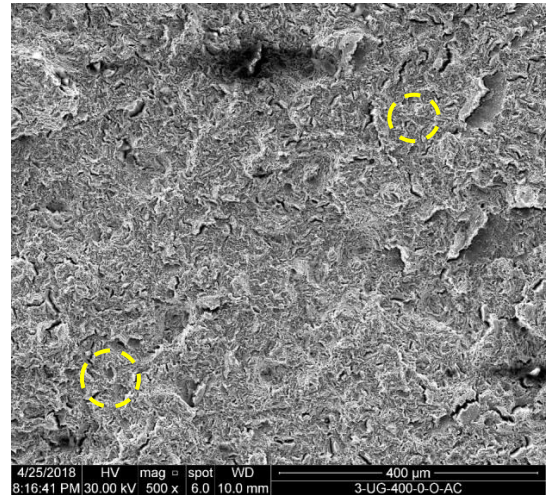
For Batch 3 ungalvanised with the Low Level of pre-stress as shown in Figure 7.40 to Figure 7.42, all test specimens at different corrosion stages had cup-cone characteristics and necking that were largely indistinguishable. For specimen M-U-L-I-O-1 (Figure 7.40 (b, c)), there are small dimples and a shear area presented in the whole fracture, indicating that the fracture is more ductile. The shear area can be seen more clearly in sample M-U-L-II-O-2 (Figure 7.41 (b)), although there are small dimples but also a brittle mechanism (identified by red dashed square), the fracture is less ductile or mix fracture mode. For specimen M-U-L-III-O-3 (Figure 7.42 (a-c)), the radial cracks appeared with the shear area and small dimples, demonstrating the fracture mechanism is a mixed fracture mode.



(a) M-U-L-I-O-1
Fracture



(b) The whole fracture surface

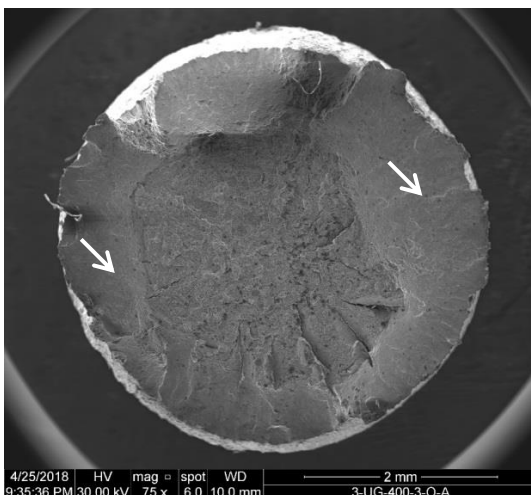


(c) The microstructure at centre

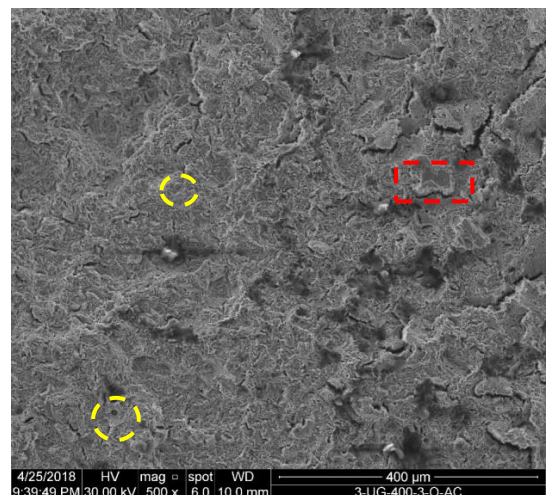
Figure 7.40 SEM images for ungalvanised tendon (M-U-L-I-O-1), 30% UTS



(a) M-U-L-II-O-2
Fracture



(b) The whole fracture surface

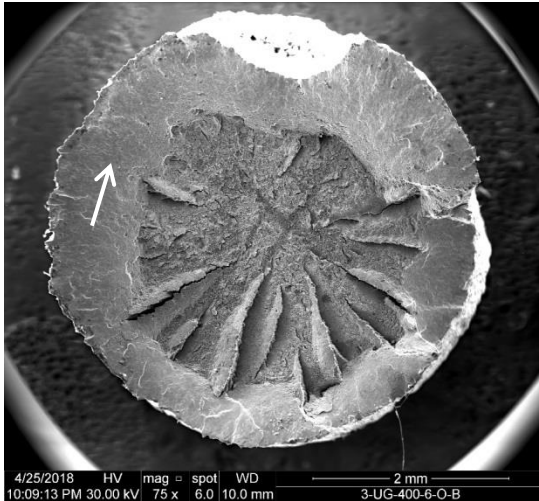


(c) The microstructure at the centre

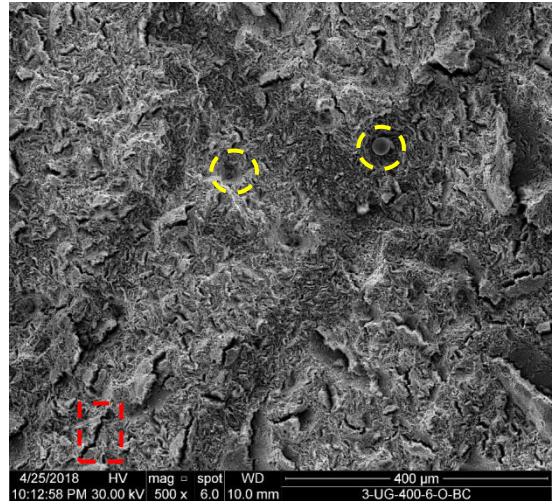
Figure 7.41 SEM images for ungalvanised tendon (M-U-L-II-O-2), 30% UTS



(a) M-U-L-III-O-3
Fracture



(b) The whole fracture surface

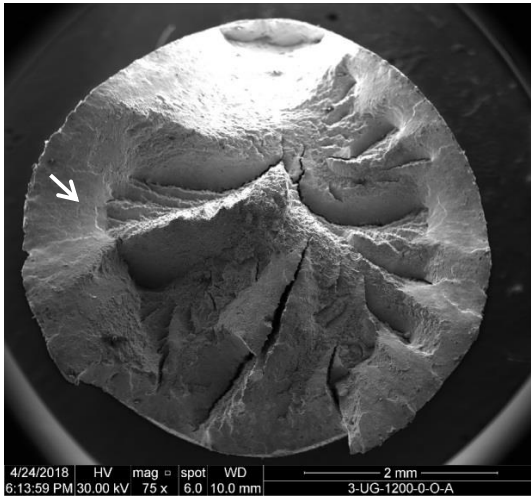


(c) The microstructure at the centre

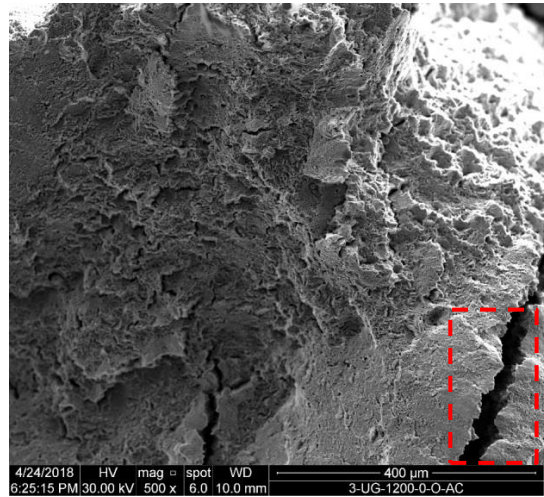
Figure 7.42 SEM images for ungalvanised tendon (M-U-L-III-O-3), 30% UTS Batch 3 ungalvanised with high level of pre-stress as shown in Figure 7.43 (a-c) to Figure 7.45 (a-c), all teste samples at different corrosion stages showed characteristic cup-cone failure and necking. The shear area and radial fractures were evident in the whole fractures, while dimples were not presented in the microstructures. This indicates the mechanism of the fracture is less ductile and more brittle.



(a) M-U-H-I-O-1
Fracture



(b) The whole fracture surface

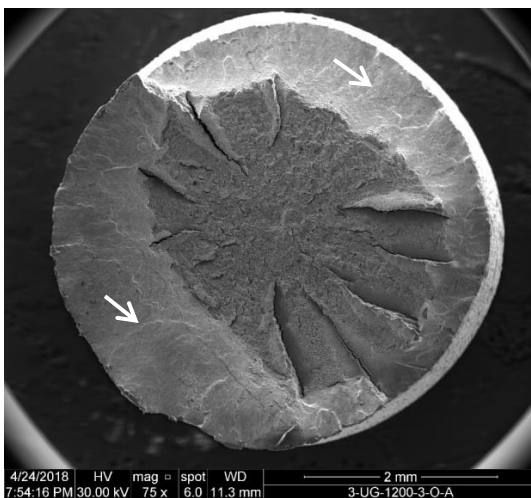


(c) The microstructure at the centre

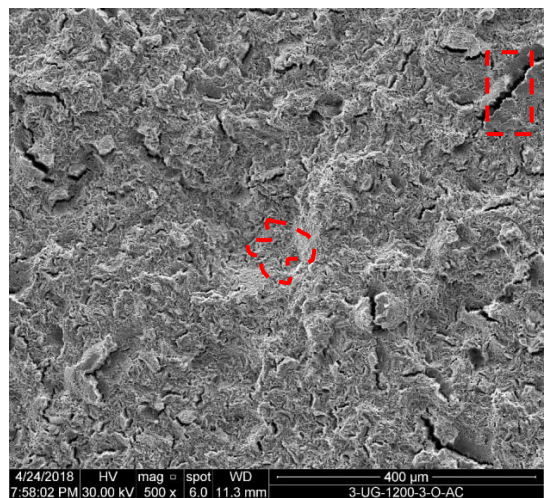
Figure 7.43 SEM images for ungalvanised tendon (M-U-H-I-O-1), 80% UTS



(a) M-U-H-II-O-2
Fracture



(b) The whole fracture surface

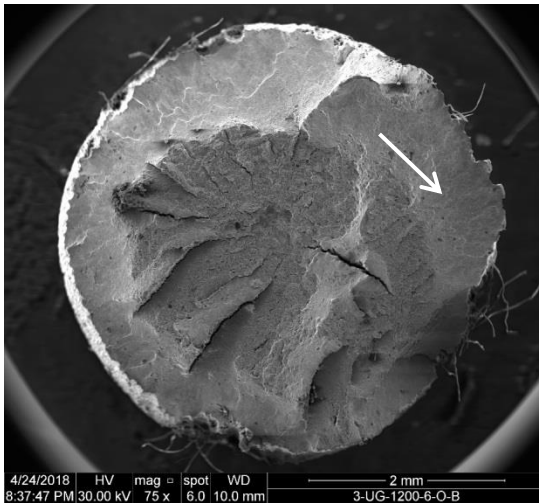


(c) The microstructure at the centre

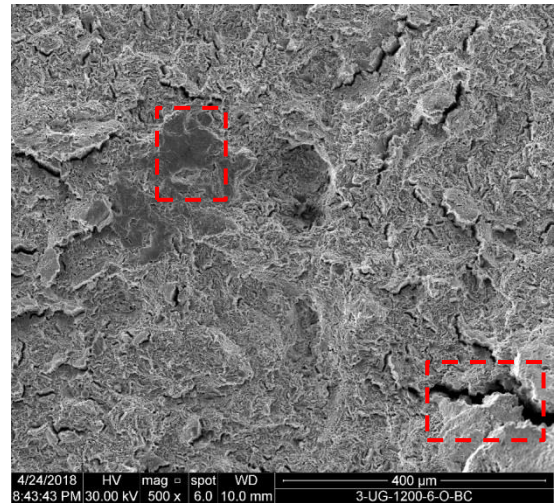
Figure 7.44 SEM images for ungalvanised tendon (M-U-H-II-O-2), 80% UTS



(a) M-U-H-III-O-3
Fracture



(b) The whole fracture surface



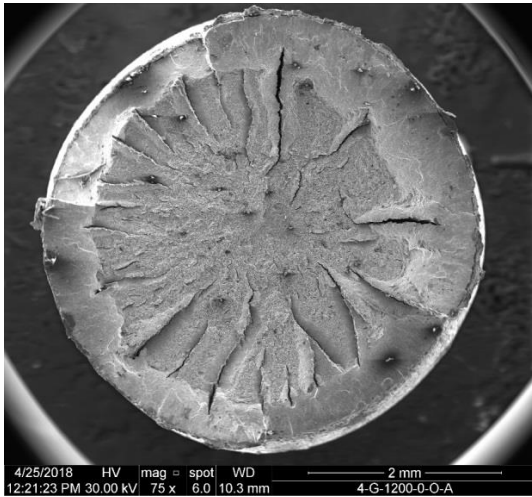
(c) The microstructure at the centre

Figure 7.45 SEM images for ungalvanised tendon (M-U-H-III-O-3), 80% UTS

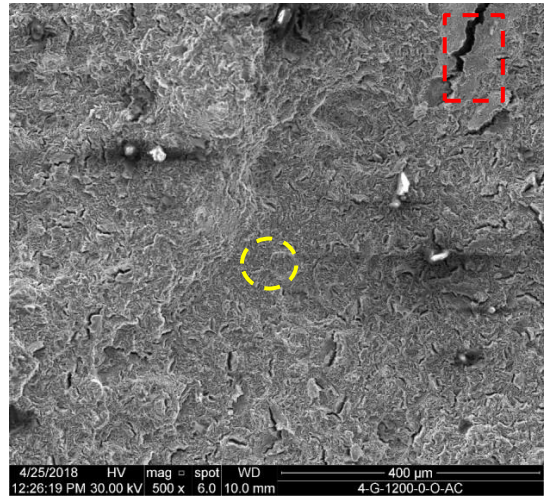
For Batch 4 galvanised with High Level of pre-stress as shown in Figure 7.46 to Figure 7.48, all test samples at different corrosion stages showed cup-cone characteristics and necking. For specimen M-G-H-I-O-1 (Figure 6.46 (b, c)), there is a small shear area in the whole fracture surface and there are very small dimples evident in the microstructure, indicating a mix of ductile (identified by yellow circle) and brittle (identified by red box) mode structure. The shear area can be seen more clearly in sample M-G-H-II-O-2 (Figure 7.47 (c, c)), although there are small dimples, but also brittle mechanism is evident (identified by red dashed square), and the fracture is less ductile or mixed fracture mode. For specimen M-U-L-III-O-3 (Figure 7.48 (b, c)), no dimples are present and the fracture mechanism is brittle fracture mode.



(a) M-G-H-I-O-1
Fracture



(b) The whole fracture surface

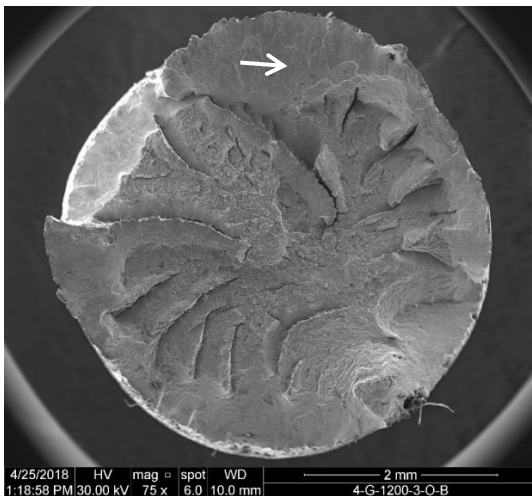


(c) The microstructure at the centre

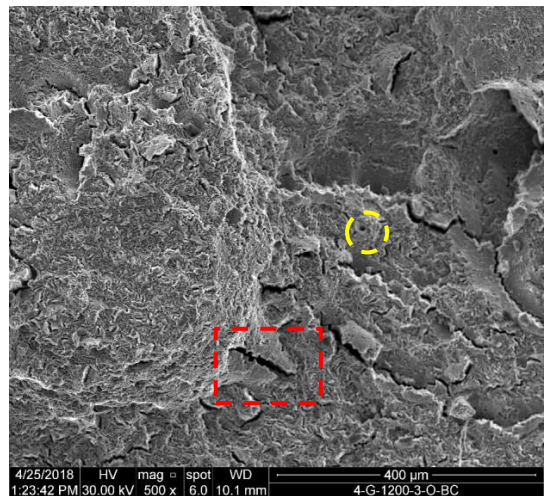
Figure 7.46 SEM images for galvanised tendon (M-G-H-I-O-1), 80% UTS



(a) M-G-H-II-O-2
Fracture



(b) The whole fracture surface



(c) The microstructure at the centre

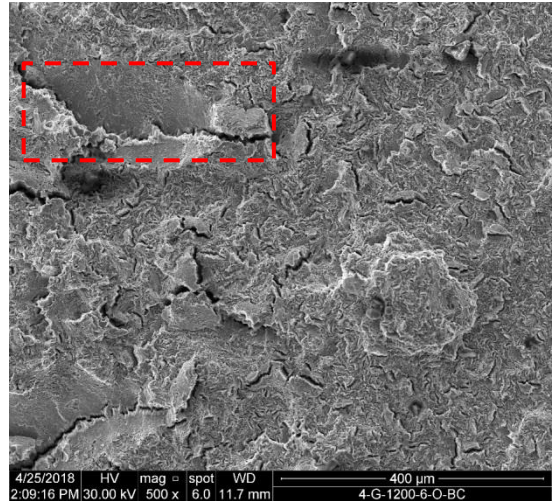
Figure 7.47 SEM images for galvanised tendon (M-G-H-II-O-2), 80% UTS



(a) M-G-H-III-O-3
Fracture



(b) The whole fracture surface



(c) The microstructure at centre

Figure 7.48 SEM images for galvanised tendon (M-G-H-III-O-3), 80% UTS

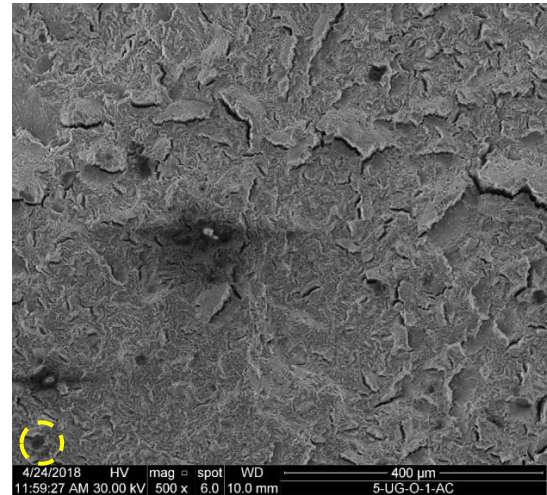
For Batch 5 ungalvanised with no corrosion and unstressed, as shown in Figure 7.49 to Figure 7.51, all test samples showed evidence of cup-cone characteristics and necking. Under powerful magnification the dimples, as presented in the microstructure images, indicate that the fracture surface was ductile.



(a) 5-U-O-1
Fracture



(b) The whole fracture surface

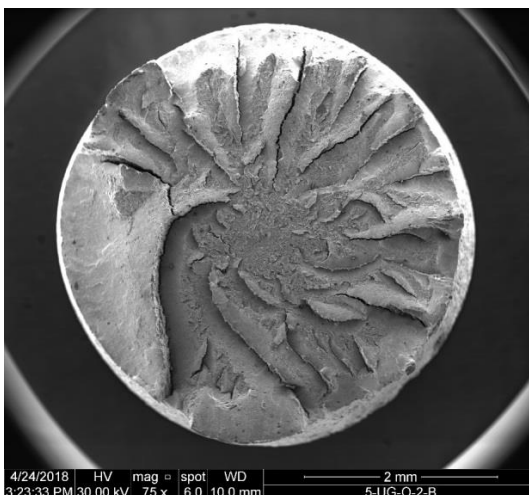


(c) The microstructure at the centre

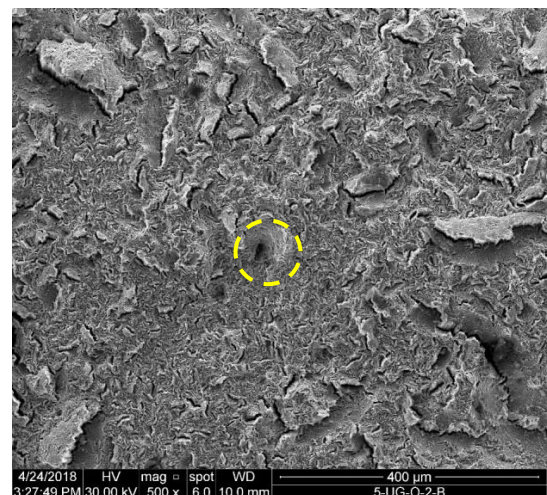
Figure 7.49 SEM images for ungalvanised tendon (5-U-O-1), Batch 5



(a) 5-U-O-2
Fracture



(b) The whole fracture surface

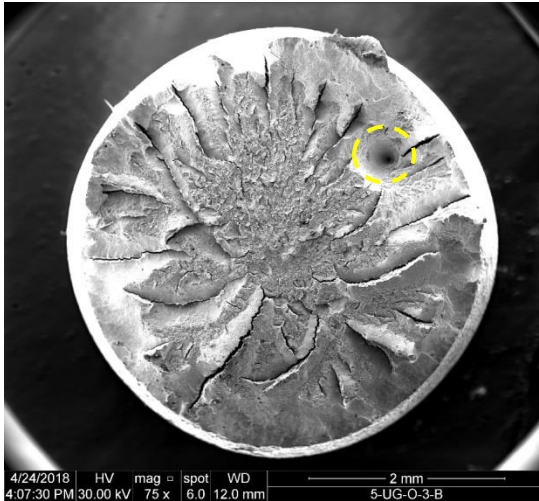


(c) The microstructure at the centre

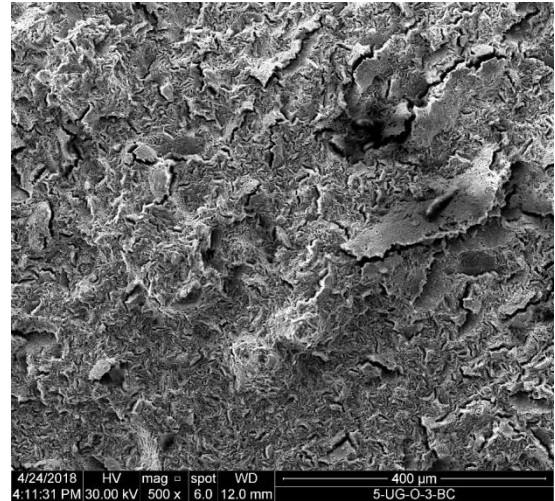
Figure 7.50 SEM images for ungalvanised tendon (5-U-O-2), Batch 5



(a) 5-U-O-3
Fracture



(b) The whole fracture surface



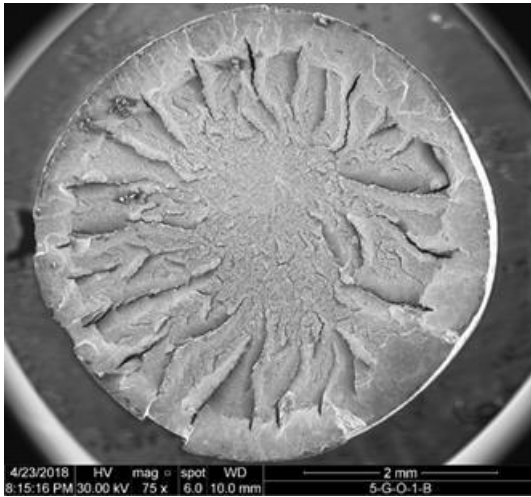
(c) The microstructure at the centre

Figure 7.51 SEM images for ungalvanised tendon (5-U-O-3), Batch 5

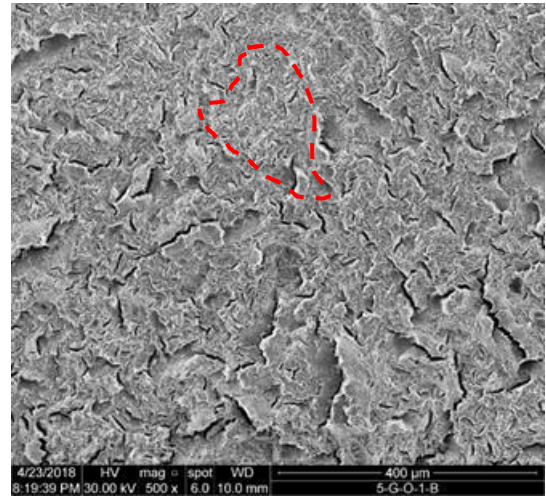
For Batch 5 galvanised with no corrosion and unstressed as shown in Figure 7.52 to Figure 7.54, although specimen 5-G-O-3 (Figure 7.54 (b, c)) has a shear area, cup-cone character and necking were still distinguishable. Under powerful magnification the dimples, as presented in the microstructure images, indicate that the fracture surfaces were ductile.



(a) 5-G-O-1
Fracture



(b) The whole fracture surface

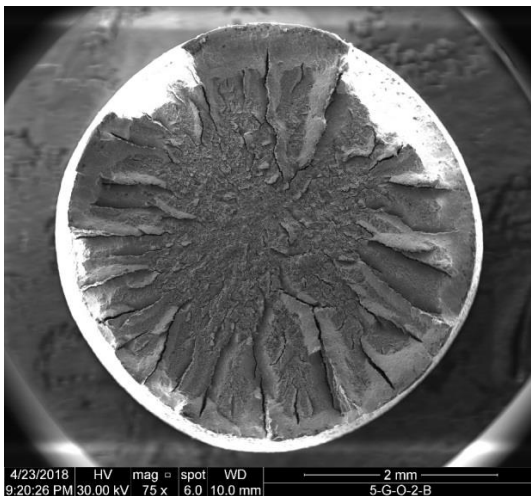


(c) The microstructure at centre

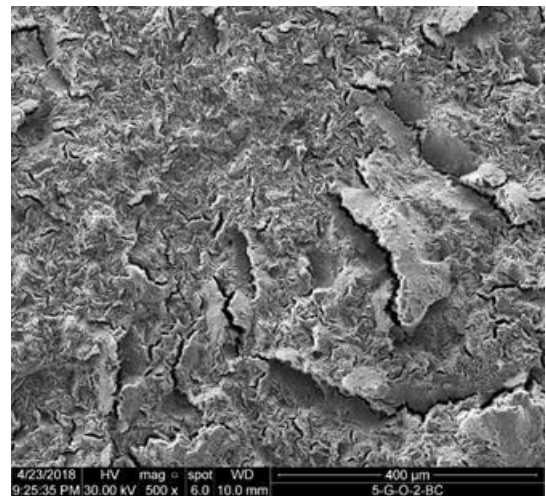
Figure 7.52 SEM images for galvanised tendon (5-G-O-1), Batch 5



(a) 5-G-O-2
Fracture



(b) The whole fracture surface

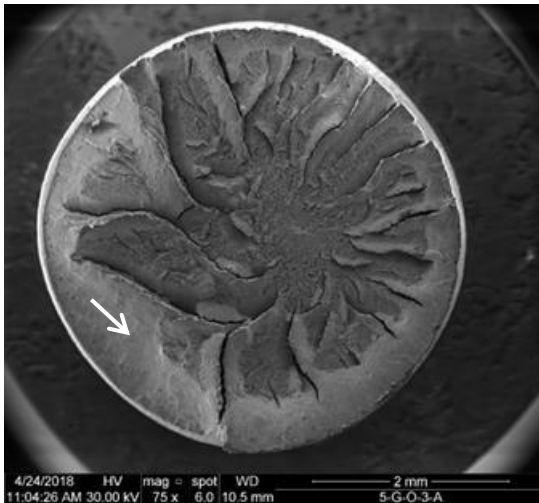


(c) The microstructure at centre

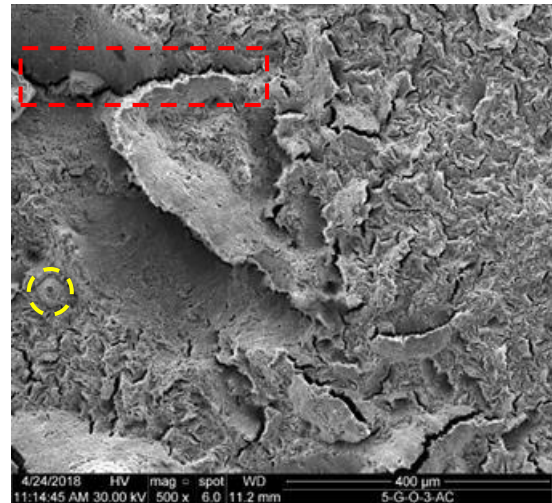
Figure 7.53 SEM images for galvanised tendon (5-G-O-2), Batch 5



(a) 5-G-O-3
Combined fracture mode



(b) The whole fracture surface



(c) The microstructure at centre

Figure 7.54 SEM images for galvanised tendon (5-G-O-3), Batch 5

7.5.7 Summary of comparison between the effects of applying cathodic protection at normal and overprotection levels

7.5.7.1 The loss in service stress

Figure 7.55 compares the loss in service stress in the ungalvanized tendon exposed to Stage II and Stage III corrosion and the application of ICCP-N and ICCP-O with Low Level and High Level of pre-stress. It can be seen from Figure 7.55 that the loss of service stress in ungalvanized tendons with High Level of pre-stress is greater than the loss with Low Level of pre-stress, as would be expected. The general trend for the loss in ungalvanized tendons with High Level of pre-stress under the application of ICCP-O is not consistent with the degree of corrosion, where the loss of stress in Stage II corrosion is more than in Stage III corrosion. In the ungalvanized tendons with Low Level of pre-stress, the losses are very small for both the application of ICCP-N and ICCP-O, being 14 MPa and 27 MPa respectively.

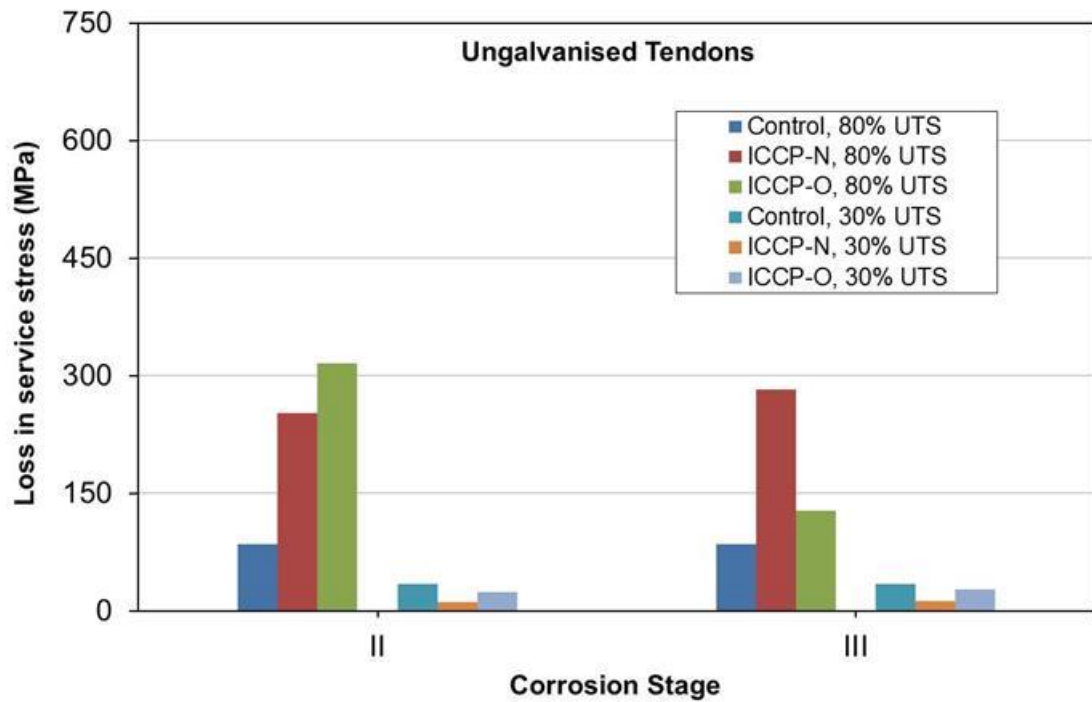


Figure 7.55 Comparison of loss in service stress for ungalvanised tendons (30% & 80% UTS)

Comparing the loss of service stress in galvanized tendons exposed to Stage II and Stage III corrosion and the application of ICCP-N and ICCP-O with High Level of pre-stress, the loss is lower than that in the ungalvanized tendons (Figure 7.55) as shown in Figure 7.56. In addition, there is little difference in the loss of stress in either ICCP-N and ICCP-O with the two Stages of Corrosion II and III and the loss associated with the control sample is negligible. This loss indicates that the effect of ICCP-N and ICCP-O on the galvanized tendons has less impact than in the ungalvanized tendon.

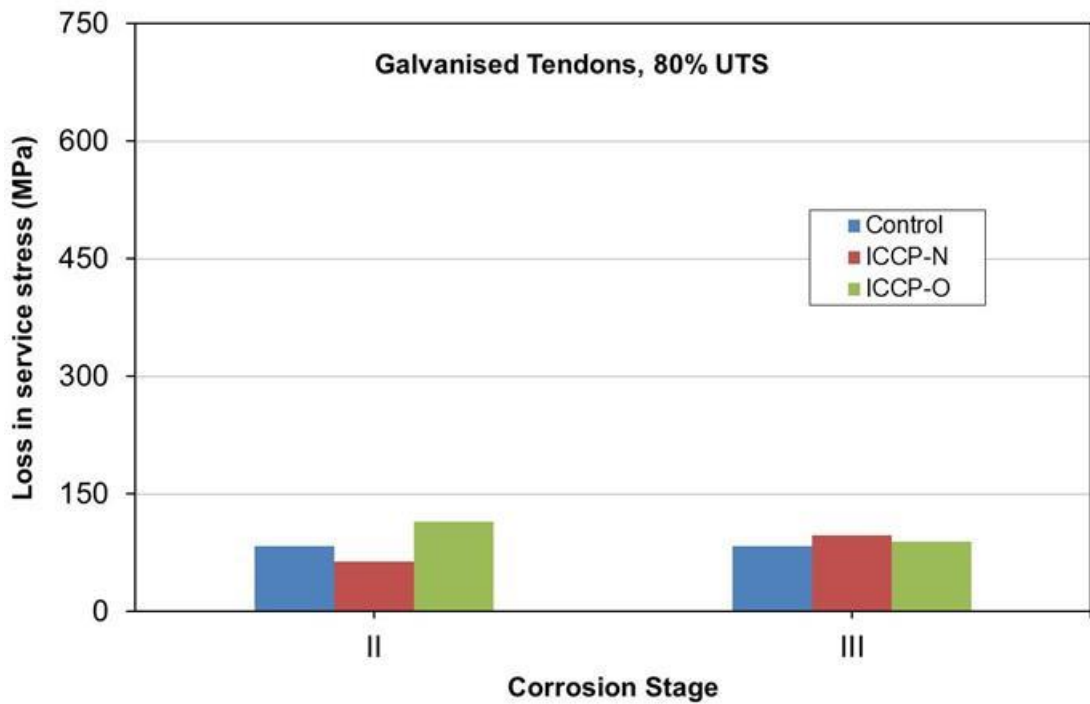


Figure 7.56 Comparison of loss in service stress for galvanised tendons (80%UTS)

7.5.7.2 Mechanical properties

A comparison of the mechanical properties for the ungalvanised tendons with Low Level and High Level pre-stress is shown in Figure 7.57 to Figure 7.60. Figure 7.57 shows the UTS, proof strength, breaking strength and Young's Modulus for all ungalvanised samples exposed to ICCP-N and ICCP-O. The results of these samples were compared to as-received samples and show that for Young's Modulus, proof strength, UTS and the breaking strength, there was no effect resulting from the application of ICCP-N & ICCP-O on the ungalvanised tendons with a Low Level of pre-stress. In Figure 7.49, shows that the trend of ductility for the samples exposed to ICCP-N or ICCP-O as similar, and as the degree of corrosion increased, the percentage of ductility decreased. However, the reduction in ductility under the application of ICCP-O is greater than for ICCP-N.

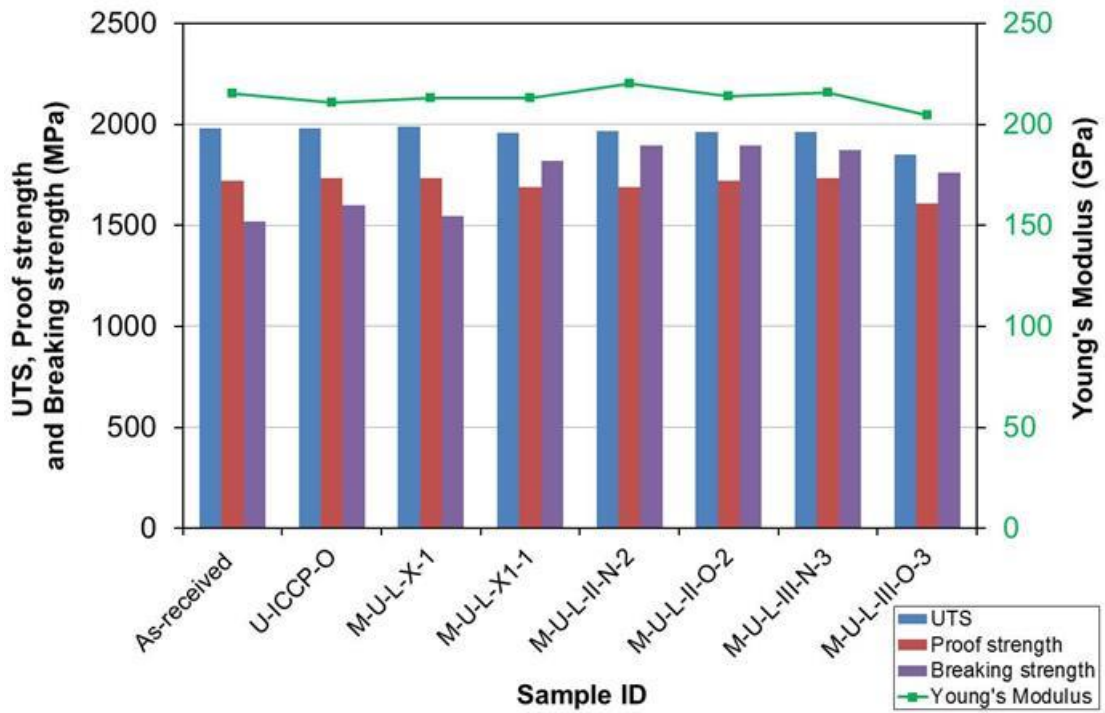


Figure 7.57 Comparison of mechanical properties for ungalvanised tendons with low level of pre-stress exposed to ICCP-N & ICCP-O (1)

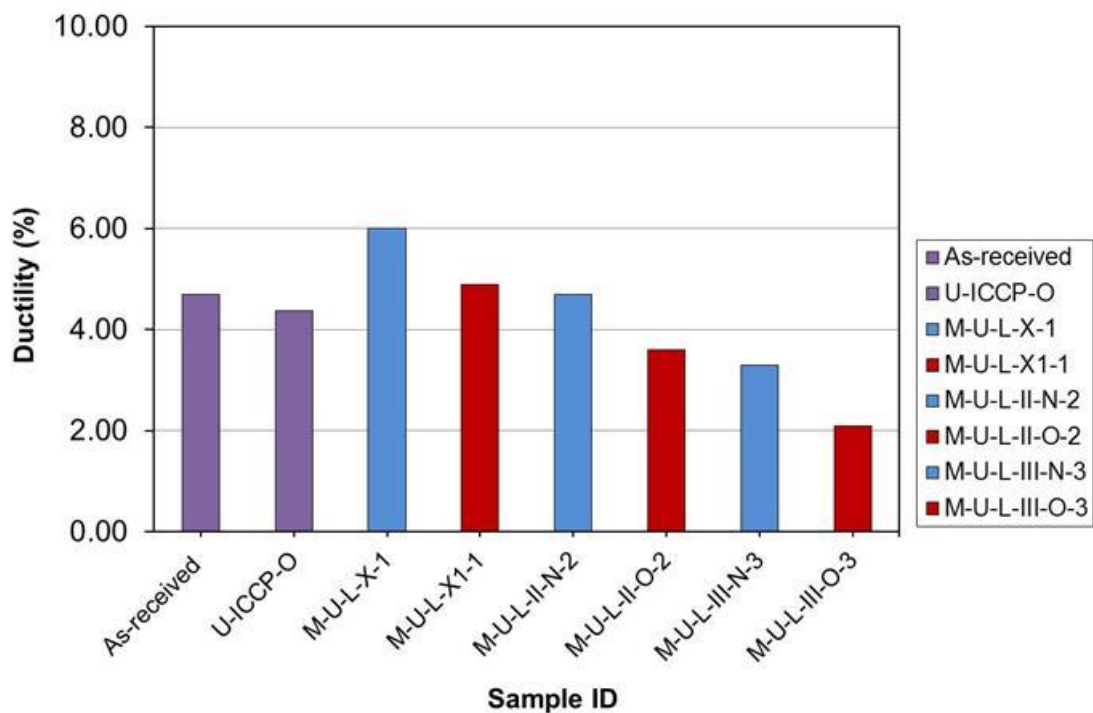


Figure 7.58 Comparison of mechanical properties for ungalvanised tendons with a low level of pre-stress exposed to ICCP-N & ICCP-O (2)

Figure 7.59 compares the UTS, proof strength, breaking strength and Young's Modulus for all ungalvanised tendons with High Level of pre-stress for samples

exposed to ICCP-N and ICCP-O. In order to investigate and compare the effect of the application of ICCP-N and ICCP-O, results of as-received and unstressed samples were plotted. It demonstrates that there is no significant effect due to ICCP-N and ICCP-O on Young's Modulus, proof strength and UTS of the tendons, relative to the as-received samples. However, breaking strength shows a different trend with the failure strength generally reduced when the degree of corrosion increased, and reduced more with ICCP-O than ICCP-N. Figure 7.60 shows the trend of ductility for the samples exposed to ICCP-N or ICCP-O and, as the degree of corrosion increased, the percentages of ductility, necking and the energy of toughness decreased. It also shows that the reduction in ductility and toughness for samples exposed to ICCP-O are greater than the samples exposed to ICCP-N. Nevertheless, failure of tendons occurred in the plastic stage.

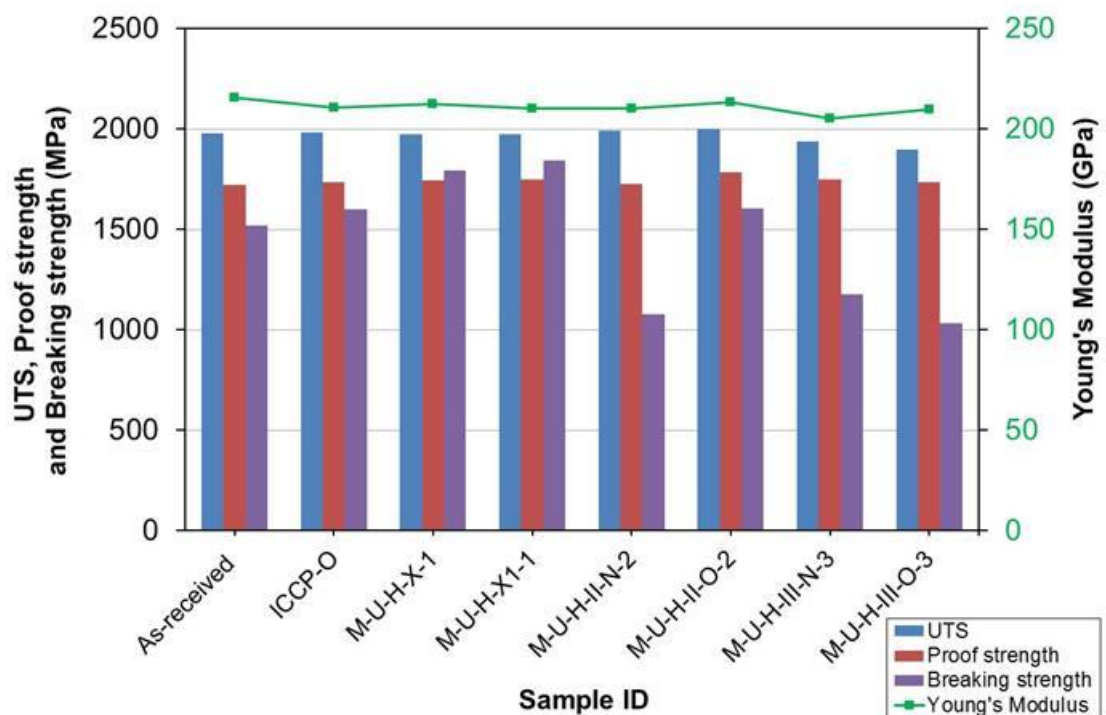


Figure 7.59 Comparison of mechanical properties for ungalvanised tendons with High Level of pre-stress exposed to ICCP-N & ICCP-O (1)

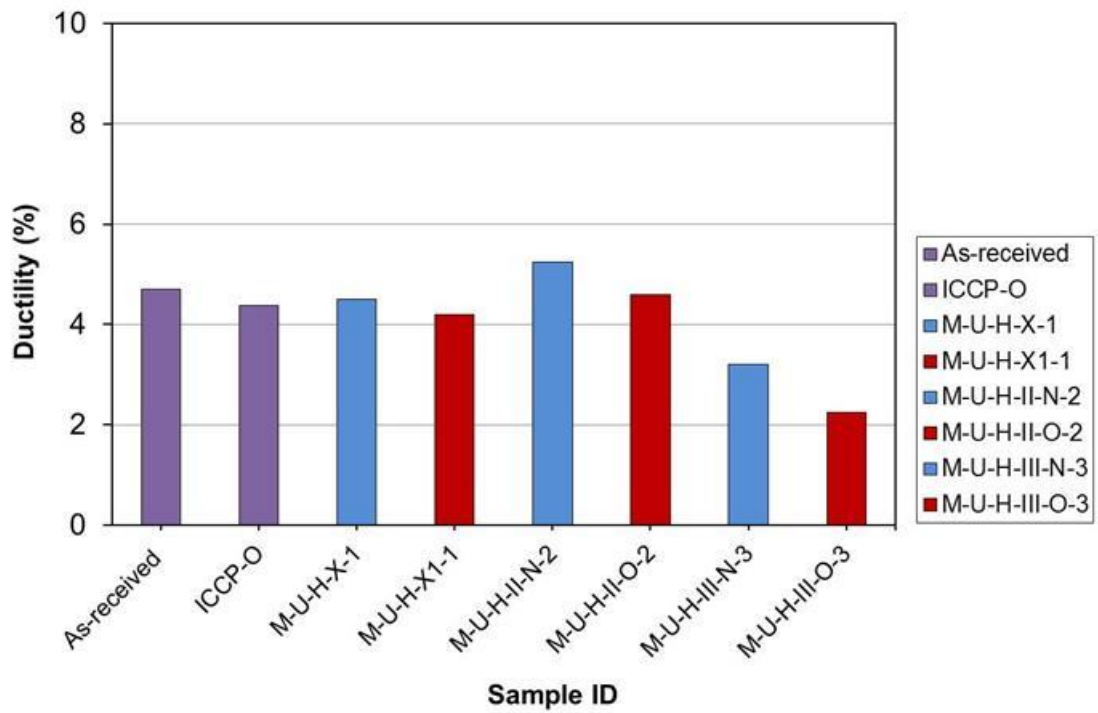


Figure 7.60 Comparison of mechanical properties for ungalvanised tendons with High Level of pre-stress exposed to ICCP-N & ICCP-O (2)

Figure 7.61 shows the comparison of UTS, proof strength, breaking strength and Young's modulus for all galvanised tendons with High Level of pre-stress and exposed to ICCP-N and ICCP-O. Results of as-received and unstressed samples are also plotted. For galvanised tendons, Young's Modulus, proof strength, UTS and breaking strength have not been affected by the application of ICCP-N or ICCP-O relative to the as-received samples. Figure 7.62 shows the trend of ductility samples exposed to ICCP-N or ICCP-O and as the degree of corrosion increased, the percentages of ductility decreased. It also shows that the reduction in ductility and toughness for samples exposed to ICCP-O are more than the samples exposed to ICCP-N. It also shows that this reduction was greater than for the ungalvanised tendons. Nevertheless, the failure of tendons occurred in the plastic stage.

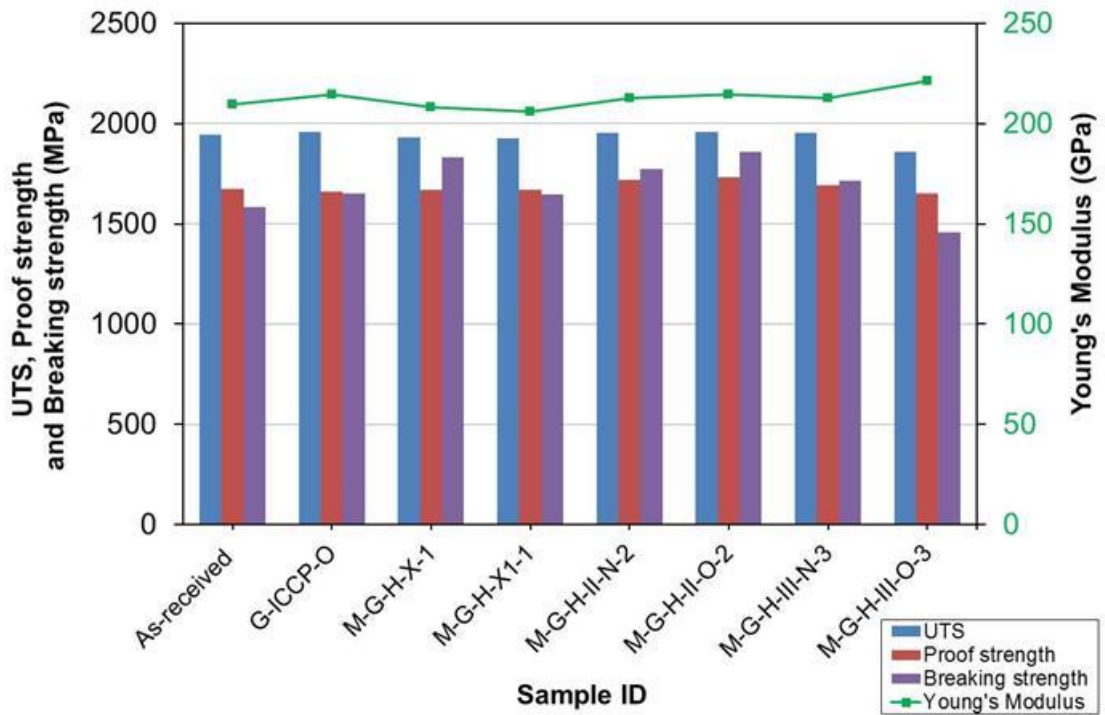


Figure 7.61 Comparison of mechanical properties for galvanised tendons with High Level of pre-stress exposed to ICCP-N & ICCP-O (1)

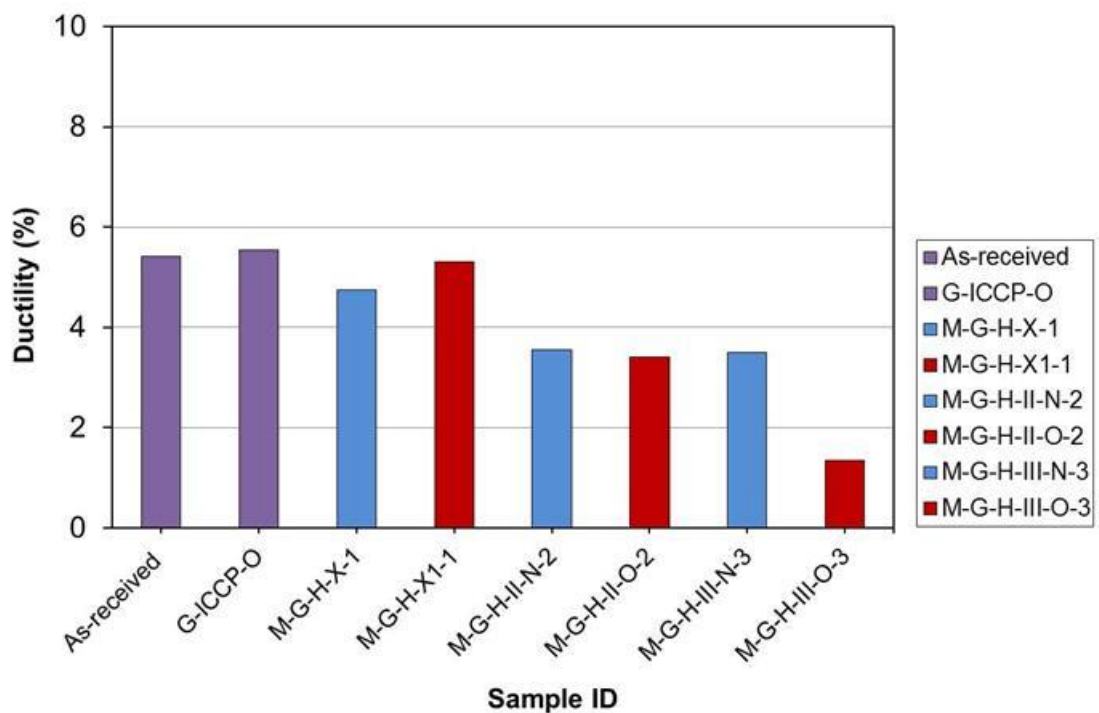


Figure 7.62 Comparison of mechanical properties for galvanised tendons with High Level of pre-stress exposed to ICCP-N & ICCP-O (2)

7.5.7.3 Embrittlement ratio

Figure 7.63 to Figure 7.66 compare the embrittlement ratio for ICCP-N and ICCP-O relative to the control samples. A description of the embrittlement ratio is given in Section 7.5.6.2. Tensile strength and proof strength ratio for all samples are close to zero. This indicates that neither tensile strength nor proof strength have been affected by hydrogen generated by either ICCP-N or ICCP-O. The ductility ratio indicates clearly how the tendons responded to the generation of hydrogen. However, it also has to be stated that the degree of corrosion is a very important factor in the reduction of ductility [122].

For the ungalvanised tendons with Low Level of pre-stress, the embrittlement ratio increased as the degree of corrosion increased for both ICCP-N and ICCP-O relative to the control. It also shows that this ratio is greater for the application of ICCP-O than ICCP-N (Figure 7.63 and Figure 7.64). However, for ungalvanised tendons with High Level pre-stress the embrittlement ratio under the application of ICCP-O is lower than for the application of ICCP-N for Stage II corrosion (Figure 7.65). For Stage III, the embrittlement ratio increased, notably for the application of ICCP-O (Figure 7.66).

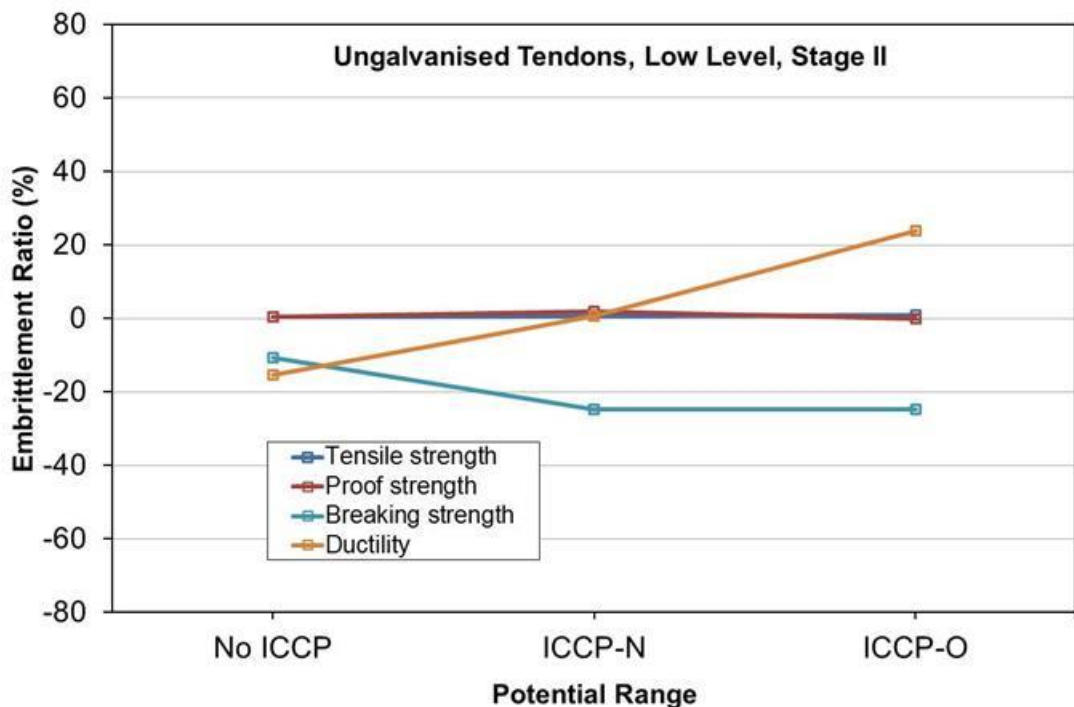


Figure 7.63 Relationship between polarisation potential and hydrogen embrittlement ratio for ungalvanised tendons, Low Level, Stage II

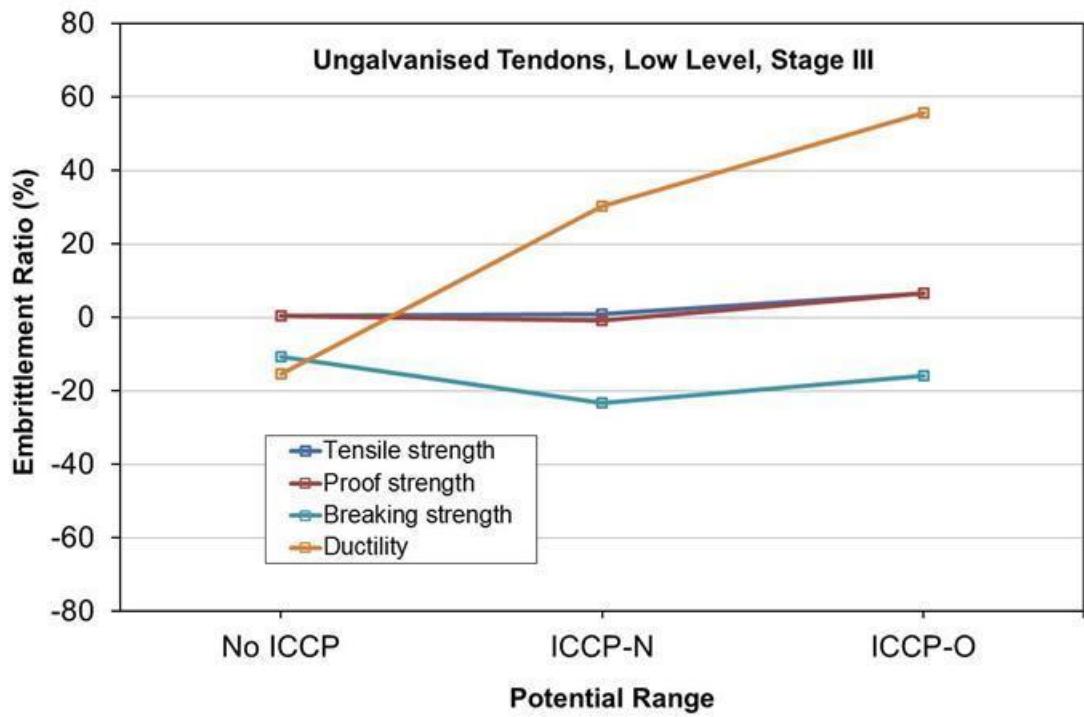


Figure 7.64 Relationship between polarisation potential and hydrogen embrittlement ratio for ungalvanised tendons, Low Level, Stage III

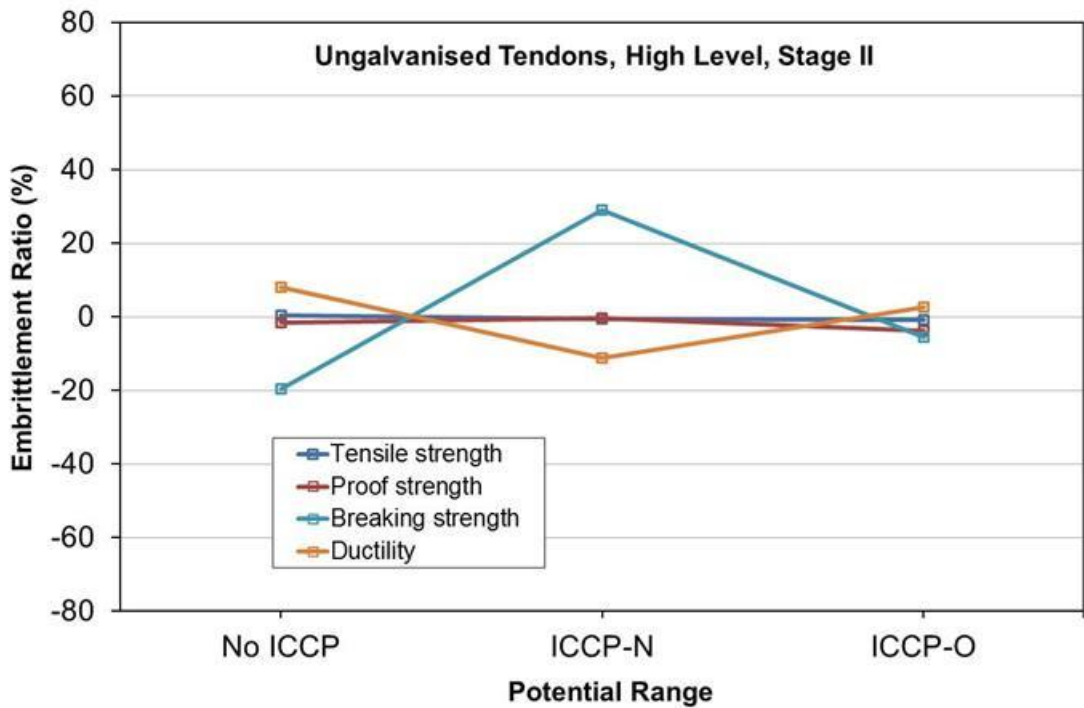


Figure 7.65 Relationship between polarisation potential and hydrogen embrittlement ratio for ungalvanised tendons, High Level, Stage II

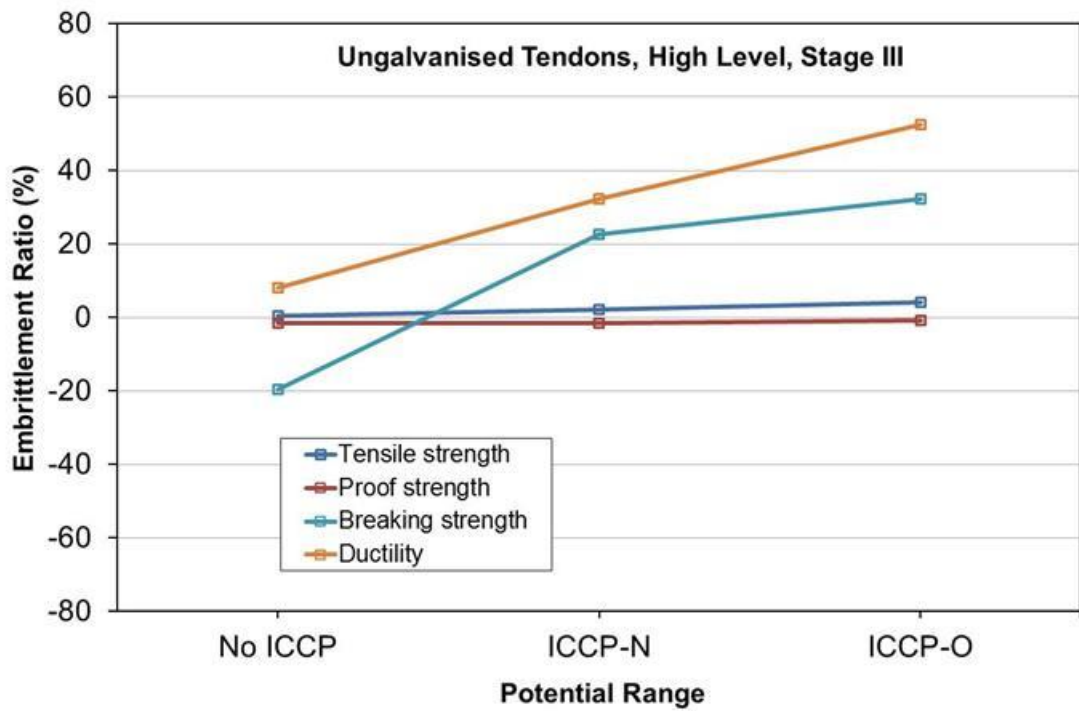


Figure 7.66 Relationship between polarisation potential and hydrogen embrittlement ratio for ungalvanised tendons, High Level, Stage III

For galvanised tendons, generally the embrittlement ratios of all mechanical properties have relatively similar behaviour as in the ungalvanised tendons (Figure 7.67 and Figure 7.68). It was observed that at Stage III corrosion, the ductility ratio became higher than the ratio of ductility for the ungalvanised tendons.

Overall, when both ungalvanised and galvanised tendons were polarized between -650 to -750 mV, the embrittlement ratio of all mechanical properties were smaller compared to polarisation between -850 to -1300mV. Therefore, at more negative potentials, the ratio of ductility, necking and breaking strength increased. The increase in ratio of ductility may indicate a higher susceptibility to hydrogen as a high embrittlement ratio indicates a greater influence by hydrogen [123].

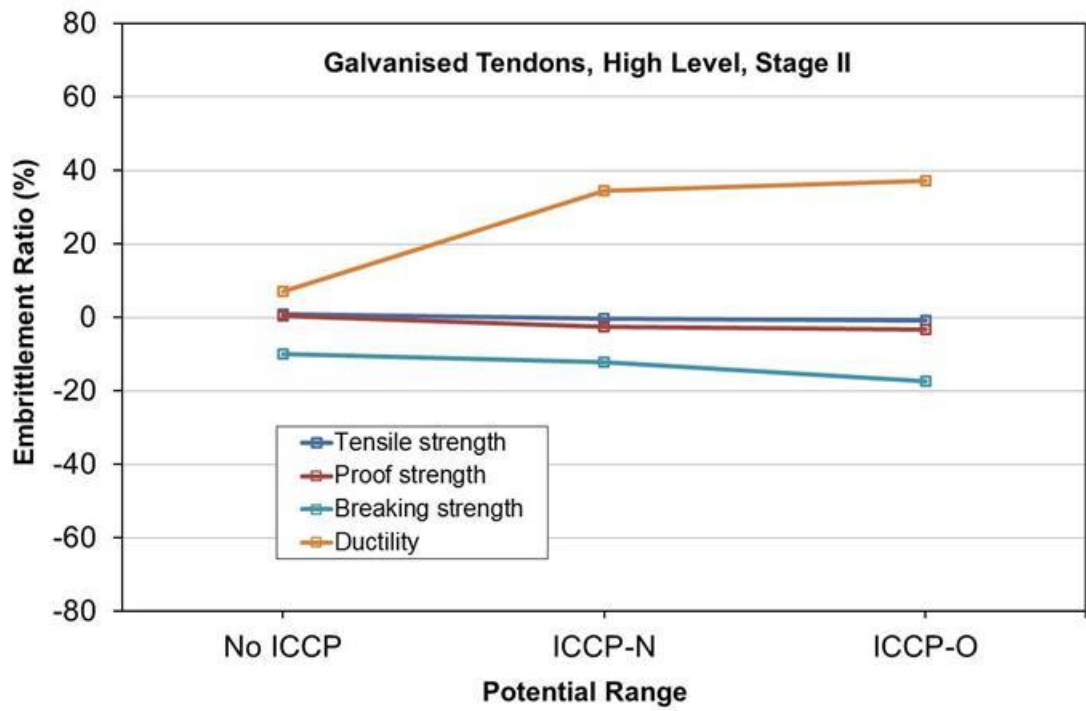


Figure 7.67 Relationship between polarisation potential and hydrogen embrittlement ratio for galvanised tendons, High Level, Stage II

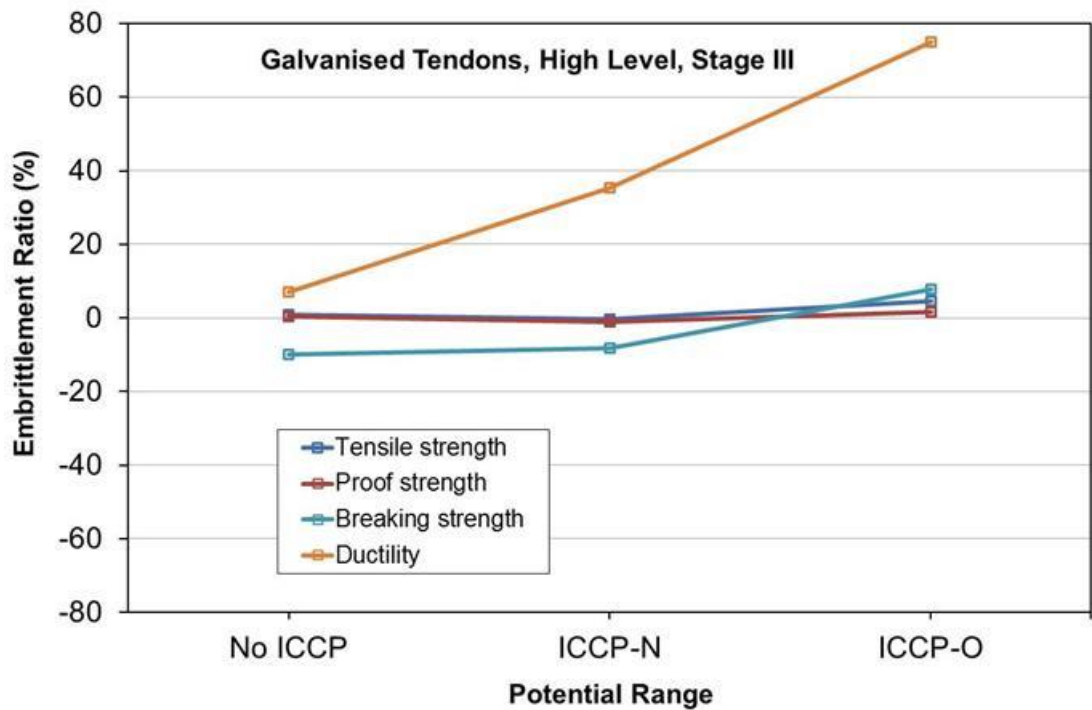


Figure 7.68 Relationship between polarisation potential and hydrogen embrittlement ratio for galvanised tendons, High Level, Stage III

7.5.7.4 Fracture mode

In order to have a better understanding of type of fracture for the tested samples, Figure 7.69 to Figure 7.72 summarise the fracture modes for both types of tendons under the effect of ICCP-N and ICCP-O. For the ungalvanised tendons with Low Level pre-stress, the fracture modes show that the shear area exists even for the samples that were not exposed to ICCP (identified by white arrows). However, the size of the shear area in the peripheral regions is greater as the degree of corrosion increased. As was discussed in Chapter 6 and in this chapter with respect to fracture mode, dimples can be seen in all fracture modes. It is also observed that in the Stage III corrosion, the dimples are fewer, and the shear area is greater. This indicates that the fracture is less ductile and is a mix of ductile and brittle [125]. Similarly, the control samples also show shear areas. This demonstrates that the effect of both ICCP-N or ICCP-O are not significant with respect to ungalvanised tendons under these conditions (Figure 7.69).

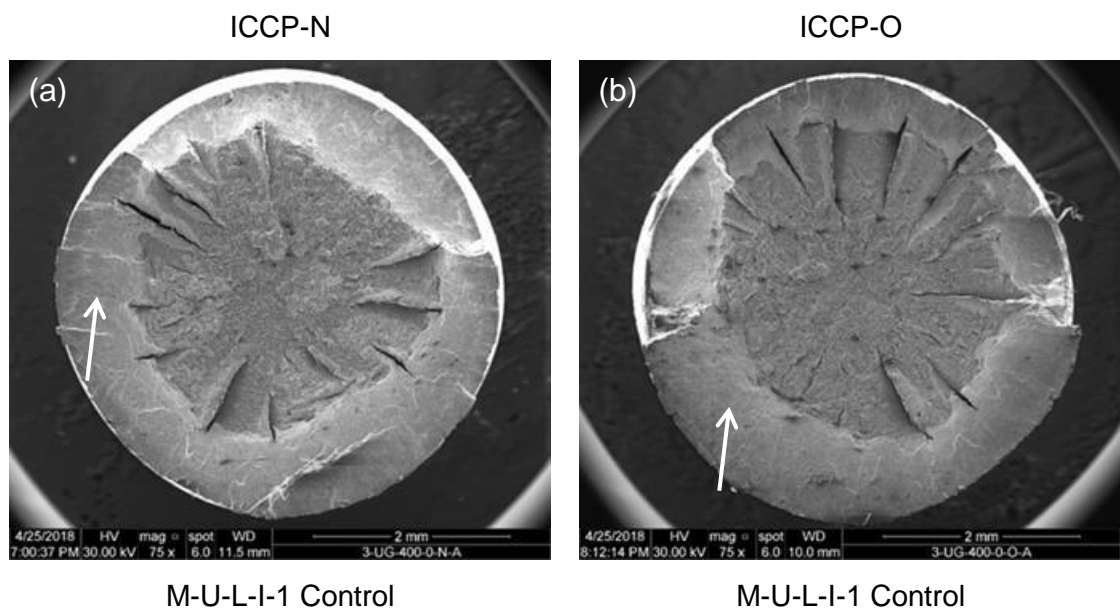


Figure 7.69 Comparison of fracture mode for ungalvanised tendons (30% UTS)

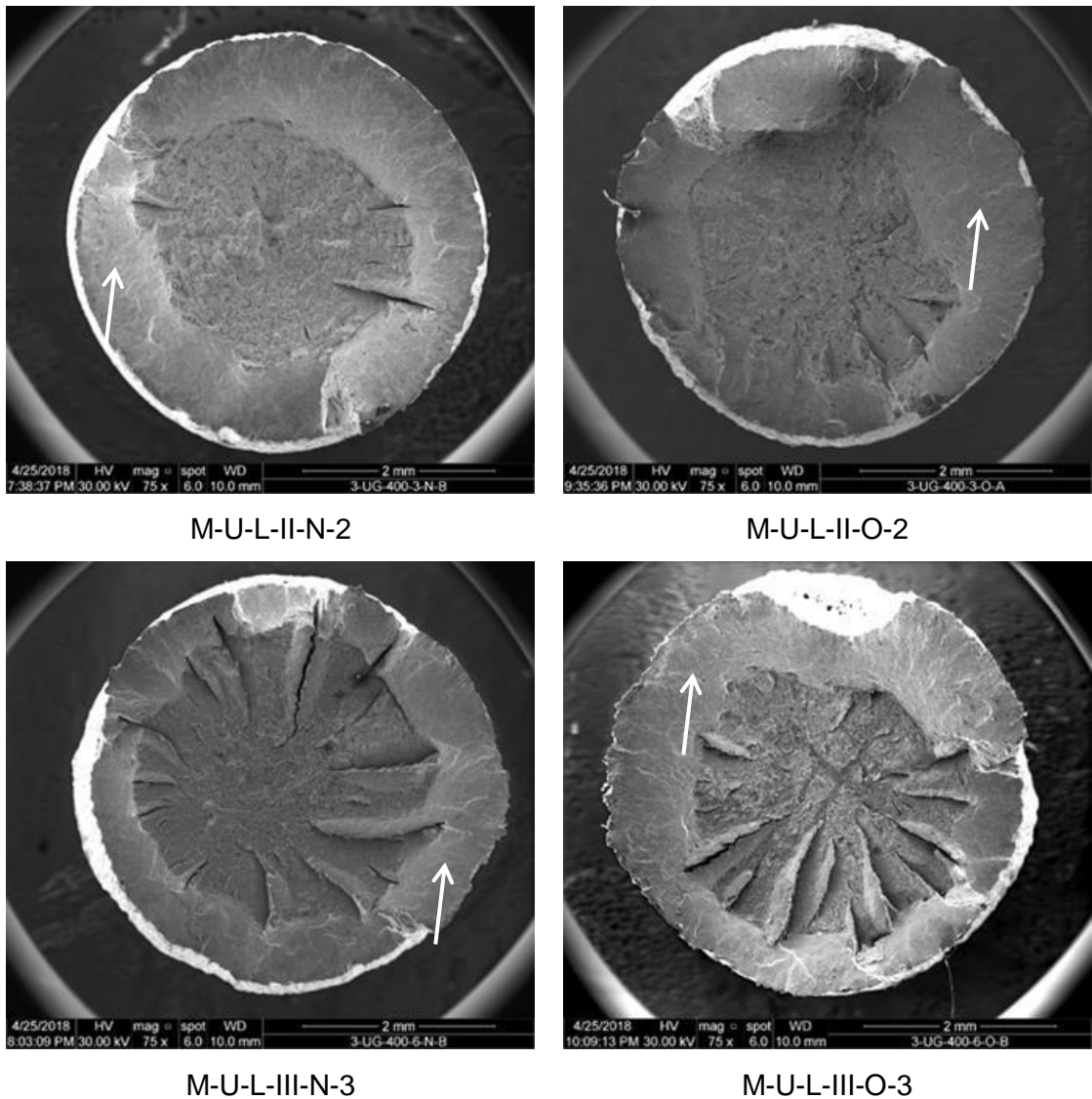


Figure 7.69 (cont.) Comparison of fracture mode for ungalvanised tendons (30% UTS)

For ungalvanised tendons with High Level of pre-stress (80% of UTS), the fracture modes show that the shear area or the damage of the surface of the fracture is more with samples exposed to the application of ICCP-O than ICCP-N, particularly in Stage III corrosion. This shows that the damage not only occurred by ICCP-O, it is combined with the degree of corrosion. Stage II corrosion does not show similar damage in the surface of the fracture as in Stage III although it was exposed to the ICCP-O with the same pre-stress. The results confirm the fracture in Stage III corrosion is a mix of ductile and brittle for samples exposed to ICCP-N but is less ductile or brittle in the samples exposed to ICCP-O (Figure 7.70).

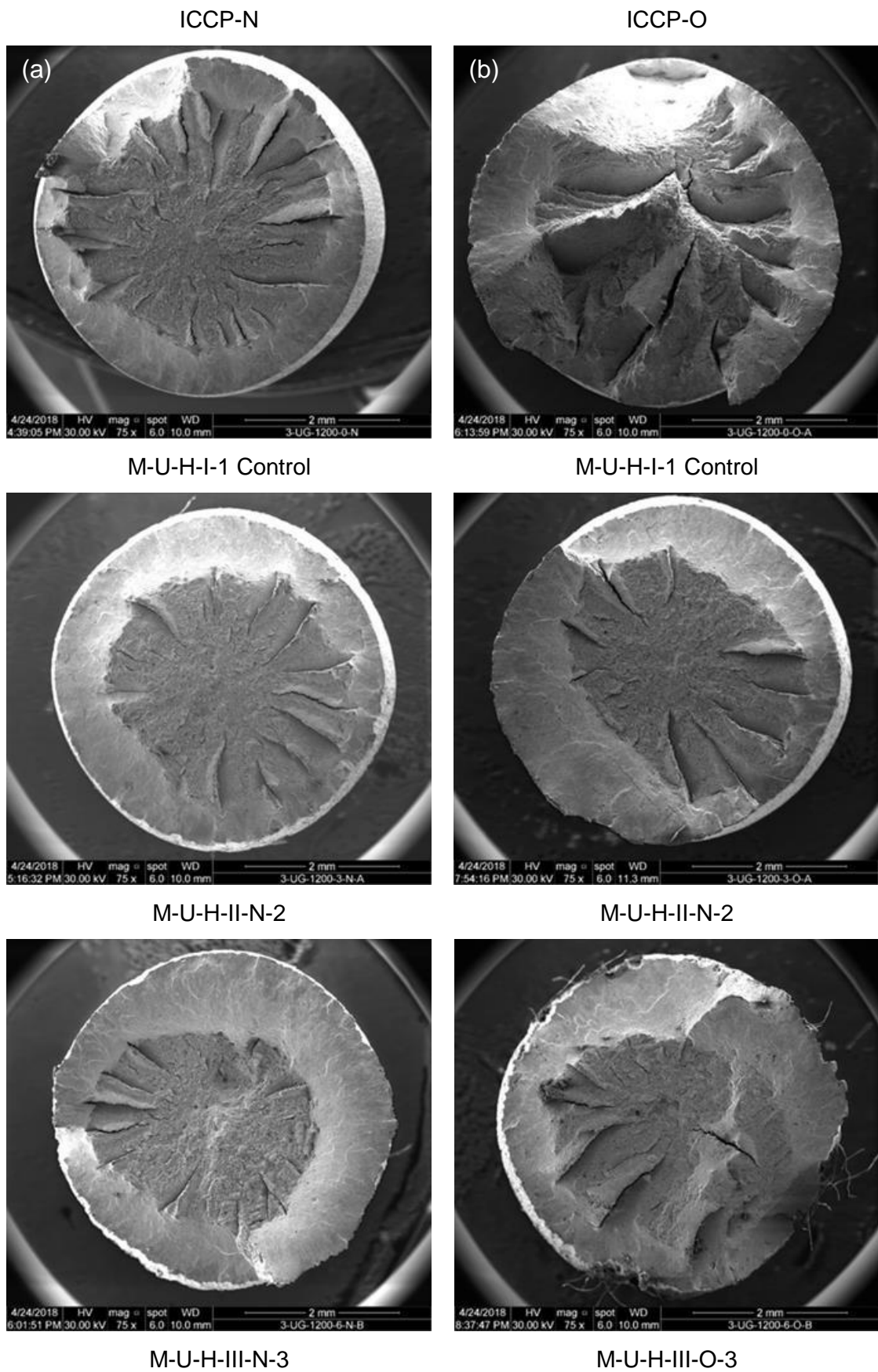


Figure 7.70 Comparison of fracture mode for ungalvanised tendons, (80% UTS)

For galvanised tendons, both ICCP-N and ICCP-O have influenced the fracture more than the ungalvanised tendons in Stage II and Stage III corrosion. However, the damage is more in ICCP-O than ICCP-N and the degree of corrosion also has to be considered as a factor that has influence on the damage of the tendons (Figure 7.71).

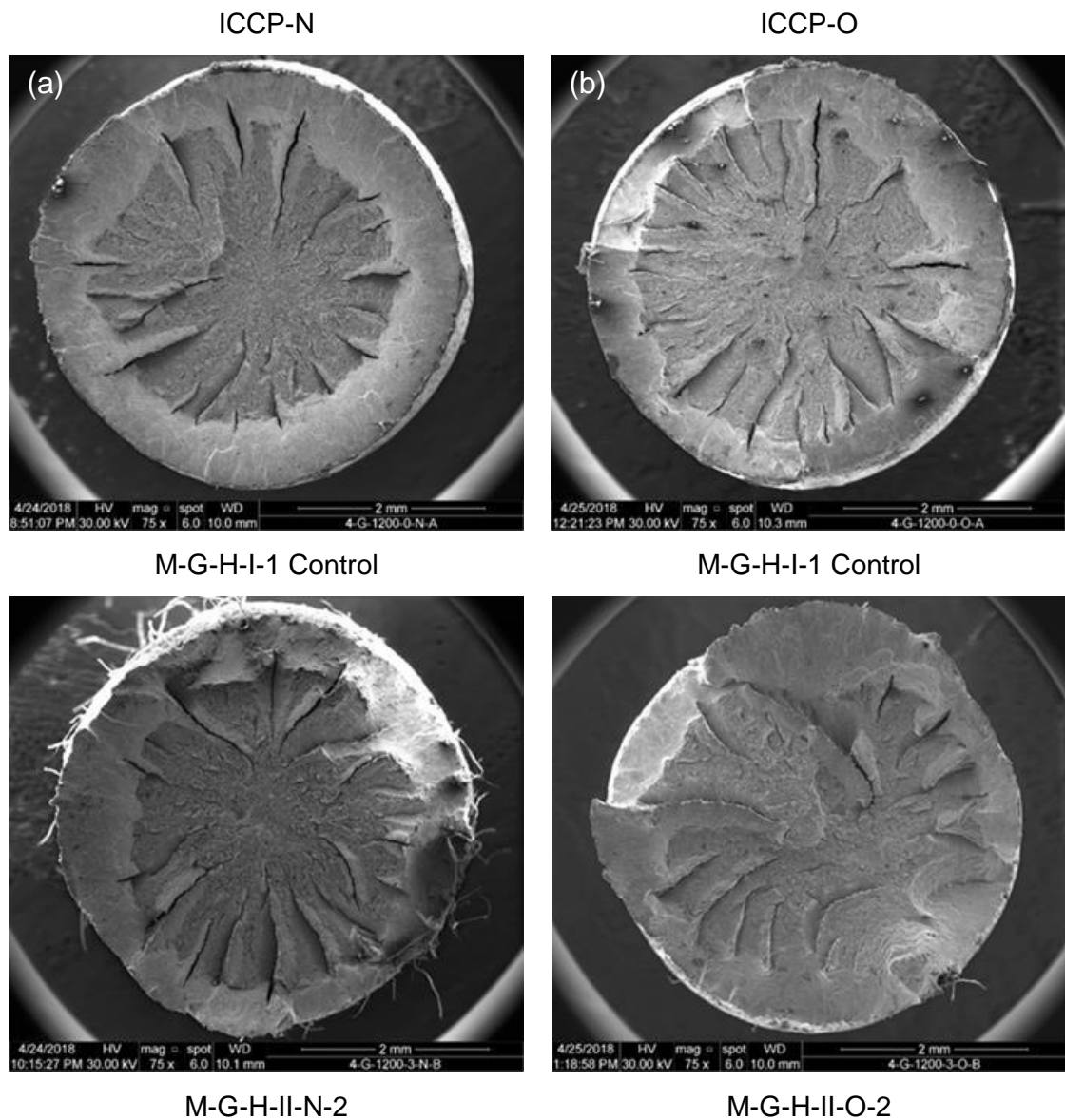
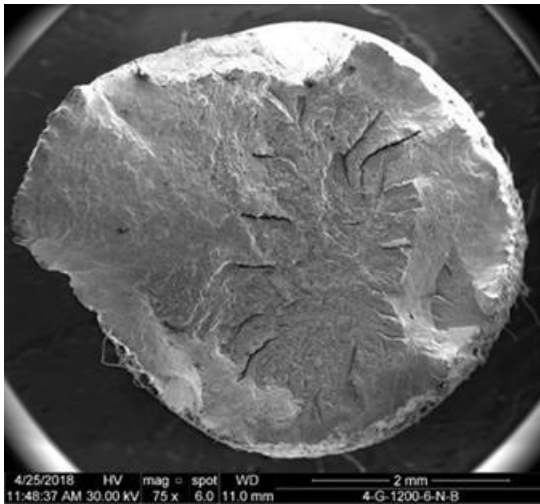


Figure 7.71 Comparison of fracture mode for galvanised tendons (80% UTS)



M-G-H-III-N-3



M-G-H-III-O-3

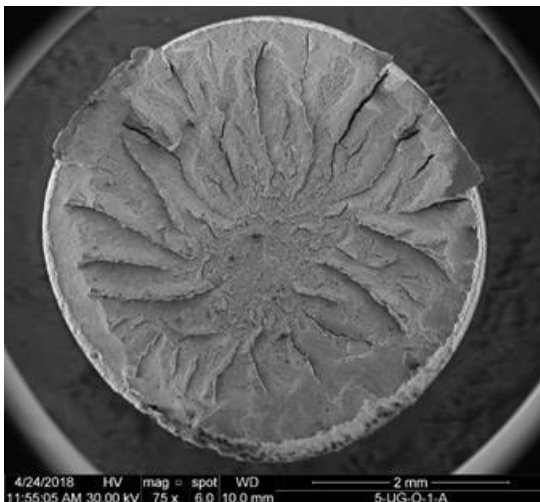
Figure 7.71 (cont.) Comparison of fracture mode for galvanised tendons

(80% UTS)

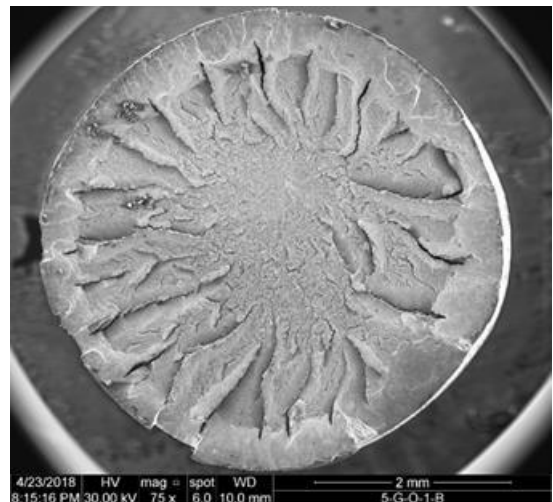
Figure 7.72 compares the fracture modes of the ungalvanised and galvanised unstressed samples. These samples were exposed to only ICCP-O (-1000 to -1300 mV) for a total period of 11,712 hrs (488 days). Shear areas are not seen in all the fracture modes as in the two types of pre-stressed tendons (Figure 7.70 and Figure 7.71). From this it can be concluded that the level of pre-stress has an influence on the degradation of the tendon as well as the degree of corrosion.

Ungalvanised

Galvanised



5-UG-O-1



5-G-O-1

Figure 7.72 Comparison of fracture mode for ungalvanised and galvanised tendons (unstressed samples)

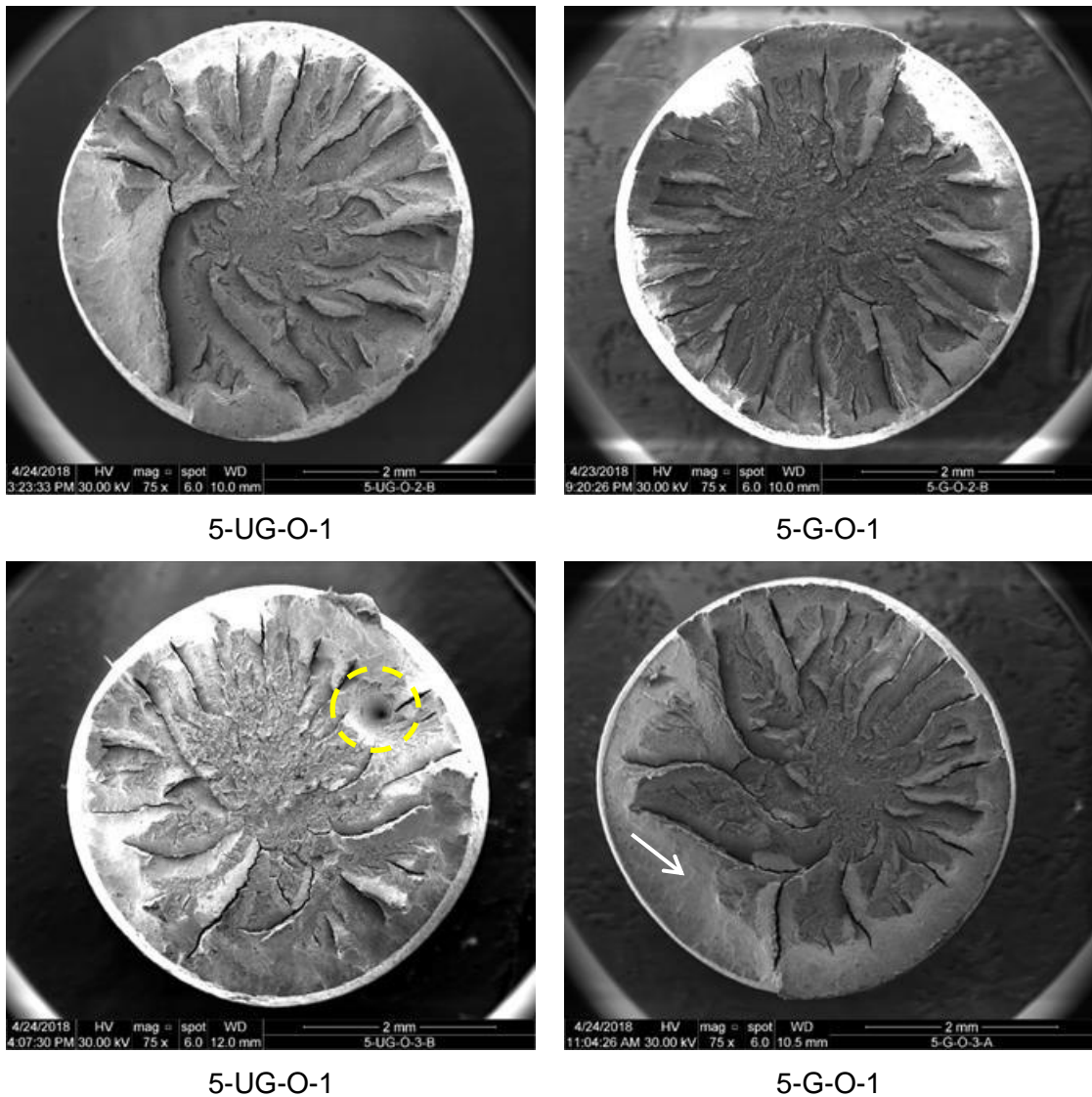


Figure 7.72 (cont.) Comparison of fracture mode for ungalvanised and galvanised tendons (unstressed samples)

7.5.8 Conclusions

7.5.8.1 Conclusion of the effect of ICCP-O on pre-stressed tendons

- The ICCP was applied for an extended period of 5,304 hours (221 days) for ungalvanized tendons, 3,288 hours (221 days) for galvanised tendons and 11,712 hours (488 days) for unstressed samples. When the ICCP-O system was interrupted for 24 hours, the potential decays were more than 100mV after 4 hours for all tendons, thus demonstrating that an adequate level of cathodic protection had been achieved

- The results indicate that there is a loss in pre-stress in both types of tendons over the test period. The behaviour of the galvanised tendon under ICCP-O application is more stable than the behaviour of the ungalvanised tendon in terms of service stress loss. The degree of corrosion also has an impact on the loss of pre-stress, particularly in ungalvanised tendons, with the tendons subjected to higher degrees of corrosion suffering higher losses which may need to be accounted for at the design stage as an additional loss. This loss of service stress can be from a combination of the degree of corrosion and the application of ICCP-O
- For mechanical properties, overall, there was no significant effect of ICCP-O on the strength of the tendons as tested. The UTS and the 0.2% proof strength in each type of tendon were similar and no significant reduction was evident. Typically, the design safety factor is set to a maximum level of load, approximately $\frac{2}{3}$ proof strength for structural engineering components. Although the ductility has been reduced by the application of the ICCP-O, the fracture occurred in the plastic zone after reaching the UTS in each type of tendon
- The embrittlement ratios indicate that hydrogen generated by ICCP-O has no effect on UTS and proof strength for either tendon type. However, for the galvanised tendon with High Level of pre-stress, the ratio was less for breaking strength and increased more for ductility. Notably, increases in the ratio of ductility and necking were apparent
- Unstressed, hydrogen exposed specimens did not show significant change in either mechanical properties or in the characteristics of the fracture. Only the galvanised specimens showed a greater shear area, and a combination of ductile and brittle fracture modes were evident

7.5.8.2 Conclusion of the comparison between the effects of applying cathodic protection normal and overprotection levels

- The loss of service stress for the two types of tendons with High Level of pre-stress is more than the loss in stress for tendons with Low Level of pre-stress. Both ICCP-N and ICCP-O have no effect on the Young's Modulus, 0.2% proof strength and UTS for either type of

pre-stressed tendon. A reduction in ductility was noticed in both types of tendons after the application of ICCP-N and ICCP-O. This reduction increased as the degree of corrosion increased. The fractures show that both ICCP-N and ICCP-O have a mixed type of fracture mode at Stage III corrosion. Nevertheless, the unstressed samples show less brittleness than the pre-stressed sample. Overall, the damage to both types of tendons is not only due to the application of ICCP as there are other factors such as the degree of corrosion and the level of pre-stress and these appears to have greater influence than the application of ICCP

8 Conclusions and Recommendations for Future Work

8.1 General conclusions

The important and unique element of this research project is replicating a potential site problem in the laboratory by achieving an extended exposure to the application of ICCP (488 days). This has developed a better understanding of the risks involving in the application of cathodic protection (ICCP) in terms of loss of service stress, risk of hydrogen embrittlement (HE) and reduction in the strength of pre-stressed ungalvanized and galvanised tendons. The loss of service stress, as monitored by vibrating wire strain gauges, was determined by the following procedure. Corrosion was generated by an acceleration technique and assessed using Faraday's Law. Impressed current cathodic protection was applied to samples of tendon at normal and excessive levels (over-protection). Mechanical properties were determined by tensile testing. Evaluation of the tested specimens was performed by Infinite Focus Microscope (IFM) and Scanning Electronic Microscopy (SEM). Embrittlement ratio, supported by inert gas fusion thermal conductivity detection, was used to investigate the possible effects of hydrogen diffusion for the tested tendons.

A novel finding is that the degree of corrosion and the level of pre-stress appear to have more influence on the strength of pre-stressed tendon than the application of cathodic protection. Although the ductility has been reduced by the application of the ICCP, the fracture occurred after reaching the ultimate strength in each type of tested tendon. In addition, the loss of service stress can also be from the combination of the degree of corrosion and the application of ICCP. Using ICCP-N is more reliable and prevents further corrosion in pre-stressed concrete structures. However, applying CP over the recommended criteria (ICCP-O) in some occasions is a lower risk than perceived, particularly in terms of yield and UTS. The research questions have been answered in that the application of ICCP on pre-stressed concrete structures can be employed with greater confidence. A summary of the significant conclusions drawn from this investigation and further research recommendations are given in this chapter.

8.2 Effect of corrosion on the tendon

- The anodic impressed current method was a practical method of generating and accelerating corrosion of both galvanised and ungalvanised pre-stressed tendons in the laboratory within a short time period. The extent of corrosion can be calculated based on Faraday's Law.
- The appearance of the corrosion products in a saline solution was yellow, brown and black, while in mortar resulted in familiar brown rust staining, followed by longitudinal cracking in the mortar surface above the tendon where a high degree of corrosion was induced.
- A corrosion current density of 1 mA/cm^2 has been used for inducing accelerated corrosion in all experiments.
- Not only general corrosion was generated by accelerated corrosion technique, some localised corrosion was observed on the corroded tendons.
- Using IFM, higher surface roughness was evident on the tendon surface as the degree of corrosion increased. Visual inspection did not identify cracks on the surface of the tendons.
- A higher degree of corrosion leads to a higher loss in pre-stress in highly pre-stressed tendons which is an additional loss to be accounted for at the design stage.
- Loss in pre-stress in ungalvanised tendons with both Stages I and II degree of corrosion is higher than the loss in pre-stressed galvanised tendons

8.3 Effect of Normal Impressed Current Cathodic Protection (ICCP-N) on the tendons

- Small yellow spots, assumed to be as a result of local acidification, appeared on the surface of the mortar around the anodic connection in the ungalvanised tendon, while in the case of the galvanised tendons, there was no sign of yellow spots.
- The ICCP was applied for an extended period of 13,272 hours for ungalvanised and 3,288 hours for galvanised tendons. The ICCP-N system was periodically interrupted for 24 hours and the potential decays were greater than 100mV after 4 hours for all tendons. This

demonstrates that an adequate level of cathodic protection had been achieved.

- The results clearly demonstrate that there is a loss in pre-stress of the ungalvanised and galvanised tendons over the entire test period due to initial slippage, mould contraction and corrosion. The galvanised tendons subject to ICCP-N application show different behaviour compared to ungalvanised tendons. Also it was noticed that the tendons subjected to higher degrees of corrosion suffer higher losses, which should be accounted for at the design stage.
- There was no a significant effect of ICCP-N on the strength of any of the tested tendons.
- The embrittlement ratio (the ratio of the mechanical properties with and without cathodic protection) indicates that hydrogen generated by ICCP-N, has no significant effect on either UTS or proof strength for both tendon types. However, for galvanised tendons with High Level of pre-stress, the ratio was reduced for breaking strength and increased for ductility.
- All as-received specimens had a ductile fracture with necking and cup-cone fracture mode. SEM images of the fracture surface of the ungalvanised tendons indicates that ductile mode failures occurred, while in the galvanised tendons two failures modes occurred, one being ductile and the other a combination of ductile and brittle.

8.4 Effect of Overprotection by Impressed Current Cathodic Protection (ICCP-O) on the tendons

- The ICCP was applied for an extended period of 5,304 hours (221 days) for ungalvanized tendons, 3,288 hours (221 days) for galvanised tendons and 11,712 hours (488 days) for unstressed samples. When the ICCP-O system was interrupted for 24 hours, the potential decays were greater than 100mV after 4 hours for all tendons, thus demonstrating that an adequate level of cathodic protection had been achieved.
- The results indicate that there is a loss in pre-stress in both types of tendons over the test period. The behaviour of the galvanised tendon

- under ICCP-O application is more stable than the behaviour of the ungalvanised tendon in terms of service stress loss. The degree of corrosion also has an impact on the loss of pre-stress, particularly in ungalvanised tendons, with the tendons subjected to higher degrees of corrosion suffering higher losses which may need to be accounted for at the design stage. This loss of service stress can be from a combination of the degree of corrosion and the application of ICCP-O
- With respect to mechanical properties, overall, there was no significant effect of ICCP-O on the strength of the tendons as tested. The ultimate tensile strength and the 0.2% proof strength in each type of tendon were similar and no significant reduction was evident that could compromise safety. Usually, the design safety factor is set to a maximum level of load, approximately $\frac{2}{3}$ proof strength for structural engineering components. Although the ductility has been reduced by the application of the ICCP-O, the fracture occurred in the plastic zone and after reaching the ultimate strength in each type of tendon.
 - The embrittlement ratios (the ratio of the mechanical properties with and without cathodic protection) indicate that hydrogen generated by ICCP-O has no effect on UTS and proof strength for both tendon types. However, for the galvanised tendon with High Level of pre-stress, the ratio was less for breaking strength and increased more for ductility. Notably, increases in the ratio of ductility and necking were apparent.
 - Unstressed, hydrogen exposed specimens did not show significant changes in either mechanical properties or the characteristics of the fracture. Only the galvanised specimen showed greater shear area and a combination of ductile and brittle fracture modes was evident.
 - The loss of service stress for the two tendon types with High Level of pre-stress is greater than the loss in stress for tendons with Low Level of pre-stress. Neither ICCP-N nor ICCP-O have any significant effect on the Young's Modulus, 0.2% proof strength and UTS for either type of pre-stressed tendon. A reduction in ductility was observed in both types of tendons after the application of ICCP-N and ICCP-O. This reduction increased as the degree of corrosion

increased. The fracture modes show that both ICCP-N and ICCP-O have a mixed type of fracture mode at Stage III corrosion. Nevertheless, the unstressed samples show less brittleness than the pre-stressed sample. Overall, the damage to both types of tendons is not only due to the application of ICCP as there are other factors such as the degree of corrosion and the level of pre-stress and these appear to have more influence than the application of ICCP alone.

8.5 Recommendations for further research

There are several areas of further study that have the possibility to expand the findings of this research but could not be pursued during the timescale and scope of this project. These are listed below as a series of recommendations:

- Further investigation is required to establish losses due to corrosion at other in-service pre-stresses as would commonly be found in structures. Although this could be estimated via interpolation, it will enable more accurate design guidance to be developed, linking losses in pre-stress to degree of corrosion for all levels of pre-stress.
- It would be beneficial for more data to be made available from actual corroded structures. This will help in the development of a correlation between laboratory results and data from existing structures.
- Further tests are required to be conducted where the specimens are pre-stressed and exposed to ICCP and compared with the pre-corroded specimens.

Appendix 1

Table A1.1 Diameter of steel tendons before and after test completion

Sample ID	Diameter (mm)											
	Before corrosion						After corrosion					
	d1	d2	d3	d4	d5	Average	d1	d2	d3	d4	d5	Average
	mm	mm	mm	mm	mm	mm	mm	mm	mm	mm	mm	mm
U-R-1	5.37	5.35	5.32	5.3	5.3	5.33						
U-R-2	5.36	5.31	5.3	5.3	5.29	5.31						
U-R-3	5.36	5.34	5.31	5.3	5.29	5.32						
U-R-4	5.29	5.31	5.31	5.31	5.36	5.32						
U-R-5	5.27	5.28	5.29	5.3	5.36	5.30						
G-R-1	5.31	5.34	5.34	5.33	5.4	5.34						
G-R-2	5.4	5.36	5.33	5.33	5.32	5.35						
G-R-3	5.39	5.37	5.32	5.33	5.3	5.34						
G-R-4	5.39	5.39	5.33	5.39	5.38	5.38						
G-R-5	5.39	5.38	5.36	5.3	5.4	5.37						
S-U-L-I-1	5.36	5.36	5.37	5.36	5.32	5.35	5.24	5.23	5.22	5.23	5.25	5.23
S-U-L-II-O-2	5.37	5.32	5.31	5.4	5.34	5.35	5.14	5.11	5.09	5.12	5.05	5.10
S-U-L-III-O-3	5.37	5.32	5.35	5.37	5.37	5.36	4.76	4.89	4.89	4.8	4.8	4.83
S-U-H-I-1	5.33	5.32	5.36	5.36	5.37	5.35	5.31	5.3	5.3	5.22	5.2	5.27
S-U-H-II-O-2	5.37	5.36	5.33	5.36	5.33	5.35	5.08	5.04	5.08	5.03	5.09	5.06
S-U-H-III-O-3	5.32	5.32	5.36	5.36	5.31	5.33	4.92	4.97	5	5.01	4.99	4.98
M-U-L-X-1	5.24	5.26	5.3	5.25	5.33	5.28	5.27	5.33	5.26	5.27	5.31	5.29
M-U-L-II-N-2	5.37	5.33	5.4	5.32	5.27	5.34	5.14	5.13	5.13	5.1	5.13	5.13
M-U-L-III-N-3	5.43	5.4	5.34	5.3	5.24	5.34	5.13	5.1	5.05	5.09	5.18	5.11

Table A1.1 (cont.) Diameter of steel tendons before and after test completion

Sample ID	Diameter (mm)											
	Before corrosion						After corrosion					
	d1	d2	d3	d4	d5	Average	d1	d2	d3	d4	d5	Average
	mm	mm	mm	mm	mm	mm	mm	mm	mm	mm	mm	mm
M-U-L-X1-1	5.24	5.24	5.32	5.3	5.33	5.29	5.27	5.27	5.26	5.26	5.32	5.28
M-U-L-II-O-2	5.35	5.33	5.34	5.35	5.33	5.34	5.2	5.13	5.13	5.09	5.06	5.12
M-U-L-III-O-3	5.37	5.34	5.32	5.32	5.25	5.32	5.03	5.08	5.07	5.11	5.03	5.06
M-U-H-X-1	5.36	5.36	5.36	5.31	5.36	5.35	5.32	5.31	5.3	5.29	5.28	5.30
M-U-H-II-N-2	5.35	5.36	5.36	5.36	5.32	5.35	5.18	5.19	5.2	5.22	5.17	5.19
M-U-H-III-N-3	5.39	5.36	5.36	5.35	5.36	5.36	5.17	5.18	5.22	5.14	5.13	5.17
M-U-H-X1-1	5.36	5.36	5.36	5.35	5.36	5.36	5.32	5.32	5.31	5.37	5.31	5.33
M-U-H-II-O-2	5.36	5.36	5.35	5.36	5.35	5.36	5.17	5.19	5.2	5.17	5.22	5.19
M-U-H-III-O-3	5.38	5.36	5.36	5.35	5.36	5.36	5.17	5.19	5.16	5.21	5.2	5.19
M-G-H-X-1	5.38	5.38	5.39	5.39	5.4	5.39	5.35	5.34	5.33	5.31	5.32	5.33
M-G-H-II-N-1	5.41	5.4	5.39	5.38	5.4	5.40	5.19	5.23	5.2	5.19	5.24	5.21
M-G-H-III-N-3	5.38	5.39	5.4	5.4	5.38	5.39	5.13	5.16	5.16	5.16	5.2	5.16
M-G-H-X1-1	5.41	5.4	5.39	5.39	5.4	5.40	5.29	5.33	5.31	5.28	5.32	5.31
M-G-H-II-O-2	5.4	5.39	5.39	5.4	5.38	5.39	5.19	5.24	5.24	5.22	5.23	5.22
M-G-H-III-O-3	5.4	5.39	5.4	5.39	5.41	5.40	5.13	5.16	5.18	5.17	5.25	5.18
5-UG-O-1	5.32	5.33	5.33	5.34	5.33	5.33	5.3	5.29	5.26	5.28	5.27	5.28
5-UG-O-2	5.32	5.33	5.32	5.34	5.32	5.33	5.26	5.28	5.3	5.3	5.28	5.28
5-UG-O-3	5.33	5.34	5.34	5.33	5.32	5.33	5.25	5.25	5.25	5.25	5.26	5.25
5-G-O-1	5.36	5.37	5.38	5.37	5.39	5.37	5.25	5.26	5.26	5.27	5.28	5.26
5-G-O-2	5.36	5.37	5.37	5.36	5.38	5.37	5.2	5.19	5.17	5.2	5.21	5.19
5-G-O-3	5.38	5.39	5.38	5.38	5.39	5.38	5.16	5.17	5.18	5.22	5.19	5.18

Appendix 2

List of Publications, conferences and competitions

- 37th Cement and Concrete Science Conference, 11-12 September 2017, University College London, conference paper and oral presentation: 'Corrosion induced losses in pre-stressed tendons' [128].
- Symposium image competition 2017, awarded as the 2017 research image winner in Material Engineering Research Institute (MERI), Sheffield Hallam University.

Further papers are currently in preparation.

References

- [1] J. Piazza, "Corrosion Control on Concrete Structures: Zinc- Hydrogel Technology," *Mar. Corros. Trop. Environ.*, vol. 52, p. 72, 2000.
- [2] R. M. Burns and W. W. Bradley, *Protective Coatings for Metals*, 3rd ed. New York: Reinhold Publishing Corporation, 1967.
- [3] P. Kotler and B. Heron, "Prestressed Concrete Tanks." Preload LTD, London, 1970.
- [4] S. El Belbol and S. Wilson, "Cathodic Protection of Steel in Concrete - Frequently Asked Questions," Corrosion Prevention Association (CPA), Technical Notes No: 8, 2002.
- [5] D. H. Lee, S. J. Han, H. E. Joo, and K. S. Kim, "Control of Tensile Stress in Prestressed Concrete Members Under Service Loads," *Int. J. Concr. Struct. Mater.*, vol. 12, no. 1, 2018.
- [6] C. S. Hanskat, "Shotcrete in Liquid-Containing Concrete Structures," *Shotcrete*, 2010.
- [7] A. A. Torres-Acosta, S. Navarro-Gutierrez, and J. Terán-Guillén, "Residual flexure capacity of corroded reinforced concrete beams," *Eng. Struct.*, vol. 29, no. 6, pp. 1145–1152, 2007.
- [8] C. Fang, K. Lundgren, L. Chen, and C. Zhu, "Corrosion influence on bond in reinforced concrete," *Cem. Concr. Res.*, vol. 34, no. 11, pp. 2159–2167, 2004.
- [9] R.I.Gilbert and N.C.Mickleborough, *Design of prestressed concrete*, vol. 5, no. 3. Taylor & Francis e-Library, 2003.
- [10] P. Pedferri, L. Bertolini, B. Elsener, E. Redaelli, and R. Polder, *Corrosion of Steel in Concrete - Prevention, Diagnosis, Repair*, 2nd ed. Singapore: Wiley-VCH, 2013.
- [11] A. M. Neville, *Properties of Concrete*, 4th ed. 2005.
- [12] E. H. Hristova, "Residual Strength of Corroded Reinforced Concrete Beams," Sheffield Hallam University (Thesis), 2006.
- [13] H. W. Song, C. H. Lee, and K. Y. Ann, "Factors influencing chloride transport in concrete structures exposed to marine environments," *Cem. Concr. Compos.*, vol. 30, no. 2, pp. 113–121, 2008.
- [14] "Cost of Corrosion Study," <http://www.nace.org/nace/content/>

publicaffairs/cocorrindex.asp., 2007. .

- [15] P. Lambert, "Reinforced Concrete – History , Properties & Durability," Corrosion Prevention Association (CPA), Technical Notes No: 1, 2002.
- [16] S. Ahmad, "Reinforcement corrosion in concrete structures, its monitoring and service life prediction - A review," *Cem. Concr. Compos.*, vol. 25, no. 4-5 SPEC, pp. 459–471, 2003.
- [17] ACI, "Guide to Design and Construction Practices to Mitigate Corrosion of Reinforcement in Concrete Structures," ACI 222.3R-11, 2011.
- [18] A. J. Kashani M. Mohammad, Crewe and N. A. Alexander, "Stress-Strain Response of Corroded Reinforcing Bars under Monotonic and Cyclic Loading," in *15 WCEE*, 2012.
- [19] J. G. Cabrera, "Deterioration of Concrete Due to Reinforcement Steel Corrosion," *Cem. Concr. Compos.*, vol. 9465, no. 95, pp. 47–59, 1996.
- [20] National Ready Mixed Concrete Association, "CIP 25 - Corrosion of Steel in Concrete," *Concrete in Practice*, no. G 15, 1995.
- [21] A. Mak, "Corrosion of Steel , Aluminum and Copper in Electrical Applications," *General Cable*, no. 770, 2002.
- [22] P. Lambert, "Corrosion Mechanisms – an Introduction to Aqueous Corrosion," Corrosion Prevention Association (CPA), Technical Notes No: 5, 2002.
- [23] P. A. Schweitzer, *Fundamentals of Corrosion-Mechanisms, Causes, and Preventative Methods*, vol. 53, no. 9. Taylor & Francis Group, 2013.
- [24] M. Fontana, *Corrosion Engineering*, 3rd ed. McGraw-Hill Book Company, 1987.
- [25] P. Roberge, *Handbook of Corrosion Engineering*. McGraw-Hill, 1999.
- [26] L. Abosrra, A. F. Ashour, and M. Youseffi, "Corrosion of steel reinforcement in concrete of different compressive strengths," *Constr. Build. Mater.*, vol. 25, no. 10, pp. 3915–3925, 2011.
- [27] Z. Ahmed, *Principle of corrosion engineering and corrosion control*, no. September. Elsevier Science & Technology Books, 2006.
- [28] C. E. Locke and A. Siman, "Electrochemistry of Reinforcing Steel in Salt-Contaminated Concrete," in *Corrosion of Reinforcing Steel in Concrete*, STP 713., D. E. Tonini and J. M. Gaidis, Eds. Philadelphia: American Society for Testing and Materials, 1980, pp. 3–16.

- [29] C. M. Hansson, "Comments on electrochemical measurements of the rate of corrosion of steel in concrete," *Cem. Concr. Res.*, vol. 14, no. 4, pp. 574–584, 1984.
- [30] J. P. Broomfield, *Corrosion of Steel in Concrete: Understanding, Investigation and Repair*. London: E & FN Spon, Chapman & Hall, London, UK, 1997.
- [31] H. Böhni, Ed., *Corrosion in reinforced concrete structures*. Cambridge: Woodhead Publishing Limited, 2005.
- [32] ACI, "Protection of Metals in Concrete Against Corrosion," ACI 222R-01, 2010.
- [33] W. Podolny, "Corrosion of prestressing steels and its mitigation," *PCI J.*, vol. 37, no. 5, pp. 34–55, 1992.
- [34] M. Raupach, "Chloride-induced macrocell corrosion of steel in concrete - Theoretical background and practical consequences," *Constr. Build. Mater.*, vol. 10, no. 5 SPEC. ISS., pp. 329–338, 1996.
- [35] C. Atkins, "Cathodic Protection of Prestressed Concrete," Corrosion Prevention Association (CPA), Technical Note 21, 2002.
- [36] W. H. Hartt, S. Lee, and F. Drive, "Corrosion Induced Bridge Tendon Failures Resulting from Deficient Grout: Part I – Model Development," 2016, no. 7121, pp. 1–12.
- [37] R. E. Melchers and T. M. Pape, "Performance of 45-year-old corroded prestressed concrete beams," *Proc. ICE - Struct. Build.*, vol. 166, no. 10, pp. 547–559, 2013.
- [38] G. Schiroky, A. Dam, A. Okeremi, and C. Speed, "Preventing pitting and crevice corrosion of offshore stainless steel tubing," *World oil*, vol. 230, no. 4, 2009.
- [39] Y. Wu and U. Nürnberger, "Corrosion-technical properties of high-strength stainless steels for the application in prestressed concrete structures," *Mater. Corros.*, vol. 60, no. 10, pp. 771–780, 2009.
- [40] J. R. Galvele, "Tafel's law in pitting corrosion and crevice corrosion susceptibility," *Corros. Sci.*, vol. 47, no. 12, pp. 3053–3067, 2005.
- [41] J. R. Galvele, "Treatise on Materials Science and Technology, Corrosion: Aqueous Processes and Passive Films," *Acad. Press*, vol. 23, pp. 1–57.
- [42] U. Nürnberger, "Corrosion Induced Failures in Prestressed Concrete

- Structures and Preventative Measures,” *Otto-Graf-Journal*, vol. 9, pp. 218–250, 1998.
- [43] M. Li, L. Q. Guo, L. J. Qiao, and Y. Bai, “The mechanism of hydrogen-induced pitting corrosion in duplex stainless steel studied by SKPFM,” *Corros. Sci.*, vol. 60, pp. 76–81, 2012.
- [44] F. J. Recio, M. C. Alonso, L. Gaillet, and M. Sánchez, “Hydrogen embrittlement risk of high strength galvanized steel in contact with alkaline media,” *Corros. Sci.*, vol. 53, no. 9, pp. 2853–2860, 2011.
- [45] R.A.Cottis, “Hydrogen Embrittlement,” *Shrier’s Corros.*, vol. 2, no. Part II, Chapter 2.10, pp. 902–922, 2010.
- [46] W. Lynes, “Some historical developments relating to corrosion,” *Electrochem. Soc.*, vol. 98, 3C, 1951.
- [47] P. M. Chess, *Cathodic Protection of Steel in Concrete and Masonry*, 2nd ed. New York: Taylor & Francis Group, 2014.
- [48] “Cathodic Protection of Steel in Concrete,” A cement and concrete industry, Technical Report No. 73, 2011.
- [49] R. Polder, A. Kranje, J. Leggedoor, A. Sajna, and I. Stipanovic, “Guideline for smart cathodic protection of steel in concrete: Assessment and Rehabilitation of Central European Highway Structures,” 2009.
- [50] J. P. Broomfield, “Cathodic Protection of Reinforced Concrete Status Report,” 1995.
- [51] R. Winston and H. Uhlig, *Corrosion and Corrosion Control Corrosion: An Introduction to Corrosion Science and Engineering*, 4th ed. New Jersey: John Wiley & Sons, Inc., Hoboken New Jersey, 2008.
- [52] V. Ashworth, “Principles of cathodic protection,” in *Shreir’s Corrosion*, vol. 2, 2010, pp. 2747–2762.
- [53] K. Wilson, M. Jawed, and V. Ngala, “The selection and use of cathodic protection systems for the repair of reinforced concrete structures,” *Constr. Build. Mater.*, vol. 39, 2013.
- [54] “World energy resources: a survey,” World Energy Council, London, 2013.
- [55] A. Byrne, N. Holmes, and B. Norton, “Cathodic Protection for Reinforced Concrete Structures: Present Practice and Moves Toward using Renewable Energy,” *Cprrosion Sci.*, 2015.

- [56] R. B. Polder, "Cathodic protection of reinforced concrete structures in the Netherlands - Experience and developments: Cathodic protection of concrete - 10 years experience." *Heron*, pp. 3–14, 1998.
- [57] J. Xu and W. Yao, "Current distribution in reinforced concrete cathodic protection system with conductive mortar overlay anode," *Constr. Build. Mater.*, vol. 23, no. 6, pp. 2220–2226, 2009.
- [58] C. Ward, S. Nanukuttan, and J. McRobert, "The performance of a cathodic protection system in reinforced concrete structure: Monitoring and Service Life Modelling The Performance of a Cathodic Protection System in Reinforced Concrete Structure: Monitoring and Service Life Modelling," *Civ. Eng. Res. Irel. Conf. (CERAI), Belfast, United Kindgom.*, no. December, pp. 1–7, 2014.
- [59] F. Pruckner, J. Theiner, J. Eri, and G. E. Nauer, "In-situ monitoring of the efficiency of the cathodic protection of reinforced concrete by electrochemical impedance spectroscopy," *Electrochim. Acta*, vol. 41, no. 7–8, pp. 1233–1238, 1996.
- [60] C. Christodoulou, G. Glass, J. Webb, S. Austin, and C. Goodier, "Assessing the long term benefits of Impressed Current Cathodic Protection," *Corros. Sci.*, vol. 52, no. 8, pp. 2671–2679, 2010.
- [61] G. K. Glass, A. M. Hassanein, and N. R. Buenfeld, "Cathodic protection afforded by an intermittent current applied to reinforced concrete," *Corros. Sci.*, vol. 43, no. 6, pp. 1111–1131, 2001.
- [62] J. P. B. Euring and B. S. W. Euring, "Cathodic Protection of Steel in Concrete: The International Perspective," Corrosion Prevention Association (CPA), Technical Notes No: 3, 2002.
- [63] R. Kean and K. Davies, "Cathodic Protection. Guide prepared British Department Trade and Industry: The UK National Physical Laboratory." pp. 2–4, 1981.
- [64] R. Brueckner, C. P. Atkins, and P. Lambert, "Life time extension of prestressed beams using cathodic protection," *Br idge Maint. , Saf ety , Manag. Resil. Sustain. Frangopol*, pp. 2814–2819, 2012.
- [65] G. K. C. and K. C. Hover, "Cathodic Protection for Prestressed Structures," *Concr. Int.*, vol. 9, no. 1.
- [66] "Design manual for roads and bridges: Cathodic protection for use in

- reinforced concrete highway structures,” High Way Agency, 2002.
- [67] J. P. Broomfield, “The Principles and Practice of Galvanic Cathodic Protection for Reinforced Concrete Structures,” Corrosion Prevention Association (CPA), Technical Notes No: 6, 2002.
- [68] G. T. Parthiban, T. Parthiban, R. Ravi, V. Saraswathy, N. Palaniswamy, and V. Sivan, “Cathodic protection of steel in concrete using magnesium alloy anode,” *Corros. Sci.*, vol. 50, no. 12, pp. 3329–3335, 2008.
- [69] P. Francis, “Cathodic Protection in Practise,” in *NPL Report*, 1998, pp. 1–22.
- [70] A. A. Sohangpurwala, *Cathodic Protection for Life Extension of Existing Reinforced Concrete Bridge Elements*. Washington: National Cooperative Highway Research Program, 2009.
- [71] J. Mietz, “Electrochemical Rehabilitation Methods for Reinforced Concrete Structures – A State of the Art Report - Publication number 24,” European Federation of Corrosion, 1998.
- [72] T. E. Evans, “Mechanism of cathodic protection in sea water,” in *Cathodic Protection - theory and practice, 2nd International conference*, 1989.
- [73] V. Ashworth and C. J. L. Booker, Eds., *Impressed current anodes, Cathodic protection: Theory and practice*. Chichester, England: Ellis Horwood Ltd., 1986.
- [74] H. C. Schell, D. G. Manning, and K. C. Clear, “Cathodic protection of bridge substructures: Burlington Bay Skyway test site, initial performance of systems 1 to 4,” *Transportation Research Record* 962, 1984.
- [75] G. Mussinelli, M. Tettamanti, and P. Pedferri, “The effect of current density on anode behaviour and on concrete in the anode region,” in *CIRIA 2nd International conference deterioration and repair of reinforced concrete in the Arabian Gulf*, 1987, p. Vol. 1, 99-120.
- [76] “State-of-the-Art Report: Criteria for cathodic protection of prestressed concrete structure,” NACE International Publication 01102, 2002.
- [77] BSI Standards, “Cathodic protection of steel in concrete,” BS EN ISO 12696, 2016.
- [78] T. Covered, P. Monitoring, T. Conductive, C. Anode, and O. Criteria, “Monitoring and Maintenance of Conductive Coating Anode Cathodic

- Protection Systems,” 2002. [Online]. Available: <http://www.azom.com/article.aspx?ArticleID=1695> P.
- [79] BSI Standards, “Cathodic protection-Part 1: Code of practice for land and marine applications (formerly CP 1021),” BS 7361-1, 1991.
- [80] T. C. Society, “Electrochemical tests for reinforcement corrosion-Concrete Society Technical Report No. 60,” The Concrete Society, 2004.
- [81] A. Fallis, “Hydrogen embrittlement of high strength steel wires under cathodic polarization,” *J. Chem. Inf. Model.*, vol. 53, no. 9, pp. 1689–1699, 2013.
- [82] F. O’Flaherty, P. Mangat, P. Lambert, and E. Browne, “Effect of under-reinforcement on the flexural strength of corroded beams,” *Mater. Struct.*, pp. 311–321, 2008.
- [83] M. Geoff, Ed., *Durability of Concrete Structures Investigation, repair, protection*, vol. 53, no. 9. E & FN Spon, an imprint of Chapman & Hall, 2013.
- [84] D. V. Val and M. G. Stewart, “Life-cycle cost analysis of reinforced concrete structures in marine environments,” *Struct. Saf.*, vol. 25, no. 4, pp. 343–362, 2003.
- [85] A. Bahadori, “Test Methods,” in *Cathodic Corrosion Protection Systems*, 2014, pp. 253–308.
- [86] G. Song and A. Shayan, “Corrosion of steel in concrete: causes. detection and prediction, A state- of-the-art review,” ARRB Transport Research Ltd, 1998.
- [87] M. S. A. Elgarf, “The Effect of Reinforcement Corrosion on the Structural Performance Concrete Flexural Members,” University of Aberdeen (Thesis), 1994.
- [88] M. Dutek and M. Hayles, “The Quanta User’s Operation Manual, 1st Edition,” 2005.
- [89] H. Schroettner, M. Schmied, and S. Scherer, “Comparison of 3D surface reconstruction data from certified depth standards obtained by SEM and an infinite focus measurement machine (IFM),” *Microchim. Acta*, vol. 155, no. 1–2, pp. 279–284, 2006.
- [90] BSI Standards, “Metallic materials — Tensile testing Part 1 : Method of test at room temperature,” BS EN ISO 6892-1, 2016.

- [91] C. Andrade, "Corrosion of steel reinforcement," in *Environmental Deterioration of Materials*, vol. 28, 2014, pp. 183–243.
- [92] W. W. Burns, R.M. Bradley, *Coatings for Metals*, 3rd ed. New York: Reinhold Publishing Corporation, 1967.
- [93] U. R. Evans, *The corrosion and oxidation of metal*. London: Edward Arnold Ltd, 1960.
- [94] S. Ahmad, "Techniques for inducing accelerated corrosion of steel in concrete," *Arab. J. Sci. Eng.*, vol. 34, no. 2 C, pp. 95–104, 2009.
- [95] S. Caré and A. Raharinaivo, "Influence of impressed current on the initiation of damage in reinforced mortar due to corrosion of embedded steel," *Cem. Concr. Res.*, vol. 37, no. 12, pp. 1598–1612, 2007.
- [96] Y. Yuan, Y. Ji, and S. P. Shah, "Comparison of two accelerated corrosion techniques for concrete structures," *ACI Struct. J.*, vol. 104, no. 3, pp. 344–347, 2007.
- [97] M. . Mangat, P.S. Elgarf, "Flexural Strength of concrete beams with corroding reinforcement," *ACI Struct. J.*, vol. 96 (1), pp. 149–158, 1999.
- [98] "Accelerated Corrosion Test Uses Electrochemical Techniques," *Materials Performance*, vol. 52, no. 4, p. 6, 2013.
- [99] B. Weber, "Accelerated Corrosion of Steel in Dry-Cast reinforced Concrete Pipes after Initiation," Florida Atlantic University (Thesis), 2014.
- [100] M. M. Mahat, A. Hisham, M. Aris, U. S. Jais, M. Fakharul, and Z. Raja, "Infinite Focus Microscope (IFM): Microbiologically Influenced Corrosion (MIC) behavior on Mild Steel by *Pseudomonas aeruginosa*," in *2011 International Symposium on Humanities, Science and Engineering Research Infinite*, 2014, no. June 2012, pp. 106–110.
- [101] C. Nguyen, "Dual function carbon fibre reinforced anode system for concrete structures," Sheffield Hallam University (Thesis), 2014.
- [102] E. Ghali, *Corrosion Resistance of Aluminum and Magnesium Alloys*. A Johan Wiley & Sons INC., 2010.
- [103] "Cathodic Protection," Department of Defense USA, 2016.
- [104] B. S. Covino Jr., S. D. Cramer, S. J. Bullard, G. R. Holcomb, and W. K. Collins, "Thermal spray anodes for impressed current cathodic protection of reinforced concrete structures," *Materials Performance*, vol. 38, no. 1, pp. 27–33, 1999.

- [105] S. C. Hall, "Cathodic protection criteria for prestressed concrete pipe - An update," *Materials Performance*, vol. 37, no. 11, p. 23, 2002.
- [106] W. Hartt, E. Joubert, and S. H. Kliszowski, "Long-Term Effects of Cathodic Protection on Prestressed Concrete Bridge Components - DRAFT," *Corrosion*, vol. 53, no. 11, pp. 891–908, 1997.
- [107] N. Perez, *Electrochemistry and Corrosion Science*. Kluwer Academic, 2004.
- [108] P. C. S. Hayfield, "Corrosion Prevention in Concrete - The Cathodic Protection of Reinforcing Steel Bars Using Platinised-Type Materials," *Platin. Met. Rev.*, vol. 30, pp. 158–166, 1986.
- [109] "Operation and maintenance: water conservation," Department of Defence USA, 2003.
- [110] E. David, "Avoidance of Potential Side Effects, in Cathodic Protection of Steel in Concrete." pp. 170–172, 2005.
- [111] NACE, "SP0169 - Standard Practice Control of External Corrosion on Underground or Submerged Metallic Piping Systems," 2013.
- [112] NACE, "TM0497-2012 - Measurement Techniques Related to Criteria for Cathodic Protection of Underground Storage Tank Systems," 2012.
- [113] BSI Standards, "Petroleum , petrochemical and natural gas industries — Collection and exchange of reliability and maintenance data for equipment," BS EN ISO 15589-1, 2017.
- [114] BSI Standards, "Cathodic Protection-Part 1: Code of practice for land and marine applications," BS7361-1, 1991.
- [115] BSI Standards, "Cathodic protection of buried or immersed metallic structures — General principles and application for pipelines," BS EN 12954, 2001.
- [116] Australian Standard, "Cathodic protection of metals Part 3: Fixed immersed structures," AS 2832.3, 2005.
- [117] NACE, "Control of External Corrosion on Buried or Submerged Metallic Piping Systems," NACE SP0169, 2007.
- [118] F. Song, B. F. M. Song, and S. Antonio, "Review Of CP Criteria In Five Standards," *Pipeline & Gas*, no. December, 2011.
- [119] J. Tinnea and R. Tinnea, "Cathodic Protection Survey Final Report," Oregon Department of Transportation, 2014.

- [120] C. Van Nguyen, P. Mangat, G. Jones, F. O'Flaherty, and P. Lambert, "The Performance of Carbon Fibre Composites as ICCP Anodes for Reinforced Concrete Structures," *ISRN Corros.*, vol. 2012, pp. 1–9, 2012.
- [121] I. B. Topçu and C. Karakurt, "Properties of reinforced concrete steel rebars exposed to high temperatures," *Adv. Mater. Sci. Eng.*, vol. 2008, no. September 2001, 2008.
- [122] W. Zhu, R. François, D. Coronelli, and D. Cleland, "Effect of corrosion of reinforcement on the mechanical behaviour of highly corroded RC beams," *Eng. Struct.*, vol. 56, pp. 544–554, 2013.
- [123] K. Ishii, H. Seki, T. Fukute, and K. Ikawa, "Cathodic protection for prestressed concrete structures," *Constr. Build. Mater.*, vol. 12(2–3), pp. 125–132, 1998.
- [124] R. N. Parkins, M. Elices, V. Sanchez-Galvez, and L. Caballero, "Environment sensitive cracking of pre-stressing steels," *Corros. Sci.*, vol. 22, no. 5, pp. 379–405, 1982.
- [125] G. Gonzalez-Mancera, V. Cortes-Suarez, and M. Mariano-Alberto, "Influence of Hydrogen on Fracture Mode API X60 Steel," *Microsc. Microanal.*, vol. 21, no. S3, pp. 283–284, 2015.
- [126] J. Sanchez, S. F. Lee, M. A. Martin-Rengel, J. Fulla, C. Andrade, and J. Ruiz-Hervías, "Measurement of hydrogen and embrittlement of high strength steels," *Eng. Fail. Anal.*, vol. 59, pp. 467–477, 2016.
- [127] I. R. Kabir and M. A. Islam, "Hardened Case Properties and Tensile Behaviours of TMT Steel Bars," *Am. J. Mech. Eng.*, vol. 2, no. 1, pp. 8–14, 2014.
- [128] F. O. Flaherty, I. R. Elomari, and P. Lambert, "Corrosion induced losses in pre-stressed tendons," in *37th Cement and Concrete Science Conference*, 2017, p. 111.